188
8/28/79

14 3667

ORNL-5551

MASTER

Analysis of the ORNL/TSF GCFR Grid-Plate Shield Design Confirmation Experiment

C. O. Slater
S. N. Cramer
D. T. Ingersoll

OAK RIDGE NATIONAL LABORATORY
OPERATED BY UNION CARBIDE CORPORATION · FOR THE DEPARTMENT OF ENERGY

BLANK PAGE

ORNL-5551
Distribution Category
UC-77 — Gas Cooled Reactor Technology

Contract W-7405-eng-26

Engineering Physics Division

ANALYSIS OF THE ORNL/TSF GCFR GRID-PLATE SHIELD DESIGN CONFIRMATION EXPERIMENT

Report Written by:

C. O. Slater

Analysis Performed by:

C. O. Slater
S. N. Cramer
D. T. Ingersoll

Experiment Performed by:

F. J. Muckenthaler
J. J. Manning
J. L. Hull

Date Published: August 1979

NOTICE

[illegible]

OAK RIDGE NATIONAL LABORATORY
Oak Ridge, Tennessee 37830
operated by
UNION CARBIDE CORPORATION
for the
DEPARTMENT OF ENERGY

CONTENTS

Abstract v
Executive Summary. vii
1.0. INTRODUCTION 1
2.0. EXPERIMENTAL CONFIGURATIONS. 2
2.1. Internal Components. 2
2.2. Basic Configuration — II.A 6
2.3. Other Configurations II. 7
2.4. Configurations III 10
2.5. Configurations IV. 10
2.6. Configurations V 10
2.7. Configurations VI. 10
3.0. DETECTORS. 10
4.0. NEUTRON SOURCE 12
5.0. CALCULATIONAL MODELS 14
5.1. Two-Dimensional Model. 14
5.2. Three-Dimensional Model. 15
6.0. CALCULATIONAL METHODS. 16
6.1. Two-Dimensional Calculations 16
6.2. Three-Dimensional Calculations 16
7.0. RESULTS. 17
7.1. Configurations II. 17
7.1.1. Configuration II.A 17
7.1.2. Configuration II.B 19
7.1.3. Configuration II.D 27
7.1.4. Configuration II.E 32
7.1.5. Configuration II.F 33
7.1.6. Examination of Discrepancies 42
7.1.6.1. Configuration II.A 42
7.1.6.2. Configuration II.B 49
7.1.6.3. Configurations II.D, II.E, and II.F. . 52
7.2. Configurations III.A, IV.A, and VI.A 52
7.3. Configuration IV.B 55
7.4. Configuration V 58
8.0. IMPLICATIONS FOR THE GCFR. 60
8.1. Axial Neutron Streaming. 60
8.2. Fast Neutron Exposure to the Grid Plate. 61
8.3. Neutron Source for the GCFR Upper Plenum 65
9.0 SUMMARY 68
REFERENCES 70
APPENDIX A: The Experimental Program Plan 73
APPENDIX B: Multigroup Response Functions 85
APPENDIX C: Special Computer Codes. 89
APPENDIX D: Group Structure, Quadrature, and Fission Spectrum . . . 129
APPENDIX E: Two-Dimensional Geometry Models, Space Mesh, and Convergence Parameters 133

ABSTRACT

The results of the analysis of the GCFR Grid-Plate Shield Design Confirmation Experiment are presented. The experiment, performed at the ORNL Tower Shielding Facility, was designed to test the adequacy of methods and data used in the analysis of the GCFR design. In particular, the experiment tested the adequacy of methods to calculate (1) axial neutron streaming in the GCFR core and axial blanket, (2) the amount and location of the maximum fast-neutron exposure to the grid plate, and (3) the neutron source leaving the top of the grid plate and entering the upper plenum. Other objectives of the experiment were to verify the grid-plate shielding effectiveness and to assess the effects of fuel-pin and subassembly spacing on radiation levels in the GCFR. The experimental mockups contained regions representing the GCFR core/blanket region, the grid-plate shield section, and the grid plate. Most core design options were covered by allowing (1) three different spacings between fuel subassemblies, (2) two different void fractions within a subassembly by variation of the number of fuel pins, and (3) a mockup of a control-rod channel.

The results were analyzed using the DOT-IV discrete ordinates, the MORSE Monte Carlo, and various auxiliary computer codes. DOT results agreed with measurements taken close behind the fuel pins and grid-plate shield configurations to within 20%. For detectors distant from those configurations, the DOT results were up to 50% higher than the measurements. The results close in behind the grid plate also showed a 50% overprediction. Results for distant detectors behind the grid plate were about twice the measured results. The MORSE results were in good agreement close behind the configurations, though there was serious underprediction close behind the grid plate. For the distant detectors, the MORSE results were somewhat better than DOT behind the fuel pins and were in excellent agreement with the measurements behind the grid plate.

BLANK PAGE

For the GCFR design, the results indicate that methods used in the analysis of the GCFR shield design are adequate for most cases. Except for locations behind the grid plate and distant locations behind the fuel pins and behind the grid-plate shields, the agreement between the calculated and measured results was much better than the desired 20% agreement. An exception was a slightly greater than 20% difference between the calculated and measured ratios of the fast neutron fluxes behind fuel-pin configurations with interassembly gap widths of 0.318 cm and 1.27 cm. The agreement between the calculated and measured fast-neutron exposure to the grid plate was excellent; the results were well within the 10% uncertainty of the measurements. The point on the grid plate at which the fast-neutron exposure was highest was also predicted well. Regarding the flux emerging from the grid plate, a calculation using a 150-angle biased quadrature overpredicted the detector responses behind the grid plate by factors of 1.5 to 2.0 (partially due to overprediction of the forward-peaked angular flux leaving the fuel pins). A calculation with a quadrature (S_{10}) frequently used in past design calculations, underpredicted the same responses by factors of 4.0 to 12.0. By analyzing the behavior of both quadratures, it was estimated that the design calculations underpredicted the neutron transmission through the grid plate by no more than a factor of 4.0. This implies a correction factor of 4.0 for radiation levels in the GCFR upper plenum. Since most calculated design radiation levels were more than a factor of 4.0 below the design constraints, the corrective factor may be accomodated with little, if any, redesign.

ANALYSIS OF THE ORNL/TSF GCFR GRID-PLATE SHIELD DESIGN CONFIRMATION EXPERIMENT*

C. O. Slater, S. N. Cramer, and D. T. Ingersoll

EXECUTIVE SUMMARY

In the proposed 300-MW(e) Gas-Cooled Fast Breeder Reactor (GCFR) demonstration plant,[1] the grid plate is the supportive structure for the fuel and blanket subassemblies which are suspended below it. Perkins and Cerbone[2] have stated that it is "essential that adequate shielding be provided to assure the structural integrity of the grid plate for the life of the plant." The shielding is said to be adequate when all design constraints are met. The calculations, however, are subject to uncertainties which, in systems involving radiation transmission through thick shields, can be quite substantial. To determine the uncertainties in the design calculations of neutron transport through the grid-plate shields and the grid plate, the GCFR Grid-Plate Shield Design Confirmation Experiment was performed at the Oak Ridge National Laboratory (ORNL) Tower Shielding Facility (TSF).[3] The experiment has as its main purpose the verification of methods used in the analysis of the GCFR grid-plate shielding design. Toward that end, the experiment was designed to verify the ability of methods used in the analysis of the GCFR shield design to calculate (1) axial neutron streaming in the GCFR core and axial blanket for a range of fuel-pin and subassembly spacings, (2) the magnitude and the location of the peak fast-neutron exposure to the grid-plate, and (3) the angular and energy distribution of the neutrons leaving the top of the grid plate and entering the upper plenum. Having accomplished the three objectives, the grid-plate shield design itself would be confirmed.

The experimental configurations were designed to provide a reasonable mockup of the GCFR design from the reactor core through the grid plate. The core was modelled by seven fuel-pin subassemblies which were surrounded by steel-lined concrete in order to have enough neutron reflection to simulate a semi-infinite fuel-pin array. The configurations were designed

---

*Research sponsored by the Division of Reactor Research and Technology of the Department of Energy under contract with Union Carbide Corp.

with a concrete shadow shield between the Tower Shielding Reactor (TSR) and the fuel pins so that the TSR neutron beam was scattered onto the fuel pins. This assured that the dominant neutron source for subsequent additions to the core configurations emanated from the fuel pins. The grid-plate shields were nearly prototypic of those for the GCFR design. The grid-plate thickness and the grid-plate penetrations were also based on GCFR design specifications.

Measurements were taken behind the configurations using fast-neutron spectrometers (NE-213 and hydrogen counter) and integral detectors (the Hornyak button and Bonner balls). The spectrometers and Bonner ball detectors provided data for absolute comparisons with the measurements. The Hornyak button, on the other hand, provided data for comparisons requiring high spatial resolution.

The calculations were performed using the discrete ordinates method on two-dimensional models of the configurations and using the Monte Carlo method on near-exact three-dimensional models. The results showed that the calculations agreed to within 20% with the measurements close behind the fuel pins and the grid-plate shields, while they agreed to within 60% close behind the grid plate. It was demonstrated that better agreement could be achieved through usage of a refined radial space mesh in the fuel-pin region of the calculational model. The peak fast-neutron flux measured behind the grid-plate shields in the absence of the grid plate was calculated to within 5%, well within the 10% uncertainty in the measurements. The measured and calculated results tend to indicate that the location of peak exposure to the grid plate is at the center of the gap between subassemblies. However, the presence of the grid plate could shift the location. The calculation with the grid plate present still showed the peak to be at the center of the subassembly gap. The measurements showed a maximum peak-to-minimum fast-neutron exposure ratio of 1.5, while the calculations showed a maximum ratio of 1.3. The flux-peaking problems in the grid plate are not serious.

The methods proved adequate for calculating axial neutron streaming within the GCFR core and axial blanket. Calculated results close behind the fuel pins generally agree with the measured results within 6%. The calculated results showed that the neutron leakage and all detector

responses varied by less than 5% when the interassembly gap width was changed from 0.318 cm to 1.27 cm. The measured 5-in. Bonner ball count rate and the Hornyak button response respectively indicate a difference of 8% in the total flux and 28% in the $E > 1.0$ MeV flux when the gap width is likewise varied. The 28% difference in the fast fluxes for the two gap widths does not cause concern because measurements taken about 2 cm from the end of the fuel pins showed less than a 5% difference on the centerline and about 8% behind the interassembly gap. These percentage differences are comparable to those calculated at 30.5 cm behind the fuel pins. The calculation may have some problems with the gap between the liner and the subassemblies (peripheral gap) when the subassemblies are spaced 0.318 cm apart. The peripheral gap is then 1.59 cm compared to 0.635 cm when the subassemblies are spaced 1.27 cm apart.

The effect of fuel-pin spacing on neutron streaming in the fuel-pin array was determined by comparing neutron leakages from heterogeneous and homogeneous calculations of a particular configuration. The streaming effect was found to be 9% to 11% for subassembly void fractions between 44.5% and 60.2%. Such increases in neutron leakage from the GCFR core were found to require about a 0.25% increase in the GCFR fissile inventory calculated with a homogeneous core model.

The methods also proved adequate for calculating the peak fast-neutron exposure to the grid plate. As mentioned before, the results were well within the 10% uncertainty of the measurements. The measured peak fast-neutron exposures to the grid plate were examined and found to increase nonlinearly with increasing gap width. For example, peak exposures were in the ratio of 1.55:1.15:1.0 for gap widths of 1.27, 0.635, and 0.3175 cm respectively. While there was a 28% difference in the measured Hornyak button response behind the fuel pins for subassembly gap sizes of 0.635 and 1.27 cm, there was a 55% difference observed behind the grid-plate shield. The peak-to-minimum fast-neutron exposure ratio was found to increase nonlinearly with increasing gap width.

The methods were somewhat lacking in their abilities to calculate the angular and energy distribution of neutrons leaking from the top of the grid plate. The Monte Carlo method did well in calculating the integral detector responses 305 cm behind the grid plate but underpredicted

results close behind the grid plate. The discrete ordinates results were sensitive to the quadrature used in the calculation. The highly biased 150-angle quadrature, used in most of the experiment calculations, gave results which were factors of 1.5 to 2.2 times the measured results. Part of the overprediction may have been due to a factor of 1.5 overprediction in the fluxes 305 cm behind the fuel pins. This translates to an overprediction in the forward-peaked angular fluxes. The forward-peaked angular fluxes from the fuel pins became more important as the source was collimated by the holes in the grid-plate shields and the grid plate. Thus the factor of 1.5 overprediction was propagated from the core through the grid plate. The calculated energy spectrum was reasonably close to the measured spectrum except for the normalization. A lower order S_{10} symmetric quadrature gave results which underpredicted fluxes close behind the grid plate by factors of 4.0 to 12.0. It was estimated that this quadrature, when used in design calculations, may underpredict fluxes in the GCFR upper plenum by factors of 2.5 to 4.0. In the past the upper axial shield design has met constraints with a margin sufficient to allow for the application of such multiplicative factors to the calculated radiation levels.

In conclusion, the calculations were able to predict radiation levels at the important positions within the GCFR shield design. In particular, the flux leaving the fuel-pin region and the peak fast-neutron exposure to the grid plate were calculated within the 10% measurement uncertainty. Streaming effects due to subassembly gap width were found to have a large effect on the peak fast-neutron exposure to the grid plate. Finally, it was determined that discrete ordinates calculations of neutron transport through the grid plate were sensitive to the quadrature. It was estimated that a quadrature frequently used in past design calculations could at worst be underestimating neutron fluxes in the GCFR upper plenum by factors of 2.5 to 4.0. The factor of 2.0 overprediction obtained using the biased quadrature, is probably an upper bound to the uncertainty in the calculations of the neutron leakage from the GCFR grid plate.

The analysis of this experiment has followed recommended practices for the implementation of required DOE and/or other Quality Assurance Standards. By official agreement, the GCFR program follows ANSI N45.2.

References

1. General Atomic Company Project Staff, "300 MW(e) Gas Cooled Fast Breeder Reactor Demonstration Plant," GA-A-13045, General Atomic Company (1974).

2. R. G. Perkins and R. J. Cerbone, "Physics Design of the 300-MW(e) Gas-Cooled Fast Breeder Reactor Demonstration Plant Grid Plate Shielding," General Atomic Company Report GA-A14124 (September 1976).

3. F. J. Muckenthaler, J. L. Hull, and J. J. Manning, "The GCFR Grid Plate Shield Design Confirmation Experiment," ORNL/TM-6580 (January 1979).

1.0 INTRODUCTION

The major support for the core of the 300-MW(e) Gas-Cooled Fast Breeder Reactor (GCFR) demonstration plant[1] comes from the GCFR grid plate. The grid plate is intended to be a lifetime component and as such must maintain its structural integrity throughout the plant lifetime.[2] Since exposure to a sufficiently high fast-neutron fluence can significantly change the mechanical properties of the grid plate, it is necessary that the fast-neutron fluence be limited to an acceptable level through the addition of shielding at strategic locations. The determination of the neutron-flux levels and the adequacy of the shielding generally rests with calculations. The calculations, however, have been subject to uncertainties which, in systems involving radiation transmission through thick shields, could be relatively large (a factor of two or greater). To determine the degree of uncertainty in the calculated neutron fluence at the GCFR grid plate and to assess the adequacy of the grid-plate shield, the GCFR Grid-Plate Shield Design Confirmation Experiment[3] was performed at the Oak Ridge National Laboratory (ORNL) Tower Shielding Facility (TSF). The chief objective of the experiment was the verification of methods used in the analysis of the GCFR shield design. In particular, emphasis was placed on verifying the ability of the methods to predict (1) the energy and angular distribution of neutrons leaving the axial blanket (i.e., the ability to calculate neutron streaming in pin geometry), (2) the maximum fast-neutron exposure to the grid plate as well as the location of and the energy spectrum at the point of maximum exposure, and (3) the energy and angular distribution of neutrons leaving the top of the grid plate. The ability to calculate with a certain precision neutron transport in the prototypic experimental configurations would indicate an ability to calculate neutron transport within the GCFR design with a similar precision.

The experiment covered a range of design options by the inclusion of a variable fuel-pin pitch and subassembly pitch in the experimental program plan. Design calculations have shown variations in fuel-pin and subassembly pitch to have significant effects on axial neutron streaming.

BLANK PAGE

By covering a large portion of the range of fuel-pin and subassembly pitches considered in the design, the experiment bracketed the effects of streaming for the most likely design parameters.

This report describes the results of the analysis of the experiment and presents some implications for the GCFR design.

2.0 EXPERIMENTAL CONFIGURATIONS

The experimental program plan (EPP) is included in Appendix A. Sections II through VI and their associated subsections (i.e., A, B, C, etc.) give brief descriptions of the various configurations. The experimental configurations described in Sections VII and VIII were designed to give a direct measurement of the streaming effect for rod or pin arrays by comparing results from the heterogeneous configuration with those from the equivalent homogeneous configuration. All of the configurations were surrounded by steel-lined concrete. Descriptions of configurations II-VI are presented in Table 1 and in the following sections.

2.1. Internal Components

The experimental configurations have four basic internal components: (1) the fuel-pin subassembly, (2) the hexagonal grid-plate shield, (3) the cylindrical grid-plate shield, and (4) the grid plate. Figure 1 shows the fuel-pin subassembly. Each is about 122 cm long and contains either 91 or 127 1.27-cm-diam fuel pins. The subassemblies containing the 127 pins contained spacers so that the pins could be spaced at either 1.27 cm, 0.635 cm, or 0.3175 cm apart. The only spacing for the subassemblies containing 91 pins was 1.27 cm.

Figure 2 shows the hexagonal grid-plate shield. The external dimensions of the shield closely approximate those of the GCFR moderate pressure drop design (220 kPa). The B_4C density (average 76.7% theoretical density) and the steel are different from design specifications, but the preanalysis showed the shield design for the experiment to be essentially equivalent to that for the GCFR demonstration plant as far as neutron transport and shielding effectiveness are concerned. The cylindrical grid-plate shield is shown in Fig. 3. Again the B_4C density and the steel are different from design specifications. But by the previous

Table 1. A Description of the GCFR Grid Plate Shield Experiment Configurations*

Configuration	Description
II.A	Empty cavity hidden by concrete shadow shield and surrounded by steel-lined concrete
II.B	II.A plus seven subassemblies spaced 1.27 cm apart and containing 127 fuel pins per subassembly
II.C	II.B plus steel-lined concrete section for grid-plate shields
II.D	II.C plus seven grid-plate shield subassemblies spaced 1.27 cm apart
II.E	II.D plus a 61-cm-thick stack of iron plates located 15.24 cm from the grid-plate shields
II.F	II.D followed by the prototypic grid-plate mockup
III.A	II.A plus seven subassemblies spaced 0.635 cm apart and containing 127 fuel pins per subassembly
III.B	III.A plus seven grid-plate shield subassemblies spaced 0.635 cm apart
III.C	III.B plus a 61-cm-thick stack of iron plates located 15.24 cm from the grid-plate shields
IV A	II.A plus seven subassemblies spaced 1.27 cm apart and containing 91 fuel pins per subassembly
IV.B	IV.A plus seven grid-plate shield subassemblies spaced 1.27 cm apart
IV.C	IV.B plus a 61-cm-thick stack of iron plates located 15.24 cm from the grid-plate shields
V.A	IV.A minus seven fuel pins from the center of the central fuel subassembly
V.B	IV.B minus seven fuel pins from the center of the central fuel subassembly
VI.A	II.A plus seven subassemblies spaced 0.318 cm apart and containing 127 fuel pins per subassembly
VI.B	VI.A plus seven grid-plate shield subassemblies spaced 0.318 cm apart

*Note that all components--the fuel pin subassemblies, the grid-plate shield subassemblies, and the grid plate--are surrounded by concrete in the radial direction.

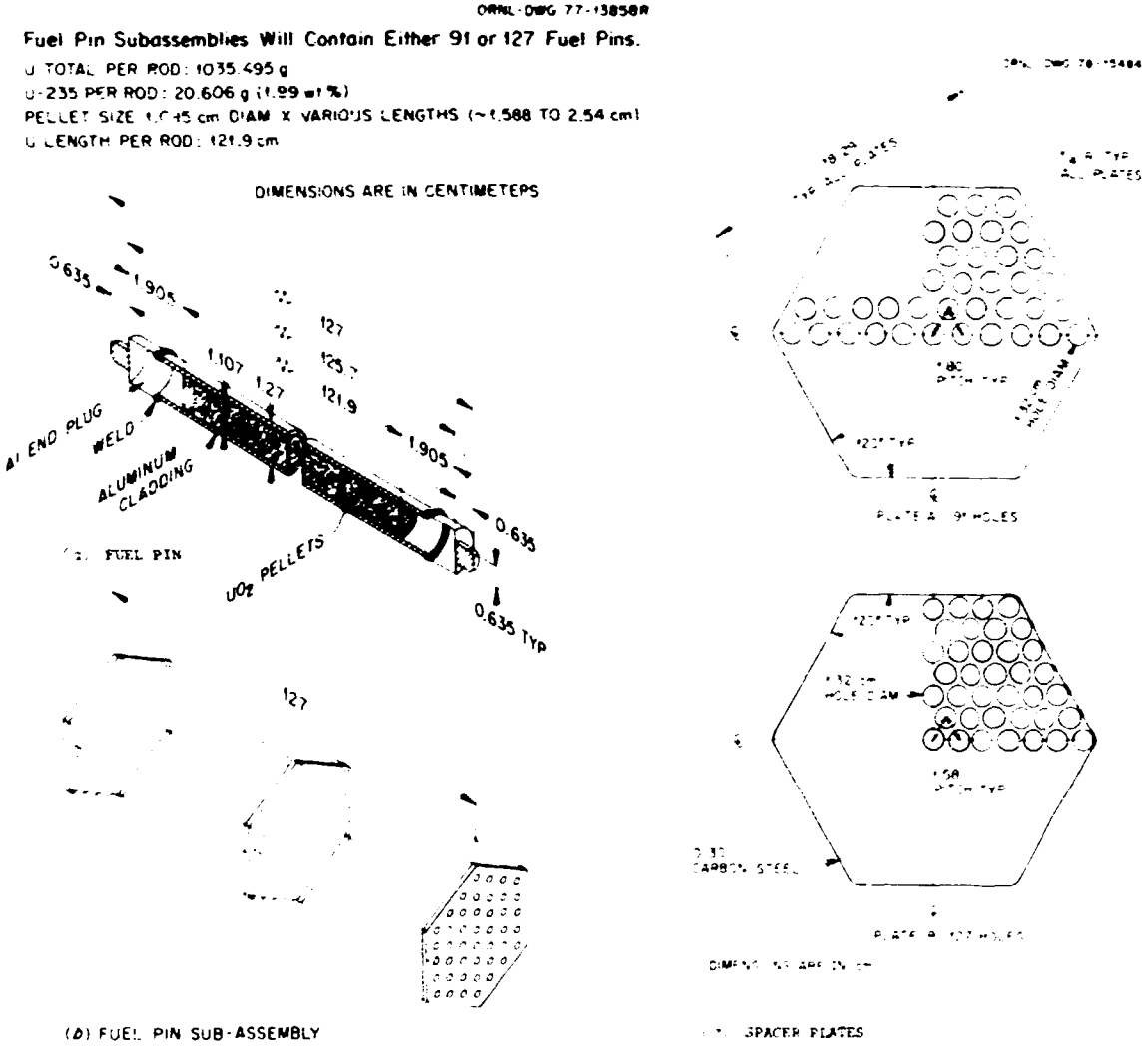

Fig. 1. Details of the Components of the Fuel-Pin Subassemblies for the GCFR Grid-Plate Experiment.

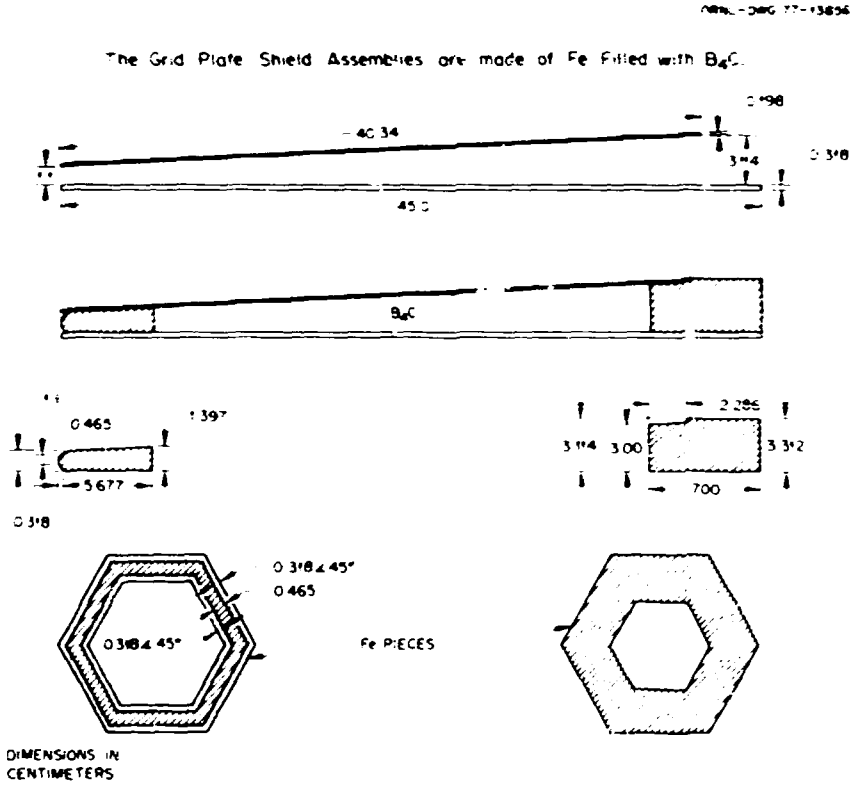

Fig. 2 Details of the GCFR Grid-Plate Shield Subassembly as Used in the GCFR Grid-Plate Shield Experiment.

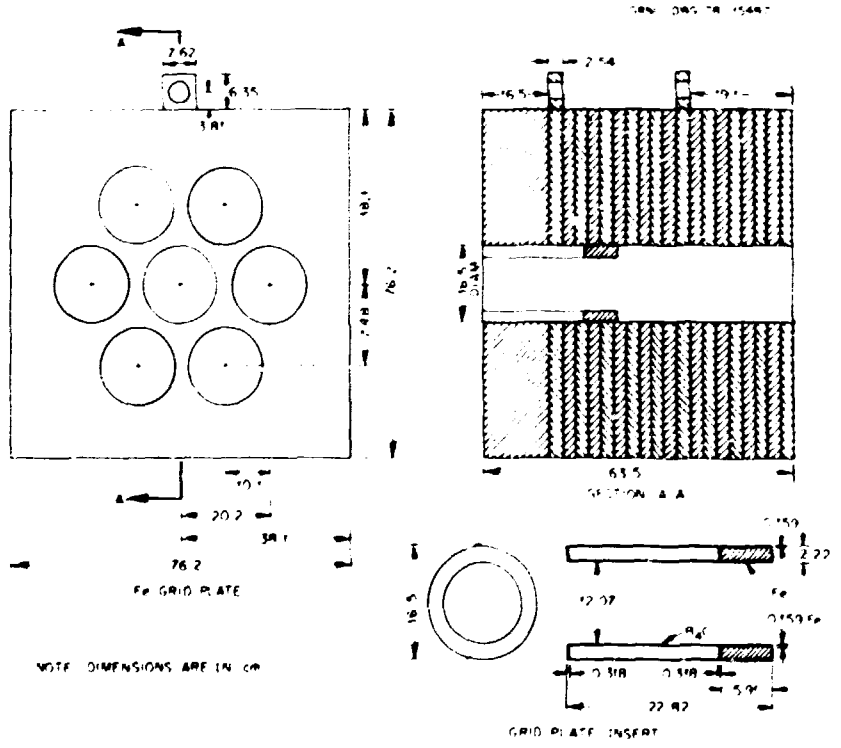

Fig. 3. Details of the Prototypic Grid Plate and Cylindrical Grid-Plate Shield Insert as Used in the GCFR Grid-Plate Shield Experiment.

argument, the shield effectiveness is believed to be nearly equivalent to that of the design shield. The grid plate is also shown in Fig. 3.

2.2. Basic Configurations -- II.A

The basic configuration, which is a part of all configurations, is the steel-lined concrete structure shown in Fig. 4. Two steel liners form a cylindrical annulus down which neutrons stream from the Tower Shielding Reactor (TSR) before they are scattered from the concrete onto the fuel pins. An 18-sided, 122-cm-long, 0.95-cm-thick steel liner supports the shadow shield and forms the cavity into which the fuel subassemblies are inserted. The shadow shield prevents TSR neutrons that would stream between the pins with few collisions from being the dominant contributors to detector responses behind the configuration. The main source is directed around the shadow shield and scatters in directions which are nearly perpendicular to the pins.

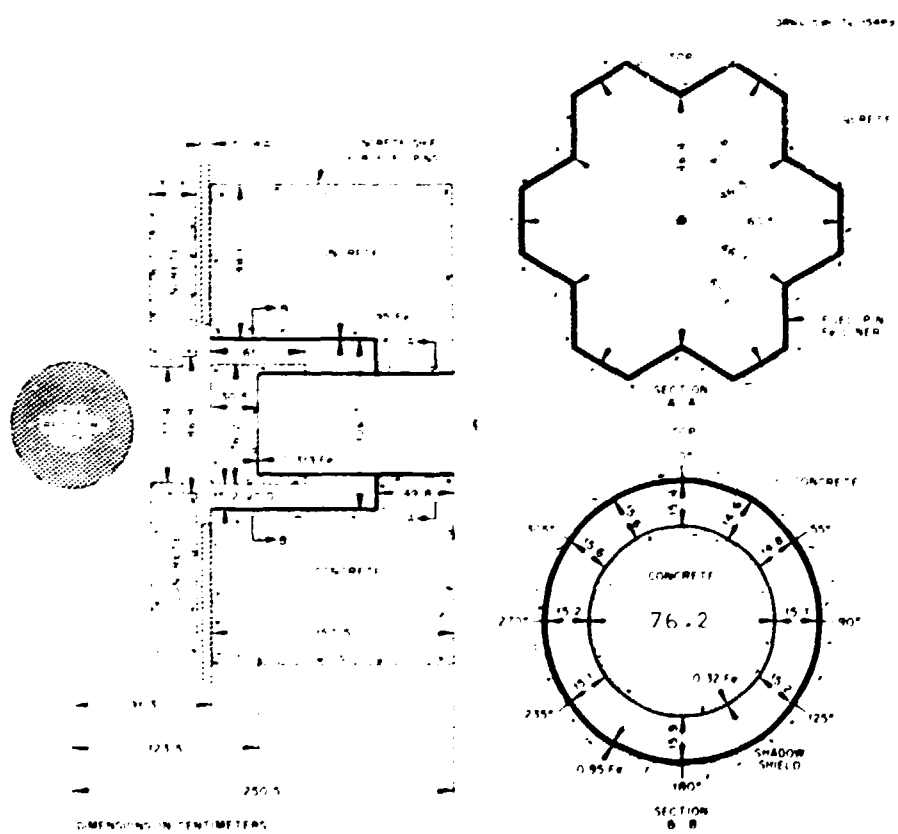

Fig. 4. The Basic GCFR Grid-Plate Shield Experiment Configuration II.A with Empty Core Cavity.

2.3. Other Configurations II

Add seven fuel subassemblies spaced 1.27 cm apart and containing 127 fuel pins per subassembly to Configuration II.A and one gets Configuration II.B as shown in Fig. 5. Configuration II.C is formed by addition of the next section of concrete with empty cavity to Configuration II.B as shown in Fig. 6. Next the grid-plate shield section with shields spaced 1.27 cm apart is added to Configuration II.C to form Configuration II.D as shown in Fig. 7. Configuration II.E in Fig. 8 has a 61-cm-thick stack of steel plates 15.24 cm from the end of Configuration II.D. Figure 9 shows Configuration II.F with a 63.5-cm-thick stack of steel plates with seven holes into which the cylindrical grid-plate shields are inserted (see Fig. 3). The cylindrical grid-plate shields are aligned with the hexagonal grid-plate shields of Configuration II.D.

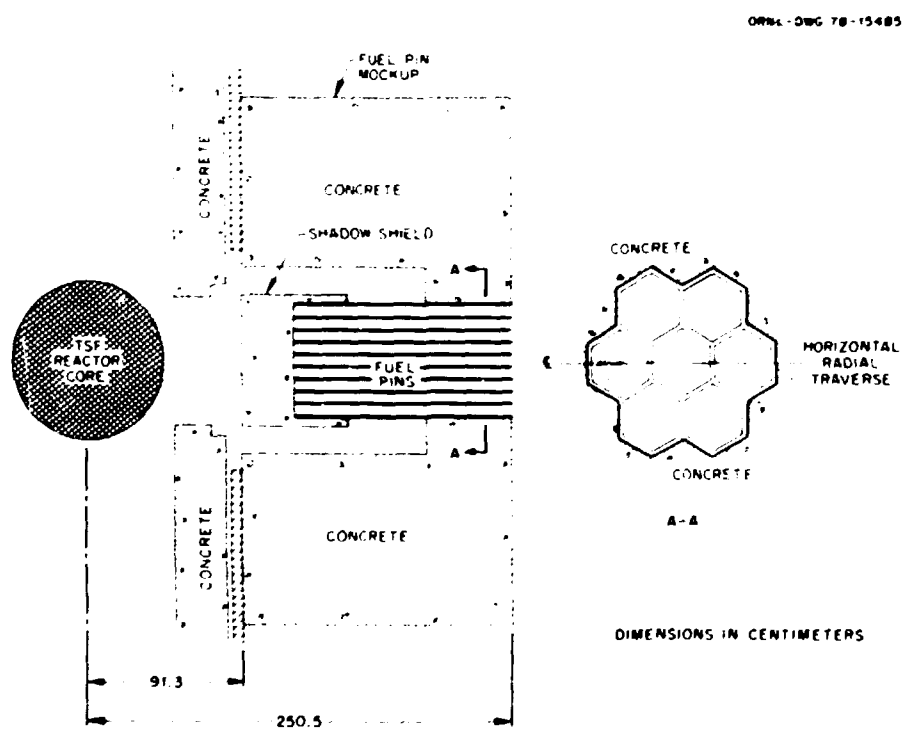

Fig. 5. Sketch of GCFR Grid-Plate Shield Experiment Configurations with Core Loaded with Fuel-Pin Subassemblies (Configurations II.B, III.A, IV.A, V.A, and VI.A).

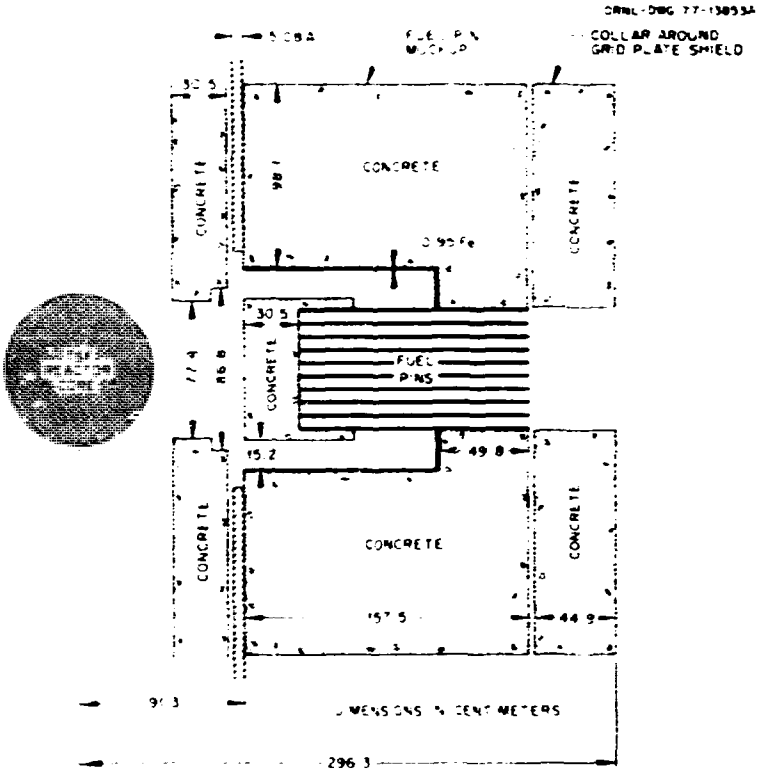

Fig. 6. Sketch of GCFR Grid-Plate Shield Experiment Configuration II.C.

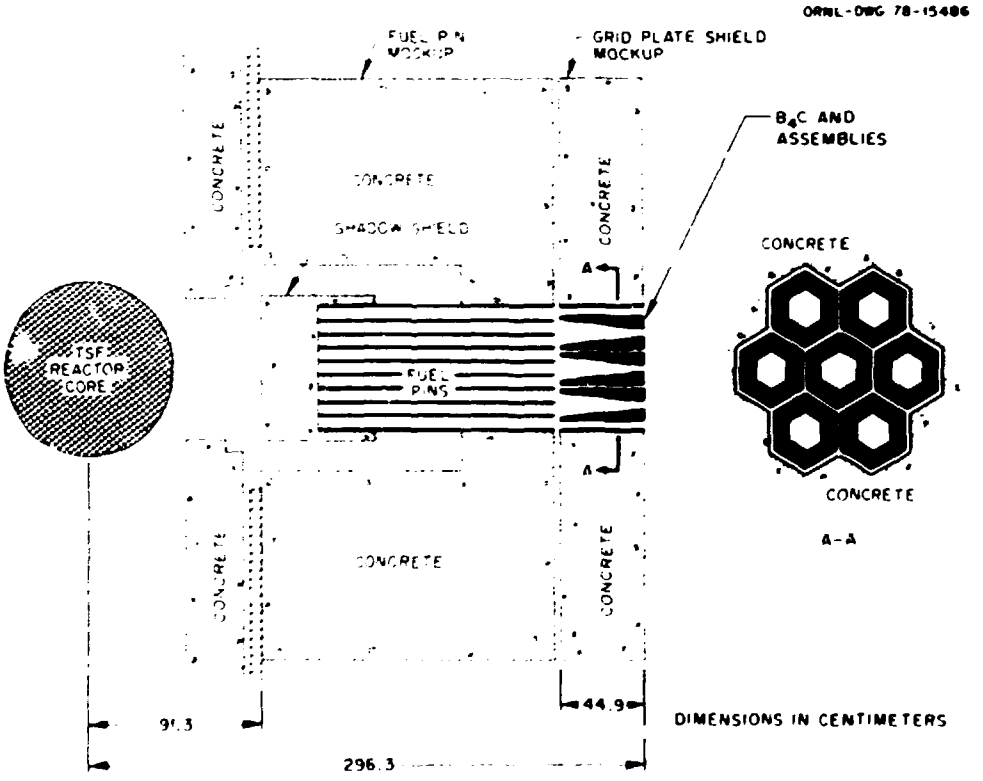

Fig. 7. Sketch of GCFR Grid-Plate Shield Experiment Configurations with Grid-Plate Shield Section Added (Configurations II.D, III.B, IV.B, V.B, and VI.B).

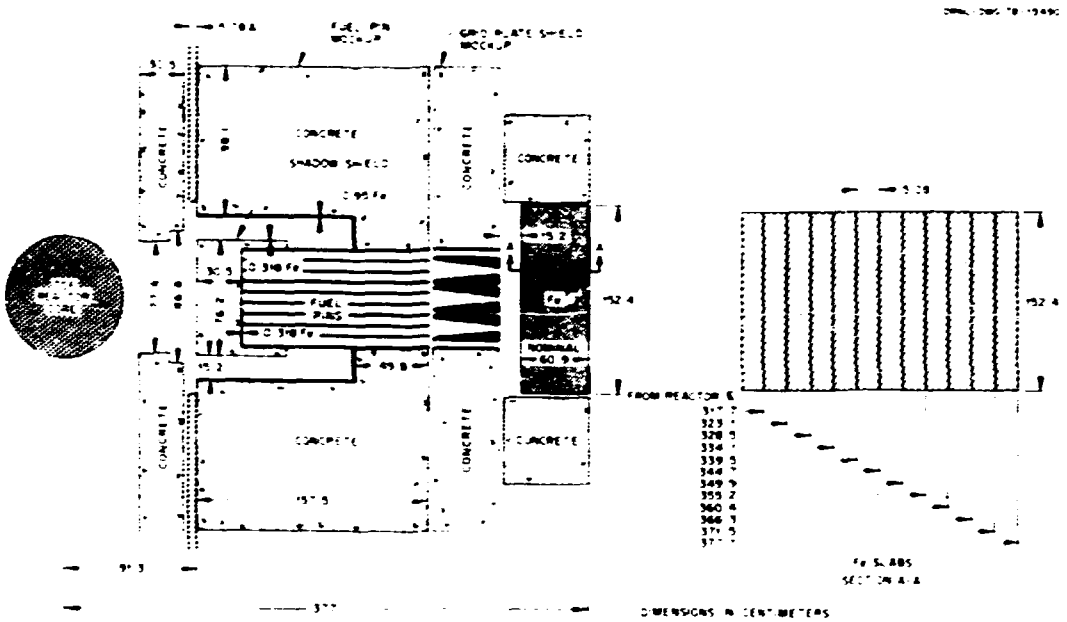

Fig. 8. Sketch of GCFR Grid-Plate Shield Experiment Configurations with the Solid Carbon Steel Plates 15.24 cm Behind the Grid-Plate Shield Section (Configurations II.E, III.C, and IV.C).

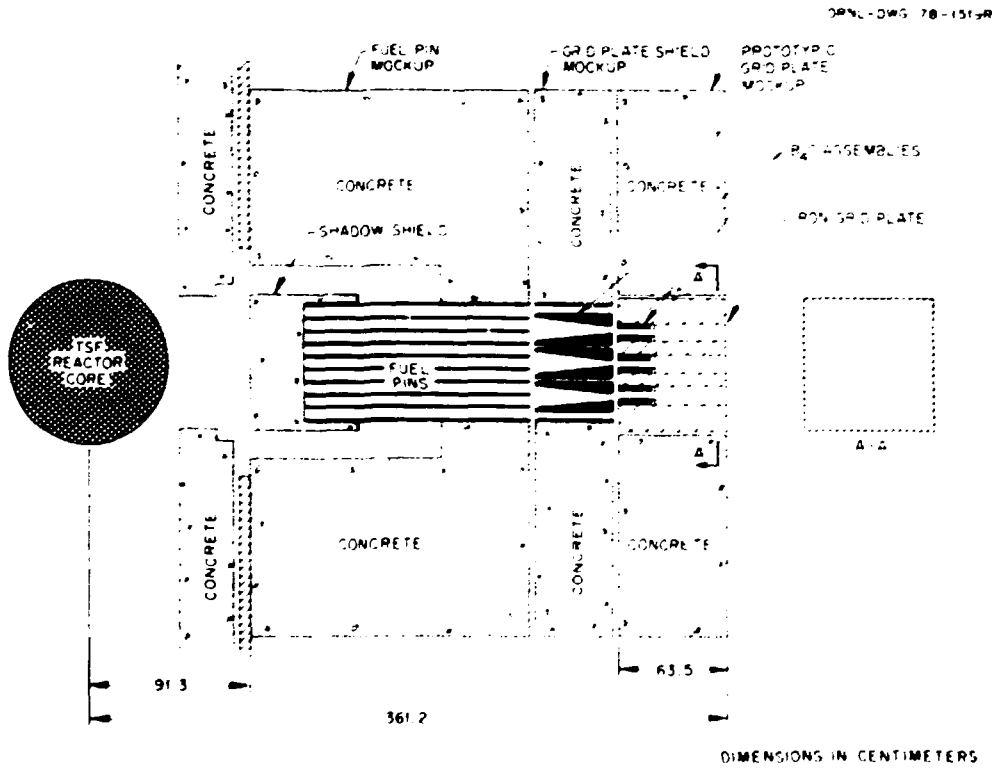

Fig. 9. Sketch of GCFR Grid-Plate Shield Experiment Configuration II.F with the Prototypic Grid Plate.

2.4. Configurations III

Configurations III are characterized by subassemblies which contain 127 fuel pins each and which are spaced 0.635 cm apart. Otherwise they are like Configurations II with III.A corresponding to II.B (Fig. 5); III.B corresponding to II.D (Fig. 7); and III.C to II.E (Fig. 8).

2.5. Configurations IV

Configurations IV are characterized by subassemblies which contain 91 fuel pins each and which are spaced 1.27 cm apart. Otherwise they are also like Configurations II with IV.A corresponding to II.B (Fig. 5); IV.B corresponding to II.D (Fig. 7); and IV.C corresponding to II.E (Fig. 8).

2.6. Configurations V

Configurations V.A and V.B correspond respectively to Configurations IV.A and IV.B with seven fuel pins removed from the center of the central fuel subassembly.

2.7. Configurations VI

Configurations VI are characterized by subassemblies which have 127 fuel pins each and which are spaced 0.3175 cm apart. Configuration VI.A is similar to II.B (Fig. 5) and VI B is similar to II.D (Fig. 7).

3.0 DETECTORS

The EPP in Appendix A lists all detectors with which measurements were to be taken and, where possible, the location of the detector behind a given configuration. Most measurements were taken with the 2-in. Cd-covered and 5-in. Bonner balls and with either a 0.635-cm-diam or a 1.27-cm-diam Hornyak button. Selected measurements were taken with the 2-in. bare, 3-in., 6-in., 8-in., 10-in., and 12-in. Bonner balls and the NE-213 and hydrogen counter spectrum detectors. Response functions in the 51-group structure for the Hornyak button and all Bonner balls except the bare one are given in Appendix B. R. E. Maerker[4] indicates a response-function uncertainty of 5% for the 2-in. Cd-covered and 3-in. Bonner balls; 10% for the 5-in. and 6-in. Bonner balls; 15% for the 8-in. and

10-in. Bonner balls; and 25% for the 12-in. Bonner ball. Major sources for the uncertainty are the upscattering effects in polyethylene and the thickness and density of the polyethylene.

The Bonner ball consists of a 5.08-cm-diam sphere filled with BF_3 gas (boron-enriched to about 96% ^{10}B by weight) at about 0.5 atm, and this sphere may be surrounded with (1) nothing (bare), (2) a 0.038-cm-thick sheet of cadmium (Cd-covered), or (3) a polyethylene spherical shell covered with a 0.038-cm-thick sheet of cadmium. As the polyethylene thickness is increased, more of the fast neutrons will be detected since they will be slowed down in the polyethylene and captured in the BF_3. The 5-in. Bonner ball response function is nearly unity over much of the energy range; hence its recorded count rate is nearly equal to the total neutron flux above 0.4 eV when that flux is expressed in the same time units as the count rate.

The Hornyak button is a thin disk of lucite in which silver-activated zinc sulfide [ZnS(Ag)] phosphor particles have been uniformly suspended. The disk is mounted on a phototube which detects light pulses (scintillations) mainly from neutron-induced proton recoils which interact with the phosphor. A threshold voltage or pulse height setting, set to discriminate against pulses resulting from gamma rays, allows only recoils above a certain energy to be detected. The direct result one gets is a count rate which one would like to convert to some more convenient integral quantity such as neutron flux or dose rate. At the TSF the count rate is converted to an energy deposition rate by means of calibration factors obtained by exposing the Hornyak button in a known neutron field and obtaining a correspondence between count rate and energy deposition rate.

The Hornyak button response function is taken to be a free-in-air tissue kerma since the calibration factor is traditionally determined by relating the energy deposition (in tissue or polyethylene) to a count rate with a known source (Po-Be, Po-B, $^{252}C_f$, etc.).[5] All groups with energies below the bias setting on the measuring equipment have zero response. The main purpose of the Hornyak button was to have a detector with great spatial resolution in order to observe streaming in the gap between fuel subassemblies. Its absolute calibration was difficult.

Part of the problem stems from the fact that the calibration factor was determined at a 6V pulse height setting (PHS), while the actual measurements were made with a 35V PHS to bias out gamma-ray contributions. At the 6V setting, the lowest contributing neutron energy was estimated to be about 100 keV. No estimate could be made for the 35 V setting. Also, the differences in the neutron spectrum between the calibrating source and the neutron spectrum from the configurations could contribute to the discrepancy since Ref. 5 has shown up to 25% difference in the energy deposition in ethylene using Po-Be and Po-B neutron sources.

4.0 NEUTRON SOURCE

The neutron source for the experiment is provided by the Tower Shielding Reactor (TSR-II). In a manner similar to that described by Maerker,[6] the angular flux on the spherical surface of the reactor is projected onto a disk (equivalent two-dimensional source) so that it may be used in two-dimensional transport calculations. The source for the first part of the experimental configurations is a boundary source at the interface of the shadow shield and the TSR iris. Figure 10 shows the two-dimensional model plus the location of the boundary source used to start the calculation and the location of the output boundary source for calculations of the experimental configurations. Note that the output boundary source comes from an interior axial interval so that in succeeding calculations the input source can be an exterior boundary source (bottom boundary in these cases).

The boundary source calculation was performed with the code DOT 3.5 (ref. 7). The code which projects the angular flux from the spherical surface onto the disk is listed in Appendix C. Like Maerker's code,[6] this code computes the angular flux only at the given quadrature direction. The calculation used 51 neutron groups, a 150-direction quadrature set, and P_5 cross sections. The group structure and quadrature are given in Appendix D.

Calculations through the grid-plate shields and the grid plate used boundary sources calculated in preceding portions of the configurations. The FACT[8] code was used to make angular and spatial mesh changes in the source. Since FACT was written for use with the DOT-III code, boundary

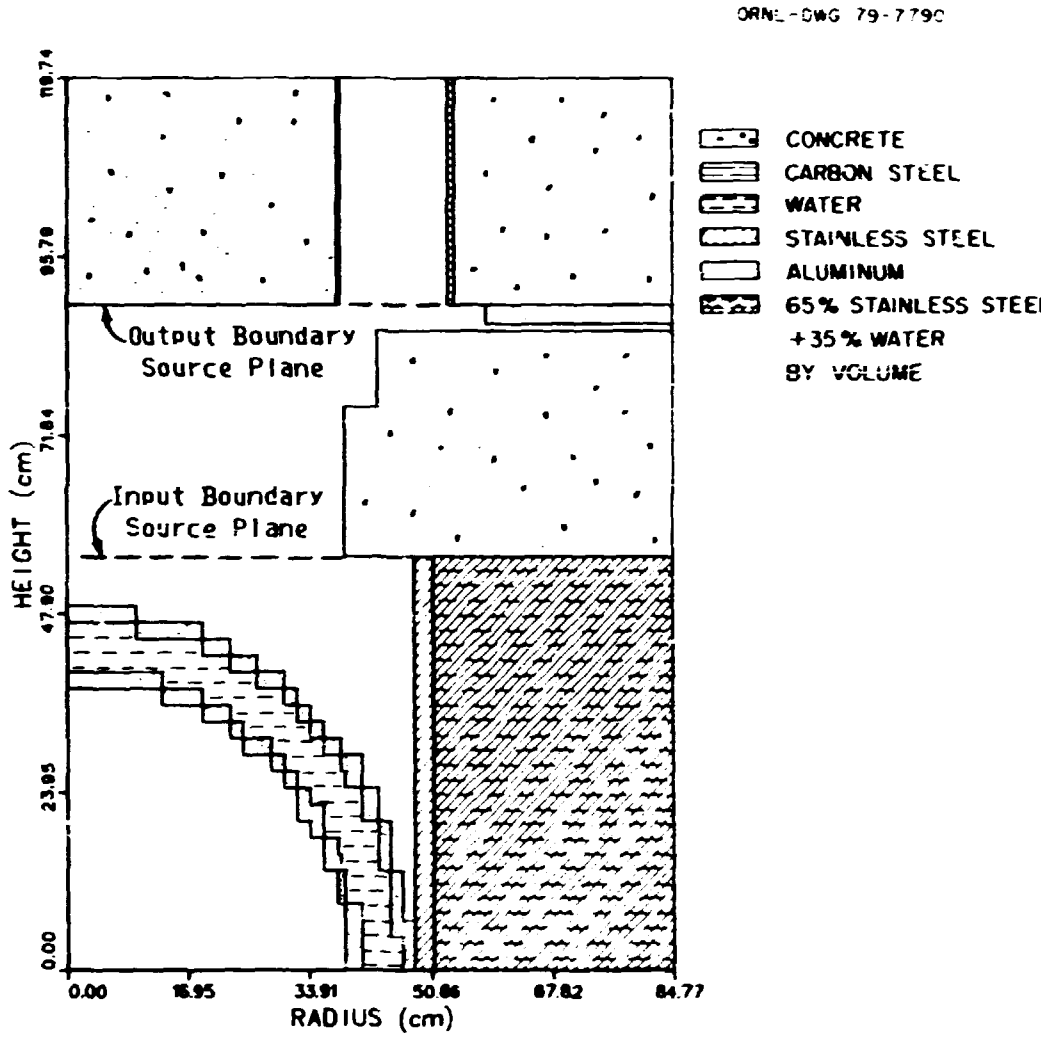

Fig. 10. Plot of the 2-D Geometry Model Used in the Generation of the Source for the Analysis of the GCFR Grid-Plate Shield Experiment

sources output from DOT-IV have to be preprocessed before being input to FACT. Similarly, the output sources from FACT have to be postprocessed before being input to DOT-IV. The processing involves removing header records and leaving only angular fluxes in a positive or negative eta- or mu-direction when the source is input to FACT and adding header records and padding the angular flux arrays with zeroes for a source input to DOT-IV. Codes to perform these operations were user written and were specific to the particular calculation.

5.0. CALCULATIONAL MODELS

5.1. Two-Dimensional Model

Material boundaries of irregular shape occurred mainly in the radial direction. These were cylindricized while conserving the volume contained within the boundary. In the fuel pin region, boundaries were determined by the envelope surrounding the outer six fuel subassemblies and by the interior envelope of these six subassemblies, in both cases excluding the void gap that sets them apart either from the concrete liner or from the central fuel subassembly. The six interior walls were converted to an equivalent cylindrical ring of steel, and the outer 18 were likewise converted. The remaining 12 walls were assumed to be intimately mixed with the fuel pins of the outer six subassemblies. The duct wall of the central subassembly also was converted to an equivalent cylinder. After the establishment of those major boundaries, the fuel-pin regions were subdivided, according to their respective volume fractions, into alternating fuel and void rings with the code RODFRAC shown in Appendix C.

In the shield region, the tapered, hex-shaped shields are converted to equivalent cylindrical, stepped shields with equal shield thickness on either side of the void. The outer six shields in both the shield region and grid-plate region extend the full 360 degrees and thus have narrower shield openings than the actual shield. Figure 11 shows the actual geometry and an equivalent 2-D geometry for the central grid-plate shield. It shows the circular cross section and the steps used to mock up the tapered section of the shield.

The spatial mesh boundaries and major convergence parameters used in the calculation of selected configurations are shown in Appendix E. Also shown are geometry plots generated using the 8$ and 9$ array from the DOT input with a minor modification to the 9$ array of Configuration II.F so that the steel of the grid-plate shield would be separated from the steel of the grid plate. The group structure, quadrature, and fission spectrum, as previously stated, are in Appendix D.

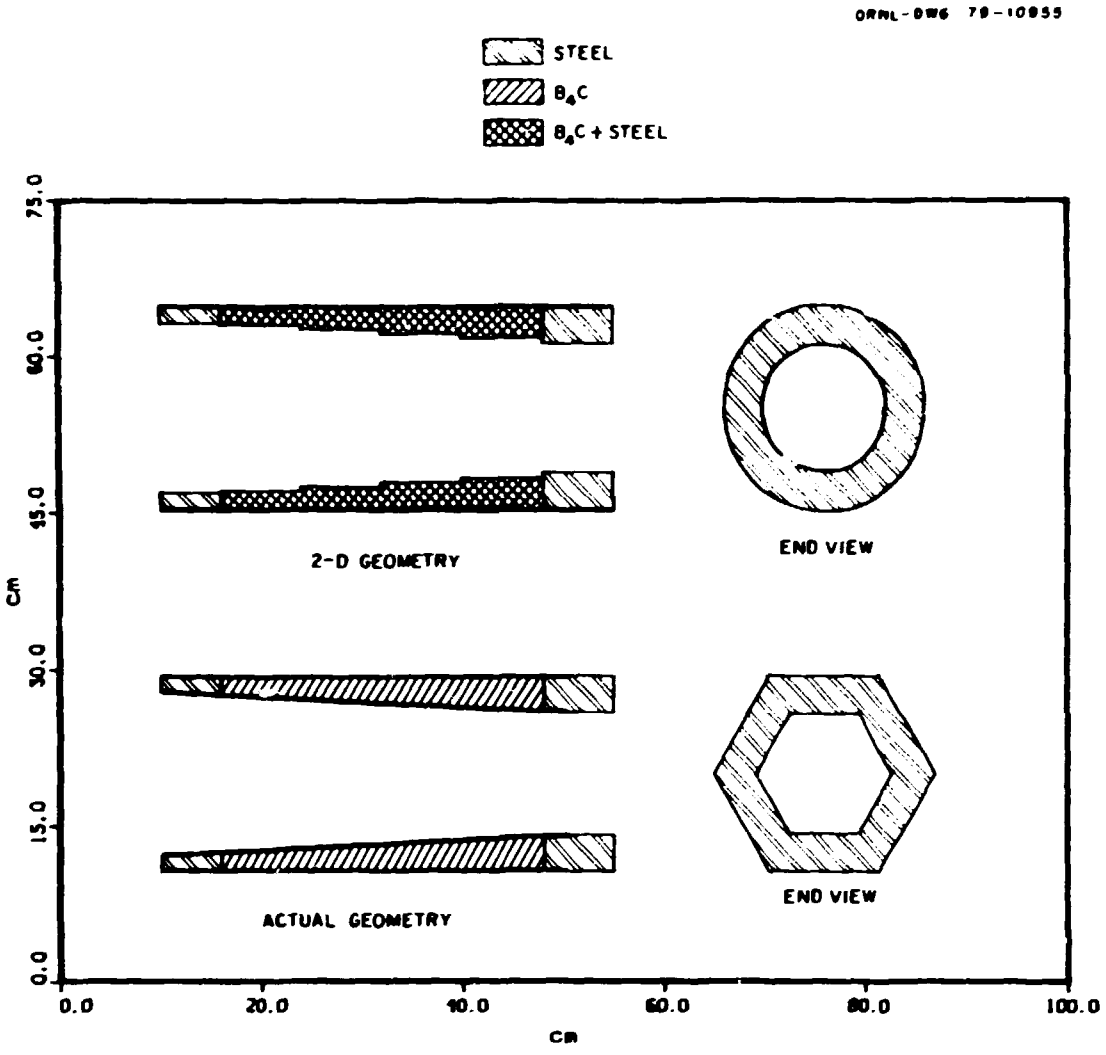

Fig. 11. Illustration of the Actual Grid-Plate Shield Geometry and a Two-Dimensional Approximation to that Geometry. (The tapered portion of the shield is first approximated by stepped hexagons and then converted to stepped cylinders.)

5.2. Three-Dimensional Model

The geometry was mocked up almost exactly with a 1/12th segment of the geometry and the proper reflective boundary conditions. Cladding and fuel regions were included for each fuel pin. A minor approximation was made when the end spacer plates were considered as homogeneous mixtures of carbon steel and aluminum rather than a carbon-steel plate penetrated by aluminum pins. The boundary source impinging on these configurations,

however, remained two-dimensional. This was also thought to be a minor approximation.

6.0. CALCULATIONAL METHODS

6.1. Two-Dimensional Calculations

Calculations in two dimensions were performed using discrete ordinates transport theory. Either discrete ordinates theory or an auxiliary technique was used to compute responses at detectors within the void behind the configurations. In the discrete ordinates method, the energy, space, and direction variables are represented by a finite number of bins or discrete variables for which fluxes are computed. The number of discrete variables is limited by computer storage and computation time considerations. Because of the narrow streaming gaps among the fuel pins, the quadrature is probably the most crucial variable as far as calculating the experiment.

Since the method is two-dimensional in its space and energy variables, one must introduce certain approximations in order to calculate three-dimensional systems. These approximations have to be made starting with the reactor source configuration and going through the experimental configuration. The results should be as good as the approximations made.

The two-dimensional method using cylindrical r-z geometry has the advantage of providing detailed energy, angular, and spatial data at reasonable cost when compared to three-dimensional methods. Localized three-dimensional effects can then be studied using sources from the two-dimensional calculation and only a portion of the geometry.

6.2. Three-Dimensional Calculations

The three-dimensional calculations were exclusively Monte Carlo calculations. These calculations used output from the two-dimensional calculations as starting sources. The Monte Carlo method has the advantage that the geometry can, in theory, be mocked up exactly. In practice, however, only those parts of the geometry to which the desired response is thought to be most sensitive receive such careful consideration.

The method appears to work well in fixed-source-only or fission-source-only problems. However, problems with both fixed and fission

sources appear to have difficulty converging the fission-source distribution, especially when the fission region is a large distance from the fixed source. The three-dimensional calculations reported herein have relied on boundary sources and fission-source distributions supplied by the two-dimensional calculations in order to avoid the aforementioned difficulties.

The particular Monte Carlo method used also has some of the same limitations as the two-dimensional method. The energy structure has been discretized and the scattering angle in collisions has been limited to discrete values based on the truncated cross-section expansion. The elastic scattering energy-loss scattering-angle relationship has been lost with the use of a group energy structure rather than a continuous energy structure. On the other hand, the method was not sought on the basis of a continuous energy and angle treatment. Rather it was chosen for its exact or near-exact treatment of the spatial variable.

While the method relies on sources from the two-dimensional method, it is still able to give an estimate of the effect of the two-dimensional approximations in the geometry on the spatial distribution of the neutron flux within the configuration beyond the source.

7.0. RESULTS

7.1. Configurations II

7.1.1. Configuration II.A

The first calculation performed was for the basic configuration, II.A, with steel-lined concrete surrounding an empty cavity. Because of the way the configuration is designed, this particular calculation appears to be the analysis of neutron streaming down a stepped, plugged, steel-lined concrete duct.

The calculation used 51 neutron groups, P_3 cross-section expansion, and a 150-direction, biased quadrature set.

Two sets of measurements were taken for this configuration: (1) axial traverses along the centerline of the cavity, and (2) radial traverses 30.5 cm behind the configuration. Calculations were performed with the DOT-IV[9] 2-D discrete ordinates code and the MORSE[10] Monte Carlo code. A comparison of calculation with measurement is shown in Fig. 12 for the

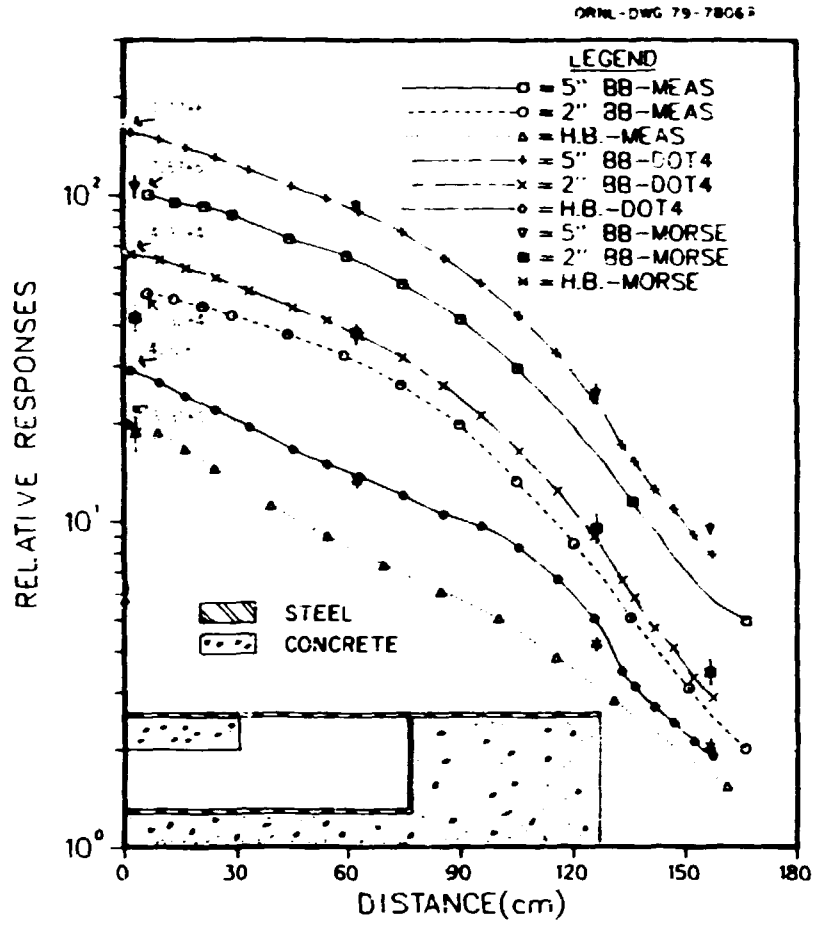

Fig. 12. Relative Measured and Calculated Responses for Axial Traverses Down the Center of the Empty Cavity of GCFR Grid-Plate Shield Experiment Configuration II.A.

axial traverse. Figure 12 shows relative responses for the 1.27-cm-diam Hornyak button and the 2-in. Cd-covered and 5-in. Bonner balls. Also shown are absolute values at the point closest to the shadow shield in units of $ergs \cdot g^{-1} \cdot h^{-1} \cdot W^{-1}$ for the Hornyak button and $counts \cdot min^{-1} \cdot W^{-1}$ for the Bonner balls.

While the shapes of the DOT-IV (or simply DOT) calculated curves agree well with the measured shapes, the calculated absolute values are all higher than the measured values. The Hornyak button results are high by 45%; the 2-in. Cd-covered Bonner ball results are high by 30%; and the 5-in. Bonner ball results are high by 55%. The discrepancy between calculation and measurement, while not excessively large, is higher than the self-imposed criterion of "less than 20% discrepancy" being considered good agreement.

Since the 150-direction set was biased in the forward direction, it was thought that the calculation employing it would have difficulty in transporting neutrons in the outer void ring, through the 90-degree turn into the central cavity and then through another 90-degree turn to either exit or impinge on the shadow shield (see Fig. 4). Consequently, the calculation was redone with a symmetric 96-direction quadrature set. The results were essentially the same as for the 150-direction calculation. Other possible explanations for the discrepancies are to be found in a later section.

The MORSE results are generally in good agreement with the DOT results except near the shadow shield, where they are close to the measured results. This seems to say that the 2D approximation is adequate and the source of the discrepancy lies either in the source or in the concrete composition since MORSE used a DOT-generated source.

The comparisons between calculations and measurement for radial traverses 30.5 cm behind the configuration are shown in Figs. 13, 14, and 15 for the Hornyak button and the 2-in. Cd-covered and 5-in. Bonner balls, respectively. (Note: On these and similar figures, the 2-D and actual geometries have been drawn to scale in abscissa units. The 2-D geometry is the upper one.) The results show the same discrepancies as the axial traverses for the portion of the traverse behind the empty cavity, though there is closer agreement between calculation and measurement behind a portion of the concrete (i.e., about 25 cm of concrete adjacent to the steel liner). Again the MORSE results agree with the DOT results. (Note that in these and succeeding radial traverse plots, the MORSE data point at r = 0 has been plotted away from the axis so that it and its error bar may be seen clearly.)

7.1.2 Configuration II.B

This configuration is designed such that the neutron source emerging from the fuel pins closely approximates that from a GCFR axial blanket at equilibrium. The subassemblies are spaced 1.27 cm apart. The fuel-pin spacing gives this configuration a void fraction per subassembly of 44.5%. This is near the void fraction found in the GCFR high-pressure-drop design (290 kPa). Measurements behind the fuel pins were made for the purpose of defining the source leaving the axial blanket region and entering the

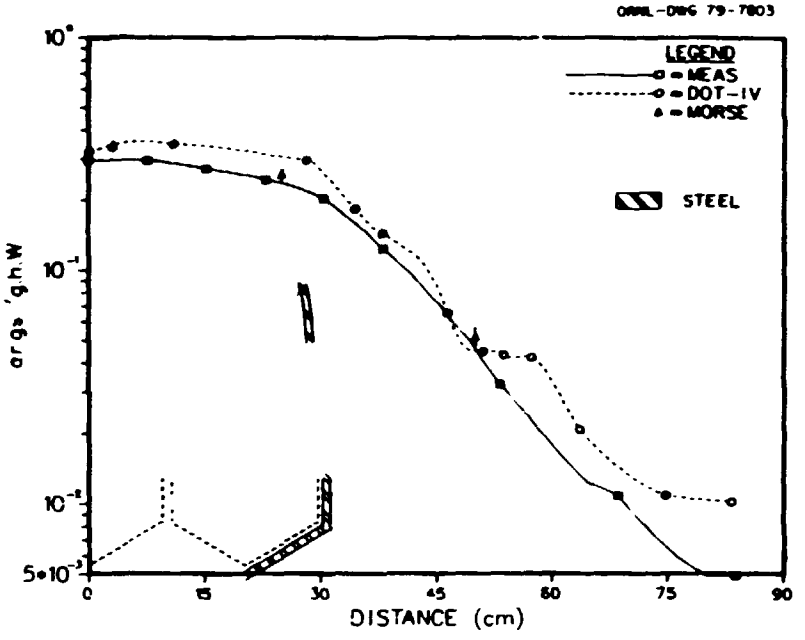

Fig. 13. Comparison of Calculated and Measured Hornyak Button Response for a Radial Traverse 30.5 cm Behind GCFR Grid-Plate Shield Experiment Configuration II.A.

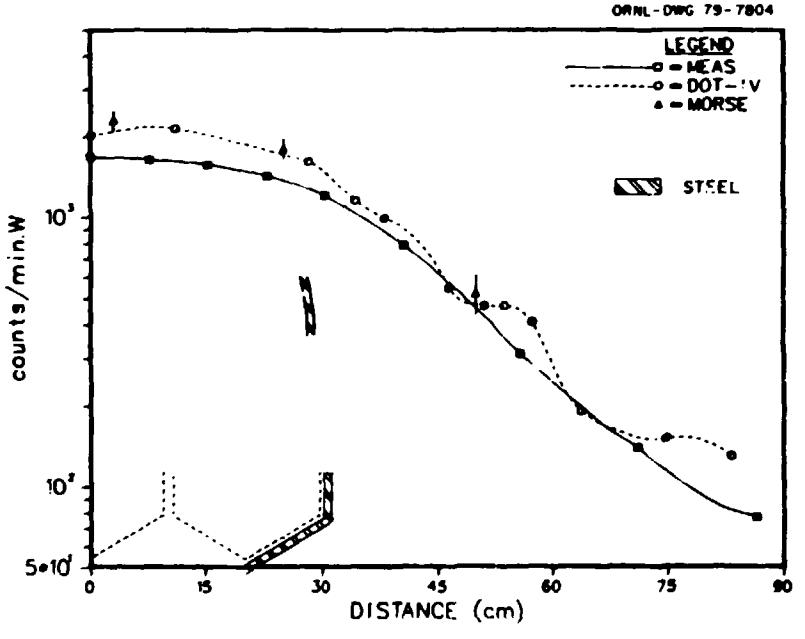

Fig. 14. Comparison of Calculated and Measured 2-in. Cd-Covered Bonner Ball Count Rate for a Radial Traverse 30.5 cm Behind GCFR Grid-Plate Shield Experiment Configuration II.A.

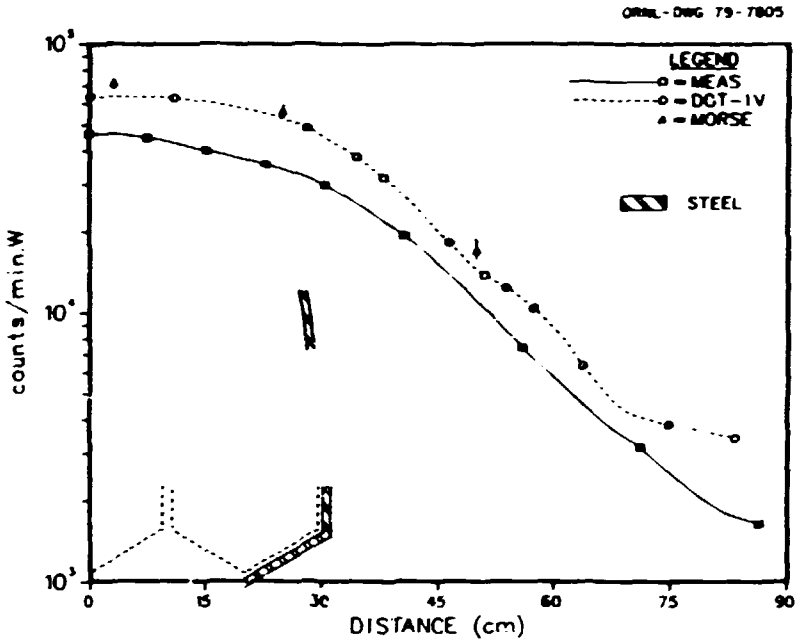

Fig. 15. Comparison of Calculated and Measured 5-in. Bonner Ball Count Rate for a Radial Traverse 30.5 cm Behind GCFR Grid-Plate Shield Experiment Configuration II.A.

grid-plate shield region. Radial traverses were made at 30.5 and 305 cm behind the configuration, and a neutron spectrum measurement was made on the axis 138.1 cm behind the configuration. The location of the latter measurement was determined by the flux level at which the detector could operate rather than being arbitrarily set in the experimental program plan (Appendix A). Bonner ball measurements were also made at 138.1 cm. Comparisons of the results for the radial traverse 30.5 cm behind the configuration are shown in Figs. 16, 17, and 18 for the 1.27-cm-diam Hornyak button and the 2-in. Cd-covered and 5-in. Bonner balls, respectively. The respective comparisons for radial traverses 305 cm behind the configuration are shown in Figs. 19, 20, and 21.

The DOT-calculated 2-in. Cd-covered and 5-in. Bonner ball results at 30.5 cm behind the configuration appear to agree well with the measured results. On the other hand, the DOT/DISKTRAN[11] calculated results at 305 cm behind the configuration are much higher than the measurements. The 1.27-cm-diam Hornyak button results are as much as 87% higher directly behind the pins and 29% to 36% higher behind the concrete. The 2-in. Cd-

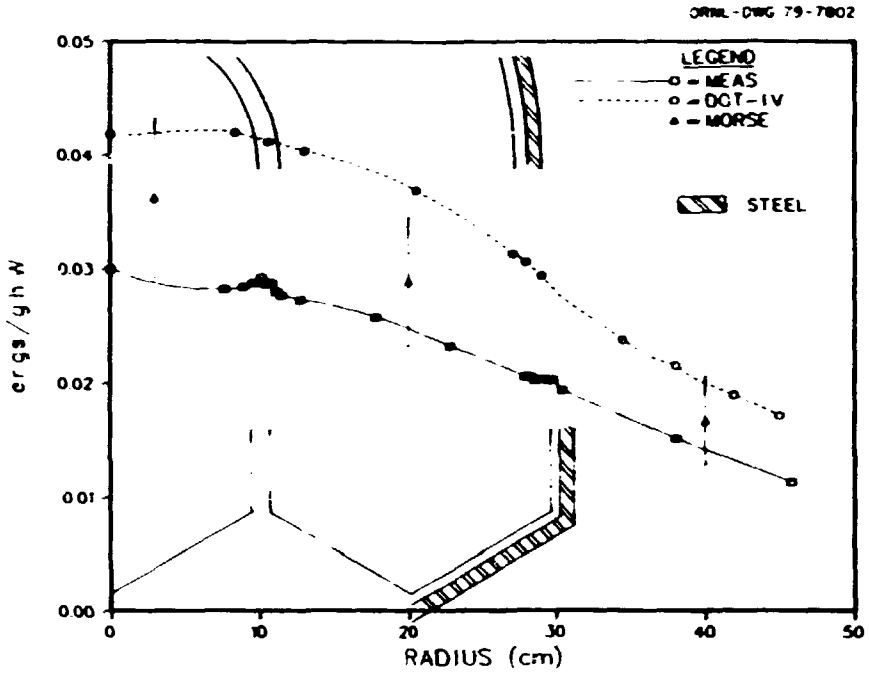

Fig. 16. Comparison of Calculated and Measured Hornyak Button Response for a Radial Traverse 30.5 cm Behind GCFR Grid-Plate Shield Experiment Configuration II.B.

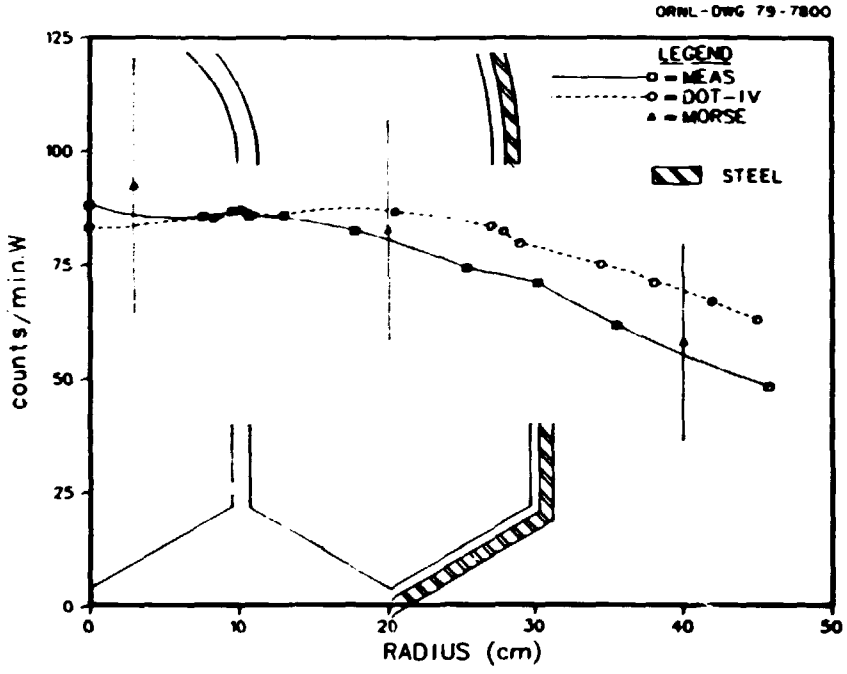

Fig. 17. Comparison of Calculated and Measured 2-in. Cd-Covered Bonner Ball Count Rates for a Radial Traverse 30.5 cm Behind GCFR Grid-Plate Shield Experiment Configuration II.B.

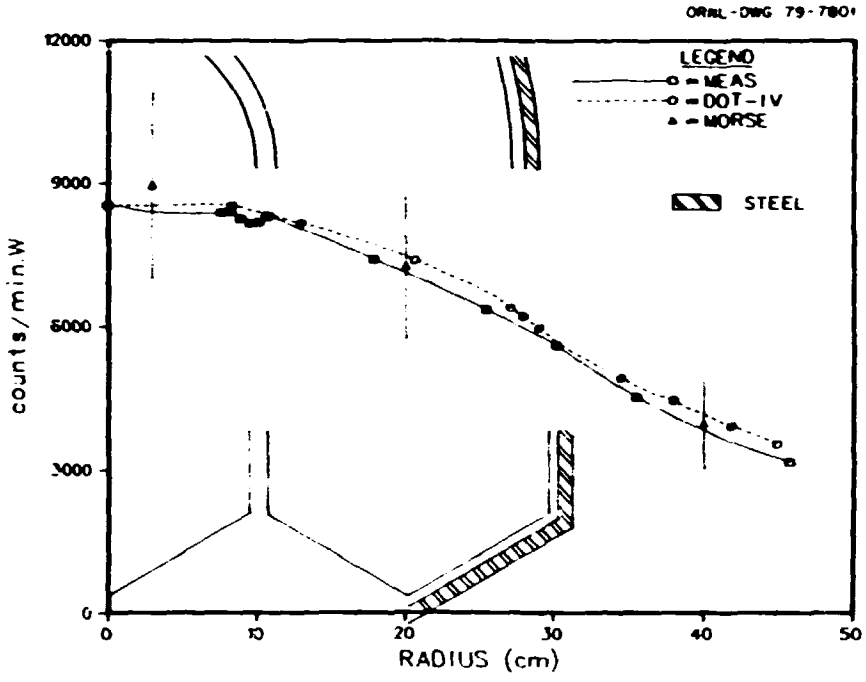

Fig. 18. Comparison of Calculated and Measured 5-in. Bonner Ball Count Rates for a Radial Traverse 30.5 cm Behind GCFR Grid-Plate Shield Experiment Configuration II.B.

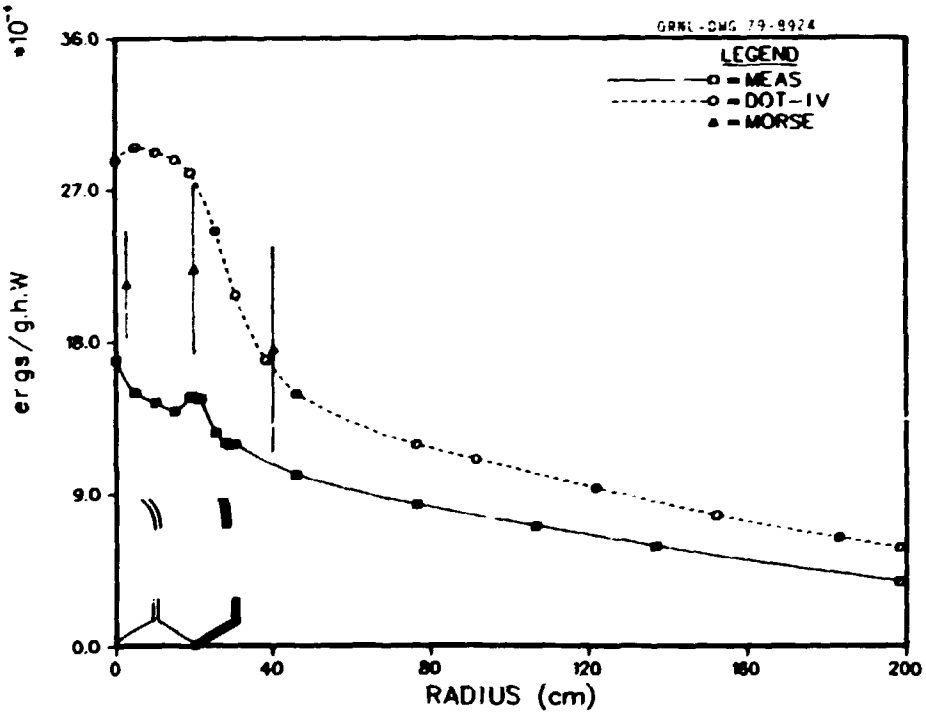

Fig. 19. Comparison of Calculated and Measured Hornyak Button Response for a Radial Traverse 305 cm Behind GCFR Grid-Plate Shield Experiment Configuration II.B.

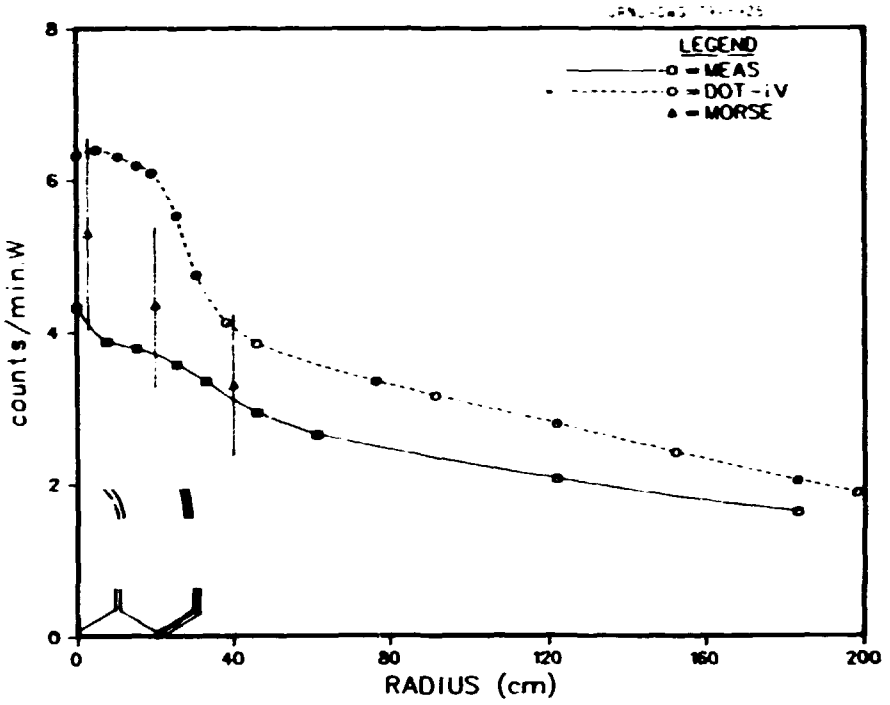

Fig. 20. Comparison of Calculated and Measured 2-in. Cd-Covered Bonner Ball Count Rate for a Radial Traverse 305 cm Behind GCFR Grid-Plate Shield Experiment Configuration II.B.

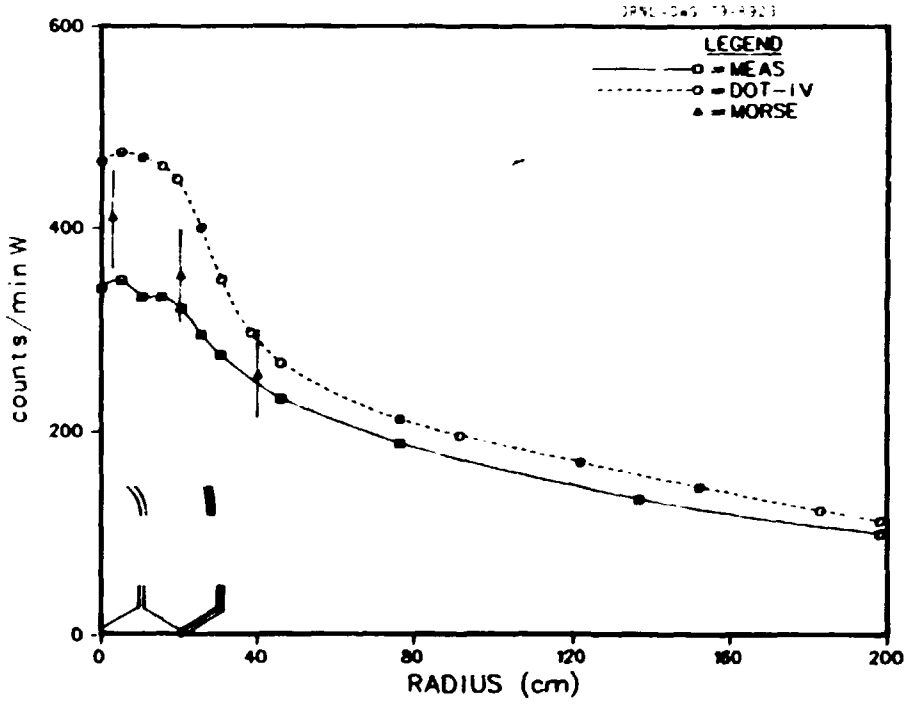

Fig. 21. Comparison of Calculated and Measured 5-in. Bonner Ball Count Rate for a Radial Traverse 305 cm Behind GCFR Grid-Plate Shield Experiment Configuration II.B.

covered Bonner ball results are as much as 63% higher directly behind the pins and 25% to 35% higher behind the concrete. The corresponding numbers for the 5-in. Bonner ball are as much as 42% higher directly behind the fuel pins and 13% to 15% higher behind the concrete. Thus, at 305 cm behind the configuration, the calculated 5-in. Bonner ball results behind the concrete are acceptable, while the results behind the fuel pins and the results for the other two detectors are not acceptable.

The better Monte Carlo calculation for this configuration was actually a combination of two calculations. The first was a fixed-source calculation using the boundary source generated in the DOT calculation. The second was also a fixed-source calculation using a fission source distributed within the fuel pins according to the DOT fission density. Only source positions within the fuel pins were used. The results were combined by multiplying the separate results for a unit source by the total source for each and adding the two results. The Monte Carlo calculation with fission led to results that varied widely according to batch size and the number of batches, even though the total number of histories was nearly the same in the "large batch size" case and in the "large number of batches" case. Besides, a Monte Carlo calculation in which a source is incident on one end of the fuel pins has much difficulty in generating the correct fission distribution within the fuel pins.

Detector responses were calculated at 30.5 and 305 cm behind the configuration at 0, 20, and 40 cm from the centerline of the configuration. The points are plotted, along with the corresponding DOT and measured results, in Figs. 16-21. At 30.5 cm behind the configuration, the statistical mean responses are 18 to 21% higher than the measurements for the Hornyak button, 4 to 7% higher for the 2-in. Cd-covered Bonner ball, and 3 to 5% higher for the 5-in. Bonner ball. The differences are larger at 305 cm behind the configuration. There, the Hornyak button response is higher than measured by 27 to 64% (27% at 0 cm); the 2-in. Cd-covered Bonner ball count rate is higher by 6 to 22% (22% at 0 cm); and the 5-in. Bonner ball count rate is higher by 4 to 21% (21% at 0 cm). Though the statistical uncertainties are large in most cases (20 to 38%), the statistical mean values certainly compare favorably with the measured values

(except, of course, the Hornyak button results 305 cm behind the configuration). The agreement is much better than that achieved with DOT.

The Monte Carlo calculations used a point detector estimation procedure developed especially for geometries which contain certain symmetries and which are mocked up with a repeating segment on which specularly reflective boundaries have been imposed. The good agreement of the Monte Carlo results with the measured results confirms the correctness of the estimation procedure.

The DOT-calculated and the measured neutron spectrum 138.1 cm behind the fuel pins are compared in Fig. 22. The energy range of the NE-213

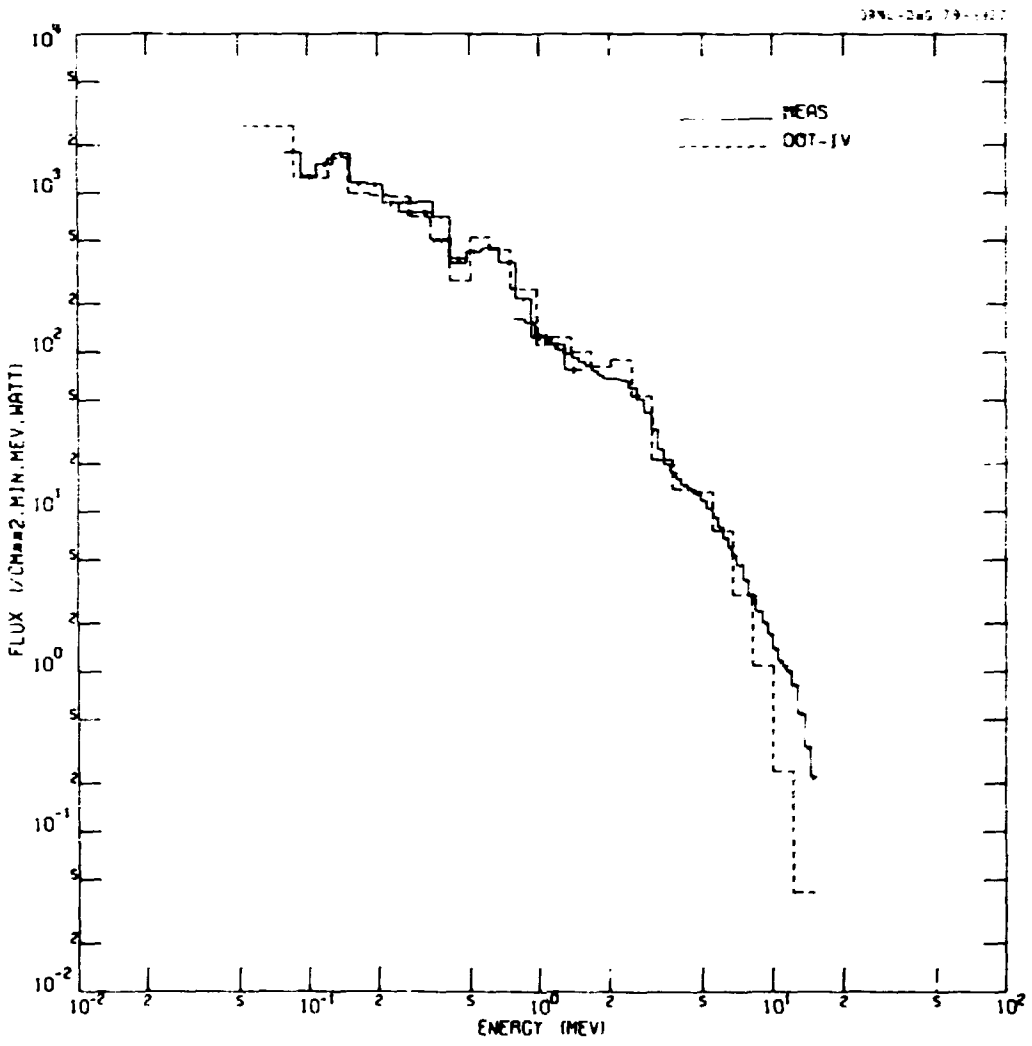

Fig. 22. Comparison of Calculated and Measured Neutron Spectra on the Centerline 138.1 cm Behind the Fuel Pins of GCFR Grid-Plate Shield Experiment Configuration II.B.

part of the spectrum is from 0.8 to 15 MeV. The hydrogen counter spectrum is in three parts, with energies between 0.08 and 1.5 MeV. Good agreement between the calculated (with DOT) and the measured spectra is evident. The measured flux was integrated over energy in the ranges 0.9 - 15 MeV and 0.12 - 15 MeV. Those integrated fluxes and the measured 3-in., 6-in., and 10-in. Bonner ball count rates are compared with the calculated results in Table 2. It is seen that the calculated results agree well with the measured results, particularly the high-energy neutron fluxes. The good agreement here tends to indicate a difficulty in the Hornyak button normalization since it shows disagreement, while the Bonner balls and spectrum detectors show good agreement.

Table 2. Comparison of DOT/DISKTRAN-Calculated and Measured Detector Responses on the Centerline 138.1 cm Behind Configuration II.B

Response Type	Response		C/E
	Calculated	Measured	
Bonner ball (counts/min·W)			
3-in. ball	356	280	1.17
6-in. ball	1470	1270	1.16
10-in. ball	647	600	1.08
Flux (neutrons/min·W)			
E > 0.9 MeV	233	219	1.06
E > 0.12 MeV	656	656	1.00

The question of why such good agreement close in behind Configuration II.B when there was such a large discrepancy in and behind the basic Configuration II.A will be discussed in a later section.

7.1.3. Configuration II.D

This configuration is formed by adding the grid-plate shield section to Configuration II.B. The shields, like the fuel subassemblies, are spaced 1.27 cm apart. The measurements included axial traverses down the center of the central grid-plate shield subassembly and radial traverses close behind the grid-plate shields. The 0.635-cm-diam Hornyak button and the 2-in. Cd-covered Bonner ball were used for these measurements.

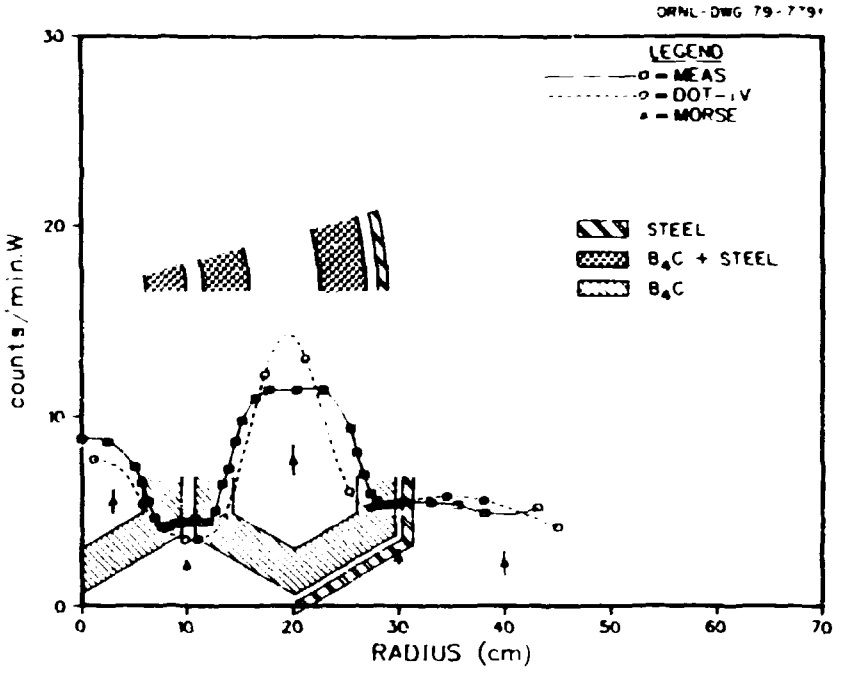

Fig. 26. Comparison of Calculated and Measured 2-in. Cd-Covered Bonner Ball Count Rate for a Radial Traverse 3.18 cm Behind GCFR Grid-Plate Shield Experiment Configuration II.D.

twice the measured values. Again, this is attributed to difficulty in normalizing the Hornyak button response function. Monte Carlo (MORSE) results agree with DOT near the entrance to the shield (a DOT-calculated boundary source is used in the MORSE calculation), but they tail off toward the measurements beyond the shield. While the statistics are good, it is believed that the drop in the MORSE results is due to underprediction. The reason for this belief is illustrated clearly in Fig. 24, where the 2-in. Cd-covered Bonner ball results are shown. The DOT results agree well with the measured results. On the other hand, the MORSE results start out agreeing well, but they underpredict beyond the shield.

The radial traverses were designed to detect the relative differences in the radiation levels behind the B_4C and those behind the interassembly gaps, the goal being to determine which part of the grid plate received the highest fast-neutron exposure. Figures 25 and 26 compare calculated and measured Hornyak button and 2-in. Cd-covered Bonner ball responses, respectively. The small-diameter (0.635 cm) Hornyak button used to obtain the traverse in Fig. 25 was able to determine the relative

peak value over the inner subassembly gap. Again, the calculated results are high due to the difficulty in normalizing the Hornyak button response. The MORSE results are generally in agreement with the DOT results. The DOT-calculated and 2-in. Cd-covered Bonner ball count rates, smoothed to take the ball size into account, agree fairly well with the measured results. Since the holes in the outer six shields were mocked up in a smaller width ring for the two-dimensional geometry, the calculated peak over the outer ring is narrower and higher than the measured peak. The DOT results underestimate over most of the range but not seriously so. MORSE, however, has trouble generating the low-energy fluxes which contribute heavily to the 2-in. Bonner ball count rate. Thus, the results are underestimated.

Centerline measurements were taken at 30.5 and 305 cm behind the configuration. DOT results are compared with the measured results in Table 3. As seen previously, the calculation-to-measurement ratios for the Hornyak button are much higher than those for the Bonner ball count rates. The calculated Bonner ball count rates show good agreement at 30.5 cm and up to 60% overprediction at 305 cm. The 5-in. Bonner ball count rate overprediction is about 15% higher than it was at 305 cm behind the fuel pins, while the overprediction for the 2-in. Cd-covered Bonner ball is smaller.

Table 3. Comparison of DOT/DISKTRAN-Calculated Detector Responses with Measured Values on the Centerline Behind Configuration II-D

Response Type	Distance from Shield (cm)	Response		C/E
		Calculated	Measured	
Hornyak Button (ergs/g•h•W)	30.5	5.94-3*	2.91-3	2.04
	305	1.25-3	5.94-4	2.10
Bonner Ball (counts/min•W)				
2-in. Cd-covered ball	30.5	5.20	4.92	1.06
	305	1.66	1.22	1.36
5-in. ball	30.5	1120	976	1.15
	305	187	118	1.58

*Read: 5.94×10^{-3}.

7.1.4. Configuration II.E

Calculational comparisons with measurements behind configurations similar to II.D have sometimes been poor in the past due to rapid drop-off in the radiation field immediately behind the configuration. To improve such comparisons, measurements have been taken with the detector between the configuration and a reflective medium a prescribed distance behind the configuration. This is part of the philosophy for Configuration II.E, where a 61-cm thick stack of solid steel plates was placed 15.24 cm behind the configuration and 2-in. Cd-covered and 5-in. Bonner ball measurements were made in the intervening void region. Another reason for this configuration was to try to simulate the reflection of the GCFR grid plate and to determine what effect it had on the peak-to-minimum "fast-neutron exposure to the grid plate" ratio.

This configuration was calculated with DOT only. A comparison of the calculated and measured curves is shown in Fig. 27 for the 2-in. Cd-covered Bonner ball and Fig. 28 for the 5-in. Bonner ball. The 2-in.

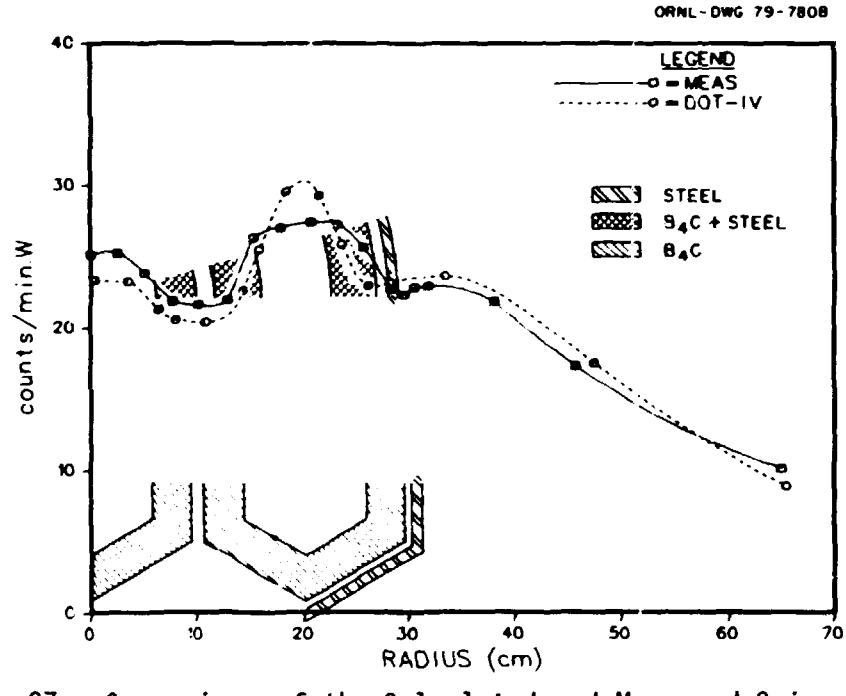

Fig. 27. Comparison of the Calculated and Measured 2-in. Cd-Covered Bonner Ball Count Rate for a Radial Traverse 4.13 cm Behind the Grid-Plate Shields of GCFR Grid-Plate Shield Experiment Configuration II.E.

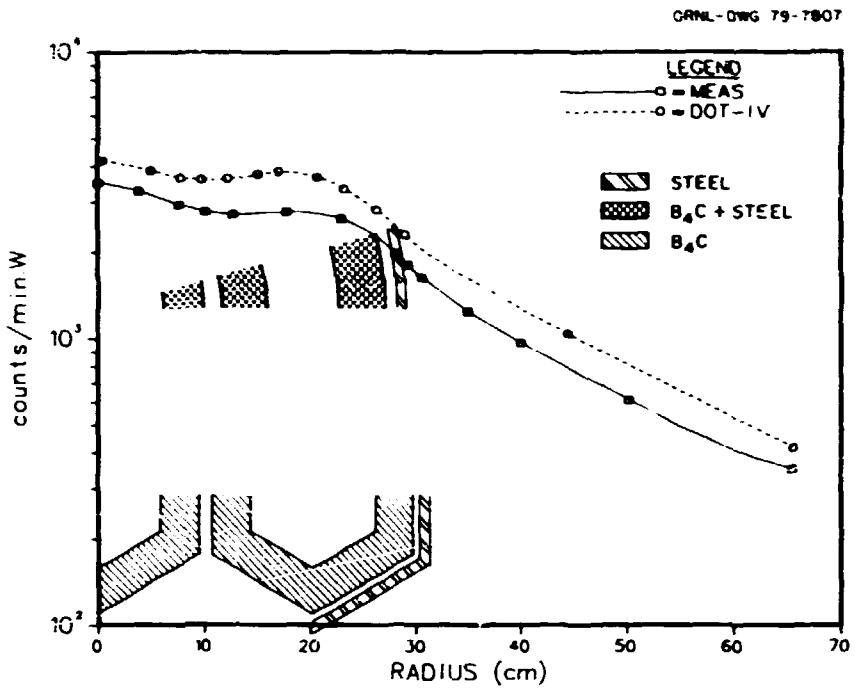

Fig. 28. Comparison of Calculated and Measured 5-in. Bonner Ball Count Rate for a Radial Traverse 7.62 cm Behind the Shields of GCFR Grid-Plate Shield Experiment Configuration II.E.

Cd-covered Bonner ball curve is generally characteristic of the one seen in Fig. 26. Calculated results (1) started out slightly lower than measured results behind the central subassembly, (2) had a relatively tall, narrow peak over the outer subassemblies, and (3) were initially slightly higher than measured behind the concrete. The presence of the iron plates cause greater than a factor of two increase in the count rate. Calculated results appear to agree with measured results to within 10%.

The 5-in. Bonner ball count rate curve shape also agrees well with the measured curve. The calculational overprediction is in general about 20%, with about 30% overprediction at the center of the outer shield.

7.1.5. Configuration II.F

This configuration includeo the prototypic grid-plate mockup, which consisted of a 76.2-cm-square by 63.5-cm-thick stack of iron plates through which seven holes were drilled. The holes were aligned with those through the grid-plate shields. The plates, surrounded by concrete, were placed adjacent to the grid-plate shield section. Into each of the cylindrical

holes in the grid plate, steel clad B_4C shields were inserted to create a shield which resembles that in the GCFR design. Thus, Configuration II.F is Configuration II.D with a prototypic mockup of the grid plate following it.

A Hornyak button measurement was taken close to the grid plate (2.62 cm). Hornyak button, 2-in. Cd-covered Bonner ball, and 5-in. Bonner ball measurements were taken at 30.5 and 305 cm behind the grid plate. Figure 29 shows results for the Hornyak button 2.62 cm behind the grid plate. The DOT results are about a factor of 3.0 times the measurements while the MORSE results are about a factor of 1.7 to 2.0 times the measurements. Assuming the MORSE results are correct except for the normalization of the Hornyak button response function, then the renormalized DOT results would be only a factor of 1.5 to 1.75 times the measured results. The shape of both the MORSE and DOT curves are good when compared to the measurements.

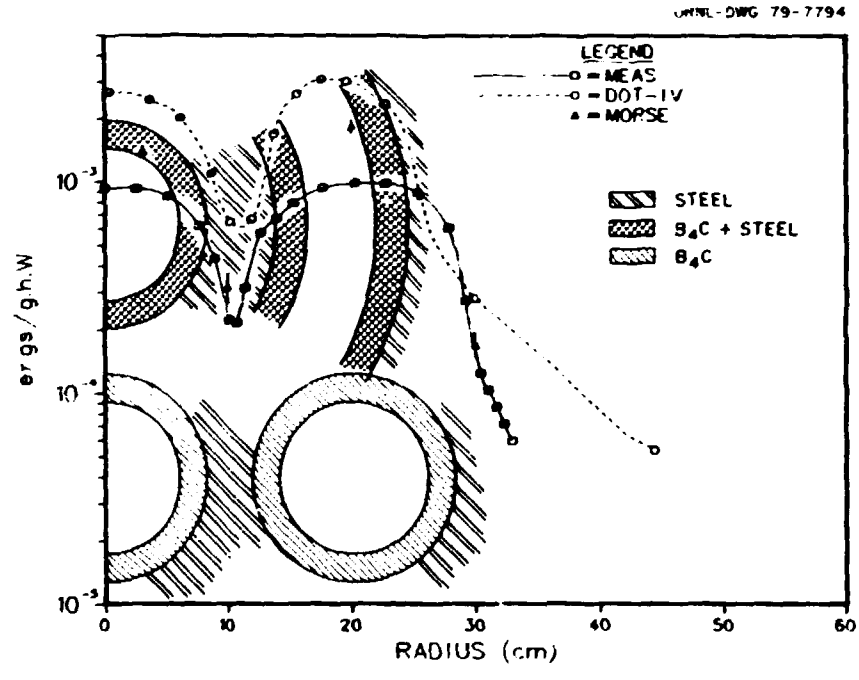

Fig. 29. Comparison of Calculated and Measured Hornyak Button Response for a Radial Traverse 2.62 cm Behind GCFR Grid-Plate Shield Experiment for Configuration II.F.

Figures 30, 31, and 32 compare calculations and measurement at 30.5 cm behind the grid plate for the Hornyak button, the 2-in. Cd-covered Bonner ball count rate, and the 5-in. Bonner ball count rate, respectively. Again the DOT-calculated Hornyak button response is a factor of 3.0 times the measured response while the MORSE results are a factor of 1.5 to 2.0 times the measured values. DOT does well in calculating the 2-in. Cd-covered Bonner ball count rate while MORSE is underpredictive overall. A MORSE calculated value behind an outer grid-plate hole agrees well with the measurement. The DOT 5-in. Bonner ball count rate is about 25% higher than the measured count rate on the centerline but becomes about 55% higher behind the outer grid-plate holes. Beyond the concrete, calculation and measurement nearly coincide. The MORSE results are about the same as seen for the 2-in. Cd-covered Bonner ball with results low near the centerline and agreement good behind the outer grid-plate holes.

Figures 33, 34, and 35 show, respectively, the results for the Hornyak button, the 2-in. Cd-covered Bonner ball, and the 5-in. Bonner ball at 305 cm behind the grid plate. Both calculated Hornyak button

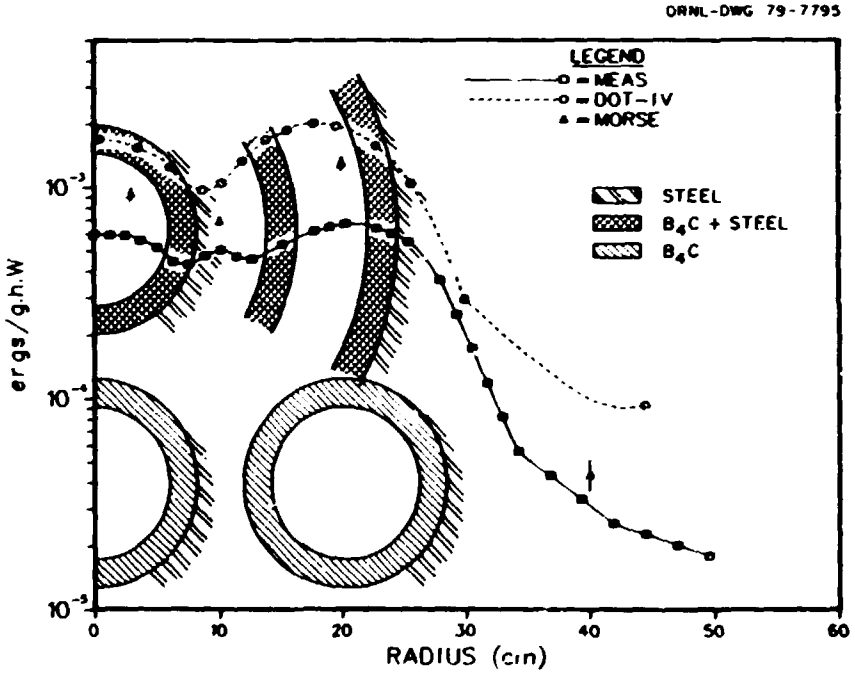

Fig. 30. Comparison of Calculated and Measured Hornyak Button Response for a Radial Traverse 30.5 cm Behind GCFR Grid-Plate Shield Experiment Configuration II.F.

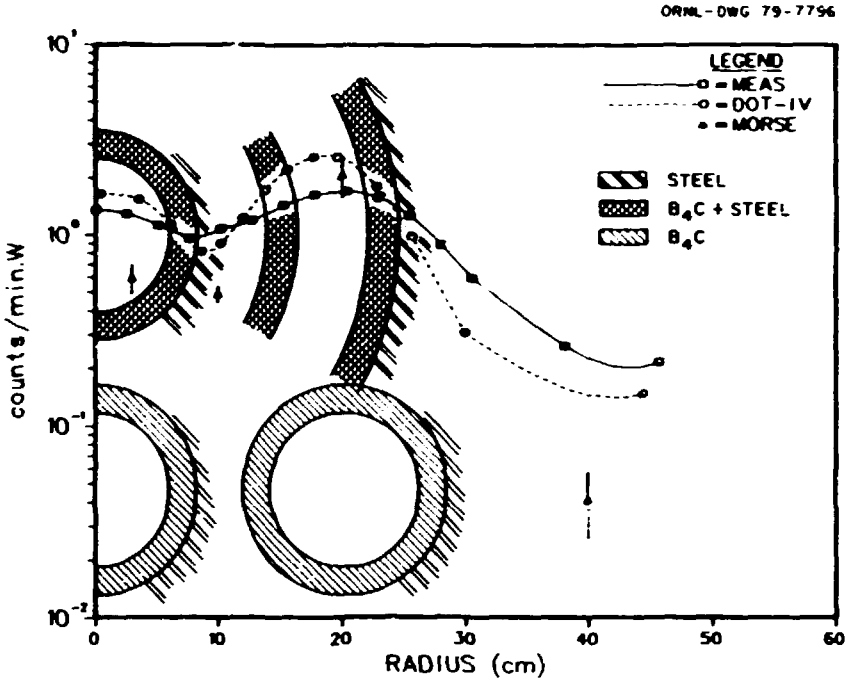

Fig. 31. Comparison of Calculated and Measured 2-in. Cd-Covered Bonner Ball Count Rate for a Radial Traverse 30.5 cm Behind GCFR Grid-Plate Shield Experiment Configuration II.F.

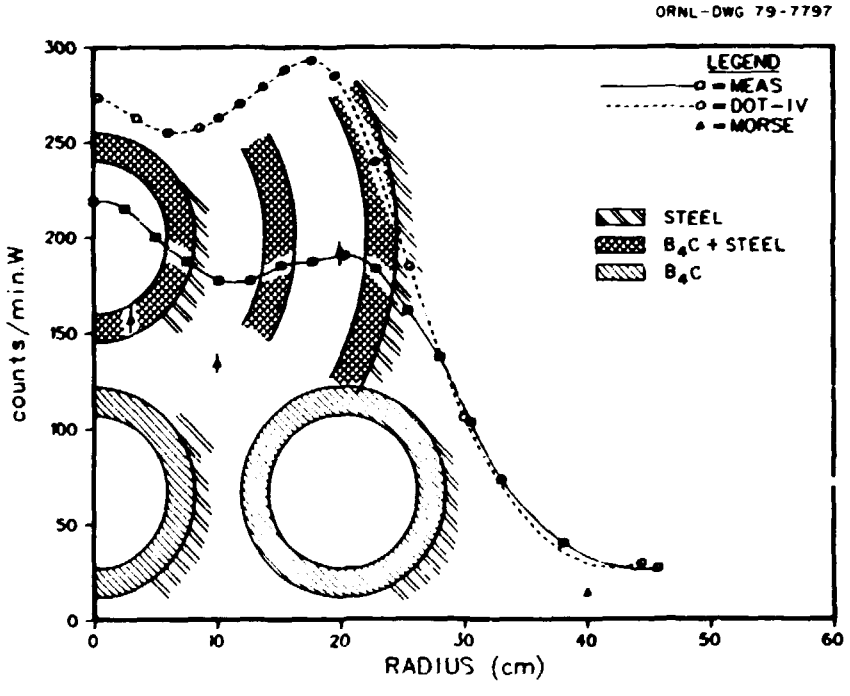

Fig. 32. Comparison of Calculated and Measured 5-in. Bonner Ball Count Rate for a Radial Traverse 30.5 cm Behind GCFR Grid-Plate Shield Experiment Configuration II.F.

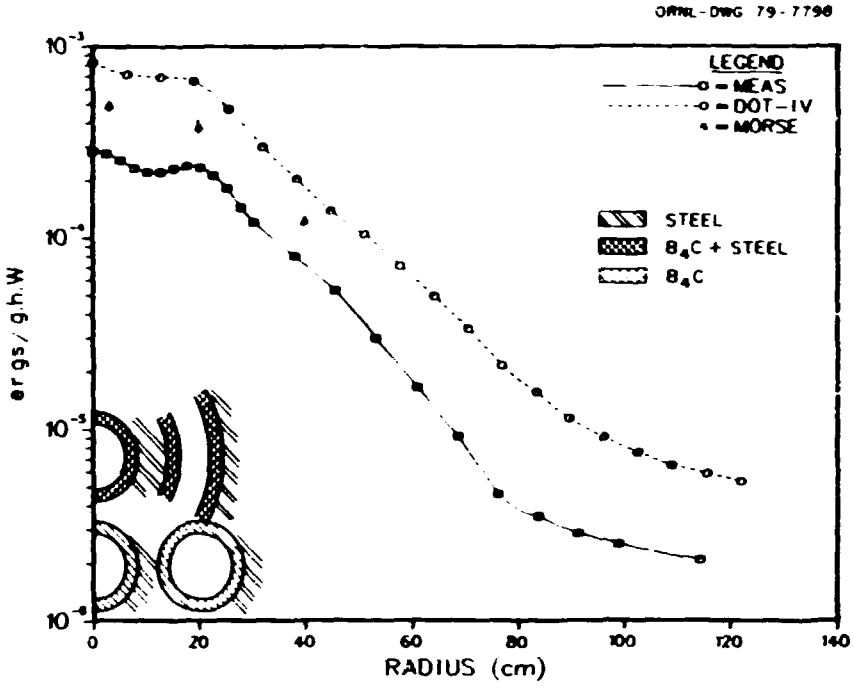

Fig. 33. Comparison of Calculated and Measured Hornyak Button Response for a Radial Traverse 305 cm Behind GCFR Grid-Plate Shield Experiment Configuration II.F.

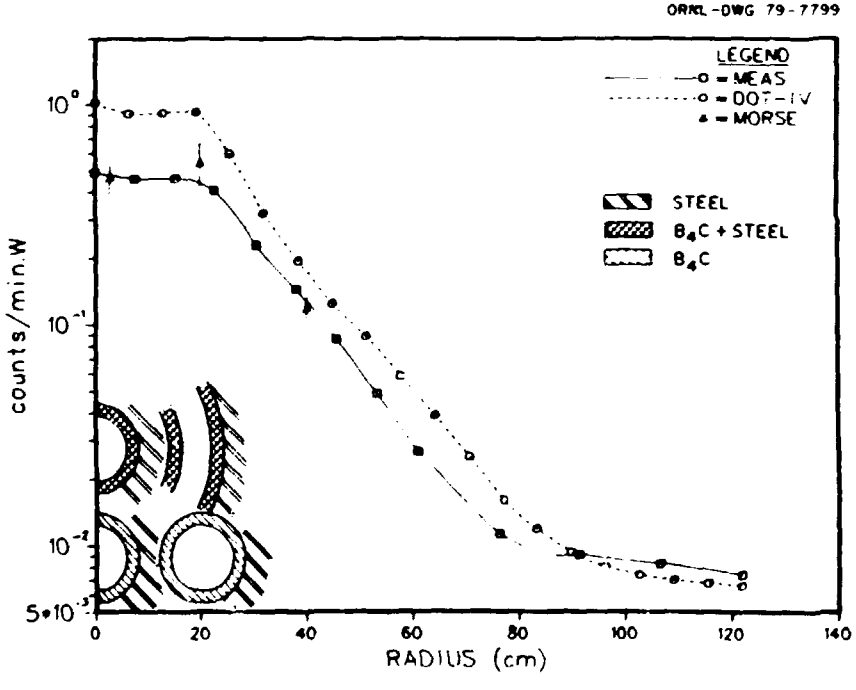

Fig. 34. Comparison of Calculated and Measured 2-in. Cd-Covered Bonner Ball Count Rate for a Radial Traverse 305 cm Behind GCFR Grid-Plate Shield Experiment Configuration II.F.

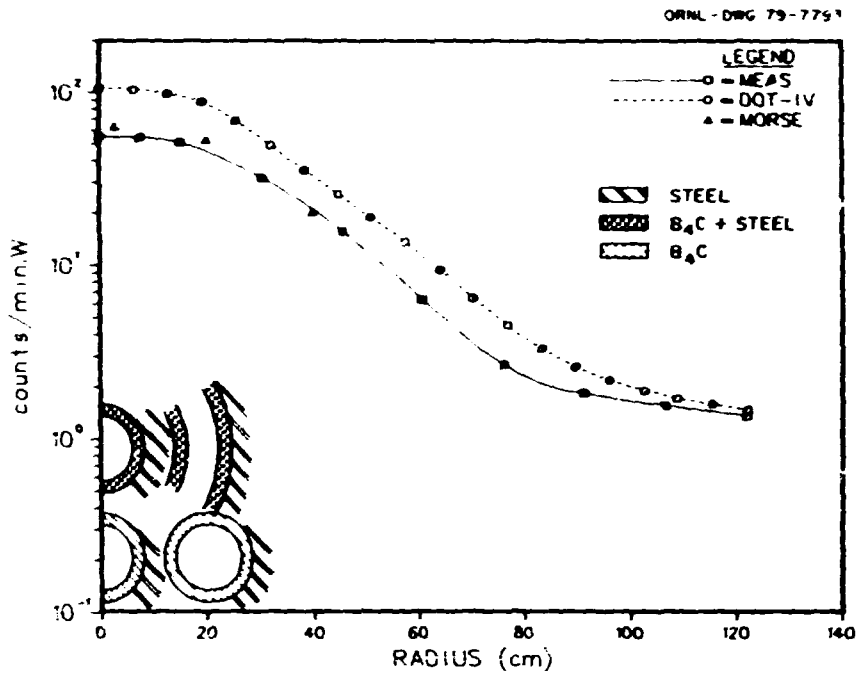

Fig. 35. Comparison of Calculated and Measured 5-in. Bonner Ball Count Rate for a Radial Traverse 305 cm Behind GCFR Grid-Plate Shield Experiment Configuration II.F.

curve shapes (Fig. 33) are similar to the measured shape though the DOT results are 2.7 times the measured results and the MORSE results are 1.7 times the measured results. Again, a portion of these large factors is attributed to inappropriate normalization of the Hornyak button response function. MORSE does well in calculating the Bonner ball count rates with statistics so low in the 5-in. Bonner ball case that the error bars are shorter than the plotting symbols and are thus not plotted. DOT results, on the other hand, are about a factor of 2 too high behind the holes but show slightly better agreement behind the steel and concrete (the concrete begins at 38.1 cm in the actual geometry and about 43 cm in 2-D cylindrical geometry). Beyond about 80 cm both Bonner ball measurements tend to flatten even though a large background component (up to 70% for the 2-in. Cd-covered Bonner ball and 28% for the 5-in. Bonner ball) has been subtracted. Probably a better comparison of the calculated and measured curves would be to continue the measured curve by maintaining the nearly constant difference between the curves in the range 40 to 80 cm. The high Bonner ball count rates at 305 cm behind the grid plate indicate that the calculated neutron source leaving the top of the GCFR design grid plate

may be very conservative. The upper plenum in the GCFR is about 450 cm high and is partially constricted by a tapered upper axial shield and a cylindrical shield plug along the axis. There are also control-rod mechanisms within the plenum. Otherwise, the upper plenum is like the grid-plate shield experiment configuration at the TSF with a large low-density (helium or air) region immediately following the grid plate. However, the experimental plenum is only partially surrounded by scattering surfaces such as the PCRV (Prestressed-Concrete Reactor Vessel) in the GCFR.

The question of whether the calculated source leaving the top of the grid plate will be conservative is left to a later section.

A neutron spectrum measurement was taken at 34.29 cm behind the grid plate. Figure 36 shows the DOT calculated spectrum compared with the

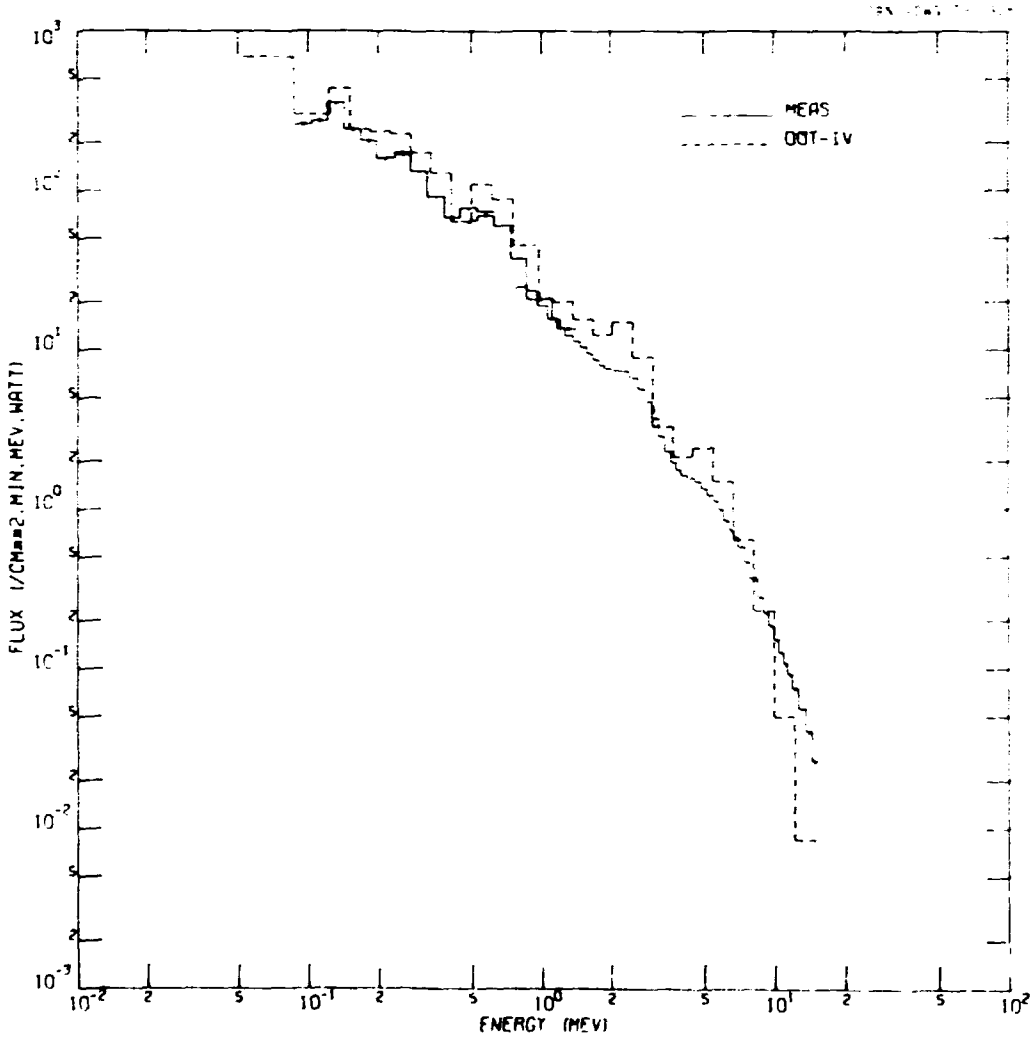

Fig. 36. Comparison of DOT-Calculated and Measured Neutron Spectra 34.3 cm Behind GCFR Grid-Plate Shield Experiment Configuration II.F.

measured spectrum and Fig. 37 shows the comparison of the MORSE results. While the shape of the DOT curve compares reasonably well, the calculated integral flux is about 50% higher than the measured flux. The MORSE calculation used broad energy bands in order to remove some of the statistical fluctuation due to undersampling certain energy ranges. There is much statistical fluctuation above 1.0 MeV, but the results have settled down to a monotonic pattern below that energy. While the spectrum is not calculated well by MORSE, the integrated E > 0.9 MeV flux agrees well with the measured flux, being a factor of 0.89 ± 0.13 times the measurement.

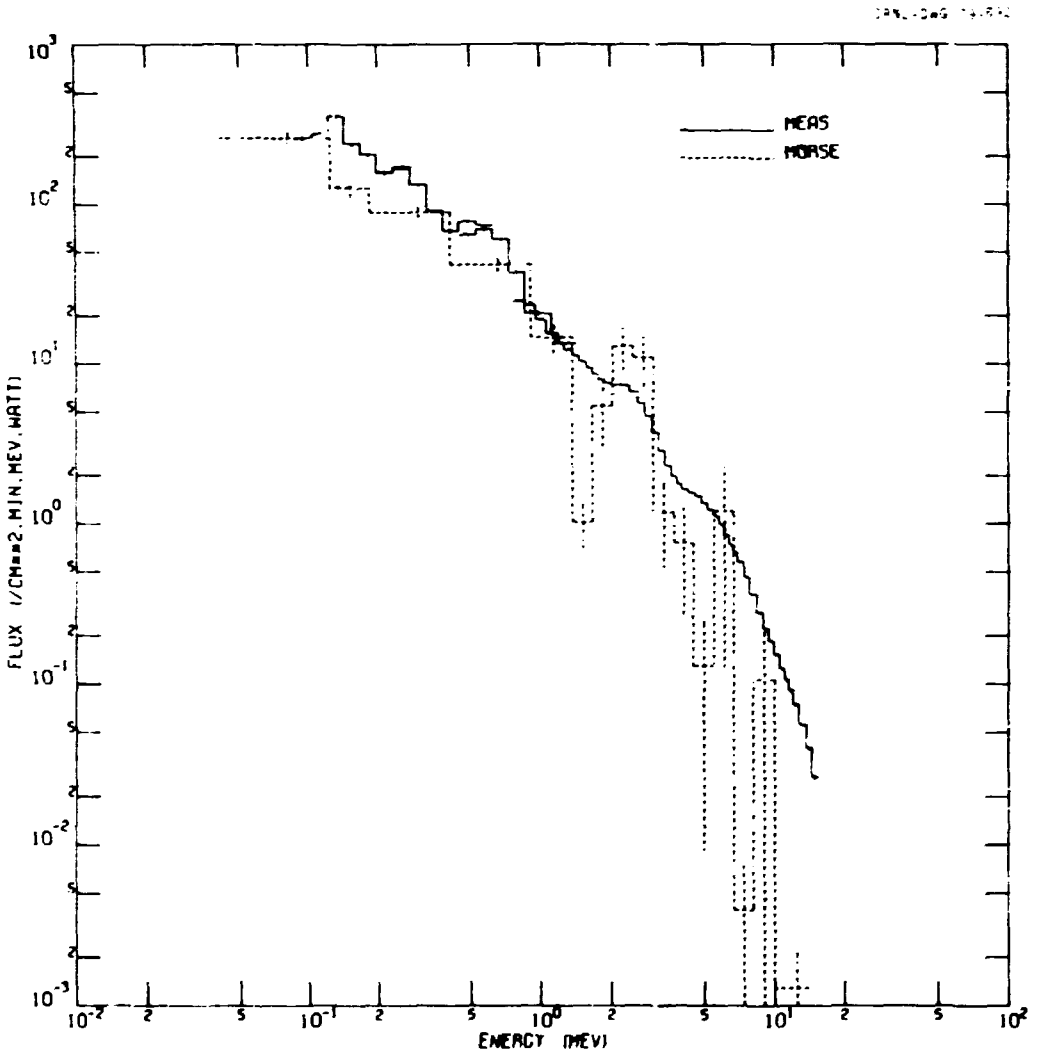

Fig. 37. Comparison of MORSE-Calculated and Measured Neutron Spectra 34.3 cm Behind GCFR Grid-Plate Shield Experiment Configuration II.F.

The flux between 0.12 MeV and 0.9 MeV was underestimated even more than that above 0.9 MeV since the total E > 0.12 MeV neutron flux was only a factor of 0.73 ± 0.04 times the measurement.

Centerline measurements were also made with Bonner balls 34.29 cm and 305 cm behind the grid plate. The calculation and measurement comparison for the flux and Bonner ball count rates are given in Table 4. It shows that close in the DOT 3-in. Bonner ball count rate is about 40% higher while the flux is about 50% higher than measured. At 305 cm behind the grid plate, all calculated Bonner ball count rates (covering most of the neutron spectrum) appear to be a factor of two higher than the measurements. These latter results indicate that the angular flux collimated through the grid plate may be a factor of two too high since it should contribute most to detector responses for detectors located large distances behind the grid plate. And as stated before, the distance at which the measurement was taken is reasonable when compared to the GCFR upper plenum. The MORSE flux comparisons presented above are also summarized in Table 4. The Bonner ball count rates calculated with MORSE agree well with the measurements.

Table 4. Comparison of Calculated and Measured Detector Responses on the Centerline Behind Configuration II-F

Response Type	Distance (cm) from Grid Plate	Measured Response	Calculated Response		C/E	
			DOT	MORSE	DOT	MORSE
Flux (neutrons/cm^2·min·W)						
E > 0.9 MeV	34.29	26.61	40.99	23.62±3.42	1.54	0.89±0.13
E > 0.12 MeV	34.29	99.22	146.4	72.0±4.38	1.48	0.73±0.04
Bonner ball (counts/min·W)						
3-in. ball	34.29	42.6	59.0	-	1.4	-
2-in. ball	305	0.493	1.08	0.462±0.074	2.1	0.94±0.15
3-in. ball	305	12.3	25.6	-	2.1	-
5-in. ball	305	55.1	116	62.6±6.89	2.1	1.14±0.12
6-in. ball	305	62.1	127	-	2.0	-
8-in. ball	305	50.8	101	-	2.0	-
10-in. ball	305	29.6	62.6	-	2.1	-
12-in. ball	305	16.8	36.4	-	2.2	-

7.1.6. Examination of Discrepancies

It was seen in the foregoing sections that there were large discrepancies (up to 55%) between the calculations and the measurements in the basic Configuration II.A. One would have expected a similar or worse discrepancy to exist when the fuel pins were added (Configuration II.B). Yet the calculations and measurements were in good agreement up to 138 cm behind the configurations. The discrepancies reappeared in calculations of detector responses large distances behind the configurations. The discrepancies also increased as more components were added to form the larger configurations. Since the larger configurations were calculated with sources generated from previous smaller configurations, only the two basic configurations (II.A and II.B) were further analyzed in order to try to resolve the discrepancies. Configuration II.F was further analyzed to see the effect of quadrature on the transmission through the grid plate.

7.1.6.1. Configuration II.A. Since a biased 150-angle quadrature was being used in the analysis, it was thought that this might account for the discrepancy in Configuration II.A. Consequently, the calculation was redone with a symmetric 96-angle (S_{12}) quadrature with slightly more angles in the -Z direction (48 angles compared to 35 angles). Both quadratures gave essentially the same results.

The configuration was further examined by sensitivity and channel theory[12] analysis to try to understand the transport through it. The VIP[13] computer code was used to generate the sensitivity matrices which were input to FORSS[14] to generate the sensitivities. The response of interest was the 5-in. Bonner ball count rate on the centerline 30.5 cm behind Configuration II.A. The adjoint calculation was performed with DOT-IV using a first-collision source from the GRTUNCL[15] computer code. Since a first-collision source was used in the adjoint calculation, only 30 angles were used. The FACT code was used to couple the forward source (with 115 forward angles) to the adjoint leakage (with 15 backward angles). The result agreed with the 5-in. Bonner ball count rate from the forward calculation to within 1%. Thus, the adjoint calculation is well defined.

The results of the sensitivity analysis are shown in Table 5. It shows that the count rate is sensitive mainly to the water content in the concrete, particularly the concrete in the shadow shield. The fluxes from

Table 5. Sensitivity of the 5-in. Bonner Ball Count Rate to Concrete Cross Sections Used in the Analysis

(Detector on axis 30.5 cm behind Configuration II.A)

Elements	Atom Densities ($barn^{-1} \cdot cm^{-1}$)* TSF Concrete	Ordinary Concrete	Sensitivity	$\frac{\Delta\Sigma}{\Sigma}$**	$\frac{\Delta R}{R}$
Na	2.73-5	1.05-3	-3.50-4	3.746+1	-1.31-2
O	4.202-2	4.385-2	-3.31-1	4.355-2	-1.44-2
Si	3.84-3	1.58-2	-2.84-2	3.115+0	-8.85-2
Mg	1.44-3	1.4-4	-1.30-2	-9.028-1	1.17-2
Fe	2.64-4	3.1-4	-2.72-3	1.742-1	-4.74-4
H	8.88-3	7.86-3	-5.00-1	-1.149-1	5.75-2
Al	4.14-4	2.39-3	-3.26-3	4.773+0	-1.56-2
Ca	1.0-2	2.92-3	-8.25-2	-7.080-1	5.84-2
K	2.34-3	6.9-4	-1.83-2	-7.051-1	1.29-2
C	7.97-3	1.0-6	-7.28-2	-9.999-1	7.28-2
S	1.015-4	1.0-6	-7.91-4	-9.901-1	7.83-4
Total			-1.054		8.19-2

*Densities computed from atom densities are 2.34 g/mc and 2.39 g/mc for ordinary and TSF concrete, respectively.

**Fractional change in the atom density (thus cross section) in going from TSF concrete to ordinary concrete.

8 shows the composition of the cement. Two other mixtures (Table 9) were obtained based on the determination of the composition of two samples by the ORNL Analytical Chemistry Division. A fifth mixture considered was an

Table 8. Composition of Cement Used in the Manufacture of the Concrete Used in the GCFR Grid-Plate Shield Experiments*

Compound	Weight percent
SiO_2	21.2
Al_2O_3	5.5
Fe_2O_3	2.6
CaO	64.5
MgO	2.7
SO_3	2.2
Na_2O	0.4
Assumed H_2O of hydration**	1.0

*Analysis performed by General Portland Cement Company of Chattanooga, Tennessee, and reported on July 21, 1978.
**Based on SO_3 percentage and the formula for gypsum [$CaO(SO_3)2H_2O$], taking the ratio of the water molecular weight to the SO_3 molecular weight and multiplying by 2.2.

Table 9. Composition of Concrete Samples as Determined by the ORNL Analytical Chemistry Division

Compound	Weight percent	
	Sample 1*	Sample 2*
H_2O	6.32	3.41
SiO_2	11.28	9.41
Fe_2O_3	0.94	0.94
Al_2O_3	1.30	1.57
CaO	33.34	36.96
MgO	13.6	13.2
Na_2O	0.01	0.022
K_2O	0.50	0.53
SO_3	0.091	0.16
P_2O_5**	0.09	0.10
CO_2	33.66	32.19
	101.1+	98.49#

*Sample 1 is from the concrete surrounding the fuel pins and sample 2 is from that surrounding the B_4C shields.
**Phosphorus combined with sulfur in calculations.
+Weight percentages normalized to 100% before use.
#Deficiency of 1.5% assumed to be water. Thus water content is 4.92%.

ordinary (Portland) concrete found in the Nuclear Engineering Handbook.[17] The sixth mixture was an ordinary (#4B) concrete used in the GCFR design analysis. The previously computed sensitivity coefficients (Table 5) were multiplied by the percent change in the atom densities of the elemental components of the concretes with respect to the TSF concrete used in the analysis and the results were summed to give a predicted change in the count rate if the given concrete is substituted for the TSF concrete. Table 10 shows the concrete compositions (elements and atom densities of each), the percent of water in the mixture, and the predicted percent change in the count rate. All concrete densities were assumed to be 2.4 g/cc.

Seven-group calculations were run using five of the above-named concrete mixtures and the results were compared with the seven-group results for the TSF concrete. As stated before, the seven-group results agreed well with the 51-group results. Six calculated curves for a 5-in. Bonner ball axial traverse down the centerline of the empty cavity are compared with the measured curve in Fig. 39. As predicted by sensitivity theory, two concrete mixtures give results comparable to the measurement (since the calculated 5-in. Bonner ball count rate was 1.55 times the measurement, the calculated results should be lowered 35% for agreement with the experiment). The two mixtures are the manufacturer's mixture with all water (MIX #1) and the ordinary concrete from the Nuclear Engineering Handbook (MIX #5). The other mixtures also give results as predicted by sensitivity analysis except for mixture #4 where the predicted change is so small (1.4%) that the sign of the change is in doubt.

These results show the effect of concrete composition on the 5-in. Bonner ball count rate. Similar effects can be expected for other detectors since the 5-in. Bonner ball has a nearly flat response over the most important energy range. Mixture #1 would be a credible mixture were it not for the fact that no water loss on setting was assumed. However, studies on the ORNL Graphite Pile Reactor Concrete Shields[18] have shown a high percentage retention of water in the portion of the concrete away from heat sources and away from exposed surfaces. The concrete around the fuel subassemblies is steel-lined and has a lateral thickness greater than 120 cm (much thicker than the 30.5 cm ordinary concrete layer on

Table 10. Compositions of Several Concrete Mixes, Water Percentages, and Predicted Percent Change in the Count Rate of a 5-in. Bonner Ball on Axis 30.5 cm Behind GCFR Grid-Plate Shield Experiment Configuration II.A When the Concrete Mix Replaces That Used in the Original Calculation

	Atom densities ($b^{-1} \cdot cm^{-1}$)*						
Element	TSF Concrete	Mix #1	Mix #2	Mix #3	Mix #4	Mix #5	Mix #6
H	8.88-3	1.361-2	7.326-3	1.067-2	8.395-3	1.494-2	7.86-3
O	4.202-2	4.713-2	4.572-2	4.654-2	4.503-2	4.153-2	4.385-2
Ca	1.0-2	8.278-3	8.686-6	8.498-3	9.257-3	1.159-2	2.92-3
Na	2.73-5	3.403-5	3.550-5	4.618-6	1.026-5	3.039-4	1.05-3
Al	4.14-4	2.844-4	2.969-4	3.658-4	4.452-4	7.372-4	2.39-3
K	2.34-3	1.527-4	1.527-4	1.504-4	1.627-4	1.217-4	6.9-4
Mg	1.44-3	5.408-3	5.640-3	4.823-3	4.733-3	1.055-3	1.4-4
Si	3.83-3	2.510-3	2.617-3	2.682-3	2.264-3	6.044-3	1.58-2
S	1.015-4	7.245-5	7.556-5	3.376-5	4.856-5	0	1.0-6
Fe	2.64-4	8.585-5	8.955-5	1.684-4	1.702-5	1.974-4	3.1-4
C	7.97-3	1.046-2	1.091-2	1.093-2	1.059-2	3.818-3	1.0-6
% water	5.53	8.48	4.57	6.18	4.92	9.38	5.02
Pred. % chg in count rate	0.0	-32.1	+3.38	-15.4	-1.37	-31.3	+8.19

*Mix #1 - Composition based on suppliers mix and concrete and sand analysis plus 0.5 wt % K_2O.
Mix #2 - Composition based on suppliers mix with about half the water retained + 0.5 wt % K_2O.
Mix #3 - Composition based on ORNL Analytical Chemistry Division analysis with total normalized to 100%.
Mix #4 - Composition based on ORNL Analytical Chemistry Division analysis with deficiency attributed to water.
Mix #5 - Ordinary (Portland) concrete from the Nuclear Engineering Handbook.[17]
Mix #6 - Ordinary (#4B) concrete as used in GCFR design analysis.

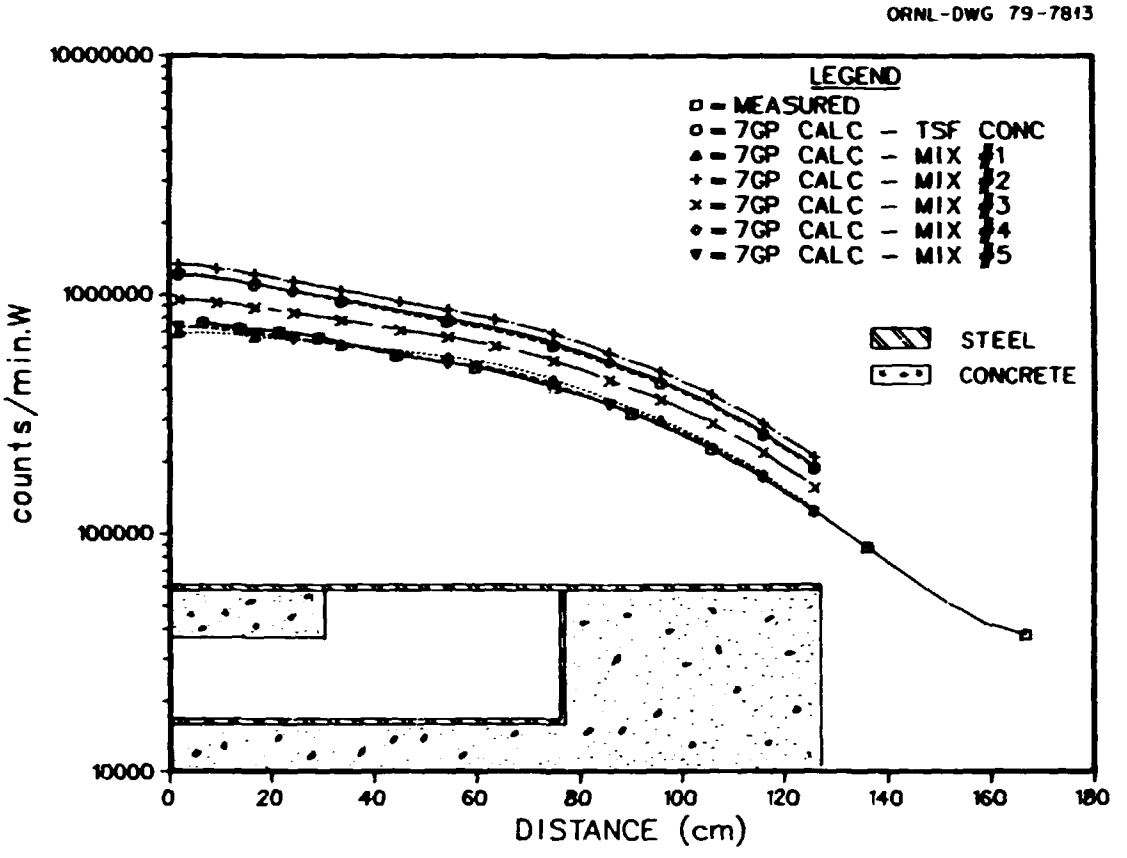

Fig. 39. Comparison of the Calculated 5-in. Bonner Ball Count Rate for Several Concrete Mixtures with the Measured Count Rate for an Axial Traverse Down the Center of GCFR Grid-Plate Shield Experiment Configuration II.A.

either side of the heavy concrete in the Graphite Reactor shield). Thus, the concrete surrounding the fuel subassemblies could indeed retain a large percentage of the water used in mixing.

The only conclusion to be drawn from these calculations is that knowledge of the concrete composition is very important if unbiased comparisons are to be made between calculations and measurements. A definitive claim that a given concrete is the correct one to use may be made only if that concrete also gives good comparisons with the fuel subassemblies present.

7.1.6.2. Configuration II.B. Two additional questions remained for Configuration II.B. First, assuming that the correct concrete mixture has been determined in the previous section, how does it affect the calculated results behind the fuel pins? Second, how does one reduce the error in calculations to detectors great distances behind the fuel pins? The first

question was answered by running seven-group calculations for Configuration II.B with the TSF concrete mixture and with Mixture #1. The results showed that the calculated 5-in. Bonner ball count rate 30.5 cm behind the fuel pins would drop 16 to 17% on the centerline and about 33% at the edge of the calculational geometry when the concrete is substituted. The thermal flux ($E < 2.38$ eV) remains about the same for both concretes. The 5-in. Bonner ball count rate at 305 cm behind the fuel pins drops 20 to 25%. At 305 cm behind the configuration, the calculated 5-in. Bonner ball count rate is 13% higher than measured on centerline and up to 16% lower than measured off centerline. Thus, the concrete which removes the discrepancy from the Configuration II.A calculation introduces discrepancies into the Configuration II.B calculations.

Two approaches were used in the analysis of the second question. First, a finer mesh was introduced in the fuel-pin region and the seven-group calculation with TSF concrete was rerun. The results were unchanged at 30.5 cm behind the fuel pins. At 305 cm behind the fuel pins, the 2-in. Cd-covered and 5-in. Bonner ball count rates drop about 20% on the centerline and remain about the same toward the outer edge of the geometry. This results in a 5-in. Bonner ball count rate 11% higher than measured on the centerline 305 cm behind the fuel pins, while the calculated count rate is 13% higher than measured off the centerline 305 cm behind the configuration. Since agreement is good both close behind the configuration and large distances behind it, it is concluded that inadequate mesh spacing, rather than grossly incorrect concrete composition, is the major source of the discrepancy between calculation and measurement for Configuration II.B. The discrepancies in the results for Configuration II.A remain unexplainable.

The second approach used to reduce the discrepancy in the results 305 cm behind the configuration was to use a different auxiliary code to compute the detector responses at detectors large distances behind the fuel pins. Unlike the DISKTRAN code, which uses a boundary source as input, the FALSTF[19] code uses a volumetric scattering-plus-fission source from which last-flight contributions are summed for each discrete volume element specified. Because the source angular distribution is given in terms of flux moments, responses of detectors close to the axis frequently are undercalculated. Consequently, the FALSTF results presented are based

on results obtained at off-axis detectors and extrapolated to those on-axis or near the axis. The results are compared with measurements in Table 11. It is seen that the Bonner ball results agree reasonably well with the measurements 30.5 cm behind the fuel pins. The Hornyak button results are characteristically high. There is also good agreement for

Table 11. Comparison of DOT/FALSTF-Calculated and Measured Responses Behind Configuration II-B

Response Type	R (cm)	Z (cm)	Value Calculated	Value Measured	C/E
Bonner ball (counts/min•W)					
2-in. Cd-covered ball	0.0	30.48	105.4	88.0	1.20
	10.16	30.48	100.7	86.8	1.16
	17.78	30.48	91.02	82.3	1.11
	30.48	30.48	82.27	68.3	1.20
	45.72	30.48	63.74	48.1	1.33
	0.0	304.8	7.053	4.32	1.63
	15.24	304.8	6.774	3.78	1.79
	25.4	304.8	6.277	3.57	1.76
	45.72	304.8	4.539	2.93	1.55
	137.16	304.8	3.488	1.95	1.79
3-in. ball	0	138.1	369.1	280.0	1.32
5-in. ball	0.0	30.48	9672	8530	1.13
	10.16	30.48	9106	8180	1.11
	17.78	30.48	7939	7390	1.07
	30.48	30.48	6243	5310	1.18
	45.72	30.48	3693	3170	1.16
	0.0	304.8	363.6	348.0	1.04
	15.24	304.8	352.0	331.0	1.06
	25.4	304.8	331.3	294.0	1.13
	45.72	304.8	258.9	231.0	1.12
	137.16	304.8	202.5	133.0	1.52
6-in. ball	0	138.1	1274	1270	1.00
10-in. ball	0	138.1	555.1	600.0	0.93
Hornyak Button (ergs/g•h•W)	0.0	30.48	4.78-2*	2.99-2	1.60
	10.16	30.48	4.50-2	2.92-2	1.54
	17.78	30.48	3.94-2	2.57-2	1.53
	30.48	30.48	3.08-2	1.93-2	1.60
	45.72	30.48	1.79-2	1.13-2	1.58
	0.0	304.8	2.03-3	1.69-3	1.20
	15.24	304.8	1.96-3	1.39-3	1.41
	25.4	304.8	1.85-3	1.26-3	1.47
	45.72	304.8	1.46-3	1.01-3	1.44
	137.16	304.8	1.09-3	5.88-4	1.86
Flux (neutrons/cm^2•min•W) E > 0.9 MeV	0.0	138.1	207.7	219.0	0.95

*Read: 4.78×10^{-2}.

the 5-in. Bonner ball count rate at 305 cm behind the fuel pins except for the position 137 cm from the axis. The 2-in. Cd-covered Bonner ball results are even higher than for the DISKTRAN calculations, while the Hornyak button results remain high due in part to uncertainty in the normalization of its response function. Except for the 3-in. Bonner ball count rate, the calculated results on centerline at 138.1 cm behind the configuration agree well with measured results. Overall, the results are not very definitive. However, they tend to show that the volumetric scattering source is well-defined since the such good agreement was achieved for the 5-in. Bonner ball count rate at both 30.5 and 305 cm behind the configuration. The inadequate mesh then allows excess neutron streaming and results in an overestimate for the source leaking the fuel pins. The FALSTF calculation is analagous to the Monte Carlo calculation with a point detector estimator. Like MORSE, some of its results agreed better with the measured results than did the DOT results.

7.1.6.3 Configurations II.D, II.E, and II.F. The discrepancies in configurations II.D, II.E, and II.F are attributed in part to the discrepancies present in Configuration II.B. The use of a finer mesh and attention to the concrete composition should eliminate the greater portion of the discrepancies in any of the configurations. The neutron source is concentrated in the fuel pins a short distance beyond the point where the source is directed onto the pins; hence, the concrete composition should have little additional effect upon calculated responses behind the follow-on configurations (II.D, II.E, and II.F) than it has on responses behind Configuration II.B. Errors in the concrete composition are believed to contribute little to the discrepancies seen behind Configuration II.B; rather, the space mesh is the controlling factor.

7.2. Configurations III.A, IV.A, and VI.A

Since a thorough analysis of Configurations II were or would be done, only selected portions of the other configurations were analyzed. Hence all the core/blanket arrangements except the one including the control-rod-channel mockup were examined. These included two variations of the subassembly-gap spacing from that of Configuration II.B. In Configuration III.A the number of fuel pins per subassembly (127) remained the same as

that of Configuration II.B, but the subassembly-gap size was reduced to 0.635 cm. Likewise, in Configuration VI.A the gap size was reduced further to 0.318 cm. The three configurations, II.B, III.A, and VI.A, thus cover a range of subassembly-gap sizes each of which might have a different effect on the location of the point of maximum fast-neutron exposure to the grid plate.

Configuration IV.A is also like Configuration II.B, except that instead of varying the subassembly gap size the number of fuel pins per subassembly has been lowered to 91. The two fuel subassemblies with 91 and 127 pins have inside void fractions of 60.2% and 44.5%, respectively. The GCFR design values have ranged from 63.3% in the low-pressure-drop design to 52.9% in the high-pressure-drop design. While the void fraction range in the experiment is shifted to the low side of that for the design, there is enough overlap so that meaningful information may be extracted and applied to the GCFR design.

The calculations were performed the same as with Configuration II.B, with adjustments to the ring geometry to account for the rearrangement of the fuel subassemblies within the core.

The DOT-calculated results on axis 30.5 cm behind each of the four configurations (II.B, III.A, IV.A, and VI.A) are compared with measured results in Table 12. The Bonner ball count rates agree very well with the measured ones. The Hornyak button results are high and, as mentioned before, the disagreement is probably due to the lack of a properly normalized response function for the Hornyak button. The C/E ratios seem to increase with decreasing subassembly-gap width (compare II.B to III.A to VI.A) and decrease with a decrease in the number of fuel pins per subassembly (compare II.B to IV.A). Changes in the neutron spectrum among the different core arrangements are chiefly responsible.

The DOT/DISKTRAN-calculated results on axis 305 cm behind each of the four configurations are compared with measured results in Table 13. These results show the calculations substantially overpredicting the measured results. Note that the calculated-to-measured ratios (C/Es) increased when the outer or peripheral-gap thickness was increased from 0.635 cm to 1.27 cm (Configuration II.B to Configuration III.A), but there is little change when the peripheral-gap thickness is increased from 1.27 cm to

Table 12. Comparison of DOT-Calculated and Measured Responses on Axis 30.5 cm Behind Various Configurations

Detector	Configuration			
	II-B	III-A	IV-A	VI-A
Bonner ball (counts/min·W)				
2-in. Cd-covered ball				
Calculated	8.30+1*	8.48+1	1.17+2	8.43+1
Measured	8.80+1	8.63+1	1.43+2	8.69+1
C/E	0.94	0.98	0.82	0.97
5-in. ball				
Calculated	8.53+3	8.38+3	1.18+4	8.15+3
Measured	8.53+3	7.95+3	1.25+4	7.88+3
C/E	1.0	1.05	0.94	1.03
Hornyak button (ergs/g·h·W)				
Calculated	4.18-2	4.10-2	6.39-2	3.97-2
Measured	2.99-2	2.55-2	4.75-2	2.34-2
C/E	1.40	1.61	1.35	1.70

*Read: 8.30×10^1.

Table 13. Comparison of DOT/DISKTRAN-Calculated and Measured Responses on Axis 305 cm Behind Various Configurations

Detector	Configuration			
	II-B	III-A	IV-A	VI-A
Bonner ball (counts/min·W)				
2-in. Cd-covered ball				
Calculated	6.32+0*	6.39+0	8.87+0	6.45+0
Measured	4.32+0	3.28+0	7.28+0	3.61+0
C/E	1.46	1.95	1.22	1.79
5-in. ball				
Calculated	4.65+2	4.96+2	6.68+2	4.91+2
Measured	3.48+2	3.16+2	5.30+2	3.03+2
C/E	1.34	1.57	1.26	1.62
Hornyak button (ergs/g·h·W)				
Calculated	2.87-3	3.13-3	4.71-3	3.09-3
Measured	1.68-3	1.43-3	2.75-3	1.35-3
C/E	1.71	2.19	1.71	2.29

*Read: 6.32×10^0.

1.59 cm (Configuration III.A to Configuration VI.A). Also, there is much improvement in the C/Es for the Bonner ball count rates in going from the 127 fuel pins per subassembly in Configuration II.B to the 91 fuel pins per subassembly in Configuration IV.A. The results for Configuration IV.A are almost acceptable. Again, part of the overprediction in the Hornyak button response is due to the difficulty in normalizing the Hornyak button response function.

The results also show the effect of void fraction within a subassembly on the neutron streaming. Configurations IV.A and II.B have the same interassembly gap but different void fractions within the subassemblies. The Hornyak button comparisons give an idea about how the fast-neutron flux ($E > 0.1$ MeV) behaves. The calculational comparisons showed that at 30.5 cm behind the configuration the higher void fraction (60.2%) Configuration IV.A gives a fast-neutron flux 1.5 times that behind the lower void fraction (44.5%) Configuration II.B. The measurement comparisons give a factor of 1.6. The higher neutron flux behind the higher void fraction configuration is due to both the lower effective material density in the core and neutron streaming among the fuel pins. The fission and scattering sources per unit volume of material within the fuel subassemblies were compared for both configurations and were found to be nearly the same. The sources per unit volume in the design calculations were also about the same for the different designs.

7.3. Configuration IV.B

The final configuration analyzed was Configuration IV.B, which was formed by adding the grid-plate shield section to Configuration IV.A. Configuration IV.A had 91 fuel pins per subassembly with subassemblies spaced 1.27 cm apart. This configuration (IV.B) is analagous to Configuration II.D in which the core contained subassemblies which were spaced 1.27 cm apart and which had 127 fuel pins each. The DOT calculation was performed using a boundary source generated during the calculation of Configuration IV.A. The boundary source was located about 64 cm into the fuel pin region so that "end effects" would not result in a source which was too low.

Radial traverses were made close behind the shields using the Hornyak button and the 2-in. Cd-covered Bonner ball. The calculated and measured curves for the Hornyak button are plotted in Fig. 40 while those for the 2-in. Cd-covered Bonner ball are plotted in Fig. 41. The agreement is similar to that seen for Configuration II.D. The calculated Hornyak button results are generally higher than measured, except over the outer shield where the narrower void channel in the 2-D mockup of the shields caused the calculated results to drop below the measured results. The shape is good in general and probably represents the average of what one would see in all the radial traverses across the shields with various angles from 0 to 90° from the horizontal. The 2-in. Cd-covered Bonner ball count rate curve has the same problem as the Hornyak button with respect to the outer shield. The narrower opening in the 2-D geometry

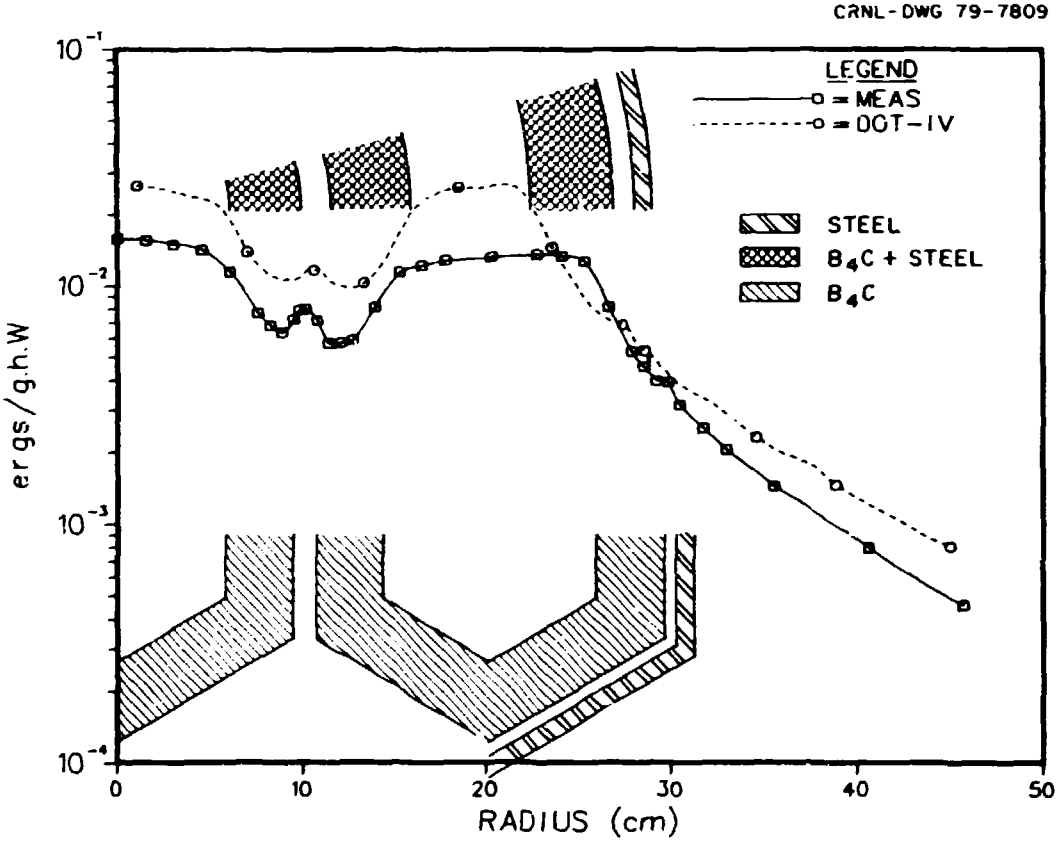

Fig. 40. Comparison of Calculated and Measured Hornyak Button Response for a Radial Traverse 2.35 cm Behind GCFR Grid-Plate Shield Experiment Configuration IV.B.

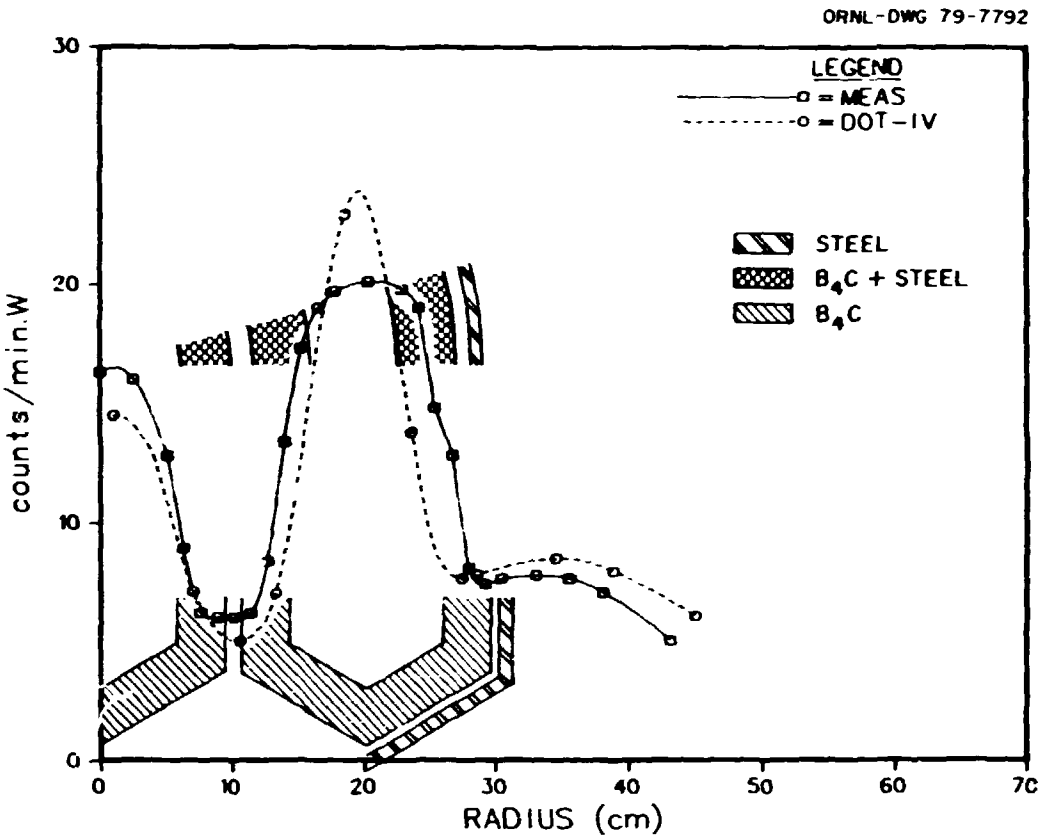

Fig. 41. Comparison of Calculated and Measured 2-in. Cd-Covered Bonner Ball Count Rate for a Radial Traverse 3.18 cm Behind GCFR Grid-Plate Shield Experiment Configuration IV.B.

causes the calculated peak to be tall and narrow when compared to the shorter and broader measured curves. While an average of all the measured results for traverses from 0 to 90° from the horizontal might produce a narrower peak, it could hardly be expected to produce a taller one. Thus the calculation would probably overpredict the count rate over the center of the outer hole by about 30%. There is about a 10% underprediction at the center.

The final comparisons are for measurements made on the centerline at either 30.5 cm or 305 cm behind the configuration. The results are shown in Table 14. About the same degree of success is achieved in calculating the results for this configuration as was achieved with Configuration II.D (Table 3). The results at 305 cm show slightly better agreement than before. In both cases the Hornyak button results are high by a factor of 2, due in part to an improperly normalized response function.

Table 14. Comparison of DOT/DISKTRAN-Calculated and Measured Response on the Centerline Behind Configuration IV.B

Response Type	Distance from Shield (cm)	Response		C/E
		Calculated	Measured	
Hornyak button	30.5	1.08-2*	5.40-3	2.00
(ergs/g·h·W)	305	1.99-3	9.58-4	2.08
Bonner ball (counts/min·W)				
2-in. Cd-covered ball	30.5	9.37	9.91	0.95
	305	2.70	2.14	1.26
5-in. ball	30.5	1730	1520	1.1[illegible]
	305	265	177	1.50

*Read: 1.08×10^{-2}.

7.4 Configuration V

Configuration V.A was designed to simulate a control rod channel mock-up within the GCFR. It is like Configuration IV.A (Section 7.2) except that seven fuel pins have been removed from the central fuel subassembly leaving the simulated control rod channel. The other Configurations V are identical to Configurations IV except for the control rod channel mock-up.

None of the Configuration V mockups were calculated, but some inferences may be made from the measured results. Results from Configurations IV are used as the standard to which results from Configurations V are compared.

Behind the fuel pins, Configuration V.A gave 5-in. Bonner ball count rates on the centerline which were 3.5% higher than those for Configuration IV.A at both 30.5 cm and 305 cm behind the configuration. The total flux would be expected to have the same behavior as the 5-in. Bonner ball count rate. The fast-neutron fluxes (inferred from Hornyak button results) were respectively 11% lower and 1.5% higher at 30.5 and 305 cm behind the configuration.

Behind the grid-plate shields, the differences between Configuration IV and Configuration V results became greater than those seen behind the fuel pins. The fast-neutron fluxes for Configuration V.B were respectively 29% and 18% higher than those for Configuration IV.B at 30.5 cm

and 305 cm behind the configurations. The total fluxes at 30.5 cm and 305 cm behind Configuration V.B were respectively 9% and 5% higher than the corresponding results for Configuration IV.B. While there was a large difference in the fast-neutron fluxes on the centerline, the peak fast-neutron exposure to the grid plate in Configuration V.B was actually 8% lower than that for Configuration IV.B.

The control rod channel mockup was included in the measurements in order to assess the importance of neutron streaming in a control subassembly in comparison to a regular fuel subassembly. Speculation was that the reduction in the fission source in the control subassembly would offset the effect of neutron streaming in the control rod channel, leaving the regular fuel subassembly as the worse case as for a neutron leakage from the core. Preanalysis calculations indicated little difference in results for the two cases. The results above indicate that the control rod channel can have a very large effect on axial neutron streaming, particularly neutron transport through the penetrations in the grid plate. On the other hand, such a subassembly mockup would give a lower fast-neutron exposure to the grid plate and would thus be nonconservative in one of the key design limiting criteria. The effect of streaming in the channel in the GCFR design is expected to be smaller than that indicated by the experiment due to the fact that the fission distribution within a design subassembly is flatter radially. The experiment had an inward flux gradient which drove the neutrons into the channel. The larger streaming path enhanced the ability of (1) neutrons from the TSR-II which penetrate the shadow shield, (2) neutrons from the TSR-II which scatter perpendicularly onto the fuel pins, and (3) fission neutrons born in the fuel pins which backscatter from the shadow shield to travel the full length of the fuel pins and leak from the fuel array.

In summary, the choice of subassembly mockups might depend upon one's major interest. Were one interested in the peak fast-neutron exposure to the grid plate, the regular fuel subassembly mockup would be preferable. The control subassembly mockup may be preferable for studies concentrating on neutron transmission through the grid plate or radiation exposure to instrumentation within a subassembly.

8.0 IMPLICATIONS FOR THE GCFR

8.1 Axial Neutron Streaming

Calculations of axial neutron streaming in the GCFR core and axial blanket are concerned mainly with that relatively and small population of source neutrons which, having been emitted in a favorable direction, suffer few, if any, collisions and only small changes in direction before crossing the axial plane of interest. They travel in relatively long flight paths in the neutronically nearly void coolant channels among the fuel pins. Their contributions to given neutron responses become more important as they move away from the source, since many of the source neutrons will be attenuated by the fuel pins and other structures. The experiment incorporated provisions for two parameter variations so that the effects of these variations on neutron streaming could be ascertained.

Four different fuel-pin configurations (II.B, III.A, IV.A, and VI.A) were calculated. From these one may obtain some idea of the effect of fuel-pin spacing and subassembly spacing on axial neutron streaming. Comparing calculations for configurations II.B, III.A, and VI.A showed that varying the interassembly-gap size from 0.318 to 1.27 cm had little effect (< 5%) on any detector response behind the configuration. Measured results, however, indicate (by the 5-in. Bonner ball count rate) a difference of 8% in the total flux and (by Hornyak button results) a difference of 28% in the E > 1.0 MeV neutron flux. The fuel-pin spacing, on the other hand, had a somewhat larger effect on the flux. The effect could not be determined directly by comparing results from configurations II.B and IV.A, since part of the increase in the neutron leakage from the configuration is due to the reduced smeared fuel density within the core of the configuration. The remainder is due to streaming. The streaming effects for the two configurations were determined separately by comparing heterogeneous and homogeneous calculations for the two configurations.

What one finds in comparing the heterogeneous and homogeneous calculations is that close behind the configurations the streaming effect due to pin streaming is about 9% for Configuration II.B (with the higher smeared fuel density) and about 11% for Configuration IV.A. Such underpredictions of neutron streaming by the homogeneous calculations ordinarily would not

be serious since larger factors of conservation are often included to account for streaming and other effects. However, when one looks at the results 305 cm behind the configurations, one finds that the homogeneous calculation underpredicts the 5-in. Bonner ball count rate by 20 to 30% for Configuration II.B and by about 40% for Configuration IV.A. The heterogenous calculations overpredict the same count rate by 35 to 50% for Configuration II.B and about 25% for Configuration IV.A. The homogeneous calculations should thus start to underpredict the neutron transport through the large penetrations in the grid-plate shields and the grid plate. Design-cell calculations have shown little difference between results from heterogeneous and homogeneous calculations when only the pin geometry portion of the cell is homogenized for the homogeneous calculation. When the grid-plate shield region and the grid-plate region are represented homogeneously, a factor of two difference has been noted between homogeneous- and heterogeneous-calculated fluxes at the bottom of the grid plate.

In general, the results indicate that the two-dimensional heterogeneous modelling used in calculations of the GCFR design is an adequate means for representing the core and axial-blanket regions of the GCFR.

8.2 Fast-Neutron Exposure to the Grid Plate

One of the major objectives of this experiment was to determine how well the calculations predict the fast-neutron exposure to the grid plate as well as the location of the point of peak exposure. It has been speculated by some that the bottom of the grid plate over the center of the interassembly gap receives a relatively high exposure when compared to the shielded portions of the grid plate. The Hornyak button measurements has such spatial resolution that a localized peak-to-minimum exposure ratio can be determined with a high degree of certainty.

Only two configurations (II.D and IV.B) were calculated. Each had the subassemblies spaced 1.27 cm apart. The Configuration II.D core contained 127 fuel pins per subassembly while the Configuration IV.B core contained 91 fuel pins per subassembly. The 1.27 cm subassembly gap was the largest for any configuration and should be the worst case of any as far as the differential in the fast-neutron exposure. Thus, the peak-to-

minimum exposure ratios should be limiting for designs which have the same or smaller subassembly gaps. Another consideration is the fact that the measurements were taken without the grid plate in place behind the shields. The presence of the grid plate has the effect of lowering the peak-to-minimum exposure ratio. The ratios measured and calculated without the grid plate should be limiting for the ratios expected with the grid plate in place.

Upon examination of the measured and calculated Hornyak button data obtained for a radial traverse behind the grid-plate shields of Configuration II.D, it was found that the measurement showed a peak-to-minimum fast-neutron exposure ratio of 1.5, compared to 1.3 for the calculation. This indicates that the calculation gives a flatter distribution across the gap and behind the shields than does the measurement. It says nothing about how well the peak exposure itself is calculated. Since it was determined that the Hornyak button response function was incorrect, it was difficult to say directly whether the peak exposure was being calculated precisely or more appropriately with a degree of conservatism. So the calculated Hornyak button curve was normalized on the centerline using the relationship between the calculated and measured 5-in. Bonner ball count rate on the centerline. At 30.5 cm behind the configuration, the calculated 5-in. Bonner ball count rate was 1.15 times the measured count rate. Normalizing the calculated Hornyak button response on the centerline to 1.15 times the measured value results in a calculated peak exposure which is 0.98 times the measured value. The difference between the calculation and the measurement is well within the uncertainty of about 10% in the measurement (see Ref. 3). The question might be asked, "What would be the result if the calculated 5-in. Bonner ball count rate were 1.0 times the measured count rate?" Since the calculation gives a smaller peak-to-minimum fast-neutron exposure ratio, it is suspected that the flux coming through the large hole in the grid-plate shield is being overpredicted. Thus, as the discrepancy in the calculated flux at the center of the hole is reduced, the peak flux should remain unchanged or change very little. The peak-to-minimum fast-neutron exposure ratio would be changed in the direction of the experimental value. It is expected that the peak exposure will be calculated well indeed.

The calculation for Configuration II.F with the grid plate in place can give an idea of the effect of the grid plate on the peak-to-minimum fast-neutron exposure ratio. A suitable measurement scheme was not available. The calculation with the grid plate present showed a peak-to-minimum exposure ratio of 1.12 compared to 1.3 without the grid plate. If a similar reduction in the measured ratio could be assumed, then one would expect a maximum peak-to-minimum fast-neutron exposure ratio of 1.3. This is certainly an acceptable differential between the peak and minimum exposures.

Configuration IV.B showed results similar to those of Configuration II.D. The measured and calculated peak-to-minimum fast-neutron exposure ratios were 1.4 and 1.2 respectively. As before, the calculated Hornyak button curve was normalized on the centerline by the ratio of the calculated-to-measured 5-in. Bonner ball count rate 30.5 cm behind the configuration. The calculated count rate was 1.14 times the measured count rate. The resulting calculated-to-measured peak fast-neutron exposure ratio was 1.00, which is excellent agreement with the measurements and is well within the 10% uncertainty in the measurements.

In all the above cases, calculation and measurement alike, the peak fast-neutron exposure occurred behind the interassembly gap. Even with the grid plate in place, the peak exposure still occurred behind the interassembly gap and at the bottom of the grid plate. However, one calculation of Configuration II.F (with the prototypic grid plate), using an S_{10} quadrature rather than the 150-angle quadrature, placed the peak exposure at the bottom of the grid plate but in the portion of the grid plate nearest the hole in the grid-plate shield. Design calculations with smaller interassembly-gap sizes have shown a similar trend where the relatively low-order S_{10} quadrature places the peak exposure near the hole in the grid-plate shield, while the high-order biased quadrature places the peak exposure behind the interassembly gap. In the calculations of the experiment, the biased quadrature gives an exposure behind the gap which is 1.13 times that given by the S_{10} quadrature. On the other hand, since the peak exposure for the S_{10} calculation is not behind the gap, the difference in the two calculated exposures is smaller. The peak exposure for the biased quadrature is 1.07 times that for the S_{10} quadrature. Thus the peak exposure is not seriously underpredicted by the lower-order quadrature.

From the above discussions, one can conclude that the peak fast-neutron exposure to the grid plate occurs at the bottom of the grid plate and most likely over the interassembly gap. Secondly, the peak exposure is calculated well with low-order and high-order quadratures. Thirdly, the estimated maximum peak-to-minimum fast-neutron exposure ratio of 1.3 (see earlier discussion in this section) indicates that there are no serious flux-peaking problems in the design grid plate.

The measurements themselves give indications of the effect of interassembly-gap size on the peak fast-neutron exposure to the grid plate. Configurations II.D, III.B, and VI.B all contained subassemblies bearing 127 pins per subassembly but had different subassembly gap widths. The gap widths were 1.27, 0.635, and 0.3175 cm for configurations II.D, III.B, and VI.B, respectively. When the fast-neutron dose rates (Hornyak button measurements) behind the shield were compared, it was found that the peak exposures for configurations II.D, III.B, and VI.B were in the ratio of 1.55:1.15:1.0. Using the results from Configuration VI.B as the base results, a parametric equation was derived for computing the ratio of results for other gap sizes to that for the 0.3175-cm gap size (Configuration VI.B). The equation for the ratio is given by

$$r = 0.8833 + 0.3150d + 0.1653d^2$$

where d is the gap width in centimeters. The equation holds for gap widths between 0.3175 and 1.27 cm and possibly for a small interval outside the ranges. Within a few decimal places it reproduces the ratios 1.55, 1.15, and 1.0 for gap sizes of 1.27, 0.635, and 0.3175 cm respectively. The ratios may be maintained with the grid plate present.

The measured results showed that the peak-to-minimum fast-neutron exposure ratio increased with increasing gap widths being 1.15 for the 0.3175-cm gap, 1.3 for the 0.635-cm gap, and 1.5 for the 1.27-cm gap width. The peak-to-minimum exposure ratio for Configuration IV.B with a 1.27-cm interassembly-gap width and 91 fuel pins per subassembly was 1.4, slightly lower than that for Configuration II.D which also had an interassembly-gap width of 1.27 cm but 127 fuel pins per subassembly. The presence of a control-rod channel (Configuration V.B) did not change this result. The peak exposure for Configuration IV.B was 1.6 times that for Configu-

ration II.D due to the reduced smeared fuel density in the core of Configuration IV.B (since calculations showed the streaming effects to be about the same for the cores of the two configurations).

Overall the results indicate that the peak fast-neutron exposure to the grid plate increases in a nonlinear fashion as the gap width increases. In a like manner, the localized flux peaking also becomes worse as the gap width increases. However, the measurements were taken without a grid plate behind the shields. Calculations have shown improvements in the flux-peaking factors in the presence of the grid plate. Thus the measurements without the grid plate give the worst possible peaking factors for a given interassembly-gap size.

8.3. Neutron Source for the GCFR Upper Plenum

Another objective for this experiment was to determine how well the neutron source for the GCFR upper plenum has been calculated in the past using methods which were used to analyze the experiment. The difficulty lies in finding a suitable two-dimensional model which can adequately represent the relatively large penetrations in the grid plate and the grid-plate shields. Inadequate representation of those penetrations can result in gross overprediction or underprediction of the neutron transport through the grid plate. The angular distribution of those neutrons as they emerge from the grid plate can also be distorted. A neutron spectrum measurement 34.29 cm behind Configuration II.F and detector measurements in a radial traverse 305 cm behind the configuration can be used to assess the ability to calculate both the energy and angular distribution of the neutrons leaving the grid plate. The detector a large distance behind the grid plate effectively sees the source at a single point and senses mainly energy and angular variations in the flux. The portion of the angular distribution measured in the distant traverses may be only that portion with cosines of 0.9 to 1.0 with respect to the normal to the source surface. The traverse close behind the grid plate verifies the angular distribution for the remaining cosines, though the source can no longer be viewed as emanating from a point.

The calculations of neutron transmission through the grid plate of the experiment (Configuration II.F) gave detector responses behind the grid

plate which were 1.5 to 2.2 times the measured values. The calculated 5-in. Bonner ball count rates 30.5 cm behind the grid plate were substantially higher than measured until the traverse was a short distance radially beyond the outer grid-plate penetrations; then the calculated and measured results nearly coincided (Fig. 32). At 305 cm (Fig. 35) the calculation overpredicted the measured results by a nearly constant factor of 2 over much of the traverse. The two sets of results, together with the fact that the fast neutron flux 34.29 cm behind the grid plate was overpredicted by a factor of 1.5, indicate that the angular fluxes in the most forward directions ($\eta > 0.9$) are too high. The results also imply that design calculations using the same biased quadrature used in the experiment analysis would give a very conservative estimate of the neutron transmission through the grid plate, which would in turn give rise to a conservative source for the GCFR upper plenum. However, design calculations in the past have used a lower-order quadrature for neutron transport calculations in the GCFR. In particular most cell calculations have been performed with S_{10} quadrature (70 angles) and full mockup calculations have been performed with an S_6 (30 angles) or S_{10} quadrature. These have 35 and 15 angles, respectively, in the forward direction compared to 115 in the biased quadrature set used in the experiment analysis. In the forward direction, the biased set is basically an S_{10} quadrature set with additional η-levels added in the most forward η-level of the S_{10} set.

The above being the case, one could not make a direct inference from the calculations of the experiment to the calculations of the design, unless of course one would use the same quadrature in the design calculations. Consequently, a design cell calculation was made using the biased quadrature used in the experiment analysis and Configuration II.F (with the prototypic grid plate) was recalculated using the S_{10} quadrature previously used in the design cell calculation. The cell calculation results showed that at the center of a penetration at the top of the grid plate, the biased quadrature gave $E > 1.0$ MeV, $E > 0.1$ MeV, and total neutron fluxes which were factors of 2.2, 1.5, and 1.4, respectively, times the results given by the S_{10} quadrature. Elsewhere, at the bottom of the grid plate and in the grid plate webbing (top and bottom), the S_{10} results were comparable to and slightly higher than the biased quadrature results.

Since the biased quadrature results were higher than the S_{10} results by the same factors by which the calculation overpredicted the measurement, it was felt that the S_{10} quadrature might have been more suited to calculating the neutron transport through the grid plate than the biased quadrature. However, results from the S_{10} calculation of the experiment Configuration II.F showed that quadrature to be quite inadequate for calculating the experiment. The ratios of the biased-quadrature-calculated E > 1.0 MeV, E > 0.1 MeV, and total neutron fluxes at the top center of the grid-plate penetration to the respective S_{10}-calculated fluxes were 6.8, 3.3, and 2.9, respectively, more than double the ratios for the design calculation. At 34.3 cm behind the grid plate, the S_{10}-quadrature calculation underpredicted the 3-in. Bonner ball count rate, the E > 0.9 MeV flux, and the E > 0.12 MeV flux by factors of 3.8, 12.3, and 5.3 respectively. These ratios might be expected to be reduced by more than half for the design calculation since flux ratios at the top of the grid plate for the experiment calculation were more than double those for the design calculation.

At 305 cm the S_{10} quadrature underpredicted Bonner ball count rates on the centerline by factors of 35 to 85. The agreement between calculation and measurement gets better off centerline. For example, the calculated 5-in. Bonner ball count rate 122 cm off the centerline is 1.2 times the measured value. Design calculations using the S_{10} quadrature are not expected to underpredict radiation levels in the upper plenum by factors of 35 to 85, due in part to the discussion above which showed that the design calculation gave less than half the underprediction of the experiment calculation. Secondly, the neutron reflections from the upper shields and the PCRV surrounding the plenum creates a more uniform flux field in the upper plenum than that in the open space behind the grid-plate Configuration II.F.

In summary, the above discussion implies that based on calculations of the experiment and the design with the biased quadrature and S_{10} quadrature, design calculations which have used an S_{10} quadrature in the past may have underestimated the E > 1.0 MeV neutron flux by a factor of 4.0 and the E > 0.1 MeV and total neutron fluxes by a factor of 2.5. These factors are perceived as upper bounds to the underpredictions. Most

design constraints for the upper axial region have been met with sufficient margin that such uncertainties can be accomodated with the present shield design.

9.0 SUMMARY

The results of the analysis of the GCFR Grid-Plate Shield Design Confirmation Experiment have been presented. The established objectives of the experiment were met. The shadow shield eliminated the direct neutron-streaming source and allowed the scattered beam to place the dominant source within the fuel pins themselves. The effects of neutron streaming on neutron leakage from the core were calculated to be between 9 and 11% for void fractions between 44.5 and 60.2%. The calculated effect of interassembly-gap size on the leakage from the core was small since there was a difference of less than 5% between the leakage for a 0.3175-cm gap width and that for a 1.27-cm gap width. Centerline measurements behind the fuel pins, however, indicated a larger effect due to gap width. A difference of 28% was noted in the Hornyak button response, indicating about a 28% difference in the $E > 1.0$ MeV neutron flux. The difference of 8% in the Bonner ball count rates (versus 5% for the calculation) means about an 8% difference in the total flux. Hence, varying the gap size between 0.3175 and 1.27 cm is expected to have only a small overall effect on neutron leakage from the GCFR axial blanket.

In terms of the peak fast-neutron exposure to the grid plate, the effect of the interassembly-gap width variation was much larger than the effect on the leakage from the axial blanket. While there was only an 18% difference in the centerline Hornyak button responses, the peak values in the grid plate differed by 55% between configurations with 0.3175 cm and 1.27 cm interassembly-gap widths. A parametric quadratic equation was derived which expressed the ratio of the fast-neutron exposure for a particular gap width between 0.3175 cm and 1.27 cm to the fast-neutron exposure for a gap width of 0.3175 cm. The equation, though based on measurements behind the grid plate shields without the grid plate, was expected to hold for configurations with the grid plate present.

The peak fast-neutron exposure to the grid plate was found to be calculated well. Calculated peak Hornyak button responses, when renor-

malized using the calculated 5-in. Bonner ball count rate and the measured Hornyak button response and 5-in. Bonner ball count rate on the centerline behind the shields, were found to lie within 2% of the measurements for two configurations. These differences between calculation and measurement were well within the 10% uncertainty in the measurements.

Lastly, initial calculations with a high-order biased quadrature gave very conservative results for the neutron leakage from the top of the grid plate. Calculated fluxes and Bonner ball count rates were 1.5 to 2.2 times the measured results. A subsequent calculation with a lower-order S_{10} symmetric quadrature greatly underpredicted detector responses behind the grid plate. It was determined that this quadrature might underpredict fluxes in the GCFR upper plenum by factors of 2.5 to 4.0. Constraints having been met by a large margin in the upper axial regions, the application of such bias factors to calculated responses can be accommodated without redesign.

In conclusion, the results presented have shown that methods and data used in the analysis of the GCFR design are adequate for calculating (1) axial neutron streaming in the GCFR core and axial blanket for a variety of fuel-pin and subassembly spacings, and (2) the amount and location of the peak fast-neutron exposure to the GCFR grid plate. The methods were found lacking when used to calculate the neutron leakage from the top of the grid plate into the upper plenum. Results were sensitive to the quadrature set chosen. Future design calculations of neutron and gamma-ray transport through the grid plate will place greater emphasis on quadrature.

REFERENCES

1. General Atomic Company Project Staff, "300 MW(e) Gas-Cooled Fast Breeder Reactor Demonstration Plant," GA-A-13045, General Atomic Company (1974).

2. R. G. Perkins and R. J. Cerbone, "Physics Design of the 300-MW(e) Gas-Cooled Fast Breeder Reactor Demonstration Plant Grid Plate Shielding," General Atomic Company Report GA-A 14124 (September 1976).

3. F. J. Muckenthaler, J. L. Hull, and J. J. Manning, "The GCFR Grid Plate Shield Design Confirmation Experiment," ORNL/TM-6580 (January 1979).

4. R. E. Maerker, private communication (December 1978).

5. H. Goldstein, *Fundamental Aspects of Reactor Shielding*, Addison-Wesley Publishing Company, Inc., Reading, Mass., 1959.

6. R. E. Maerker and F. J. Muckenthaler, "The Absolute Neutron Spectrum Emerging Through the Large Beam Collimator from the TSR-II Reactor at the Tower Shielding Facility," ORNL/TM-5183 (January 1976).

7. W. A. Rhoades and F. R. Mynatt, "The DOT-III Two-Dimensional Discrete Ordinates Transport Code," ORNL/TM-4280 (September 1973).

8. M. L. Gritzner, W. W. Engle, Jr., W. A. Rhoades, D. R. Vondy, and L. R. Williams, "FACT: A Computer Code to Process the Neutron and Gamma Angular Flux and Fold Regular and Adjoint Results on a Coupling Surface for Response Analysis," draft report.

9. W. A. Rhoades, D. B. Simpson, R. L. Childs, and W. W. Engle, Jr., "The DOT-IV Two-Dimensional Discrete Ordinates Transport Code with Space-Dependent Mesh and Quadrature," ORNL/TM-6529 (January 1979).

10. M. B. Emmett, "The MORSE Monte Carlo Radiation Transport Code System," ORNL-4972 (February 1975).

11. DISKTRAN is a code written by C. O. Slater. It uses the angular fluxes from the DOT scalar flux and moments data set to calculate responses at detectors within a void. Only disk sources are allowed. See Appendix C.

12. M. L. Williams and W. W. Engle, Jr., "The Concept of Spatial Channel Theory Applied to Reactor Shielding Analysis," ORNL/TM-5467 (July 1976).

13. R. L. Childs, "VIP, A Computer Program Using Two-Dimensional Discrete Ordinates Transport Calculations for Cross-Section Sensitivity Analysis," UCCND-CSD-1 (to be published).

14. C. R. Weisbin, E. M. Oblow, J. H. Marable, R. W. Peelle, and J. L. Lucius, "Applications of Sensitivity and Uncertainty Methodology to Fast Reactor Integral Experiment Analysis," *Nucl. Sci. Eng.*, 66, 307-333 (1978).

15. R. L. Childs and J. V. Pace, III, "DOT IV Great UNCL Input" in *DOS: The Discrete Ordinates System*, by W. A. Rhoades and D. B. Simpson (Draft Report).

16. D. T. Ingersoll, "FORM: Perspective Plotting Code for One- and Two-Dimensional Fluxes," ORNL/TM-6396 (May 1978).

17. H. Etherington, Editor, *Nuclear Engineering Handbook*, McGraw Hill Book Company, New York, 1958.

18. T. V. Blosser *et al.*, "A Study of the Nuclear and Physical Properties of the ORNL Graphite Reactor Shield," ORNL-2195 (August 1958).

19. R. L. Childs, "FALSTF User's Manual," draft report.

Appendix A

THE EXPERIMENTAL PROGRAM PLAN

GCFR GRID PLATE SHIELD DESIGN EXPERIMENT (FY-78)
(DATA PLAN)

I. Reactor Source Comparison.

A. 10.16-cm Fe + 2.54-cm Boral.

1. 3-, 6-, and 10-in.-diam Bonner balls on centerline at 30.5 cm behind Boral.

II. Fuel Pin Shield Assembly (1.27-cm void between subassemblies, 889 fuel pins) (Priority 1A).

A. Fuel pin-concrete shield without fuel pin subassemblies.

1. Traverses along beam centerline from zero to 457.2 cm beyond concrete shadow shield using the
   a) Bare, Cd-covered, and 5-in.-diam Bonner balls.
   b) Hornyak button (1.27 cm).

2. Horizontal traverse perpendicular to beam centerline (121.9 cm each side) at 30.5 cm beyond concrete shield using the
   a) Cd-covered and 5-in.-diam Bonner balls.
   b) Hornyak button (1.27 cm).

3. Traverse perpendicular to beam centerline (121.9 cm each side at an angle of 60° with respect to the horizontal plane at 30.5 cm beyond concrete shield using the
   a) Hornyak button (1.27 cm).

4. 3-, 6-, and 10-in.-diam Bonner balls on centerline at 370 cm beyond shadow shield.

B. Fuel pin-concrete shield with seven subassemblies of fuel pins (127 pins each).

BLANK PAGE

1. Horizontal traverse perpendicular to beam centerline (121.9 cm each side) directly behind the fuel pins using the
   a) Hornyak button (0.635 cm).
2. Horizontal traverse perpendicular to beam centerline (121.9 cm each side) at 30.5 cm beyond fuel pin subassemblies using the
   a) Cd-covered and 5-in.-diam Bonner balls.
   b) Hornyak button (1.27 cm).
3. Horizontal traverse perpendicular to beam centerline (487.7 cm each side) at 305 cm beyond fuel pin subassemblies using the
   a) Cd-covered and 5-in.-diam Bonner balls.
   b) Hornyak button (1.27 cm).
4. NE213 neutron spectrum measurement on centerline as close to the fuel pin subassemblies as feasible.
5. Hydrogen counter (1D) neutron spectrum measurements on centerline at same location as NE213.
6. Centerline measurements at same location as NE213 using the
   a) 3-, 6-, and 10-in.-diam Bonner balls.

C. Fuel pin-concrete shield with seven subassemblies of fuel pins (127 pins each) plus grid plate shield mockup without boron subassemblies.

1. Centerline measurements at 30.5 cm beyond concrete shield using the
   a) Cd-covered and 5-in.-diam Bonner balls.
   b) Hornyak button (1.27 cm).

D. Fuel pin-concrete shield with seven subassemblies of fuel pins (127 pins each) plus grid plate shield mockup with seven boron subassemblies.

1. Horizontal traverse perpendicular to beam centerline (121.9 cm each side) directly behind the boron subassemblies using the
   a) Cd-covered Bonner ball.
   b) Hornyak button (0.635 cm).
2. Centerline measurements at 30.5 cm behind boron subassemblies using the
   a) Bare, Cd-covered, and 5-in.-diam Bonner balls.
   b) Hornyak button (1.27 cm).
3. Centerline measurements at 305 cm behind boron subassemblies using the
   a) Cd-covered and 5-in.-diam Bonner balls.
   b) Hornyak button (1.27 cm).
4. Axial traverse through grid plate shield from fuel pin subassemblies to 30.5 cm beyond grid plate shield using the
   a) CD-covered Bonner ball.
   b) Hornyak button (1.27 cm).

E. Fuel pin-concrete shield with seven subassemblies of fuel pins (127 pins each) plus grid plate shield mockup with seven boron subassemblies plus 15.24-cm void plus 61-cm Fe. Surround Fe and void with concrete.

1. Horizontal traverse (152.4 cm) in the void perpendicular to the beam centerline as close as feasible to the boron subassemblies using the
   a) Cd-covered and 5-in.-diam Bonner balls.

F. Fuel pin-concrete shield with seven subassemblies of fuel pins (127 pins each) plus grid plate shield mockup with seven boron subassemblies plus prototypic grid plate.

1. Horizontal traverse perpendicular to beam centerline (121.9 cm each side) at 30.5 cm beyond grid plate using the

a) Cd-covered Bonner ball (without B_4C cylindrical inserts).

b) 5-in.-diam Bonner ball (with and without B_4C cylindrical inserts).

c) Hornyak button (1.27 cm) (with and without B_4C cylindrical inserts).

2. Horizontal traverse perpendicular to beam centerline (487.7 cm each side) at 305 cm beyond grid plate using the

a) Cd-covered and 5-in.-diam Bonner balls.

b) Hornyak button (1.27 cm).

3. Horizontal traverse perpendicular to beam centerline directly behind grid plate using the

a) Hornyak button (1.27 cm).

4. NE213 neutron spectrum measurements on centerline as close to the grid plate as feasible.

5. Hydrogen counter (1D) neutron spectrum measurements on centerline at same location as NE213.

6. Centerline measurements at 305 cm behind grid plate using the

a) 3-, 6-, 8-, and 10-in.-diam Bonner balls.

III. Fuel pin-concrete shield assembly (0.635 cm void, 889 pins) (Priority 1B).

A. Fuel pin-concrete shield with seven subassemblies of fuel pins (127 pins each).

1. Horizontal traverse perpendicular to beam centerline (121.9 cm each side) directly behind the fuel pins using the

a) Hornyak button (0.635 cm).

2. Centerline measurements at 30.5 cm beyond fuel pin subassemblies using the

a) Cd-covered and 5-in.-diam Bonner balls.

b) Hornyak button (1.27 cm).

3. Centerline measurements at 305 cm beyond fuel pin subassemblies using the

a) Cd-covered and 5-in.-diam Bonner balls.

b) Hornyak button (1.27 cm).

B. Fuel pin-concrete shield with seven subassemblies of fuel pins (127 pins each) plus grid plate shield mockup with seven boron subassemblies.

1. Horizontal traverse perpendicular to beam centerline (121.9 cm each side) directly behind the boron subassemblies using the

a) Cd-covered Bonner ball.

b) Hornyak button (0.635 cm).

2. Centerline measurements at 30.5 cm beyond boron subassemblies using the

a) Bare, Cd-covered, and 5-in.-diam Bonner balls.

b) Hornyak button (1.27 cm).

3. Centerline measurements at 305 cm beyond boron subassemblies using the

a) Cd-covered and 5-in.-diam Bonner balls.

b) Hornyak button (1.27 cm).

C. Fuel pin-concrete shield with seven subassemblies of fuel pins (127 pins each) plus grid plate shield mockup with seven boron subassemblies plus 15.24-cm void plus 61-cm Fe. Surround Fe and void with concrete.

1. Horizontal traverse 152.4 cm in the void perpendicular to the beam centerline directly behind the boron subassemblies using the

a) Cd-covered and 5-in.-diam Bonner balls.

IV. Fuel pin shield assembly (1.27-cm void, 637 pins) (Priority 1C).

A. Fuel pin-concrete shield with seven subassemblies of fuel pins (91 pins each).

1. Centerline measurements at 30.5 cm beyond concrete shield using the
   a) Cd-covered and 5-in.-diam Bonner balls.
   b) Hornyak button (1.27 cm).

2. Centerline measurements at 305 cm beyond fuel pin subassemblies using the
   a) Cd-covered and 5-in.-diam Bonner balls.
   b) Hornyak button (1.27 cm).

B. Fuel pin-concrete shield with seven subassemblies of fuel pins (91 pins each) plus grid plate shield mockup with seven boron subassemblies.

1. Horizontal traverse perpendicular to beam centerline (121.9 cm each side) directly behind the boron subassemblies using the
   a) Cd-covered Bonner ball.
   b) Hornyak button (0.635 cm).

2. Centerline measurements at 30.5 cm beyond boron subassemblies using the
   a) Cd-covered and 5-in.-diam Bonner balls.
   b) Hornyak button (1.27 cm).

3. Centerline measurements at 305 cm beyond boron subassemblies using the
   a) Cd-covered and 5-in.-diam Bonner balls.
   b) Hornyak button (1.27 cm).

C. Fuel pin-concrete shield with seven subassemblies of fuel pins (91 pins each) plus grid plate shield mockup with seven boron subassemblies plus 15.24-cm void plus 61-cm Fe. Surround Fe and void with concrete.

1. Horizontal traverse 152.4 cm in the void perpendicular to beam centerline directly behind the boron subassemblies using the
   a) Cd-covered and 5-in.-diam Bonner balls.

V. Fuel pin-concrete shield assembly (1.27-cm void, 637 pins) with seven pins removed from center of central subassembly. (Priority 2).

A. Fuel pin-concrete shield for seven subassemblies of fuel pins the center subassembly having seven pins removed from its center.

1. Centerline at 30.5 cm beyond subassemblies using the,
   a) Cd-covered and 5-in.-diam Bonner balls.
   b) Hornyak button (1.27 cm).

2. Centerline measurements at 305 cm beyond subassemblies using the
   a) Bare, Cd-covered, and 5-in.-diam Bonner balls.
   b) Hornyak button (1.27 cm).

3. Horizontal traverse perpendicular to beam centerline (121.9 cm each side) directly behind the fuel pins using the
   a) Hornyak button (0.635 cm).

B. Fuel pin-concrete shield with seven subassemblies of fuel pins, the center subassembly having seven pins removed from its center, plus grid plate shield mockup with seven boron subassemblies.

1. Horizontal traverse perpendicular to beam centerline (121.9 cm each side) directly behind the boron subassemblies using the
   a) Cd-covered Bonner ball.
   b) Hornyak button (0.635 cm).

2. Centerline measurements at 30.5 cm beyond the boron subassemblies using the
   a) Cd-covered and 5-in.-diam Bonner balls.
   b) Hornyak button (1.27 cm).

3. Centerline measurements at 305 cm beyond the boron subassemblies using the
   a) Cd-covered and 5-in.-diam Bonner balls.
   b) Hornyak button (1.27 cm).

4. Axial traverse through the grid plate shield from the fuel pin assembly to 30.5 cm beyond grid plate shield using the
   a) Cd-covered Bonner ball.
   b) Hornyak button (1.27 cm).

VI. Fuel pin-concrete shield assembly (0.318-cm void, 889 pins) (Priority 3)

A. Fuel pin-concrete shield with seven subassemblies of fuel pins (127 pins each).

1. Centerline measurements at 30.5 cm beyond fuel pin subassemblies using the
   a) Cd-covered and 5-in.-diam Bonner balls.
   b) Hornyak button (1.27 cm).

2. Centerline measurements at 305 cm beyond fuel pin subassemblies using the
   a) Cd-covered and 5-in.-diam Bonner balls.
   b) Hornyak button (1.27 cm).

3. Horizontal traverse perpendicular to beam centerline (121.9 cm each side) directly behind the fuel pin subassemblies using the
   a) Hornyak button (0.635 cm).

B. Fuel pin-concrete shield with seven subassemblies of fuel pins (127 pins each) plus grid plate shield mockup with seven boron subassemblies.

1. Horizontal traverse perpendicular to beam centerline (121.9 cm each side) behind the boron subassemblies using the
   a) Cd-covered Bonner ball.
   b) Hornyak button (0.635 cm).

2. Centerline measurements at 30.5 cm beyond boron subassemblies using the
   a) Bare, Cd-covered, and 5-in.-diam Bonner balls.
   b) Hornyak button (1.27 cm).

3. Centerline measurements at 305 cm beyond boron subassemblies using the
   a) Cd-covered and 5-in.-diam Bonner balls.
   b) Hornyak button (1.27 cm).

VII. Fuel pin-concrete shield with Fe-pin assembly (967 pins).

A. Traverse along beam centerline from zero to 152.4 cm beyond Fe pins using
   1) Cd-covered and 5-in.-diam Bonner balls.
   2) Hornyak button (1.27 cm).

B. Horizontal traverse perpendicular to beam centerline (91.5 cm each side) directly behind Fe pins using
   1) Cd-covered Bonner ball.
   2) Hornyak button (1.27 cm).

C. Horizontal traverse perpendicular to beam centerline (91.5 cm each side) at 30.5 cm behind Fe pins using
   1) Cd-covered and 5-in.-diam Bonner balls.
   2) Hornyak button (1.27 cm).

D. Horizontal traverse perpendicular to beam centerline (91.5 cm each side) at 305 cm behind Fe pins using
   1) Cd-covered and 5-in.-diam Bonner balls.
   2) Hornyak button (1.27 cm).

VIII. Fuel pin-concrete shield with Fe-plate assembly.

A. Traverse along beam centerline from zero to 152.4 cm beyond Fe plates using the

1) Cd-covered and 5-in.-diam Bonner balls.
2) Hornyak button (1.27 cm).

B. Horizontal traverse perpendicular to beam centerline (91.5 cm each side) directly behind Fe plates using the

1) Cd-covered Bonner ball.
2) Hornyak button (1.27 cm).

C. Horizontal traverse perpendicular to beam centerline (91.5 cm each side) at 30.5 cm behind Fe plates using the

1) Cd-covered and 5-in.-diam Bonner balls.
2) Hornyak button (1.27 cm).

D. Horizontal traverse perpendicular to beam centerline (91.5 cm each side) at 305 cm behind Fe plates using the

1) Cd-covered and 5-in.-diam Bonner balls.
2) Hornyak button (1.27 cm).

Appendix B

MULTIGROUP RESPONSE FUNCTIONS

NEUTRON DETECTOR 51-GROUP RESPONSE FUNCTIONS*

GRP.	RESP 1	RESP 2	RESP 3	RESP 4	RESP 5	RESP 6	RESP 7	RESP 8
1	3.72000E-05	8.07940E-05	3.44607E-03	1.20640E-01	2.29426E-01	4.32222E-01	5.78793E-01	6.49817E-01
2	3.48000E-05	9.64320E-05	4.36709E-03	1.55440E-01	2.93310E-01	5.39835E-01	7.00675E-01	7.59885E-01
3	3.252C0E-05	1.15170E-04	5.50525E-03	1.98610E-01	3.71410E-01	6.67260E-01	8.39550E-01	8.80150E-01
4	3.01800E-05	1.38940E-04	6.85514E-03	2.47830E-01	4.54975E-01	7.86115E-01	9.46620E-01	9.49120E-01
5	2.808C0E-05	1.82030E-04	9.24671E-03	3.09150E-01	5.50901E-01	9.07770E-01	1.04565E 00	1.00640E 00
6	2.616C0E-05	1.88700E-04	1.10360E-02	3.50810E-01	6.16360E-01	9.90133E-01	1.10785E 00	1.03165E 00
7	2.52C00E-05	1.69180E-04	1.34925E-02	4.11500E-01	7.03019E-01	1.06950E 00	1.12520E 00	9.82514E-01
8	2.340C0E-05	1.53390E-04	1.69491E-02	4.80390E-01	7.96009E-01	1.14895E 00	1.14495E 00	9.44992E-01
9	2.100C0E-05	1.66160E-04	2.11140E-02	5.59550E-01	9.03610E-01	1.24835E 00	1.18825E 00	9.37484E-01
10	1.872C0E-05	1.94740E-04	2.61091E-02	6.44110E-01	1.01274E 00	1.33619E 00	1.21060E 00	9.07036E-01
11	1.782C0E-05	2.41790E-04	3.19911E-02	7.27630E-01	1.11019E 00	1.39025E 00	1.18985E 00	8.30172E-01
12	1.602C0E-05	1.70950E-04	3.88255E-02	8.07900E-01	1.19294E 00	1.41070E 00	1.13345E 00	7.47410E-01
13	1.464C0E-05	1.36140E-04	4.67552E-02	8.84120E-01	1.26249E 00	1.40780E 00	1.06005E 00	6.52339E-01
14	1.332C0E-05	1.45410E-04	5.58243E-02	9.54920E-01	1.31920E 00	1.38560E 00	9.77195E-01	5.61006E-01
15	1.204C0E-05	1.76200E-04	6.60058E-02	1.01830E 00	1.35925E 00	1.34705E 00	8.90184E-01	4.77345E-01
16	1.062C0E-05	2.37200E-04	7.72051E-02	1.07320E 00	1.38585E 00	1.29415E 00	8.03746E-01	4.03566E-01
17	9.480C0E-06	3.25040E-04	8.94274E-02	1.12000E 00	1.40045E 00	1.23805E 00	7.22249E-01	3.41144E-01
18	8.520C0E-06	3.84330E-04	1.02503E-01	1.15810E 00	1.40360E 00	1.17530E 00	6.47183E-01	2.89369E-01
19	7.680C0E-06	3.98190E-04	1.16205E-01	1.18730E 00	1.39685E 00	1.11080E 00	5.79972E-01	2.46609E-01
20	7.080C0E-06	4.81690E-04	1.30270E-01	1.20940E 00	1.38385E 00	1.04940E 00	5.22500E-01	2.13140E-01
21	6.420C0E-06	6.04350E-04	1.44604E-01	1.22430E 00	1.36455E 00	9.89866E-01	4.72383E-01	1.86106E-01
22	5.820C0E-06	6.75590E-04	1.59109E-01	1.23390E 00	1.34200E 00	9.34567E-01	4.29672E-01	1.64541E-01
23	5.160C0E-06	7.35080E-04	1.73588E-01	1.23970E 00	1.31795E 00	8.84574E-01	3.93894E-01	1.47467E-01
24	4.560C0E-06	7.57470E-04	1.87970E-01	1.24230E 00	1.29335E 00	8.39644E-01	3.63825E-01	1.33905E-01
25	0.0	8.93190E-04	2.07019E-01	1.24260E 00	1.24111E 00	7.87467E-01	3.31217E-01	1.19684E-01
26	0.0	1.08160E-03	2.35800E-01	1.24040E 00	1.21710E 00	7.23154E-01	2.93770E-01	1.04215E-01
27	0.0	1.28550E-03	2.60260E-01	1.23880E 00	1.18460E 00	6.78790E-01	2.49360E-01	9.44994E-02
28	0.0	1.45530E-03	2.76679E-01	1.23960E 00	1.16770E 00	6.55691E-01	2.57060E-01	8.97135E-02
29	0.0	1.64770E-03	2.92979E-01	1.24050E 00	1.15250E 00	6.35520E-01	2.46580E-01	8.56879E-02
30	0.0	1.86470E-03	3.09628E-01	1.24340E 00	1.14050E 00	6.18591E-01	2.37851E-01	8.23641E-02
31	0.0	2.11100E-03	3.26290E-01	1.24570E 00	1.12880E 00	6.02980E-01	2.29990E-01	7.94079E-02
32	0.0	2.71540E-03	3.61414E-01	1.25470E 00	1.11190E 00	5.78143E-01	2.17579E-01	7.47628E-02
33	0.0	3.67970E-03	4.07410E-01	1.26700E 00	1.09400E 00	5.51764E-01	2.04695E-01	7.00002E-02
34	0.0	4.42659E-03	4.37121E-01	1.27370E 00	1.08340E 00	5.37199E-01	1.97793E-01	6.74759E-02
35	0.0	5.00900E-03	4.59530E-01	1.27970E 00	1.07790E 00	5.28640E-01	1.93730E-01	6.59978E-02
36	0.0	5.62170E-03	4.81039E-01	1.28640E 00	1.07300E 00	5.20650E-01	1.89960E-01	6.45288E-02
37	0.0	6.42709E-03	5.04909E-01	1.29220E 00	1.06720E 00	5.12420E-01	1.84170E-01	6.32609E-02
38	0.0	7.30459E-03	5.30180E-01	1.29850E 00	1.06210E 00	5.04730E-01	1.82640E-01	6.19920E-02
39	0.0	8.27689E-03	5.55100E-01	1.30090E 00	1.05360E 00	4.95600E-01	1.74640E-01	6.05699E-02
40	0.0	1.06450E-02	6.07196E-01	1.29930E 00	1.03173E 00	4.75850E-01	1.70307E-01	5.76350E-02
41	0.0	1.55510E-02	6.98578E-01	1.30250E 00	1.00457E 00	4.50636E-01	1.59810E-01	5.39605E-02
42	0.0	2.22480E-02	7.76323E-01	1.25910E 00	9.43920E-01	4.12809E-01	1.45259E-01	4.89535E-02
43	0.0	3.18790E-02	7.87410E-01	1.22890E 00	8.95746E-01	4.01933E-01	1.53974E-01	5.85789E-02
44	0.0	4.73180E-02	8.18811E-01	1.23420E 00	8.76602E-01	3.85776E-01	1.47154E-01	5.59389E-02
45	0.0	7.00349E-02	9.40476E-01	1.21010E 00	8.38305E-01	3.62754E-01	1.37944E-01	5.24047E-02
46	0.0	1.01500E-01	1.04550E 00	1.14300E 00	7.73980E-01	3.30358E-01	1.25458E-01	4.75943E-02
47	0.0	1.46600E-01	1.13840E 00	1.05080E 00	6.97597E-01	2.94714E-01	1.11705E-01	4.23865E-02
48	0.0	2.07670E-01	1.18447E 00	9.13930E-01	5.96960E-01	2.50454E-01	9.48917E-02	3.59817E-02
49	0.0	2.28620E-01	8.67015E-01	5.47850E-01	3.52845E-01	1.47263E-01	5.57594E-02	2.11041E-02
50	0.0	0.0	0.0	0.0	0.0	0.0	0.0	0.0
51	0.0	0.0	0.0	0.0	0.0	0.0	0.0	0.0

*Hornyak Button units (erg·cm^2·min/g·h·neutron); Bonner ball units (counts·cm^2/neutron); Response functions are for: The Hornyak button and the 2-in. Cd-covered, 3-in., 5-in., 6-in., 8-in., 10-in., and 12-in. Bonner balls respectively.

Appendix C

SPECIAL COMPUTER CODES

```
LEVEL 21.0 ( JUN 74 )                                    OS/360  FORTRAN H

          COMPILER OPTIONS - NAME=  MAIN,OPT=02,LINECNT=60,SIZE=0000K,
                             SOURCE,EBCDIC,NOLIST,NODECK,LOAD,MAP,NOEDIT,ID,NOXREF
  ISN 0002            COMMON /TRASH/D(1),LIM,N5,N6,DIM( 75000),DUM
  ISN 0003            N5=5
  ISN 0004            N6=6
  ISN 0005            LIM=(LOC(DUM)-LOC(DIM(1)))/4
  ISN 0006            CALL WORKER
  ISN 0007            STOP
  ISN 0008            END
```

```
LEVEL 21.8 ( JUN 74 )                                    OS/360  FORTRAN H

          COMPILER OPTIONS - NAME=  MAIN,OPT=02,LINECNT=60,SIZE=0000K,
                             SOURCE,EBCDIC,NOLIST,NODECK,LOAD,MAP,NOEDIT,ID,NOXREF
  ISN 0002            SUBROUTINE WORKER
  ISN 0003            COMMON /TRASH/D(1),LIM1,N5,N6,LFIX,LFLT,LWTS,LOMU,LETA,LXN,LAMU,
                     1 LBMU,LX,LY,LRBNG,LRBAR,LXNR,LXNN,IGM,ISM,NRING,IA04,N7,DZ,RS,RD
  ISN 0004            DIMENSION KD(1)
  ISN 0005            EQUIVALENCE(KD(1),D(1))
  ISN 0006            DIMENSION TITLE(18)
  ISN 0007            READ(N5,5)(TITLE(I),I=1,18)
  ISN 0008          5 FORMAT(18A4)
  ISN 0009            WRITE(N6,10)(TITLE(I),I=1,18)
  ISN 0010         10 FORMAT(1H1,18A4//)
  ISN 0011            J4=0
  ISN 0012            LFIX=19
  ISN 0013            LFLT=24
  ISN 0014            LWTS=27
                C
                C     READ BLOCK 1
                C
  ISN 0015            J3=0
  ISN 0016            CALL FIDO(5,J3,N5,N6,D,D,D)
  ISN 0017            IF(J3.GT.0)CALL EXIT
  ISN 0019            IST=LFLT-1
  ISN 0020            WRITE(N6,15)(KD(I),I=LFIX,IST)
  ISN 0021         15 FORMAT(1H0,'  IGM NO. OF ENERGY GROUPS',34X,I5
                     1 /1X,'  ISM NO. OF 1-D SN ANGLES ENTERED',26X,I5
                     2 /1X,'NRING NO. OF RADII ON SURFACE DETECTOR',22X,I5
                     3 /1X,' IA04 NO. ANGLES IN 2-D QUADRATURE',26X,I5
                     4  /1X,'   N7 UNIT NO. FOR OUTPUT OF BOUNDARY SOURCE',16X,I5//)
  ISN 0022            IST=LWTS-1
  ISN 0023            WRITE(N6,20)(D(I),I=LFLT,IST)
  ISN 0024         20 FORMAT(1H0,' DZ Z LEVEL OF DISK SURFACE DETECTOR',17X,1PE12.5
                     1 /1X,' RS RADIUS OF SOURCE SPHERE',25X,1PE12.5
                     2 /1X,' RD RADIUS OF DISK DETECTOR SURFACE',18X,1PE12.5//)
  ISN 0025            IA05=IA04+1
  ISN 0026            LOMU=LWTS+IA04
  ISN 0027            LETA=LOMU+2*IA04
                C
                C     READ BLOCKS 2 & 3
                C
  ISN 0028            CALL FIDO(2,J3,N5,N6,D,D,D)
  ISN 0029            J4=J4+J3
  ISN 0030            CALL FIDO(2,J3,N5,N6,D,D,D)
  ISN 0031            J4=J4+J3
  ISN 0032            LETA=LOMU+IA04
  ISN 0033            LXN=LETA+IA04
  ISN 0034            LAMU=LXN+IGM*ISM
  ISN 0035            LBMU=LAMU+ISM
  ISN 0036            LX=LBMU+ISM+1
  ISN 0037            LY=LX+IGM
  ISN 0038            LRBNG=LY
  ISN 0039            LRBAR=LRBNG+NRING+1
  ISN 0040            LXNR=LRBAR+NRING
  ISN 0041            LXNN=LXNR+IGM*(ISM+1)
  ISN 0042            LIM=LXNN+NRING*IA05
  ISN 0043            IF(LIM.LE.LIM1)GO TO 40
  ISN 0045            LEM=LIM-LIM1
  ISN 0046            WRITE(N6,30)LEM
```

```
ISN 0047        30 FORMAT('0STORAGE EXCEEDED BY',I7,3X,'LOCATIONS'/)
ISN 0048           CALL EXIT
ISN 0049        40 CONTINUE
ISN 0050           WRITE(N6,45)LIM
ISN 0051        45 FORMAT('0',I7,3X,'LOCATIONS ARE REQUIRED FOR THIS PROBLEM'//)
              C
              C    READ BLOCK 4
              C
ISN 0052           J3=0
ISN 0053           CALL FIDO(8,J3,N5,N6,0,0,0)
ISN 0054           J4=J4+J3
              C
              C   END OF INPUT DATA
              C
ISN 0055           IF(J4.GT.0)CALL EXIT
ISN 0057           IRB=LRBAR-1
ISN 0058           IRC=LRBNG-1
ISN 0059           DO 60 IR=1,NRING
ISN 0060        60 D(IRB+IR)=0.5*(D(IRC+IR)+D(IRC+IR+1) )
ISN 0061           DO 75 IG=1,IGM
ISN 0062           LCX=LXN*(IG-1)*ISM-1
ISN 0063           DO 75 I=1,ISM
ISN 0064           D(LCX+I)=D(LCX+I)*D(LX+IG-1)
ISN 0065        75 CONTINUE
ISN 0066           WRITE(N6,70)
ISN 0067        70 FORMAT(1H1,7X,'BDRY RADII',3X,'MID-RADII',4X,'WEIGHTS',8X,'ETA',
                  1 11X,'MU',10X,'AMU',10X,'BMU',9X,'SCALE'//)
ISN 0068           CALL WDTB(15,16, 7, 0, 8,11,12,13,N6)
ISN 0069           WRITE(N6,50)
ISN 0070        50 FORMAT('0ANGULAR FLUXES AT MID-COSINE INTERVAL'//)
ISN 0071           CALL WDT(D(LXN),IGM,ISM,1,'ANGL','GRP.',0)
ISN 0072           ISQ=ISM+1
ISN 0073           CALL FLUXB(D(LXN),D(LXNB),D(LAMU),D(LBMU),ISM,ISQ,IGM,N6)
ISN 0074           CALL COEFF(D(LXNB),D(LBMU),D(LRBAR),D(LDMU),D(LETA),D(LWTS),
                  1 D(LXNN),IGM,ISM,NRING,IA04,IA05,N5,N6,N7,ISQ,0Z,25,RD)
ISN 0075           RETURN
ISN 0076           END
```

```
LEVEL 21.8 ( JUN 74 )                                    OS/360  FORTRAN H

          COMPILER OPTIONS - NAME=  MAIN,OPT=02,LINECNT=60,SIZE=0000K,
                             SOURCE,EBCDIC,NOLIST,NODECK,LOAD,MAP,NOEDIT,ID,NOXREF
 ISN 0002            SUBROUTINE COEFF(XNN,RMU,RBAR,DMU,ETA,WTS,XNN,IGM,ISM,NRING,IA04,
                    1 IA05,N5,N6,N7,ISQ,DZ,RS,RD)
 ISN 0003            DIMENSION XNR(ISQ,1),RMU(1),RBAR(1),DMU(1),ETA(1),WTS(1),
                    1 XNN(IA05,1)
 ISN 0004            DATA ISQT/1/
 ISN 0005            REWIND N7
 ISN 0006            YR=0.0
 ISN 0007            ZR=DZ
 ISN 0008            DO 600 IG=1,IGM
 ISN 0009            DO 510 I=1,IA05
 ISN 0010            DO 510 IR=1,NRING
 ISN 0011        510 XNN(I,IR)=0.0
 ISN 0012            DO 400 IR=1,NRING
 ISN 0013            XR=RBAR(IR)
 ISN 0014            IF(XR.GT.RD)GO TO 400
 ISN 0015            DO 350 I=1,IA04
 ISN 0017            CMZ=ETA(I)
 ISN 0018            IF(CMZ*DZ.LT.0.0)GO TO 350
 ISN 0020            SM=SQRT(1.0-CMZ**2)
 ISN 0021            CMX=DMU(I)
 ISN 0022            SUM=CMX**2+CMZ**2
 ISN 0023            IF(SUM-1.015,10,10
 ISN 0024          5 CMY=SQRT(1.0-SUM)
 ISN 0025            GO TO 15
 ISN 0026         10 CMX=SIGN(SM,CMX)
 ISN 0027            CMY=0.0
 ISN 0028         15 CONTINUE
 ISN 0029            BR=CMX*XR+CMY*YR+CMZ*ZR
 ISN 0030            CC=RS**2-XR**2-YR**2-ZR**2
 ISN 0031            DISC=BR**2+CC
 ISN 0032            IF(DISC.LT.0.0)GO TO 350
 ISN 0034            DISC=SQRT(DISC)
 ISN 0035            DIS=BR-DISC
 ISN 0036            IF(DIS.LE.0.0)GO TO 350
 ISN 0038            X=XR-DIS*CMX
 ISN 0039            Y=YR-DIS*CMY
 ISN 0040            Z=ZR-DIS*CMZ
 ISN 0041            DOT=(X*CMX+Y*CMY+Z*CMZ)/RS
 ISN 0042            DO 20 IA=1,ISM
 ISN 0043            IF(DOT.LE.RMU(IA+1))GO TO 30
 ISN 0045         20 CONTINUE
 ISN 0046            IA=ISM
 ISN 0047         30 CONTINUE
 ISN 0048            SLOPE=(XNR(IA+1,IG)-XNR(IA,IG))/(RMU(IA+1)-RMU(IA))
 ISN 0049            FLX=XNR(IA,IG)+SLOPE*(DOT-RMU(IA))
 ISN 0050            XNN(I,IR)=FLX*DOT/ABS(CMZ)
 ISN 0051        350 CONTINUE
 ISN 0052        400 CONTINUE
 ISN 0053            DO 570 I=1,IA04
 ISN 0054            IF(ETA(I)*DZ.LE.0.0)GO TO 570
 ISN 0056            DO 565 IR=1,NRING
 ISN 0057            IF(XNN(I,IR).LT.0.0)XNN(I,IR)=0.0
 ISN 0059        565 XNN(IA05,IR)=XNN(IA05,IR)+XNN(I,IR)*WTS(I)
 ISN 0060        570 CONTINUE
                 C
                 C  PRINTS GROUP 1 FLUXES ONLY IF ISQT .GT. 0
                 C
 ISN 0061            IF(ISQT.GT.0.AND.IG.GT.1)GO TO 595
 ISN 0063            WRITE(N6,590)IG
 ISN 0064        590 FORMAT('0ANGULAR FLUXES FOR GROUP',I5//)
 ISN 0065            CALL WCT(XNN,NRING,IA05,1,'ANGL','RING',0)
 ISN 0066        595 CONTINUE
 ISN 0067            WRITE(N7)((XNN(I,IR),I=1,IA04),IR=1,NRING)
 ISN 0068        600 CONTINUE
 ISN 0069            REWIND N7
 ISN 0070            RETURN
 ISN 0071            END
```

```
LEVEL 21.8 ( JUN 74 )                                    OS/360  FORTRAN H

          COMPILER OPTIONS - NAME=  MAIN,OPT=02,LINECNT=60,SIZE=0000K,
                             SOURCE,EBCDIC,NOLIST,NODECK,LOAD,MAP,NOEDIT,ID,NOXREF
  ISN 0002            SUBROUTINE FLUX*(XN,XNB,AMU,RMU,ISM,ISQ,IGM,N6)
  ISN 0003            DIMENSION XN(ISM,1),XNB(ISQ,1),AMU(1),RMU(1)
  ISN 0004            DO 20 IG=1,IGM
  ISN 0005            SLOPE=(XN(ISM,IG)-XN(ISM-1,IG))/(AMU(ISM)-AMU(ISM-1))
  ISN 0006            XNB(ISQ,IG)=XN(ISM-1,IG)+SLOPE*(RMU(ISQ)-AMU(ISM-1))
  ISN 0007            DO 10 I=2,ISQ
  ISN 0008            IA= ISQ+1-I
  ISN 0009            XNB(IA,IG)=2.0*XN(IA,IG)-XNB(IA+1,IG)
  ISN 0010            IF(XNB(IA,IG).LE.0.0)XNB(IA,IG)=XN(IA,IG)
  ISN 0012         10 CONTINUE
  ISN 0013         20 CONTINUE
  ISN 0014            WRITE(N6,30)
  ISN 0015         30 FORMAT('0ANGULAR FLUXES AT COSINE BOUNDARIES'//)
  ISN 0016            CALL WDT(XNB,IGM,ISQ,1,'ANGL','GRP.',0)
  ISN 0017            RETURN
  ISN 0018            END
```

```
LEVEL 21.8 ( JUN 74 )                                    OS/360  FORTRAN H

          COMPILER OPTIONS - NAME=  MAIN,OPT=02,LINECNT=60,SIZE=0000K,
                             SOURCE,ERRORS,NOLIST,NODECK,LOAD,MAP,NOREF,ID,NOXREF
 ISN 0002            SUBROUTINE FIND(L12,J3,N5,N6,J,LDTK,LBB)                          ANSN 507
                 C   *** GENERALIZED INPUT ROUTINE - NOTE ABSENCE OF SPACE MASTING GO TO ANSN 508
                 C       FOUND IN DTF-II                                                ANSN 509
 ISN 0003            DIMENSION IN(37),K(37),V(37),LDTK(1),FMT(3),VMT(19),D(1),LBA(1)   ANSN 510
 ISN 0004            EQUIVALENCE (B9,LBB)                                              ANSN 511
 ISN 0005            DATA LDL,LS,LRL,LI,LT,LSS/'S   ','D   ','R   ','I   ','T   ',     ANSN 512
                    1'S   '/                                                           ANSN 513
 ISN 0006            DATA FMT(1),E1,E2,E3,E4/'(1X,','10E1','2.5','10I1','2)  '/        ANSN 514
 ISN 0007            DATA LF,L1,LAP,LPL,LMI/'F   ','A   ','E   ','+   ','-   '/         ANSN 515
 ISN 0008            DATA LZ,LV,LU,BP/'Z   ','V   ','U   ','.   '/                      ANSN 516
 ISN 0009            DATA LO,LM,LN/'O   ','M   ','N   '/,LE/'E   '/,LLI/'L   '/        ANSN 517
 ISN 0010            DATA LKI/'K   '/                                                   ANSN 518
 ISN 0011            DIMENSION PRT(3)                                                   ANSN 519
 ISN 0012            DATA LC,LC,PRT(1),PRT(2),PRT(3),IPRTSG/'C   ','C   ','PRE ',      ANSN 520
                    1  'PRT ','CPU ','-1'/                                              ANSN 521
 ISN 0013            J=0                                                                ANSN 522
 ISN 0014            J3=0                                                               ANSN 523
 ISN 0015            III=0                                                              ANSN 524
 ISN 0016            IVMT=0                                                             ANSN 525
 ISN 0017            NCOUNT=0                                                           ANSN 526
 ISN 0018          1 CALL FFREAD(IN,K,V,NF,NE,N4,IPRTSG)                                ANSN 527
 ISN 0019            DO 27 I=1,NF                                                       ANSN 528
 ISN 0020            IF(K(I).NE.LPL .AND. K(I).NE.LAP .AND. K(I).NE.LMI)GO TO 27        ANSN 529
                 C   *** EXPONENTIATION (E,+,-)                                         ANSN 530
 ISN 0022            L=IN(I)                                                            ANSN 531
 ISN 0023            IF(L.EQ.0)GO TO 27                                                 ANSN 532
 ISN 0025            E=10.0**L                                                          ANSN 533
 ISN 0026            IF(K(I).EQ.LMI)GO TO 28                                            ANSN 534
 ISN 0028            V(I)=V(I)*E                                                        ANSN 535
 ISN 0029            GO TO 27                                                           ANSN 536
 ISN 0030         28 V(I)=V(I)/E                                                        ANSN 537
 ISN 0031         27 CONTINUE                                                           ANSN 538
 ISN 0032       1002 DO 2 I=1,NF                                                        ANSN 539
 ISN 0033            IF(III.EQ.0)GO TO 4                                                ANSN 540
 ISN 0035            IF(III-2)3,44,48                                                   ANSN 541
 ISN 0036          4 III=0                                                              ANSN 542
 ISN 0037            IF(K(I).EQ.LBB)GO TO 14                                            ANSN 543
 ISN 0039            IF(K(I).EQ.LDL)GO TO 5                                             ANSN 544
 ISN 0041            IF(K(I).EQ.LS )GO TO 6                                             ANSN 545
 ISN 0043            IF(K(I).EQ.LRL)GO TO 7                                             ANSN 546
 ISN 0045            IF(K(I).EQ.LI )GO TO 8                                             ANSN 547
 ISN 0047            IF(K(I).EQ.LT )GO TO 9                                             ANSN 548
 ISN 0049            IF(K(I).EQ.LSS)GO TO 11                                            ANSN 549
 ISN 0051            IF(K(I).EQ.LF)GO TO 23                                             ANSN 550
 ISN 0053            IF(K(I).EQ.LA)GO TO 26                                             ANSN 551
 ISN 0055            IF(K(I).EQ.LZ)GO TO 31                                             ANSN 552
 ISN 0057            IF(K(I).EQ.LE)GO TO 39                                             ANSN 553
 ISN 0059            IF(K(I).EQ.LO)GO TO 35                                             ANSN 554
 ISN 0061            IF(K(I).EQ.LM .OR. K(I).EQ.LN)GO TO 36                             ANSN 555
 ISN 0063            IF(K(I).EQ.LU)GO TO 33                                             ANSN 556
 ISN 0065            IF(K(I).EQ.LV)GO TO 34                                             ANSN 557
 ISN 0067            IF(K(I).EQ.LLI)GO TO 42                                            ANSN 558
 ISN 0069            IF(K(I).EQ.LKI)GO TO 46                                            ANSN 559
 ISN 0071            IF(K(I).EQ.LD)GO TO 55                                             ANSN 560
 ISN 0073            IF(K(I).EQ.LC)GO TO 56                                             ANSN 561
 ISN 0075            GO TO 14                                                           ANSN 562
                 C   *** TERMINATE (T)                                                  ANSN 563
 ISN 0076          9 J2=0                                                               ANSN 564
 ISN 0077            ITEST=IN(I)                                                        ANSN 565
 ISN 0078            IF(J.EQ.0)GO TO 16                                                 ANSN 566
 ISN 0080            GO TO 12                                                           ANSN 567
                 C   *** VARIABLE FORMAT CONTROL (U,V)                                  ANSN 568
 ISN 0081         33 READ(N5,80)VMT                                                     ANSN 569
 ISN 0082         34 IVMT=1                                                             ANSN 570
```

```
                C    *** BEGIN NEW ARRAY (*,S)
ISN 0083          6 KKK=0
ISN 0084            GO TO 13
ISN 0085          5 KKK=1
ISN 0086         13 IF(NCOUNT+J .EQ. 0)GO TO 15
ISN 0088            J2=1
ISN 0089         12 WRITE (N6,20) LL,LB,J
ISN 0090            IF(J.EQ.NCOUNT)GO TO 16
ISN 0092            IMAX=J1 + J - 1
ISN 0093            IMAX=MIN0(IMAX,J1+999)
ISN 0094            WRITE (N6,30) NCOUNT,LL,LB
ISN 0095            FMT(2)=F1
ISN 0096            FMT(3)=F2
ISN 0097            IF(KK.NE.1)GO TO 22
ISN 0099            FMT(2)=F3
ISN 0100            FMT(3)=F4
ISN 0101         22 WRITE (N6,FMT) (D(II),II=J1,IMAX)
ISN 0102            J3=J3 + 1
ISN 0103         16 IF(J2.NE.0)GO TO 15
ISN 0105            WRITE(N6,50,IN(I),LT
ISN 0106            RETURN
ISN 0107         15 LL=IN(I)
ISN 0108            LL3=LL + LL2 - 1
ISN 0109            KK=KKK
ISN 0110            LB=K(I)
ISN 0111            J=V(I)
ISN 0112            J1=LBA(LL3) + J
ISN 0113            NCOUNT=LBA(LL3+1) - LBA(LL3) - J
ISN 0114         41 J=0
ISN 0115            IF(IVMT.EQ.0)GO TO 2
                C    *** VARIABLE FORMAT CONTROL (U,V)
ISN 0117         32 IF(NCOUNT.EQ.0)GO TO 1
ISN 0119            J=NCOUNT
ISN 0120            NCC=J1 + NCOUNT - 1
ISN 0121            READ(N5,VMT) (D(J2),J2=J1,NCC)
ISN 0122            IVMT=0
ISN 0123            GO TO 1
                C    *** FILL ARRAY (F)
ISN 0124         23 IF(J.GE.NCOUNT)GO TO 25
ISN 0126            NCC=J+1
ISN 0127            DO 24 II=NCC,NCOUNT
ISN 0128            J2=J1 + II -1
ISN 0129            D(J2)=V(I)
ISN 0130         24 IF(KK.NE.0)LDTK(J2)=V(I)
ISN 0132            J=NCOUNT
ISN 0133            GO TO 2
ISN 0134         25 WRITE (N6,60) LL,LB
ISN 0135            GO TO 2
                C    *** END ARRAY (E)
ISN 0136         39 IF(J.LE.NCOUNT)J=NCOUNT
ISN 0138            GO TO 2
                C    *** ADDRESS MODIFICATION (A)
ISN 0139         26 J=V(I)
ISN 0140            IF(J.GT.NCOUNT .OR. J.LE.0)WRITE(N6,70)J,LL,LB
ISN 0142            J=J-1
ISN 0143            GO TO 2
                C    *** SKIP (S)
ISN 0144         11 J=J + IN(I)
ISN 0145            GO TO 2
                C    *** TURN PRINT TRIGGER ON/OFF
ISN 0146         55 IPRTRG=-IPRTRG
ISN 0147            WRITE(N6,110)PRT(2),PRT(IPRTRG+2),IN(I),LD
ISN 0148        110 FORMAT(' ',T53,2A4,I7,A1)
ISN 0149            GO TO 2
                C    *** PRINT COUNT IN CURRENT ARRAY
ISN 0150         56 WRITE(N6,90)LL,LB,J,IN(I),LC
ISN 0151            GO TO 2
ISN 0152         90 FORMAT(T90,I5,A1,' ARRAY',I7,' ENTRIES READ AT',I4,A1)
                C    *** NO MODIFICATION
ISN 0153         14 CONTINUE
ISN 0154         17 J2=J1 + J
ISN 0155            D(J2)=V(I)
ISN 0156            IF(KK.NE.0)LDTK(J2)=V(I)
ISN 0158            J=J + 1
ISN 0159            GO TO 2
```

```
C     *** ZERO (Z)
   31 IN(I)=V(I) + IN(I)
      V(I)=0.0
C     *** REPEAT (R)
    7 L=IN(I)
      DO 18 II=1,L
      J2=J1 + J
      D(J2)=V(I)
      IF(KK.NE.0)LDTK(J2)=V(I)
   18 J=J + 1
      GO TO 2
C     *** SEQUENCE REPEAT (Q)
   35 L=V(I) + IN(I)
      LSEQ=1
      IF(V(I).EQ.0.0  .OR.  IN(I).EQ.0)GO TO 51
      L=V(I)
      LSEQ=IN(I)
   51 DO 52 LSQ=1,LSEQ
      DO 37 II=1,L
      J2=J1 + J
      J4=J2 - L
      D(J2)=D(J4)
   37 J=J + 1
   52 CONTINUE
      GO TO 2
C     *** INVERTED SEQUENCE REPEAT (N)
   36 L=V(I) + IN(I)
      LSEQ=1
      IF(V(I).EQ.0.0  .OR.  IN(I).EQ.0)GO TO 53
      L=V(I)
      LSEQ=IN(I)
   53 DO 54 LSQ=1,LSEQ
      DO 38 II=1,L
      J2=J1 + J
      J4=J2 - II - II + 1
      D(J2)=D(J4)
C     *** REVERSED SIGN INVERTED SEQUENCE REPEAT (M)
      IF(K(I).NE.LM)GO TO 38
      IF(KK.NE.0)GO TO 57
      D(J2)=-D(J2)
      GO TO 38
   57 LDTK(J2)=-LDTK(J2)
   38 J=J + 1
   54 CONTINUE
      GO TO 2
C     *** LOGARITHMIC INTERPOLATION (L)
   42 L=IN(I) + 1
      VV=V(I)
      III=2
      GO TO 2
   44 DEL=EXP(ALOG(V(I)/VV)/L)
      J2=J1 + J
      D(J2)=VV
      J=J + 1
      DO 45 II=2,L
      J2=J1 + J
      D(J2)=DEL*D(J2-1)
   45 J=J + 1
      IF(III.NE.0)GO TO 4
      GO TO 2
C     *** FIXED 10 LOG INTERP.  (K)
   46 L=IN(I) + 1
      VV=V(I)
      III=3
      GO TO 2
   48 DIF=(V(I)-VV)*.1111111
      DEL=EXP(2.302585/L)
      J2=J1 + J
      D(J2)=VV
      VV=VV-DIF
      J=J+1
      DO 49 II=2,L
      J2=J1 + J
      DIF=DIF*DEL
      D(J2)=VV + DIF
   49 J=J+1
      IF(III.NE.0)GO TO 4
      GO TO 2
```

```
                C    *** INTERPOLATE (I)                                                  ANSN 724
ISN 0238          8 L=IN(I) + 1                                                          ANSN 725
ISN 0239            VV=V(I)                                                              ANSN 726
ISN 0240            III=1                                                                ANSN 727
ISN 0241            GO TO 2                                                              ANSN 728
ISN 0242          3 DEL=(V(I)-VV)/FLOAT(L)                                               ANSN 729
ISN 0243            DO 21 II=1,L                                                         ANSN 730
ISN 0244            J2=J1 + J                                                            ANSN 731
ISN 0245            DELT=DEL*FLOAT(II-1) + VV                                            ANSN 732
ISN 0246            D(J2)=      DELT                                                     ANSN 733
ISN 0247            IF(KK.NE.0)LDTK(J2)=DELT + SIGN(0.5,DEL)                             ANSN 734
ISN 0249         21 J=J + 1                                                              ANSN 735
ISN 0250            IF(III.NE.0)GO TO 4                                                  ANSN 736
ISN 0252            GO TO 2                                                              ANSN 737
ISN 0253          2 CONTINUE                                                             ANSN 738
ISN 0254            GO TO 1                                                              ANSN 739
ISN 0255         20 FORMAT(1H0,I5,A1,6H ARRAY,I7,13H ENTRIES READ)                       ANSN 740
ISN 0256         30 FORMAT(14H0****** ERROR I7,20H ENTRIES REQUIRED IN I3,A1,6H ARRAY/ANSN 741
                  1 '          FIRST 1000 ENTRIES PRINTED')                              ANSN 742
ISN 0257         50 FORMAT(1H0,I5,A1)                                                    ANSN 743
ISN 0258         60 FORMAT(31H0****** FILL OPTION IGNORED IN I2,A1,6H ARRAY)             ANSN 744
ISN 0259         70 FORMAT(24H0****** WARNING  ADDRESS I7,20H IS BEYOND LIMITS OF I3,A1,ANSN 745
                  1 6H ARRAY)                                                            ANSN 746
ISN 0260         80 FORMAT(18A4)                                                         ANSN 747
ISN 0261            END                                                                  ANSN 748
```

```
LEVEL 21.9 ( JUN 74 )                          OS/360  FORTRAN H

        COMPILER OPTIONS - NAME=  MAIN,OPT=02,LINECNT=60,SIZE=0000K,
                           SOURCE,EBCDIC,NOLIST,NODECK,LOAD,MAP,NOEDIT,ID,NOXREF
 ISN 0002          SUBROUTINE FEREAD(IN,K,V,NF,N5,N6,IPRTRG)                          ANSN 749
 ISN 0003          DIMENSION NY(80),IN(2),K(2),V(2),N(10)                             ANSN 750
 ISN 0004          DATA NT,NBB,NDP,NPL,NPA,NMI/'T    ','    ','.    ','+    ','F    ',  ANSN 751
                  1                                '-    '/,NSS/'S    '/                ANSN 752
 ISN 0005          DATA NOL,NS,NF/'*    ','*    ','F    '/                             ANSN 753
 ISN 0006          DATA NO,NM,NN/'O    ','M    ','N    '/                             ANSN 754
 ISN 0007          DATA NR,NI,NFF,NA,NL,NK/'R    ','I    ','F    ','A    ','L    ','K    '/ANSN 755
 ISN 0008          DATA NSL/Z7040404D/                                                ANSN 756
 ISN 0009          DATA IFREF,N/0,'0    1    2    3    4    5    6    7    8    9    '/  ANSN 757
 ISN 0010     1998 DO 1 I=1,37                                                        ANSN 758
 ISN 0011          IN(I)=0                                                            ANSN 759
 ISN 0012          V(I)=0.0                                                           ANSN 760
 ISN 0013        1 K(I)=NBB                                                           ANSN 761
 ISN 0014          IEXP=0                                                             ANSN 762
 ISN 0015          NSCL=0                                                             ANSN 763
 ISN 0016          NDPN=0                                                             ANSN 764
 ISN 0017          IEX=0                                                              ANSN 765
 ISN 0018          NUM=0                                                              ANSN 766
 ISN 0019          ISGN=1                                                             ANSN 767
 ISN 0020          IBLNK=0                                                            ANSN 768
 ISN 0021          NF=1                                                               ANSN 769
 ISN 0022          NCC=1                                                              ANSN 770
 ISN 0023          IEC=0                                                              ANSN 771
 ISN 0024          IDS=0                                                              ANSN 772
 ISN 0025      112 READ (N5,10) NY                                                    ANSN 773
 ISN 0026          IF(IPRTRG.GT.0)WRITE(N6,30)NY                                      ANSN 774
 ISN 0028       30 FORMAT(' ',T53,80A1)                                               ANSN 775
 ISN 0029          IF(NY(1).NE.NSL)GO TO 111                                          ANSN 776
 ISN 0031          WRITE(N6,10)(NY(I),I=2,80)                                         ANSN 777
 ISN 0032          GO TO 112                                                          ANSN 778
 ISN 0033       10 FORMAT(80A1)                                                       ANSN 779
 ISN 0034      111 NYNCC=NY(NCC)                                                      ANSN 780
 ISN 0035          IF(IFREF.EQ.0)GO TO 122                                            ANSN 781
 ISN 0037          IEC=IEC+1                                                          ANSN 782
 ISN 0038          IF(IEC.GT.12)IEC=1                                                 ANSN 783
 ISN 0040          IF(IEC.EQ.3)GO TO 124                                              ANSN 784
 ISN 0042          IF(IEC.EQ.11 .AND. IEX.NE.0 .AND. NYNCC.EQ.NBB)GO TO 106           ANSN 785
 ISN 0044          IF(NYNCC.EQ.NF .AND. IEC.GT.4)GO TO 203                            ANSN 786
 ISN 0046      122 IF(NYNCC.EQ.NBB)GO TO 101                                          ANSN 787
 ISN 0048          IF(NYNCC.EQ.NPL .OR. NYNCC.EQ.NPA)GO TO 103                        ANSN 788
 ISN 0050          IF(NYNCC.EQ.NMI)GO TO 104                                          ANSN 789
 ISN 0052          IF(NYNCC.EQ.NF .AND. IBLNK.EQ.1)GO TO 203                          ANSN 790
 ISN 0054          IBLNK=1                                                            ANSN 791
 ISN 0055          IF(NYNCC.EQ.NDP)GO TO 102                                          ANSN 792
 ISN 0057      124 DO 1024 I=1,10                                                     ANSN 793
 ISN 0058          IF(NYNCC.NE.N(I))GO TO 1024                                        ANSN 794
 ISN 0060          NUMM=I-1                                                           ANSN 795
 ISN 0061          IF(IEX.NE.0)GO TO 107                                              ANSN 796
 ISN 0063          GO TO 105                                                          ANSN 797
 ISN 0064     1024 CONTINUE                                                           ANSN 798
 ISN 0065      121 IF(K(NF).NE.NBB .AND. NYNCC.EQ.NBB)GO TO 101                       ANSN 799
 ISN 0067          K(NF)=NYNCC                                                        ANSN 800
 ISN 0068          IN(NF)=NUM                                                         ANSN 801
 ISN 0069          NUM=0                                                              ANSN 802
 ISN 0070          IBLNK=0                                                            ANSN 803
 ISN 0071          IF(NYNCC.EQ.NBB)GO TO 106                                          ANSN 804
 ISN 0073          IF(K(NF).NE.NOL .AND. K(NF).NE.NS)GO TO 113                        ANSN 805
 ISN 0075          IFREF=0                                                            ANSN 806
 ISN 0076          IDS=1                                                              ANSN 807
 ISN 0077          IF(NF.EQ.1)GO TO 108                                               ANSN 808
 ISN 0079          IF(K(NF).NE.K(NF-1))GO TO 108                                      ANSN 809
 ISN 0081          IDS=0                                                              ANSN 810
 ISN 0082          K(NF)=NBB                                                          ANSN 811
 ISN 0083          GO TO 106                                                          ANSN 812
```

```
ISN 0084      113 IF(IFREE.EQ.0 .AND.                                                  ANSN 813
                 1   NYNCC.NE.NR .AND. NYNCC.NE.NI .AND. NYNCC.NE.NEE .AND.            ANSN 814
                 1   NYNCC.NE.NA .AND. NYNCC.NE.NL .AND. NYNCC.NE.NK .AND.             ANSN 815
                 2   NYNCC.NE.NO .AND. NYNCC.NE.NM .AND. NYNCC.NE.NN )GO TO 108         ANSN 816
ISN 0086          IF(IFREE.EQ.1 .AND. NYNCC.EQ.NSS)GO TO 108                           ANSN 817
ISN 0088          IF(NCC.EQ.72)WRITE(NE,20)NY                                          ANSN 818
ISN 0090       20 FORMAT('0 ****** INCOMPLETE FIELD AT END OF CARD, SOME DATA MAY BE   ANSN 819
                 1 LOST'/'          CARD IMAGE FOLLOWS'/' '80A1)                       ANSN 820
ISN 0091          GO TO 106                                                            ANSN 821
ISN 0092      105 NUM=NUM*10 + NUMM                                                    ANSN 822
ISN 0093          NSCL=NSCL + NDPN                                                     ANSN 823
ISN 0094          GO TO 206                                                            ANSN 824
ISN 0095      102 NDPN=-1                                                              ANSN 825
ISN 0096          GO TO 206                                                            ANSN 826
ISN 0097      107 IEXP=IEXP*10 + IEX*NUMM                                              ANSN 827
ISN 0098      206 IF(IFC.EQ.12)GO TO 301                                               ANSN 828
ISN 0100          GO TO 106                                                            ANSN 829
ISN 0101      103 IF(NUM.NE.0)GO TO 203                                                ANSN 830
ISN 0103          ISGN=1                                                               ANSN 831
ISN 0104          GO TO 106                                                            ANSN 832
ISN 0105      203 IEX=1                                                                ANSN 833
ISN 0106          GO TO 106                                                            ANSN 834
ISN 0107      104 IF(NUM.NE.0)GO TO 204                                                ANSN 835
ISN 0109          ISGN=-1                                                              ANSN 836
ISN 0110          GO TO 106                                                            ANSN 837
ISN 0111      204 IEX=-1                                                               ANSN 838
ISN 0112          GO TO 106                                                            ANSN 839
ISN 0113      123 IFREE=1                                                              ANSN 840
ISN 0114          IDS=0                                                                ANSN 841
ISN 0115          GO TO 109                                                            ANSN 842
ISN 0116      101 IF(IDS.EQ.1)GO TO 123                                                ANSN 843
ISN 0118          IF(IFREE.EQ.1 .AND. IFC.EQ.12 .AND. K(NE).NE.NBB)GO TO 301           ANSN 844
ISN 0120          IF(IBLNK.EQ.0)GO TO 106                                              ANSN 845
ISN 0122          IF(IFREE.EQ.1 .AND. IFC.NE.12)GO TO 106                              ANSN 846
ISN 0124      301 VNUM=ISGN*NUM                                                        ANSN 847
ISN 0125          V(NE)=VNUM*10.0**(IEXP+NSCL)                                         ANSN 848
ISN 0126          NDPN=0                                                               ANSN 849
ISN 0127          IEX=0                                                                ANSN 850
ISN 0128          IEXP=0                                                               ANSN 851
ISN 0129          NSCL=0                                                               ANSN 852
ISN 0130          IBLNK=0                                                              ANSN 853
ISN 0131          NUM=0                                                                ANSN 854
ISN 0132          ISGN=1                                                               ANSN 855
ISN 0133      108 NE=NE + 1                                                            ANSN 856
ISN 0134          IF(NYNCC.EQ.NSS)GO TO 106                                            ANSN 857
ISN 0136      109 IFC=0                                                                ANSN 858
ISN 0137          IF(IFREE.EQ.1)NCC=((NCC+11)/12)*12                                   ANSN 859
ISN 0139          IF(K(NE-1).EQ.NT)GO TO 999                                           ANSN 860
ISN 0141      106 IF(NCC.GE.73)GO TO 999                                               ANSN 861
ISN 0143          NCC=NCC+1                                                            ANSN 862
ISN 0144          IF(NCC.LE.72)GO TO 111                                               ANSN 863
ISN 0146          GO TO 101                                                            ANSN 864
ISN 0147      999 NE=NE-1                                                              ANSN 865
ISN 0148          IF(NE.LE.0)GO TO 1998                                                ANSN 866
ISN 0150          RETURN                                                               ANSN 867
ISN 0151          END                                                                  ANSN 868
```

```
LEVEL 21.8 ( JUN 74 )                                    OS/360  FORTRAN H

          COMPILER OPTIONS - NAME=  MAIN,OPT=02,LINECNT=60,SIZE=0000K,
                             SOURCE,EBCDIC,NOLIST,NODECK,LOAD,MAP,NOEDIT,ID,NOXREF
 ISN 0002            SUBROUTINE WOT(X,NCOL,LTBL,LG,TOP1,TOP2,TOP3)
 ISN 0003            DIMENSION X(LTBL,NCOL,1)
 ISN 0004            N6=6
 ISN 0005            DO 1 L=1,LG
 ISN 0006            IO2=0
 ISN 0007            IO3=(NCOL+7)/8
 ISN 0008            IF(LG.GT.1)WRITE(N6,10)TOP3,L
 ISN 0010         10 FORMAT(/1H0,2X,A4,I5)
 ISN 0011            DO 2 I=1,IO3
 ISN 0012            IO1=IO2+1
 ISN 0013            IO2=MIN0(IO1+7,NCOL)
 ISN 0014            WRITE(N6,20)TOP1,(TOP2,J,J=IO1,IO2)
 ISN 0015            DO 3 K=1,LTBL
 ISN 0016            IF(K.EQ.1)GO TO 4
 ISN 0018            DO 6 J=IO1,IO2
 ISN 0019            IF(X(K,J,L).NE.X(K-1,J,L))GO TO 7
 ISN 0021          6 CONTINUE
 ISN 0022            IF(KE.EQ.KS)GO TO 3
 ISN 0024            KE=K
 ISN 0025            IF(K.EQ.LTBL)GO TO 7
 ISN 0027            GO TO 3
 ISN 0028          8 IF(K.EQ.LTBL)GO TO 4
 ISN 0030            DO 9 J=IO1,IO2
 ISN 0031            IF(X(K,J,L).NE.X(K+1,J,L))GO TO 4
 ISN 0033          9 CONTINUE
 ISN 0034            KE=KE+1
 ISN 0035            GO TO 3
 ISN 0036          7 IF(KE.EQ.KS)GO TO 4
 ISN 0038            WRITE(N6,40)TOP1,KS,TOP1,KE
 ISN 0039            IF(K.EQ.LTBL.AND.KE.EQ.K)GO TO 3
 ISN 0041         40 FORMAT(8X,A4,I5,6H THRU ,A4,I5,14H SAME AS ABOVE )
 ISN 0042          4 WRITE(N6,30)K,(X(K,J,L),J=IO1,IO2)
 ISN 0043            KS=K+1
 ISN 0044            KE=KS
 ISN 0045          3 CONTINUE
 ISN 0046          2 CONTINUE
 ISN 0047          1 CONTINUE
 ISN 0048         20 FORMAT(2H0 ,A4,3X,A4,I3,7(6X,A4,I3))
 ISN 0049         30 FORMAT(I6,1PBE13.5)
 ISN 0050            RETURN
 ISN 0051            END
```

```
LEVEL 21.8 ( JUN 74 )                          OS/360  FORTRAN H

        COMPILER OPTIONS - NAME=  MAIN,OPT=02,LINECNT=50,SIZE=0000K,
                           SOURCE,EBCDIC,NOLIST,NODECK,LOAD,MAP,NOEDIT,ID,NOXREF
 ISN 0002          SUBROUTINE WOTB(L1,L2,L3,L4,L5,L6,L7,L8,NOU)                    ANSN0010
             C   *** WOTB  WILL WRITE UP TO EIGHT ONE-DIMENSIONAL ARRAYS OF VARYING  ANSN0020
             C       LENGTHS IN COLUMNS ACROSS A PAGE. L1,L2,ETC. ARE THE POSITIONS  ANSN0030
             C       IN COMMON OF THE BASE ADDRESSES OF THE ARRAYS TO BE WRITTEN.    ANSN0040
 ISN 0003          COMMON /TRASH/ D(1)
             C       IF ANY LN IS ZERO THE N-TH COLUMN WILL BE BLANK.                ANSN0050
 ISN 0004          DIMENSION EPT(19),ENT(6),L(8),M(8),Z(8),LD(1)                   ANSN0070
 ISN 0005          EQUIVALENCE (D(1),LD(1))                                        ANSN0080
 ISN 0006          DATA B/'    '/                                                  ANSN0090
 ISN 0007          DATA K,EPT(1),EPT(2),EPT(19)/100000,'(1P1','6   ','1'   '/      ANSN0100
 ISN 0008          DATA  ENT(1),ENT(2),ENT(3),ENT(4),ENT(5),ENT(6)/',F13','5   ',  ANSN0110
                 1 ',I9,','5X  ','9X,','A4  '/                                     ANSN0120
 ISN 0009          L(1)=L1                                                         ANSN0130
 ISN 0010          L(2)=L2                                                         ANSN0140
 ISN 0011          L(3)=L3                                                         ANSN0150
 ISN 0012          L(4)=L4                                                         ANSN0160
 ISN 0013          L(5)=L5                                                         ANSN0170
 ISN 0014          L(6)=L6                                                         ANSN0180
 ISN 0015          L(7)=L7                                                         ANSN0190
 ISN 0016          L(8)=L8                                                         ANSN0200
 ISN 0017          N=0                                                             ANSN0210
 ISN 0018          DO 1 I=1,8                                                      ANSN0220
 ISN 0019          LL=L(I)                                                         ANSN0230
 ISN 0020          M(I)=0                                                          ANSN0240
 ISN 0021          IF(LL.NE.0)M(I)=LD(LL+1)-LD(LL)                                 ANSN0250
 ISN 0023        1 N=MAX0(N,M(I))                                                  ANSN0260
 ISN 0024          DO 2 I=1,N                                                      ANSN0270
 ISN 0025          DO 3 J=1,8                                                      ANSN0280
 ISN 0026          IF(M(J).GE.I) GO TO 4                                           ANSN0290
 ISN 0028          Z(J)=B                                                          ANSN0300
 ISN 0029          EPT(2*J+1)=ENT(5)                                               ANSN0310
 ISN 0030          EPT(2*J+2)=ENT(6)                                               ANSN0320
 ISN 0031          GO TO 3                                                         ANSN0330
 ISN 0032        4 LL=L(J)                                                         ANSN0340
 ISN 0033          LL=LD(LL) + I - 1                                               ANSN0350
 ISN 0034          Z(J)=D(LL)                                                      ANSN0360
 ISN 0035          EPT(2*J+1)=ENT(1)                                               ANSN0370
 ISN 0036          EPT(2*J+2)=ENT(2)                                               ANSN0380
 ISN 0037          IF(K.LE.IABS(LD(LL)))GO TO 3                                    ANSN0390
 ISN 0039          EPT(2*J+1)=ENT(3)                                               ANSN0400
 ISN 0040          EPT(2*J+2)=ENT(4)                                               ANSN0410
 ISN 0041        3 CONTINUE                                                        ANSN0420
 ISN 0042        2 WRITE (NOU,EPT) I,(Z(J),J=1,8)                                  ANSN0430
 ISN 0043          RETURN                                                          ANSN0440
 ISN 0044          END                                                             ANSN0450
```

DISKTRAN

DISKTRAN is a computer code which uses the angular fluxes from the DOT scalar flux and moments data set (or any disk boundary source) to calculate responses at detectors within a void. The angular flux in a localized quadrature is computed at the detector position and is summed with weights to give the total flux. Variation of the angular flux over the DOT quadrature is allowed to be constant, linear, or exponential in both the azimuthal and polar directions. Linear and exponential variation with radius are options.

DISKTRAN Input

R-Z Problem top and bottom boundary angular fluxes (all directions) are input on unit 1.

1$ [12 entries]

IGM	Number of groups
IM	Number of I-intervals for boundary source
MM	Number of directions in boundary source quadrature
ND	Number of detectors
NRESP	Number of response functions
NN	Spare (enter 0)
INTRPA	0/1/2 = constant/linear/exponential angular flux in μ
INTRPP	0/1/2 = constant/linear/exponential angular flux in η
NAZL	Number of divisions in the azimuthal direction in localized quadrature at detector (0 means 2n in polar level n).
NPRL	Number of divisions in the polar direction in localized quadrature at the detector
ISTAT	0/1 = print responses by group and detector/print responses by detector

2* [one entry]

ZSOR	Z location of boundary source
T	Block termination.
3*	MU's [MM entries]

4* ETA's [MM entries]

5* WEIGHTS [MM entries]

8* Radii for boundary source [IM+1 entries]

9* Radii for detectors [ND entries]

10* Heights for detectors [ND entries]

11* Scale factors by response function [NRESP entries]

12* Response functions by group [IGM* NRESP entries]

13$ Triggers to punch responses [NL entries]

T Block Terminator

A listing follows except for some input and output subroutines which are obtained from a local library at execution time.

```
LEVEL 21.8 ( JUN 74 )                                    OS/360  FORTRAN H

          COMPILER OPTIONS - NAME=  MAIN,OPT=02,LINECNT=60,SIZE=0000K,
                             SOURCE,EBCDIC,NOLIST,NODECK,LOAD,MAP,NOEDIT,ID,NOXREF
  ISN 0002            COMMON D(1),LINY,LFLT,LMU,LETA,LWTS,LPHIA,LPWT,LRAD,LRDET,LZDET,
                     1 LSCALE,LRESP,LIPUN,LPHI,LNPHI,LNCNP,LPOL,LFDET,LDOS,LXNF,LAST,
                     2 ICNT,NGMX,ITER,NP,LENGTH,IGM,IM,MM,ND,NRESP,NN,INTRPA,INTRPP,
                     3 INTRPR,NAZL,NPRL,ISTAT,ZSOR
                     4 ,DUMY(1000001),X
  ISN 0003            DIMENSION ID(1)
  ISN 0004            EQUIVALENCE (D(1),ID(1))
  ISN 0005            LENGTH=(LOC(X)-LOC(D(1)))/4
  ISN 0006            LNG=LENGTH
  ISN 0007            DO 10 I=1,LNG
  ISN 0008         10 D(I)=0.0
  ISN 0009            LENGTH=LNG
  ISN 0010            LINY=28
  ISN 0011            LFLT=40
  ISN 0012            LMU=41
  ISN 0013            CALL FIDAS(0,0,0,2,J3,5,6)
  ISN 0014            IGP=IGM+1
  ISN 0015            LETA=LMU+MM
  ISN 0016            LWTS=LETA+MM
  ISN 0017            LPHIA=LWTS+MM
  ISN 0018            LPWT=LPHIA+MM
  ISN 0019            LRAD=LPWT+MM
  ISN 0020            LRDET=LRAD+IM+1
  ISN 0021            LZDET=LRDET+ND
  ISN 0022            LSCALE=LZDET+ND
  ISN 0023            LRESP=LSCALE+NRESP
  ISN 0024            LIPUN=LRESP+IGM*NRESP
  ISN 0025            ICNU=ND*NRESP
  ISN 0026            IF(ISTAT.GT.0)ICNU=NRESP
  ISN 0028            LPHI=LIPUN+ICNU
  ISN 0029            CALL FIDAS(0,0,0,2,J3,5,6)
  ISN 0030            ISNTRP=INTRPA+INTRPP
  ISN 0031            LNPHI=LPHI+3*MM
  ISN 0032            LNCNP=LNPHI+MM
  ISN 0033            LPOL=LNCNP+MM
  ISN 0034            CALL QUAD(D(LMU),D(LETA),D(LWTS),D(LPHI),D(LNPHI),D(LNCNP),
                     1 D(LPOL),MM,NP,ISNTRP )
  ISN 0035            DO 30 I=1,NP
  ISN 0036            ID(LPHI+MM+I-1)=ID(LNPHI+I-1)
  ISN 0037            ID(LPHI+MM+NP+I-1)=ID(LNCNP+I-1)
  ISN 0038            D(LPHI+MM+2*NP+I-1)=D(LPOL+I-1)
  ISN 0039         30 CONTINUE
  ISN 0040            LNPHI=LPHI+MM
  ISN 0041            LNCNP=LNPHI+NP
  ISN 0042            LPOL=LNCNP+NP
  ISN 0043            LFDET=LPOL+NP
  ISN 0044            LDOS=LFDET
  ISN 0045            IF(ISTAT.GT.0)LDOS=LFDET+ND*NRESP
  ISN 0047            LXNF=LDOS+ND*IGP*NRESP
  ISN 0048            ICNT=MM*IM
  ISN 0049            NGMX=(LENGTH-LXNF)/ICNT
  ISN 0050            LAST=LXNF+NGMX*ICNT
  ISN 0051            ITER=(IGM+NGMX-1)/NGMX
  ISN 0052            WRITE(6,40)IGM,IM,MM,ND,NRESP,NN,INTRPA,INTRPP,INTRPR,NAZL,NPRL,
                     1 ISTAT,NP,ITER,NGMX,LENGTH,LAST,ZSOR
  ISN 0053         40 FORMAT(7H1   IGM,I7/7H     IM,I7/7H     MM,I7/7H     ND,I7/
```

```
                 1 7H  NRESP,I7/7H      NN,I7/7H INTRPA,I7/7H INTRPP,I7/7H INTRPR,I7/
                 2 7H   NAZL,I7/7H    NPRL,I7/7H  ISTAT,I7/7H      NP,I7/7H    ITER,I7/
                 3 7H   NGMX,I7/7H LENGTH,I7/7H   LAST,I7//1H   ZSTR,1PE15.5
                 4 //3H  T//)
ISN 0054            WRITE(6,50)
ISN 0055         50 FORMAT(1H1,44X,2(4X,'ALPHA',4X)/12X,'MU',10X,'ETA',9X,'WEIGHT',
                  1 7X,'ANGLES',7X,'WEIGHT',7X,'RADII',9X,'RDET',9X,'ZDET'/)
ISN 0056            CALL WOT8(4,5,6,7,8,9,10,11,6,0,0)
ISN 0057            WRITE(6,60)
ISN 0058         60 FORMAT(1H1,9X,'SCALE',9X,'NPHI',9X,'NCMP',9X,'PHI',10X,'POL'/)
ISN 0059            CALL WOT8(12,16,17,15,18,0,0,0,6,0,0)
ISN 0060            WRITE(6,70)
ISN 0061         70 FORMAT('1RESPONSE FUNCTIONS BY GROUP'//)
ISN 0062            CALL WOT(D(LRESP),NRESP,IGM,1,'GRP.','RESP',0)
ISN 0063            MD=MO
ISN 0064            IF(ISTAT.GT.0)MD=1
ISN 0066            WRITE(6,80)
ISN 0067         80 FORMAT('1SIGNALS TO PUNCH RESPONSE OR SPECTRUM'//)
ISN 0068            CALL IWOT(D(LTPUN),MD,NRESP,1,'RESP','DET.',0)
ISN 0069            IF(J3.GT.0)CALL EXIT
ISN 0071            CALL CALDOS(D(LPHIA),D(LPWT),D(LRAD),D(LRDET),D(LZDET),D(LSCALE),
                  1 D(LRESP),D(LPHI),D(LNPHI),D(LNCMP),D(LPOL),D(LDOS),D(LXNF),
                  2 D(LMU),D(LETA),D(LWTS),D(LTPUN),D(LRDET),IGP)
ISN 0072            WRITE(6,90)
ISN 0073         90 FORMAT(1H1)
ISN 0074            STOP
ISN 0075            END
```

```
LEVEL 21.8 ( JUN 74 )                          OS/360  FORTRAN H

          COMPILER OPTIONS - NAME=  MAIN,OPT=02,LINECNT=60,SIZE=0000K,
                             SOURCE,EBCDIC,NOLIST,NODECK,LOAD,MAP,NOEDIT,ID,NOXREF
  ISN 0002            SUBROUTINE QUAD(MU,ETA,WTS,PHI,NPHI,NCMP,POL,MM,NP,ISNTRP)
  ISN 0003            DIMENSION MU(1),ETA(1),WTS(1),PHI(1),NPHI(1),NCMP(1),POL(1)
  ISN 0004            REAL MU
  ISN 0005            REAL*8 SUM,SUMM,SUMT
  ISN 0006            DATA PI/3.1415927/
  ISN 0007            NP=0
  ISN 0008            SUMT=0.0
  ISN 0009            DO 50 M=1,MM
  ISN 0010            SUMT=SUMT+WTS(M)
  ISN 0011            IF(WTS(M).NE.0.0)GO TO 30
  ISN 0013            NP=NP+1
  ISN 0014            POL(NP)=ETA(M)
  ISN 0015            SW=ABS(MU(M))
  ISN 0016            PHI(M)=-PI
  ISN 0017            NPHI(NP)=1
  ISN 0018            IF(NP.EQ.1)GO TO 20
  ISN 0020            NCMP(NP)=NCMP(NP-1)+NPHI(NP-1)
  ISN 0021         20 CONTINUE
  ISN 0022            GO TO 50
  ISN 0023         30 CONTINUE
  ISN 0024            NPHI(NP)=NPHI(NP)+1
  ISN 0025            CSM=MU(M)/SW
  ISN 0026            PHI(M)=-ARCOS(CSM)
  ISN 0027         50 CONTINUE
  ISN 0028            I=1
  ISN 0029         60 IJ=I+1
  ISN 0030            PMIN=POL(I)
  ISN 0031            K=I
  ISN 0032            DO 70 J=IJ,NP
  ISN 0033            PNOW=POL(J)
  ISN 0034            IF(PNOW.GE.PMIN)GO TO 70
  ISN 0036            K=J
  ISN 0037            PMIN=PNOW
  ISN 0038         70 CONTINUE
  ISN 0039            IF(K.EQ.I)GO TO 80
  ISN 0041            PNOW=POL(I)
  ISN 0042            POL(I)=PMIN
  ISN 0043            POL(K)=PNOW
  ISN 0044            NHI=NPHI(I)
  ISN 0045            NPHI(I)=NPHI(K)
  ISN 0046            NPHI(K)=NHI
  ISN 0047            NCP=NCMP(I)
  ISN 0048            NCMP(I)=NCMP(K)
  ISN 0049            NCMP(K)=NCP
  ISN 0050         80 CONTINUE
  ISN 0051            I=I+1
  ISN 0052            IF(I.LT.NP)GO TO 60
  ISN 0054            IF(ISNTRP.GE.2)RETURN
  ISN 0056            SUMM=0.0
  ISN 0057            DO 120 IP=1,NP
  ISN 0058            MM=NPHI(IP)
  ISN 0059            MMM=MM-1
  ISN 0060            NMM=NCMP(IP)
  ISN 0061            SUM=0.0
  ISN 0062            DO 90 N=2,MM
  ISN 0063         90 SUM=SUM+WTS(NMM+N)
  ISN 0064            SUMM=SUMM+SUM
  ISN 0065            POL(IP)=-1.0+2.0*SUMM/SUMT
  ISN 0066            DO 100 N=2,MMM
  ISN 0067        100 PHI(NMM+N)=PHI(NMM+N-1)+PI*WTS(NMM+N)/SUM
  ISN 0068            PHI(NMM+MM)=0.0
  ISN 0069        120 CONTINUE
  ISN 0070            RETURN
  ISN 0071            END
```

```
LEVEL 21.8 ( JUN 74 )                                    OS/360  FORTRAN H

          COMPILER OPTIONS - NAME=  MAIN,OPT=02,LINECNT=60,SIZE=2000K,
                             SOURCE,EBCDIC,NOLIST,NODECK,LOAD,MAP,NOEDIT,ID,NOXREF
  ISN 0002            SUBROUTINE CALDOS(PHIA,PWT,RAD,RDET,ZDET,SCALE,RESP,PHI,NPHI,
                     1 NCMP,POL,DOS,XNF,MU,ETA,WTS,IPUN,FDET,IGP)
  ISN 0003            COMMON D(1),LINT,LFLT,LMU,LETA,LWTS,LPHIA,LPWT,LRAD,LRDET,LZDET,
                     1 LSCALE,LRESP,LIPUN,LPHI,LNPHI,LNCMP,LPOL,LFDET,LDOS,LXNF,LAST,
                     2 ICNT,NGMX,ITER,NP,LENGTH,IGM,IM,MM,ND,NRESP,NN,INTRPA,INTRPP,
                     3 INTRPR,NAZL,NPRL,ISTAT,ZSOR
  ISN 0004            DIMENSION PHIA(1),PWT(1),RAD(1),RDET(1),ZDET(1),SCALE(1),PHI(1),
                     1 RESP(IGM,1),NPHI(1),NCMP(1),POL(1),DOS(IGP,NRESP,1),XNF(MM,IM,1)
  ISN 0005            DIMENSION MU(1),ETA(1),WTS(1),FDET(1),IPUN(1)
  ISN 0006            REAL MU
  ISN 0007            DATA PI/3.1415927/
  ISN 0008            REWIND 1
  ISN 0009            ISNTPP=INTRPA+INTRPP
  ISN 0010            ICALL=1
  ISN 0011            IF(ISNTPP.GE.2)ICALL=2
  ISN 0013            RMAX=RAD(IM+1)
  ISN 0014            DO 1000 KD=1,ND
  ISN 0015            DO 1000 NR=1,NRESP
  ISN 0016            DO 1000 IG=1,IGP
  ISN 0017       1000 DOS(IG,NR,KD)=0.0
  ISN 0018            IC=0
  ISN 0019            DO 100 IT=1,ITER
  ISN 0020            ICA=ICB+1
  ISN 0021            ICB=MIND(ICA+NGMX-1,IGM)
  ISN 0022            NGP=ICB+1-ICA
  ISN 0023            DO 1005 IG=1,NGP
  ISN 0024            READ(1)((XNF(M,I,IG),M=1,MM),I=1,IM)
  ISN 0025       1005 CONTINUE
  ISN 0026            DO 90 KD=1,ND
  ISN 0027            RD=RDET(KD)
  ISN 0028            ZD=ZDET(KD)
  ISN 0029            DDET=SQRT(RD**2+(ZD-ZSOR)**2)
  ISN 0030            CX=RD/DDET
  ISN 0031            CZ=(ZD-ZSOR)/DDET
  ISN 0032            DC=SQRT((RD-RMAX)**2+(ZD-ZSOR)**2)
  ISN 0033            ETLO=((RD-RMAX)*RD+(ZD-ZSOR)**2)/(DC*DDET)
  ISN 0034            NPLL=NPRL*NAZL
  ISN 0035            IF(NAZL.LE.0)NPLL=NPRL*(NPRL+1)
  ISN 0037            WTF=(1.0-ETLO)/(2.0*NPLL)
  ISN 0038            WATF=WTF
  ISN 0039            DLET=(1.0-ETLO)/NPRL
  ISN 0040            IF(NAZL.LE.0)DLET=(1.0-ETLO)/NPLL
  ISN 0042            RMN=AMIN1(RD,RMAX)
  ISN 0043            DMN=SQRT((RD-RMN)**2+(ZD-ZSOR)**2)
  ISN 0044            ET1=(ZD-ZSOR)/DMN
  ISN 0045            DMX=SQRT((RD+RMAX)**2+(ZD-ZSOR)**2)
  ISN 0046            ET2=(ZD-ZSOR)/DMX
  ISN 0047            ETMN=AMIN1(ET1,ET2)
  ISN 0048            ETMX=AMAX1(ET1,ET2)
  ISN 0049            DO 1010 JPA=2,NP
  ISN 0050            IF(ETMN.LE.POL(JPA))GO TO 1020
  ISN 0052       1010 CONTINUE
  ISN 0053            JPA=NP
  ISN 0054       1020 CONTINUE
  ISN 0055            DO 1030 JPB=JPA,NP
  ISN 0056            IF(ETMX.LE.POL(JPB))GO TO 1040
  ISN 0058       1030 CONTINUE
  ISN 0059            JPB=NP
  ISN 0060       1040 CONTINUE
  ISN 0061            DO 80 IPL=1,NPRL
  ISN 0062            WTE=WATF
  ISN 0063            UZ=ETLO+(IPL-0.5)*DLET
  ISN 0064            IF(NAZL.GT.0)GO TO 5
  ISN 0066            UZ=1.0-IPL**2*DLET
  ISN 0067          5 CONTINUE
  ISN 0068            SUZ=SQRT(1.0-UZ**2)
  ISN 0069            ANZ=NAZL
  ISN 0070            IF(NAZL.LE.0)NNZ=2*IPL
  ISN 0072            IF(RD.GT.0.0)GO TO 6
  ISN 0074            NNZ=1
  ISN 0075            WTE=2.0*IPL*WATF
  ISN 0076          6 CONTINUE
  ISN 0077            DAZ=PI/NNZ
  ISN 0078            DO 70 IAZ=1,NNZ
  ISN 0079            AZ=(IAZ-0.5)*DAZ
  ISN 0080            UX=SUZ*COS(AZ)
  ISN 0081            ET=-CX*UX+CZ*UZ
  ISN 0082            DD=(ZD-ZSOR)/ET
  ISN 0083            IF(DD.LT.0.0)GO TO 70
  ISN 0085            ANU=CZ*UX+CX*UZ
```

```
ISN 0086          SW=SQRT(1.0-ET**2)
ISN 0087          DISC=SW**2-AMU**2
ISN 0088          IF(DISC.LT.0.0)DISC=0.0
ISN 0090          DMY=SQRT(DISC)
ISN 0091          X=RD-DD*AMU
ISN 0092          Y=-DD*DMY
ISN 0093          R=SQRT(X**2+Y**2)
ISN 0094          IF(R.GT.RMAX)GO TO 80
ISN 0096          DDS=SQRT((RD-X)**2+Y**2)
ISN 0097          DDT=((RD-X)*X-Y*Y)/(DDS*R)
ISN 0098          IF(ABS(DDT).GT.1.0)GO TO 7
ISN 0100          PH=-ARCCS(DDT)
ISN 0101          GO TO 8
ISN 0102        7 CONTINUE
ISN 0103          PH=0.5*(-1.0+SIGN(1.0,DDT))*PI
ISN 0104        8 CONTINUE
ISN 0105          DO 10 IP=JPA,JPB
ISN 0106          IF(ET.LE.POL(IP))GO TO 15
ISN 0108       10 CONTINUE
ISN 0109          IP=JPB
ISN 0110       15 CONTINUE
ISN 0111          GO TO (20,25),ICALL
ISN 0112       20 CALL CONFLX(POL,NPHI,NCMP,IP,XMF,MM,IM,PH,PHI)
ISN 0113          GO TO 30
ISN 0114       25 CALL VARFLX(POL,NPHI,NCMP,IP,XMF,MM,IM,PH,PHI)
ISN 0115       30 CONTINUE
ISN 0116          DO 40 I=2,IM
ISN 0117          RRB=0.5*(RAD(I)+RAD(I+1))
ISN 0118          IF(R.LE.RRB)GO TO 45
ISN 0120       40 CONTINUE
ISN 0121          I=IM
ISN 0122       45 CONTINUE
ISN 0123          RRA=0.5*(RAD(I-1)+RAD(I))
ISN 0124          PR=(R-RRA)/(RRB-RRA)
ISN 0125          DO 60 IG=IGA,IGB
ISN 0126          IIG=IG+1-IGA
ISN 0127          GO TO (53,55),ICALL
ISN 0128       53 CALL CONFLI(FLZ,IIG,I,PR)
ISN 0129          GO TO 58
ISN 0130       55 CALL VARFLI(FLZ,IIG,I,PR)
ISN 0131       58 CONTINUE
ISN 0132          TRM=FLZ*WTE
ISN 0133          DDS(IG,1,KD)=DDS(IG,1,KD)+TRM
ISN 0134       60 CONTINUE
ISN 0135       70 CONTINUE
ISN 0136       80 CONTINUE
ISN 0137       90 CONTINUE
ISN 0138      100 CONTINUE
ISN 0139          DO 108 KD=1,ND
ISN 0140          DO 108 IG=1,IGM
ISN 0141          DO 105 NR=1,NRESP
ISN 0142          KR=NRESP+1-NR
ISN 0143          DDS(IG,KR,KD)=DDS(IG,1,KD)*RESP(IG,KR)*SCALE(KR)
ISN 0144          DDS(IGP,KR,KD)=DDS(IGP,KR,KD)+DDS(IG,KR,KD)
ISN 0145      105 CONTINUE
ISN 0146      108 CONTINUE
ISN 0147          IF(ISTAT.GT.0)GO TO 130
ISN 0149          DO 120 KD=1,ND
ISN 0150          WRITE(6,110)KD,RDET(KD),ZDET(KD)
ISN 0151      110 FORMAT('1DETECTOR',I5,5X,'RADIUS=',1PE15.5,5X,'HEIGHT=',1PE15.5//)
ISN 0152          IDDS=LDDS+(KD-1)*NRESP*IGP
ISN 0153          CALL WOT(D(IDDS),NRESP,IGP,1,'GRP.','RESP',0)
ISN 0154          DO 115 KR=1,NRESP
ISN 0155          LL=(KD-1)*NRESP+KR
ISN 0156          IF(IPUN(LL).LE.0)GO TO 115
ISN 0158          CALL FFPUN(DDS(1,KR,KD),IGM,LL)
ISN 0159      115 CONTINUE
ISN 0160      120 CONTINUE
ISN 0161          RETURN
ISN 0162      130 CONTINUE
ISN 0163          DO 140 KD=1,ND
ISN 0164          DO 140 NR=1,NRESP
ISN 0165          L=(NR-1)*ND+KD
ISN 0166      140 FDET(L)=DDS(IGP,NR,KD)
ISN 0167          WRITE(6,150)
ISN 0168      150 FORMAT('1TOTAL RESPONSES BY DETECTOR POSITION AND RESPONSE'//)
ISN 0169          CALL WOT(FDET,NRESP,ND,1,'DET.','RESP',0)
ISN 0170          DO 160 NR=1,NRESP
ISN 0171          IF(IPUN(NR).LE.0)GO TO 160
ISN 0173          L=(NR-1)*ND+1
ISN 0174          CALL FFPUN(FDET(L),ND,NR)
ISN 0175      160 CONTINUE
ISN 0176          RETURN
ISN 0177          END
```

```
LEVEL 21.9 ( JUN 74 )                                    OS/360  FORTRAN H

          COMPILER OPTIONS - NAME=  MAIN,OPT=02,LINECNT=60,SIZE=0000K,
                             SOURCE,EBCDIC,NOLIST,NODECK,LOAD,MAP,NOEDIT,ID,NOXREF
 ISN 0002            SUBROUTINE (POL,NPHI,NCMP,JP,XNF,MM,IM,PH,PHI,ET)
 ISN 0003            COMMON DUM(33),INTRPA,INTRPP,INTRPR
 ISN 0004            DIMENSION POL(1),NPHI(1),NCMP(1),XNF(MM,IM,1),PHI(1)
 ISN 0005            LOGICAL TSN
 ISN 0006            IP=MAX0(JP,2)
 ISN 0007            TSN=SIGN(1.0,POL(IP)).NE.SIGN(1.0,POL(IP-1))
 ISN 0008            IF(TSN.AND.ET.LE.0.0)IP=IP-1
 ISN 0009            IF(TSN.AND.ET.GT.0.0)IP=IP+1
 ISN 0010            IL1=NCMP(IP-1)
 ISN 0011            IL2=NCMP(IP)
 ISN 0012            NZ1=NPHI(IP-1)
 ISN 0013            NZ2=NPHI(IP)
 ISN 0014            DO 20 IZ1=3,NZ1
 ISN 0015            IF(PH.LE.PHI(IL1+IZ1))GO TO 25
 ISN 0016         20 CONTINUE
 ISN 0017            IZ1=NZ1
 ISN 0018         25 CONTINUE
 ISN 0019            DO 30 IZ2=3,NZ2
 ISN 0020            IF(PH.LE.PHI(IL2+IZ2))GO TO 35
 ISN 0021         30 CONTINUE
 ISN 0022            IZ2=NZ2
 ISN 0023         35 CONTINUE
 ISN 0024            PE=(ET-POL(IP-1))/(POL(IP)-POL(IP-1))
 ISN 0025            IZX=IL1+IZ1
 ISN 0026            PZ1=(PH-PHI(IZX-1))/(PHI(IZX)-PHI(IZX-1))
 ISN 0027            IZY=IL2+IZ2
 ISN 0028            PZ2=(PH-PHI(IZY-1))/(PHI(IZY)-PHI(IZY-1))
 ISN 0029            RETURN
 ISN 0030            ENTRY VARFL1(FLZ,IIG,I,PR)
 ISN 0031            J=I-1
 ISN 0032            RX1=XNF(IZX-1,J,IIG)
 ISN 0033            RX2=XNF(IZX,J,IIG)
 ISN 0034            RX3=XNF(IZX-1,I,IIG)
 ISN 0035            RX4=XNF(IZX,I,IIG)
 ISN 0036            RY1=XNF(IZY-1,J,IIG)
 ISN 0037            RY2=XNF(IZY,J,IIG)
 ISN 0038            RY3=XNF(IZY-1,I,IIG)
 ISN 0039            RY4=XNF(IZY,I,IIG)
 ISN 0040            CALL NTERP(RX1,RX3,RX5,PR,INTRPR)
 ISN 0041            CALL NTERP(RX2,RX4,RX6,PR,INTRPR)
 ISN 0042            CALL NTERP(RX5,RX6,FLX,PZ1,INTRPA)
 ISN 0043            CALL NTERP(RY1,RY3,RY5,PR,INTRPR)
 ISN 0044            CALL NTERP(RY2,RY4,RY6,PR,INTRPR)
 ISN 0045            CALL NTERP(RY5,RY6,FLY,PZ2,INTRPA)
 ISN 0046            CALL NTERP(FLX,FLY,FLZ,PE,INTRPP)
 ISN 0047            RETURN
 ISN 0048            END
```

```
LEVEL 21.9 ( JUN 74 )                                    OS/360  FORTRAN H

          COMPILER OPTIONS - NAME=  MAIN,OPT=02,LINECNT=60,SIZE=0000K,
                             SOURCE,EBCDIC,NOLIST,NODECK,LOAD,MAP,NOEDIT,ID,NOXREF
 ISN 0002            SUBROUTINE (POL,NPHI,NCMP,IP,XNF,MM,IM,PH,PHI)
 ISN 0003            COMMON DUM(33),INTRPA,INTRPP,INTRPR
 ISN 0004            DIMENSION POL(1),NPHI(1),NCMP(1),XNF(MM,IM,1),PHI(1)
 ISN 0005            IL2=NCMP(IP)
 ISN 0006            NZ2=NPHI(IP)
 ISN 0007            DO 30 IZ2=2,NZ2
 ISN 0008            IF(PH.LE.PHI(IL2+IZ2))GO TO 35
 ISN 0010         30 CONTINUE
 ISN 0011            IZ2=NZ2
 ISN 0012         35 CONTINUE
 ISN 0013            IZY=IL2+IZ2
 ISN 0014            RETURN
 ISN 0015            ENTRY CONFL1(FLZ,IIG,I,PR)
 ISN 0016            J=I-1
 ISN 0017            RX1=XNF(IZY,J,IIG)
 ISN 0018            RX2=XNF(IZY,I,IIG)
 ISN 0019            CALL NTERP(RX1,RX2,FLZ,PR,INTRPR)
 ISN 0020            RETURN
 ISN 0021            END
```

```
LEVEL 21.8 ( JUN 74 )                                    OS/360  FORTRAN H

          COMPILER OPTIONS - NAME=  MAIN,OPT=02,LINECNT=60,SIZE=0000K,
                             SOURCE,EBCDIC,NOLIST,NODECK,LOAD,MAP,NOEDIT,ID,NOXREF
  ISN 0002              SUBROUTINE NTEMP(F1,F2,F3,P,INTRP)
  ISN 0003              GO TO (10,20),INTRP
  ISN 0004           10 F3=(1.0-P)*F1+P*F2
  ISN 0005              RETURN
  ISN 0006           20 CONTINUE
  ISN 0007              ISGA=(SIGN(1.0,F1)+3.2)/2.0
  ISN 0008              ISGB=(SIGN(1.0,F2)+3.2)/2.0
  ISN 0009              IF(ISGA.EQ.ISGB)GO TO 50
  ISN 0011              GO TO (30,40),ISGA
  ISN 0012           30 F1=0.01*F2
  ISN 0013              GO TO 50
  ISN 0014           40 F2=0.01*F1
  ISN 0015           50 CONTINUE
  ISN 0016              ARG=ALOG(F2/F1)*P
  ISN 0017              F3=F1*EXP(ARG)
  ISN 0018              RETURN
  ISN 0019              END
```

```
LEVEL 21.8 ( JUN 74 )                                    OS/360  FORTRAN H

          COMPILER OPTIONS - NAME=  MAIN,OPT=02,LINECNT=60,SIZE=0000K,
                             SOURCE,EBCDIC,NOLIST,NODECK,LOAD,MAP,NOEDIT,ID,NOXREF
  ISN 0002              SUBROUTINE WDTB(L1,L2,L3,L4,L5,L6,L7,L8,NOU,D,LD)
                  C     *** WDTB  WILL WRITE UP TO EIGHT ONE-DIMENSIONAL ARRAYS OF VARYING
                  C        LENGTHS IN COLUMNS ACROSS A PAGE. L1,L2,ETC. ARE THE POSITIONS
                  C        IN COMMON OF THE BASE ADDRESSES OF THE ARRAYS TO BE WRITTEN.
                  C        IF ANY LN IS ZERO THE N-TH COLUMN WILL BE BLANK.
  ISN 0003              DIMENSION FPT(19),FNT(6),L(8),N(8),Z(8),LD(1),D(1)
  ISN 0004              DATA B/'    '/
  ISN 0005              DATA K,FPT(1),FPT(2),FPT(19)/100000,'(1PI','6   ',')   '/
  ISN 0006              DATA  FNT(1),FNT(2),FNT(3),FNT(4),FNT(5),FNT(6)/',E13','.5  ',
                       1 ',I8,','5X  ',',9X,','A4  '/
  ISN 0007              L(1)=L1
  ISN 0008              L(2)=L2
  ISN 0009              L(3)=L3
  ISN 0010              L(4)=L4
  ISN 0011              L(5)=L5
  ISN 0012              L(6)=L6
  ISN 0013              L(7)=L7
  ISN 0014              L(8)=L8
  ISN 0015              N=0
  ISN 0016              DO 1 I=1,8
  ISN 0017              LL=L(I)
  ISN 0018              IF(LL.GT.0)N(I)=LD(LL+1)-LD(LL)
  ISN 0020              IF(LL.EQ.0)N(I)=0
  ISN 0022            1 N=MAX0(N,N(I))
  ISN 0023              DO 2 I=1,N
  ISN 0024              DO 3 J=1,8
  ISN 0025              IF(N(J).GE.I) GO TO 4
  ISN 0027              Z(J)=B
  ISN 0028              FPT(2*J+1)=FNT(5)
  ISN 0029              FPT(2*J+2)=FNT(6)
  ISN 0030              GO TO 3
  ISN 0031            4 LL=L(J)
  ISN 0032              LL=LD(LL) + I - 1
  ISN 0033              Z(J)=D(LL)
  ISN 0034              FPT(2*J+1)=FNT(1)
  ISN 0035              FPT(2*J+2)=FNT(2)
  ISN 0036              IF(K.LE.IABS(LD(LL)))GO TO 3
  ISN 0038              FPT(2*J+1)=FNT(3)
  ISN 0039              FPT(2*J+2)=FNT(4)
  ISN 0040            3 CONTINUE
  ISN 0041            2 WRITE (NOU,FPT) I,(Z(J),J=1,8)
  ISN 0042              RETURN
  ISN 0043              END
```

```
LEVEL 21.8 ( JUN 74 )                                    OS/360  FORTRAN H

          COMPILER OPTIONS - NAME=  MAIN,OPT=02,LINECNT=60,SIZE=0000K,
                             SOURCE,EBCDIC,NOLIST,NODECK,LOAD,MAP,NOEDIT,ID,NOXREF
 ISN 0002            SUBROUTINE INOTE(M,NCOL,LTBL,LG,TOP1,TOP2,TOP3)
 ISN 0003            DIMENSION M(LTBL,NCOL,1)
 ISN 0004            N6=6
 ISN 0005            DO 1 L=1,LG
 ISN 0006            I02=0
 ISN 0007            I03=(NCOL+9)/10
 ISN 0008            IF(LG.GT.1)WRITE(N6,10)TOP3,L
 ISN 0010         10 FORMAT(/1H0,2X,A4,I5)
 ISN 0011            DO 2 I=1,I03
 ISN 0012            I01=I02+1
 ISN 0013            I02=MIN0(I01+9,NCOL)
 ISN 0014            WRITE(N6,20)TOP1,(TOP2,J,J=I01,I02)
 ISN 0015            DO 3 K=1,LTBL
 ISN 0016            IF(K.EQ.1)GO TO 4
 ISN 0018            DO 6 J=I01,I02
 ISN 0019            IF(M(K,J,L).NE.M(K-1,J,L))GO TO 7
 ISN 0021          6 CONTINUE
 ISN 0022            IF(KE.EQ.KS)GO TO 8
 ISN 0024            KE=K
 ISN 0025            IF(K.EQ.LTBL)GO TO 7
 ISN 0027            GO TO 3
 ISN 0028          8 IF(K.EQ.LTBL)GO TO 4
 ISN 0030            DO 9 J=I01,I02
 ISN 0031            IF(M(K,J,L).NE.M(K+1,J,L))GO TO 4
 ISN 0033          9 CONTINUE
 ISN 0034            KE=KE+1
 ISN 0035            GO TO 3
 ISN 0036          7 IF(KE.EQ.KS)GO TO 4
 ISN 0038            WRITE(N6,40)TOP1,KS,TOP1,KE
 ISN 0039            IF(K.EQ.LTBL.AND.KE.EQ.K)GO TO 3
 ISN 0041         40 FORMAT(8X,A4,I5,6H THRU ,A4,I5,14H SAME AS ABOVE )
 ISN 0042          4 WRITE(N6,30)K,(M(K,J,L),J=I01,I02)
 ISN 0043            KS=K+1
 ISN 0044            KE=KS
 ISN 0045          3 CONTINUE
 ISN 0046          2 CONTINUE
 ISN 0047          1 CONTINUE
 ISN 0048         20 FORMAT(2H0 ,A4,10(3X,A4,I3,2X))
 ISN 0049         30 FORMAT(I6,10(4X,I4,4X))
 ISN 0050            RETURN
 ISN 0051            END
```

RODFRAC

RODFRAC is a computer code which computes the rod fractions within specified annular regions and subdivides the annuli according to the rod fraction therein. It assumes rods on a triangular pitch contained within hexagonal elements themselves on a triangular pitch. The volume fraction for the walls of the hexagonal duct containing the fuel rods is allowed to be included with the rod fraction. Allowance is also made for including a separate region for grid spacers, thus partitioning a single annular region into three heterogeneous subregions.

The code assumes the geometry is divided into five zones as shown in Fig. C.1. Zone 1 represents a control rod channel and the surrounding wall. Zone 2 is a fuel pin region inside the centrally located fuel subassembly. Zone 3 represents the subassembly duct walls and gap surrounding the central subassembly. Zone 4 represents the other subassemblies with fuel pins and blanket pins, duct walls and gaps included. Zone 5 represents structure surrounding the core. A rod may be composed of up to four regions as shown in Fig. C.2.

RODFRAC Input

Title card (20A4)

1$ [13 entries]

NCYL1	Number of intervals in Zone 1
NCYL2	Number of rings in Zone 2. Rings will be subdivided by code.
NCYL3	Number of intervals in Zone 3
NCYL4	Number of rings in Zone 4. Rings will be subdivided by code.
NCYL5	Number of intervals in Zone 5
NCYT	NCYL1 + NCYL2 + NCYL3 + NCYL4 + NCYL5
IKTY	1/2/3 = 1 fuel subassembly/7 fuel subassemblies/up to 39 rows of subassemblies, 19 per row.
NCOPY	Number of times to punch the final radii
NROW	Number of rows of pins per subassembly

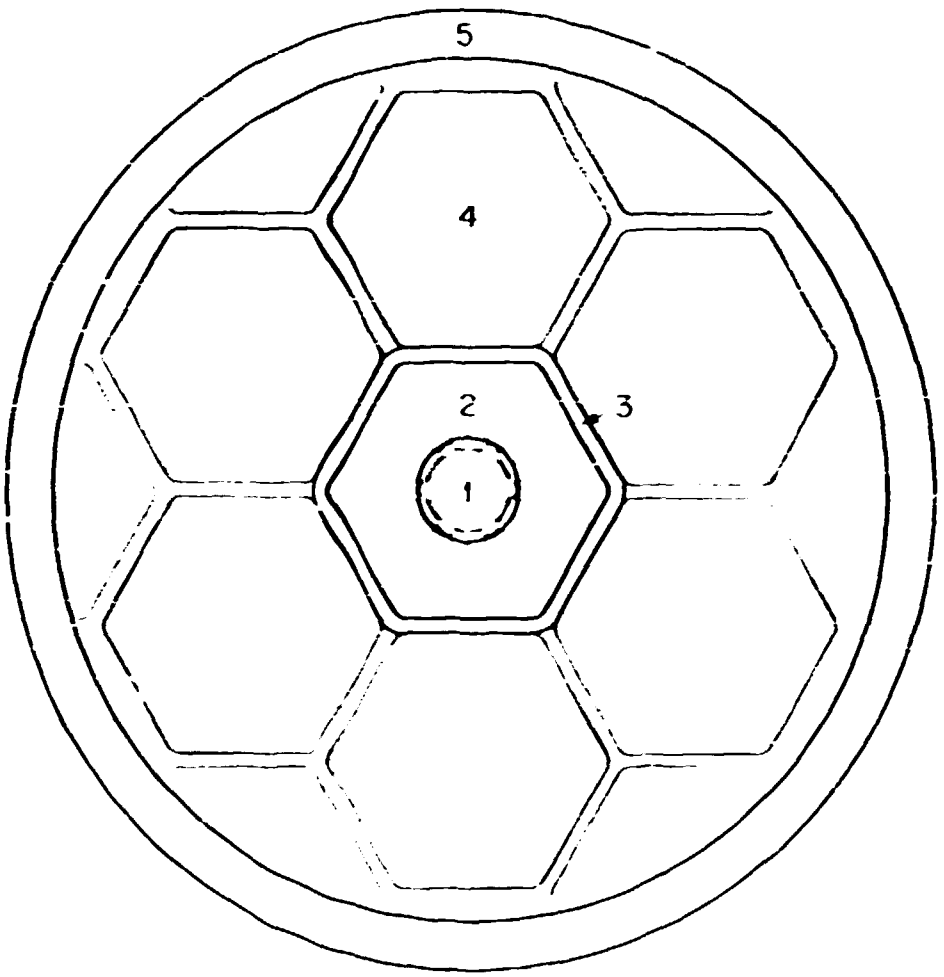

Fig. C.1. Five-Zoned Model for Which RODFRAC Computes Heterogeneous Subrings in Zones 2 and 4 and Combines These with the Input Radii in Zones 1, 3, and 5 to Give the Final Output Radii.

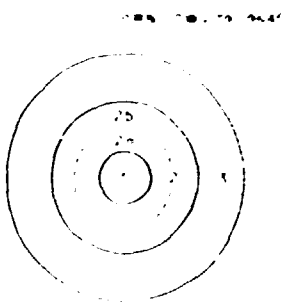

Fig. C.2. Multiregion Rod Surrounded by Coolant in Region 3 and Containing Coolant in Region 1. Region 2 May Contain a Single Material or Two Different Materials in Zones 2a and 2b.

IROT 0/1 = Hex flats in Y-direction/Hex flats in X-direction (see Fig. C.3). Note: XROW, PITCH, DELY, HPITCH, and HDELY depend on value of IROT. Fig. C.4 shows HPITCH and HDELY as a function of IROT.

Fig. C.3. Illustration of the Parameters XROW, PITCH, and DELY as a Function of IROT.

ORNL-DWG 79-11924

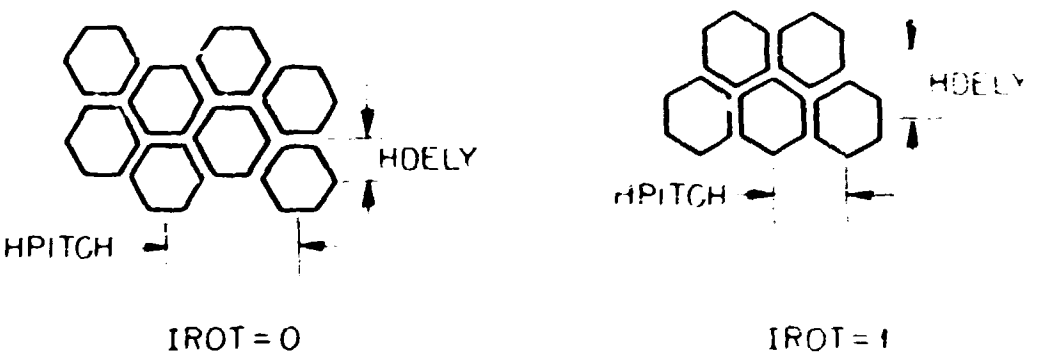

Fig. C.4. Illustration of the Parameters HPITCH and HDELY as a Function of IROT.

IOTHR Greater than zero if other material besides fuel pins, duct walls, or coolant is to be included as a separate heterogeneous subring. Volume fractions in Zones 2 and 4 (Fig. C.1) are input in the 5* array.

I4ZN Greater than zero if rods consist of a 3- or 4-region cylinder (see Fig. C.2) with coolant in the central and outer regions. Read volume fractions for region 1 in the 7* array.

I4OTH If greater than zero, region 2 (Fig. C.2) is subdivided into an inner region 2a and an outer region 2b. The outer radius of region 2b is specified as the rod radius. Volume fractions for the material in region 2a are input in the 6* array.

2* [10 entries]

RROD Radius of fuel pin (or rod)

RMAX Maximum radius of region containing fuel pins

PITCH Distance between centers of pins

DELY Center-to-center spacing between rows of pins

HPITCH Center-to-center spacing between subassemblies in a row

HDELY Center-to-center spacing between rows of elements

SIDEI Internal length of a side of a subassembly duct wall

SIDEO External length of a side of a subassembly duct wall

GRDF Volume fraction occupied by grid spacers (use 0.0 if separate ring is not desirable).

FLATC Distance across flats of duct enclosing Zone 1 of Fig. C.1.

T Block Terminator

3* Input radii (NCYT+1 values)

4* Subassembly duct wall volume fractions for each ring in Zones 2 and 4 (NCYL2 + NCYL4 values). Read zeroes for Zone 2 intervals.

5* Volume fractions in each ring of Zones 2 and 4 of material to be included in a third heterogeneous subring. (NCYL2 + NCYL4 values)

6* Volume fraction for each ring in Zones 2 and 4 (NCYL2 + NCYL4 values) of material in region 2a of Fig. C.2.

7* Volume fractions for each of the rings in Zones 2 and 4 of the coolant region 1 of Fig. C.2.

T Block Terminator

(stacked cases)

NOTE: The volume fractions to be input in the 6* and 7* arrays may be determined using RODFRAC by running several cases with the different region radii and differencing the results for the desired region.

A listing follows except for some input and output subroutines which are obtained from a local library at execution.

```
LEVEL 21.8 ( JUN 74 )                                  OS/360  FORTRAN H

          COMPILER OPTIONS - NAME=  MAIN,OPT=02,LINECNT=60,SIZE=0000K,
                             SOURCE,EBCDIC,NOLIST,NODECK,LOAD,MAP,NOEDIT,ID,NOXREF
  ISN 0002            COMMON D(31),DUMY( 5000),DEND
  ISN 0003            LCXS=(LOC(DEND)-LOC(D(1)))/4
  ISN 0004            DO 1 I=1,LCXS
  ISN 0005          1  D(I)=0.0
  ISN 0006            CALL MANIPL(LCXS)
  ISN 0007            WRITE(6,5)
  ISN 0008          5 FORMAT(1H1)
  ISN 0009            STOP
  ISN 0010            END


LEVEL 21.8 ( JUN 74 )                                  OS/360  FORTRAN H

          COMPILER OPTIONS - NAME=  MAIN,OPT=02,LINECNT=60,SIZE=0000K,
                             SOURCE,EBCDIC,NOLIST,NODECK,LOAD,MAP,NOEDIT,ID,NOXREF
  ISN 0002            SUBROUTINE STPERR(A,J)
  ISN 0003            WRITE(6,10)J,A
  ISN 0004         10 FORMAT(1H0,I7,3X,'ERRORS WERE ENCOUNTERED IN THE',1X,A4,1X,
                    1 'BLOCK'/)
  ISN 0005            RETURN
  ISN 0006            END


LEVEL 21.8 ( JUN 74 )                                  OS/360  FORTRAN H

          COMPILER OPTIONS - NAME=  MAIN,OPT=02,LINECNT=60,SIZE=0000K,
                             SOURCE,EBCDIC,NOLIST,NODECK,LOAD,MAP,NOEDIT,ID,NOXREF
  ISN 0002            SUBROUTINE INTSEC(XO,YO,RHO,RCC,THETA,PHI,IER)
  ISN 0003            DATA PI/3.1415927/
  ISN 0004            REAL*8 A,B,C
  ISN 0005            IER=0
  ISN 0006            RO=SQRT(XO**2+YO**2)
  ISN 0007            A=RHO
  ISN 0008            B=RO
  ISN 0009            C=RCC
  ISN 0010            CSA=(B**2+C**2-A**2)/(2.0*B*C)
  ISN 0011            IF(ABS(CSA).GT.1.0)GO TO 20
  ISN 0013            ALPHA=ARCOS(CSA)
  ISN 0014            PHI=2.0*ALPHA
  ISN 0015            CST=(A**2+B**2-C**2)/(2.0*A*B)
  ISN 0016            THETA=ARCOS(CST)
  ISN 0017            THETA=2.0*(PI-THETA)
  ISN 0018            RETURN
  ISN 0019         20 IER=1
  ISN 0020            RETURN
  ISN 0021            END


LEVEL 21.8 ( JUN 74 )                                  OS/360  FORTRAN H

          COMPILER OPTIONS - NAME=  MAIN,OPT=02,LINECNT=60,SIZE=0000K,
                             SOURCE,EBCDIC,NOLIST,NODECK,LOAD,MAP,NOEDIT,ID,NOXREF
  ISN 0002            SUBROUTINE AREAC(RHO,RCC,THETA,PHI,AREA)
  ISN 0003            DATA PI/3.1415927/
  ISN 0004            SSP=SIN(PHI)
  ISN 0005            SST=SIN(THETA)
  ISN 0006            AREB=PI*RHO**2
  ISN 0007            IF(THETA.GT.PI)GO TO 50
  ISN 0009            AREA=0.5*(2.0*PI-THETA+SST)*RHO**2+0.5*(PHI-SSP)*RCC**2
  ISN 0010            RETURN
  ISN 0011         50 AREA=0.5*(THETA-SST)*RHO**2-0.5*(PHI-SSP)*RCC**2
  ISN 0012            AREA=AREB-AREA
  ISN 0013            RETURN
  ISN 0014            END
```

```
LEVEL 21.8 ( JUN 74 )                                    OS/360  FORTRAN H

          COMPILER OPTIONS - NAME=  MAIN,OPT=02,LINECNT=60,SIZE=0000K,
                             SOURCE,EBCDIC,NOLIST,NODECK,LOAD,MAP,NOEDIT,ID,NOXREF
  ISN 0002            SUBROUTINE MANIPL(LCXS)
  ISN 0003            COMMON D(1),LFIX,LFLT,LRCYL,LVCF,LOTHR,LO4TH,LEXVF,LROUT,LFR,LRFA,
                     * LCAREA,LCMARE,LEND,NCYL1,NCYL2,NCYL3,NCYL4,NCYL5,NCYT,IKTY,NCOPY,
                     1 NROW,IROT,IOTHR,I4ZN,I4OTH,RROD,
                     2 RMAX,PITCH,DELY,HPITCH,HDELY,SIDEI,SIDEO,GRIDF,FLATC
  ISN 0004            DIMENSION TITLE(20)
  ISN 0005          5 READ(5,10,END=40)TITLE
  ISN 0006         10 FORMAT(20A4)
  ISN 0007            WRITE(6,20)TITLE
  ISN 0008         20 FORMAT(1H0,20A4//)
                C
  ISN 0009            LFIX=15
  ISN 0010            LFLT=28
  ISN 0011            LRCYL=38
                C
  ISN 0012            J4=0
  ISN 0013            CALL FIDAS(0,0,0,2,J3,5,6)
  ISN 0014            J4=J4+J3
  ISN 0015            IF(J4.GT.0)CALL STPERR('1ST ',J3)
  ISN 0017            GRDF=GRIDF
                C
  ISN 0018            WRITE(6,22)NCYL1,NCYL2,NCYL3,NCYL4,NCYL5,NCYT,IKTY,NCOPY,NROW,
                     * IROT,IOTHR,I4ZN,I4OTH,
                     1 RROD,RMAX,PITCH,DELY,HPITCH,HDELY,SIDEI,SIDEO,GRDF,FLATC
  ISN 0019         22 FORMAT(7H0 NCYL1,I5/7H  NCYL2,I5/7H  NCYL3,I5/7H  NCYL4,I5/
                     1 7H  NCYL5,I5/7H   NCYT,I5/7H   IKTY,I5/7H  NCOPY,I5/7H   NROW,I5/
                     * 7H   IROT,I5/7H   IOTHR,I5/7H   I4ZN,I5/7H  I4OTH,I5/
                     2/7H   RROD,1PE13.5/7H   RMAX,1PE13.5/7H  PITCH,1PE13.5/7H   DELY,
                     3 1PE13.5/7H HPITCH,1PE13.5/7H  HDELY,1PE13.5 /7H  SIDEI,1PE13.5/
                     4 7H  SIDEO,1PE13.5/7H   GRDF,1PE13.5/7H  FLATC,1PE13.5//2H T//)
                C
                C
  ISN 0020            NCY24=NCYL2+NCYL4
  ISN 0021            LVCF=LRCYL+NCYT+1
  ISN 0022            LOTHR=LVCF+NCY24
  ISN 0023            LO4TH=LOTHR+NCY24
  ISN 0024            LEXVF=LO4TH+NCY24
  ISN 0025            LROUT=LEXVF+NCY24
  ISN 0026            LFR=LROUT+NCYT+3*NCY24+1
  ISN 0027            LRFA=LFR
  ISN 0028            LCAREA=LRFA+NCY24
  ISN 0029            LCMARE=LCAREA+NCYT
  ISN 0030            LEND=LCMARE+6*NCYT
                C
  ISN 0031            WRITE(6,50)LEND,LCXS
  ISN 0032            IF(LEND.GT.LCXS)GO TO 40
  ISN 0034            ILS=LEND-1
  ISN 0035            DO 25 I=LRCYL,ILS
  ISN 0036         25 D(I)=0.0
  ISN 0037            CALL FIDAS(0,0,0,2,J3,5,6)
  ISN 0038            J4=J4+J3
  ISN 0039            IF(J3.GT.0)CALL STPERR('2ND ',J3)
  ISN 0041            IF(J4.GT.0)GO TO 5
  ISN 0043            CALL RINGO(D(LRCYL),D(LROUT),D(LRFA),D(LCAREA),D(LVCF),D(LEXVF),
                     1 D(LCMARE),D(LOTHR),D(LO4TH) )
  ISN 0044            GO TO 5
  ISN 0045         40 CONTINUE
  ISN 0046         50 FORMAT(1H0,I8,2X,'LOCATIONS REQUIRED VS',I8,2X,'AVAILABLE'/)
  ISN 0047            RETURN
  ISN 0048            END
```

```
LEVEL 21.8 ( JUN 74 )                                    OS/360  FORTRAN H

          COMPILER OPTIONS - NAME=  MAIN,OPT=02,LINECNT=60,SIZE=0000K,
                             SOURCE,EBCDIC,NOLIST,NODECK,LOAD,MAP,NOEDIT,ID,NOXREF
 ISN 0002            SUBROUTINE RINGO(RCYL,ROUT,RFA,CAREA,VCF,EXVF,CHAREA,OTHR,O4TH)
 ISN 0003            COMMON D(1),LFIX,LFLT,LRCYL,LVCF,LOTHR,LO4TH,LEXVF,LROUT,LFR,LRFA,
                    * LCAREA,LCHARE,LEND,NCYL1,NCYL2,NCYL3,NCYL4,NCYL5,NCYT,IKTY,NCOPY,
                    1 NROW,IROT,IOTHR,I4ZN,I4OTH,RROD,
                    2 RMAX,PITCH,DELY,HPITCH,HDELY,SIDEI,SIDEO,GRIDF,FLATC
 ISN 0004            DIMENSION RCYL(1),ROUT(1),RFA(1),CAREA(1),VCF(1),EXVF(1),CHAREA(1)
 ISN 0005            DIMENSION OTHR(1),O4TH(1)
 ISN 0006            DATA PI/3.1415927/
 ISN 0007            RDAREA=PI*RROD**2
 ISN 0008            AFUELA=0.0
 ISN 0009            AFUELB=0.0
 ISN 0010            AGRIDA=0.0
 ISN 0011            AGRIDB=0.0
 ISN 0012            AVOIDA=0.0
 ISN 0013            AVOIDB=0.0
 ISN 0014            IRAT=IROT
 ISN 0015            IROT=MOD(IROT,2)
 ISN 0016            KAY=1
 ISN 0017            IF(IKTY.EQ.2.AND.IRAT.GT.1)KAY=2
 ISN 0019            IRCD=0
 ISN 0020            NR2=NROW/2
 ISN 0021            NR3=(NROW+1)/2
 ISN 0022            IXMAX=10
 ISN 0023            IYMAX=20
 ISN 0024            IF(MOD(IKTY+2,3).LE.1)IXMAX=1
 ISN 0026            IF(MOD(IKTY+2,3).EQ.0)IYMAX=1
 ISN 0028            IF(MOD(IKTY+2,3).EQ.1)IYMAX=3
 ISN 0030            SQ3=SQRT(3.0)
 ISN 0031            FLAT=SIDEI*SQ3
 ISN 0032            DO 5 I=1,NCYT
 ISN 0033          5 CAREA(I)=PI*(RCYL(I+1)**2-RCYL(I)**2)
 ISN 0034            IY=1
 ISN 0035            IH=0
 ISN 0036         10 CONTINUE
 ISN 0037            YHC=(IY-1)*HDELY
 ISN 0038            NO=0
 ISN 0039            IF(IH.GT.0)
                    .CALL XCLUD(XHC,YHC,SIDEO,IROT,1,NO,RMAX,XHC,YHC,RROD)
 ISN 0041            IF(NO.GT.0)GO TO 220
 ISN 0043            IX=1
 ISN 0044         20 CONTINUE
 ISN 0045            IH=IH+1
 ISN 0046            XHC=(IX-1+0.5*MOD(IY+1,2))*HPITCH
 ISN 0047            IF(IH.GT.1)
                    *CALL XCLUD(XHC,YHC,SIDEO,IROT,2,NO,RMAX,XHC,YHC,RROD)
 ISN 0049            IF(NO.GT.0)GO TO 210
 ISN 0051            IR1=NCYL1+1
 ISN 0052            IR2=IR1+NCYL2-1
 ISN 0053            K=0
 ISN 0054            IF(IH.EQ.1.AND.NCYL2.GT.0)GO TO 30
 ISN 0056            IR1=NCYL1+NCYL2+NCYL3+1
 ISN 0057            IR2=IR1+NCYL4-1
 ISN 0058            K=NCYL2
 ISN 0059         30 CONTINUE
 ISN 0060            II=IR1
 ISN 0061            IO=IR2
 ISN 0062            YSTRT=YHC-NR2*DELY
 ISN 0063            DO 200 NR=1,NROW
 ISN 0064            YC=YSTRT+(NR-1)*DELY
 ISN 0065            IF(YC.LT.0.0)GO TO 200
 ISN 0067            NN=NROW-ABS(NR-NR2-1)
 ISN 0068            IF(IROT.EQ.0)GO TO 32
 ISN 0070            NN=NR
 ISN 0071            IF(NN.GT.NR3)NN=2*NR3-NR
 ISN 0073         32 CONTINUE
 ISN 0074            ANN=NN
 ISN 0075            XSTRT=XHC-0.5*(ANN-1.0)*PITCH
 ISN 0076            NP=0
 ISN 0077            DO 190 NX=1,NN
 ISN 0078            XC=XSTRT+(NX-1)*PITCH
 ISN 0079            IF(XC.LT.0.0)GO TO 190
 ISN 0081            GO TO (33,34),KAY
```

```
ISN 0082          33 CONTINUE
ISN 0083             CALL XCLUD(XC,YC,SIDEI,IROT,3,N1,FLATC,XHC,YHC,RROD)
ISN 0084             IF(NO.GT.0)GO TO 190
ISN 0086          34 CONTINUE
ISN 0087             RC=SQRT(XC**2+YC**2)
ISN 0088             AT=0.0
ISN 0089             FAC=1.0
ISN 0090             IF(ABS(XC*YC).LE.1.0E-6.AND.RC.GT.1.0E-6)FAC=2.0
ISN 0092             IF(ABS(XC*YC).GT.1.0E-6)FAC=4.0
ISN 0094             IFAC=FAC+0.1
ISN 0095             RI=RC-RROD
ISN 0096             RO=RC+RROD
ISN 0097             GO TO (36,37),KAY
ISN 0098          36 CONTINUE
ISN 0099             IF(RI.GT.RMAX)GO TO 190
ISN 0101             IF(FLATC.GT.0.0.AND.RI.LT.0.5*FLATC)GO TO 190
ISN 0103             IROD=IROD + IFAC
ISN 0104             NM=NM+1
ISN 0105             GO TO 38
ISN 0106          37 CONTINUE
ISN 0107             IROD=IROD + IFAC
ISN 0108             NM=NM+1
ISN 0109             IF(RI.GT.RMAX)GO TO 170
ISN 0111          38 CONTINUE
ISN 0112             IF(RC.LE.0.0)GO TO 90
ISN 0114             DO  40 II=IR1,IR2
ISN 0115             R2=RCYL(II+1)
ISN 0116             IF(IH.EQ.1.AND.II.EQ.IR2)R2=SIDEO
ISN 0118             IF(RI.LT.R2)GO TO 50
ISN 0120          40 CONTINUE
ISN 0121             WRITE(6,45)IX,IY,IH,NR,NX,IROD,RI,RO
ISN 0122          45 FORMAT('0****  REGION NOT FOUND FOR THIS ROD'//
                    1 ' IX IY IH NR NX IROD RI RO :',2X,6I6,1P2E15.5/)
ISN 0123             RETURN
ISN 0124          50 CONTINUE
ISN 0125             IF(RO.LT.RCYL(II+1))GO TO 120
ISN 0127             DO 60 IO=II,IR2
ISN 0128             R2=RCYL(IO+1)
ISN 0129             IF(IH.EQ.1.AND.IO.EQ.IR2)R2=SIDEO
ISN 0131             IF(RO.LT.R2)GO TO 70
ISN 0133          60 CONTINUE
ISN 0134             IF(RO.GT.RMAX)GO TO 65
ISN 0136             WRITE(6,45)IX,IY,IH,NR,NX,IROD,RI,RO
ISN 0137             RETURN
ISN 0138          65 CONTINUE
ISN 0139             IO=IR2
ISN 0140          70 CONTINUE
ISN 0141             IOM=IO-1
ISN 0142             IF(IOM.LT.II)GO TO 85
                C   ROD DIVIDED BY SEVERAL RINGS
ISN 0144             DO 80 IP=II,IOM
ISN 0145             RCC=RCYL(IP+1)
ISN 0146             CALL INTSEC(XC,YC,RROD,RCC,THETA,PHI,IER)
ISN 0147             IF(IER.GT.0)GO TO 410
ISN 0149             CALL AREAC(RROD,RCC,THETA,PHI,AREA)
ISN 0150             RFA(K+IP+1-IR1)=RFA(K+IP+1-IR1)+(AREA-AT)*FAC
ISN 0151             AT=AREA
ISN 0152          80 CONTINUE
ISN 0153          85 CONTINUE
ISN 0154             IF(RO.GT.RMAX)GO TO 130
                C   PORTION OF ROD AREA IN LAST RING SPANNED
ISN 0156             IF(AT.GT.1.001*RDAREA)GO TO 390
ISN 0158             XCESS=RDAREA-AT
ISN 0159             IF(XCESS.LT.0.0)XCESS=0.0
ISN 0161             RFA(K+IO+1-IR1)=RFA(K+IO+1-IR1)+XCESS*FAC
ISN 0162             GO TO 190
ISN 0163          90 CONTINUE
                C   CENTRAL ROD SPANS SEVERAL ANNULI
ISN 0164             AT=0.0
ISN 0165             DO 100 II=IR1,IR2
ISN 0166             IF(RO.LT.RCYL(II+1))GO TO 110
ISN 0168             AX=CAREA(II)
ISN 0169             AT=AT+AX
ISN 0170             RFA(K+II+1-IR1)=RFA(K+II+1-IR1)+AX*FAC
ISN 0171         100 CONTINUE
ISN 0172             GO TO 190
```

```
                C   PORTION OF ROD AREA IN LAST RING SPANNED
ISN 0173          110 XCESS=ROAREA-AT
ISN 0174              IF(XCESS.LT.-0.001*ROAREA)GO TO 390
ISN 0176              IF(XCESS.LT.0.0)XCESS=0.0
ISN 0178              RFA(K+II+1-IR1)=RFA(K+II+1-IR1)+XCESS*FAC
ISN 0179              GO TO 190
                C   ROD LIES ENTIRELY WITHIN SINGLE ANNULUS
ISN 0180          120 CONTINUE
ISN 0181              RFA(K+II+1-IR1)=RFA(K+II+1-IR1)+ROAREA*FAC
ISN 0182              GO TO 190
                C   PORTION OF ROD LIES BEYOND 'RMAX'. COMPUTE AREA IN RING 'IR2'
ISN 0183          130 CONTINUE
ISN 0184              GO TO (135,140),KAY
ISN 0185          135 CONTINUE
ISN 0186              RCC=RMAX
ISN 0187              CALL INTSEC(XC,YC,RROD,RCC,THETA,PHI,IER)
ISN 0188              IF(IER.GT.0)GO TO 410
ISN 0190              CALL AREAC(RROD,RCC,THETA,PHI,AREA)
ISN 0191              GO TO 145
ISN 0192          140 AREA=ROAREA
ISN 0193          145 CONTINUE
ISN 0194              RFA(K+IO+1-IR1)=RFA(K+IO+1-IR1)+(AREA-AT)*FAC
ISN 0195              GO TO 190
ISN 0196          170 CONTINUE
ISN 0197              AREA=ROAREA
ISN 0198              AT=0.0
ISN 0199              IO=IR2
ISN 0200              RFA(K+IO+1-IR1)=RFA(K+IO+1-IR1)+(AREA-AT)*FAC
ISN 0201          190 CONTINUE
ISN 0202              IF(IH.LE.5)WRITE(6,185)NR,NM,XSTRT,YC
ISN 0204          185 FORMAT(1X,' NR  NM  XSTRT YC:',2X,2I6,1P2E15.5)
ISN 0205          200 CONTINUE
ISN 0206              IX=IX+1
ISN 0207              IF(IX.LE.IXMAX)GO TO 20
ISN 0209          210 CONTINUE
ISN 0210              IY=IY+1
ISN 0211              IF(IY.LE.IYMAX)GO TO 10
ISN 0213          220 CONTINUE
ISN 0214              K=1
ISN 0215              M=0
ISN 0216              L=0
ISN 0217              ROUT(1)=RCYL(1)
                C   ZONE 1
ISN 0218              IF(NCYL1.LE.0)GO TO 240
ISN 0220              DO 230 I=1,NCYL1
ISN 0221              K=K+1
ISN 0222              L=L+1
ISN 0223              ROUT(K)=RCYL(L+1)
ISN 0224          230 CONTINUE
ISN 0225          240 CONTINUE
                C   ZONE 2
ISN 0226              IF(NCYL2.LE.0)GO TO 270
ISN 0228              DO 260 I=1,NCYL2
ISN 0229              M=M+1
ISN 0230              L=L+1
ISN 0231              RFA(M)=RFA(M)/CAREA(L)
ISN 0232              C4T=O4TH(M)
ISN 0233              FRAC=RFA(M)*VCF(M)
ISN 0234              GRDF=GRIDF
ISN 0235              IF(IOTHR.GT.0)GRDF=OTHR(M)
ISN 0237              IF(IOTHR.LE.0)OTHR(M)=GRIDF
ISN 0239              R1=RCYL(L)
ISN 0240              R2=RCYL(L+1)
ISN 0241              IF(FRAC.LE.0.0)GO TO 250
ISN 0243              IF(I4ZN .LE.0)GO TO 245
ISN 0245              FRAC=FRAC-EXVF(M)
ISN 0246              IF(IOTHR.GT.0)FRAC=FRAC-GRDF
ISN 0248              RFA(M)=FRAC
```

```
ISN 0249        245 CONTINUE
ISN 0250            AFUELA=AFUELA+FRAC*CAREA(L)
ISN 0251            IK=L
ISN 0252            CMAREA(IK)=CMAREA(IK)+CAREA(L)*FRAC
ISN 0253            K=K+1
ISN 0254            ROUT(K)=SQRT((1.0-FRAC)*R1**2+FRAC*R2**2)
ISN 0255        250 CONTINUE
ISN 0256            IF(FRAC.GE.1.0)GO TO 260
ISN 0258            IF(GRDF.LE.0.0)GO TO 255
ISN 0260            AGRIDA=AGRIDA+GRDF*CAREA(L)
ISN 0261            IK=NCYT+L
ISN 0262            CMAREA(IK)=CMAREA(IK)+CAREA(L)*GRDF
ISN 0263            K=K+1
ISN 0264            FRAC=AMIN1(FRAC+GRDF,1.0)
ISN 0265            ROUT(K)=SQRT((1.0-FRAC)*R1**2+FRAC*R2**2)
ISN 0266        255 CONTINUE
ISN 0267            EXVF(M)=1.0-FRAC-O4T
ISN 0268            XVFM=EXVF(M)
ISN 0269            IF(FRAC.GE.1.0)GO TO 260
ISN 0271            TXM=XVFM*CAREA(L)
ISN 0272            AVOIDA=AVOIDA+TXM
ISN 0273            IK=2*NCYT+L
ISN 0274            CMAREA(IK)=CMAREA(IK)+TXM
ISN 0275            K=K+1
ISN 0276            ROUT(K)=SQRT(O4T*R1**2+(1.0-O4T)*R2**2)
ISN 0277            IF(O4T.LE.0)GO TO 260
ISN 0279            K=K+1
ISN 0280            ROUT(K)=R2
ISN 0281        260 CONTINUE
              C   ZONE 3
ISN 0282        270 IF(NCYL3.LE.0)GO TO 290
ISN 0284            DO 280 I=1,NCYL3
ISN 0285            K=K+1
ISN 0286            L=L+1
ISN 0287        280 ROUT(K)=RCYL(L+1)
              C   ZONE 4
ISN 0288        290 IF(NCYL4.LE.0)GO TO 320
ISN 0290            DO 310 I=1,NCYL4
ISN 0291            M=M+1
ISN 0292            L=L+1
ISN 0293            R1=RCYL(L)
ISN 0294            R2=RCYL(L+1)
ISN 0295            RFA(M)=RFA(M)/CAREA(L)
ISN 0296            FRAC=RFA(M)+VCF(M)
ISN 0297            C4T=O4TH(M)
ISN 0298            GRDF=GRIDF
ISN 0299            IF(IOTHR.GT.0)GRDF=OTHR(M)
ISN 0301            IF(IOTHR.LE.0)OTHR(M)=GRIDF
ISN 0303            IF(FRAC.LE.0.0)GO TO 300
ISN 0305            IF(I4ZN.LE.0)GO TO 295
ISN 0307            FRAC=FRAC-EXVF(M)
ISN 0308            IF(IOTHR.GT.0)FRAC=FRAC-GRDF
ISN 0310            RFA(M)=FRAC
ISN 0311        295 CONTINUE
ISN 0312            AFUELB=AFUELB+FRAC*CAREA(L)
ISN 0313            IK=3*NCYT+L
ISN 0314            CMAREA(IK)=CMAREA(IK)+CAREA(L)*FRAC
ISN 0315            K=K+1
ISN 0316            ROUT(K)=SQRT((1.0-FRAC)*R1**2+FRAC*R2**2)
ISN 0317        300 CONTINUE
ISN 0318            IF(FRAC.GE.1.0)GO TO 310
ISN 0320            IF(GRDF.LE.0.0)GO TO 305
ISN 0322            AGRIDB=AGRIDB+GRDF*CAREA(L)
ISN 0323            IK=4*NCYT+L
ISN 0324            CMAREA(IK)=CMAREA(IK)+CAREA(L)*GRDF
ISN 0325            FRAC=AMIN1(FRAC+GRDF,1.0)
ISN 0326            K=K+1
ISN 0327            ROUT(K)=SQRT((1.0-FRAC)*R1**2+FRAC*R2**2)
```

```
ISN 0328        305 CONTINUE
ISN 0329            EXVF(M)=1.0-FRAC-O4T
ISN 0330            XVFM=EXVF(M)
ISN 0331            IF(FRAC.GE.1.0)GO TO 310
ISN 0333            TXM=XVFM*CAREA(L)
ISN 0336            AVOIDB=AVOIDB+TXM
ISN 0335            IK=5*NCYT+L
ISN 0336            CMAREA(IK)=CMAREA(IK)+TXM
ISN 0337            K=K+1
ISN 0338            ROUT(K)=SQRT(O4T*R1**2+(1.0-O4T)*R2**2)
ISN 0339            IF(O4T.LE.0.0)GO TO 310
ISN 0341            K=K+1
ISN 0342            ROUT(K)=R2
ISN 0343        310 CONTINUE
              C   ZONE 5
ISN 0344        320 IF(NCYL5.LE.0)GO TO 340
ISN 0346            DO 330 I=1,NCYL5
ISN 0347            K=K+1
ISN 0348            L=L+1
ISN 0349            ROUT(K)=RCYL(L+1)
ISN 0350        330 CONTINUE
ISN 0351        340 CONTINUE
ISN 0352            DO 345 I=1,6
ISN 0353            DO 345 L=2,NCYT
ISN 0354            IK=(I-1)*NCYT+L
ISN 0355            IL=IK-1
ISN 0356        345 CMAREA(IK)=CMAREA(IK)+CMAREA(IL)
ISN 0357            LFR=LROUT+K
ISN 0358            WRITE(6,350)
ISN 0359        350 FORMAT(1H1,75X,'AREA'/10X,'INPUT',7X,'ROD DUCT',5X,'COOLANT',7X,
                   1 'OUTPUT',8X,'ROD',8X,'BETWEEN',7X,'OTHER'/10X,'RADII',7X,
                   2 'FRACTION',5X,'FRACTION',6X,'RADII',7X,'FRACTION',3X,
                   3 'INPUT RADII',4X,'FRACTION',3X,'4TH FRACTION'/)
ISN 0360            CALL WOT8(4,5,8,9,11,12,6,7,6,0,0)
ISN 0361            WRITE(6,351)
ISN 0362        351 FORMAT('OCUMULATIVE AREAS-ROD,OTHER&COOLANT-FOR ZONES 2&4'//)
ISN 0363            CALL WOT(CMAREA,6,NCYT,1,'INT.','QUAN',0)
ISN 0364            WRITE(6,360)IROD
ISN 0365        360 FORMAT('ONO. RODS OR PARTIAL RODS INCLUDED',I8)
ISN 0366            WRITE(6,365)AFUELA,AGRIDA,AVOIDA,AFUELB,AGRIDB,AVOIDB
ISN 0367        365 FORMAT('OSYSTEM SUMMARY'//' ZONE 2 ROD,OTHER AND COOLANT AREAS',
                   1 2X,1P3E15.5//' ZONE 4 ROD,OTHER AND COOLANT AREAS',2X,1P3E15.5//)
ISN 0368            IF(NCOPY.LE.0)GO TO 380
ISN 0370            DO 370 I=1,NCOPY
ISN 0371            CALL FFPUN(ROUT,K,1)
ISN 0372        370 CONTINUE
ISN 0373        380 CONTINUE
ISN 0374            RETURN
ISN 0375        390 WRITE(6,400)IX,IY,IH,NR,NX,IROD,II,IO
ISN 0376        400 FORMAT('OROD AREA TOTALS MORE THAN TRUE AREA'//
                   1 (1X,'IX IY IH NR NX IROD II IO',8I6))
ISN 0377            RETURN
ISN 0378        410 WRITE(6,420)IX,IY,IH,NR,NX,IROD,II,IO
ISN 0379        420 FORMAT('OROD INTERSECTS NO RINGS'//
                   1 (1X,'IX IY IH NR NX IROD II IO',8I6))
ISN 0380            RETURN
ISN 0381            END
```

```
LEVEL 21.8 ( JUN 74 )                                    OS/360  FORTRAN H

          COMPILER OPTIONS - NAME=  MAIN,OPT=02,LINECNT=60,SIZE=0000K,
                             SOURCE,EBCDIC,NOLIST,NODECK,LOAD,MAP,NOEDIT,ID,NOXREF
  ISN 0002            SUBROUTINE XCLUD(XC,YC,SIDE,IROT,KEY,NO,RM,XHC,YHC,ROD)
  ISN 0003            SQ3=SQRT(3.0)
  ISN 0004            NO=0
  ISN 0005            GO TO (10,20,50),KEY
  ISN 0006         10 CONTINUE
  ISN 0007            YLOW=YC-SIDE
  ISN 0008            YLOW=AMAX1(YLOW,0.0)
  ISN 0009            IF(IROT.EQ.0)YLOW=YC-0.5*SQ3*SIDE
  ISN 0011            IF(YLOW.GT.RM)NO=1
  ISN 0013            RETURN
  ISN 0014         20 CONTINUE
  ISN 0015            IF(IROT.GT.0)GO TO 30
  ISN 0017            Y1=YC-0.5*SQ3*SIDE
  ISN 0018            X1=XC-0.5*SIDE
  ISN 0019            X1=AMAX1(X1,0.0)
  ISN 0020            Y2=YC
  ISN 0021            X2=XC-SIDE
  ISN 0022            GO TO 40
  ISN 0023         30 Y1=YC-0.5*SIDE
  ISN 0024            Y1=AMAX1(Y1,0.0)
  ISN 0025            X1=XC-0.5*SQ3*SIDE
  ISN 0026            Y2=YC-SIDE
  ISN 0027            X2=XC
  ISN 0028         40 R1=SQRT(X1**2+Y1**2)
  ISN 0029            R2=SQRT(X2**2+Y2**2)
  ISN 0030            RA=AMIN1(R1,R2)
  ISN 0031            IF(RA.GT.RM)NO=1
  ISN 0033            RETURN
  ISN 0034         50 IF(IROT.EQ.0)RETURN
  ISN 0036            RA=ABS(XC-XHC)
  ISN 0037            IF(RA+ROD.GT.0.5*SQ3*SIDE)NO=1
  ISN 0039            RETURN
  ISN 0040            END
```

Appendix D

GROUP STRUCTURE, QUADRATURE, AND FISSION SPECTRUM

TG	GROUP ENERGY BOUNDARIES	FISSION SPECTRUM
1	1.4920E 07	3.6136E-04
2	1.2214E 07	1.5676E-03
3	1.0000E 07	4.9778E-03
4	8.1870E 06	1.2211E-02
5	6.7032E 06	2.4720E-02
6	5.4881E 06	4.0751E-02
7	4.4933E 06	5.7917E-02
8	3.6788E 06	7.3990E-02
9	3.0120E 06	8.5661E-02
10	2.4660E 06	9.1551E-02
11	2.0190E 06	9.1590E-02
12	1.6530E 06	8.6772E-02
13	1.3530E 06	7.8604E-02
14	1.1080E 06	6.8732E-02
15	9.0760E 05	5.8308E-02
16	7.4270E 05	4.8264E-02
17	6.0810E 05	3.9153E-02
18	4.9790E 05	3.1294E-02
19	4.0760E 05	2.4608E-02
20	3.3370E 05	1.9155E-02
21	2.7320E 05	1.4763E-02
22	2.2370E 05	1.1323E-02
23	1.8320E 05	8.6710E-03
24	1.5000E 05	6.5339E-03
25	1.2280E 05	7.8050E-03
26	8.6520E 04	6.1710E-03
27	5.2480E 04	1.7610E-03
28	4.0860E 04	1.7070E-03
29	3.1830E 04	8.3501E-04
30	2.4790E 04	5.7659E-04
31	1.9030E 04	3.9790E-04
32	1.5030E 04	5.9209E-04
33	7.1020E 03	1.5103E-04
34	4.3070E 03	4.2304E-05
35	3.3550E 03	2.9111E-05
36	2.6130E 03	2.0070E-05
37	2.0350E 03	1.3769E-05
38	1.5850E 03	9.4614E-06
39	1.2340E 03	6.5050E-06
40	9.6110E 02	9.6562E-06
41	4.5400E 02	3.1357E-06
42	2.1450E 02	1.0169E-06
43	1.0130E 02	3.2923E-07
44	4.7850E 01	1.0663E-07
45	2.2600E 01	3.4077E-08
46	1.0680E 01	1.0622E-08
47	5.0430E 00	3.2778E-09
48	2.3820E 00	1.0756E-09
49	1.1250E 00	3.3913E-10
50	4.1400E-01	0
51	1.0000E-01	0
52	1.0000E-05	

1	0	-2.7994E-01	-9.7941E-01	76	2.1037E-04	-9.7924E-01	9.9874E-01
2	1.6668E-02	-1.4987E-01	-9.7391E-01	77	2.3337E-04	9.7924E-01	9.9874E-01
3	1.6668E-02	1.4887E-01	-9.7391E-01	78	0	-5.5109E-02	9.9781E-01
4	0	-5.2166E-01	-8.6506E-01	79	2.3037E-04	-4.3363E-02	9.9781E-01
5	2.6667E-02	-4.3360E-01	-8.6506E-01	80	2.3337E-04	4.3363E-02	9.9781E-01
6	1.2921E-02	-1.4887E-01	-8.6506E-01	81	0	-9.5786E-02	9.9598E-01
7	1.2921E-02	1.4887E-01	-8.6506E-01	82	2.2319E-04	-5.8765E-02	9.9598E-01
8	2.6667E-02	4.3360E-01	-8.6506E-01	83	2.2319E-04	5.8765E-02	9.9598E-01
9	0	-7.3376E-01	-6.7941E-01	84	0	-1.2192E-01	9.9254E-01
10	7.7011E-02	-6.7941E-01	-6.7941E-01	85	9.9414E-04	-7.9977E-02	9.9254E-01
11	8.5501E-03	-4.3360E-01	-6.7941E-01	86	9.9414E-04	7.9977E-02	9.9254E-01
12	1.9210E-02	-1.4887E-01	-6.7941E-01	87	0	-1.5413E-01	9.8895E-01
13	1.9210E-02	1.4887E-01	-6.7941E-01	88	1.2451E-03	-1.3111E-01	9.8895E-01
14	8.5501E-03	4.3360E-01	-6.7941E-01	89	1.2451E-03	1.3111E-01	9.8895E-01
15	2.7311E-02	6.7941E-01	-6.7941E-01	90	0	-1.9821E-01	9.8251E-01
16	0	-9.5120E-01	-4.3360E-01	91	1.5035E-03	-1.2715E-01	9.8251E-01
17	2.6667E-02	-8.6506E-01	-4.3360E-01	92	1.5035E-03	1.2715E-01	9.8251E-01
18	8.5501E-03	-6.7941E-01	-4.3360E-01	93	0	-2.1800E-01	9.7593E-01
19	2.7668E-02	-4.3360E-01	-4.3360E-01	94	1.7670E-03	-1.4300E-01	9.7593E-01
20	6.8571E-03	-1.4887E-01	-4.3360E-01	95	1.7670E-03	1.4300E-01	9.7593E-01
21	6.8571E-03	1.4887E-01	-4.3360E-01	96	0	-2.4971E-01	9.6832E-01
22	2.7668E-02	4.3360E-01	-4.3360E-01	97	2.0180E-03	-1.6321E-01	9.6832E-01
23	8.5501E-03	6.7941E-01	-4.3360E-01	98	2.0180E-03	1.6301E-01	9.6832E-01
24	2.6667E-02	8.6506E-01	-4.3360E-01	99	0	-2.8110E-01	9.5968E-01
25	0	-9.8886E-01	-1.4887E-01	100	2.2715E-03	-1.8439E-01	9.5968E-01
26	1.6668E-02	-9.7391E-01	-1.4887E-01	101	2.2715E-03	1.8439E-01	9.5968E-01
27	1.2921E-02	-8.6506E-01	-1.4887E-01	102	0	-3.1216E-01	9.5003E-01
28	1.9210E-02	-6.7941E-01	-1.4887E-01	103	2.5250E-03	-2.0477E-01	9.5003E-01
29	6.8571E-03	-4.3360E-01	-1.4887E-01	104	2.5250E-03	2.0477E-01	9.5003E-01
30	1.8225E-02	-1.4887E-01	-1.4887E-01	105	0	-3.4791E-01	9.3937E-01
31	1.8225E-02	1.4887E-01	-1.4887E-01	106	2.7735E-03	-2.2494E-01	9.3937E-01
32	6.8571E-03	4.3360E-01	-1.4887E-01	107	2.7735E-03	2.2494E-01	9.3937E-01
33	1.9210E-02	6.7941E-01	-1.4887E-01	108	0	-5.0167E-01	8.6508E-01
34	1.2921E-02	8.6506E-01	-1.4887E-01	109	2.6297E-02	-4.3360E-01	8.6508E-01
35	1.6668E-02	9.7391E-01	-1.4887E-01	110	1.2844E-02	-1.4888E-01	8.6508E-01
36	0	-1.4142E-03	1.0000E 00	111	1.2844E-02	1.4888E-01	8.6508E-01
37	1.0000E-06	-9.2832E-04	1.0000E 00	112	2.6297E-02	4.3360E-01	8.6508E-01
38	1.0000E-06	9.2832E-04	1.0000E 00	113	0	-7.3377E-01	6.7942E-01
39	0	-4.6742E-03	9.9999E-01	114	2.6850E-02	-6.7942E-01	6.7940E-01
40	9.9504E-06	-2.9356E-03	9.9999E-01	115	8.4997E-03	-4.3360E-01	6.7940E-01
41	9.9504E-06	2.9356E-03	9.9999E-01	116	1.9094E-02	-1.4888E-01	6.7940E-01
42	0	-7.7358E-03	9.9997E-01	117	1.9094E-02	1.4888E-01	6.7940E-01
43	4.9504E-06	-5.0745E-03	9.9997E-01	118	8.4997E-03	4.3360E-01	6.7940E-01
44	4.9504E-06	5.0745E-03	9.9997E-01	119	2.6850E-02	6.7942E-01	6.7940E-01
45	0	-9.9829E-03	9.9[illegible]95E-01	120	0	-9.0171E-01	4.3339E-01
46	4.9504E-06	-6.5486E-03	9.9995E-01	121	2.4294E-02	-8.5507E-01	4.3339E-01
47	4.9504E-06	6.5486E-03	9.9995E-01	122	8.4997E-03	-6.7941E-01	4.3339E-01
48	0	-1.1813E-02	9.9993E-01	123	2.7304E-02	-4.3360E-01	4.3339E-01
49	4.9504E-06	-7.7471E-03	9.9993E-01	124	6.8163E-03	-1.4887E-01	4.3339E-01
50	4.9504E-06	7.7471E-03	9.9993E-01	125	6.8163E-03	1.4887E-01	4.3339E-01
51	0	-1.3390E-02	9.9991E-01	126	2.7304E-02	4.3360E-01	4.3339E-01
52	4.9504E-06	-8.7835E-03	9.9991E-01	127	8.4997E-03	6.7941E-01	4.3339E-01
53	4.9504E-06	8.7835E-03	9.9991E-01	128	2.4294E-02	8.5507E-01	4.3339E-01
54	0	-1.6403E-02	9.9987E-01	129	0	-9.7371E-01	2.2778E-01
55	1.7327E-05	-1.3760E-02	9.9987E-01	130	8.3635E-03	-9.5899E-01	2.2778E-01
56	1.7327E-05	1.0760E-02	9.9987E-01	131	6.4835E-03	-9.5182E-01	2.2778E-01
57	0	-2.0209E-02	9.9980E-01	132	9.6393E-03	-6.6900E-01	2.2778E-01
58	1.7327E-05	-1.3757E-02	9.9980E-01	133	3.4407E-03	-4.2676E-01	2.2778E-01
59	1.7327E-05	1.3757E-02	9.9980E-01	134	9.1647E-03	-1.4659E-01	2.2778E-01
60	0	-2.3606E-02	9.9973E-01	135	9.1647E-03	1.4659E-01	2.2778E-01
61	1.7327E-05	-1.5356E-02	9.9973E-01	136	3.4407E-03	4.2676E-01	2.2778E-01
62	1.7327E-05	1.5356E-02	9.9973E-01	137	6.6393E-03	6.6900E-01	2.2778E-01
63	0	-2.6214E-02	9.9966E-01	138	6.4835E-03	8.5182E-01	2.2778E-01
64	1.7327E-05	-1.7196E-02	9.9966E-01	139	8.3635E-03	9.5899E-01	2.2778E-01
65	1.7327E-05	1.7196E-02	9.9966E-01	140	0	-9.9709E-01	7.6250E-02
66	0	-2.8751E-02	9.9959E-01	141	8.5642E-03	-9.8201E-01	7.6250E-02
67	1.7327E-05	-1.8860E-02	9.9959E-01	142	6.6391E-03	-8.7227E-01	7.6250E-02
68	1.7327E-05	1.8860E-02	9.9959E-01	143	9.8706E-03	-6.8507E-01	7.6250E-02
69	0	-3.2717E-02	9.9946E-01	144	3.5233E-03	-4.3700E-01	7.6250E-02
70	4.3316E-05	-2.3461E-02	9.9946E-01	145	9.3642E-03	-1.5011E-01	7.6250E-02
71	4.3316E-05	2.3461E-02	9.9946E-01	146	9.3642E-03	1.5011E-01	7.6250E-02
72	0	-3.7607E-02	9.9929E-01	147	3.5233E-03	4.3700E-01	7.6250E-02
73	4.3316E-05	-2.6709E-02	9.9929E-01	148	9.8706E-03	6.8507E-01	7.6250E-02
74	4.3316E-05	2.6709E-02	9.9929E-01	149	6.6391E-03	8.7227E-01	7.6250E-02
75	0	-5.0191E-02	9.9876E-01	150	8.5642E-03	9.8201E-01	7.6250E-02

Appendix E

TWO-DIMENSIONAL GEOMETRY MODELS, SPACE MESH, AND CONVERGENCE PARAMETERS

Convergence and Other Parameters Used in DOT-IV
Two-Dimensional Calculations

Parameter*	Description	Value
ISCTM	Maximum scattering by zone	3
IGM	Number of energy groups	51; 7
MM	Number of directions in quadrature	150
MODE	Method used reduce unknowns in angular flux calculation	3 (weighted)
IACC	Type of rebalance	2 (space dependent)
KALF	Rebalance method	0 (J)
IBFSCL	Number flux iterations before space scaling	2
INTSCL	Number of flux iterations between space scalings	1
ITMSCL	Maximum number of scale factor iterations	60
EPS	Eigenvalue convergence criterion	0.0001
EPP	Pointwise flux convergence criterion	0.001
EPV	Volumetric flux convergence criterion	0.0001
CONACC	Rebalance acceptance criterion	0.001
CONSCL	Spatial rebalance convergence criterion	0.0001
WSOLOI	Rebalance source iteration coefficient	1.0
WSOLII	Rebalance flux iteration coefficient	1.0
WSOLCN	Rebalance constant	0.0

*All variables as they appear in DOT-IV Output.

SPATIAL FINE MESH

RADIAL AND AXIAL BOUNDARIES FOR CONFIGURATION II.A

I/J	Z (CM)	SET 1 R (CM)
1	0	0
2	3.0160E 00	2.0000E-01
3	6.0320E 00	3.2944E 00
4	9.0480E 00	6.3889E 00
5	1.2064E 01	9.4833E 00
6	1.5080E 01	1.2578E 01
7	1.8096E 01	1.5672E 01
8	2.1112E 01	1.8767E 01
9	2.4128E 01	2.1861E 01
10	2.7144E 01	2.4956E 01
11	3.0160E 01	2.8050E 01
12	3.0320E 01	2.8420E 01
13	3.0480E 01	2.8790E 01
14	3.4250E 01	2.9160E 01
15	3.8020E 01	3.1315E 01
16	4.1790E 01	3.3470E 01
17	4.5560E 01	3.5625E 01
18	4.6330E 01	3.7780E 01
19	5.3100E 01	3.7940E 01
20	5.6870E 01	3.8100E 01
21	6.0640E 01	3.9624E 01
22	6.0800E 01	4.1148E 01
23	6.0960E 01	4.2672E 01
24	6.3246E 01	4.4196E 01
25	6.5532E 01	4.5720E 01
26	6.7818E 01	4.7244E 01
27	7.0104E 01	4.8768E 01
28	7.2390E 01	5.0292E 01
29	7.4676E 01	5.1816E 01
30	7.6962E 01	5.3340E 01
31	7.9248E 01	5.3657E 01
32	8.1534E 01	5.3973E 01
33	8.3820E 01	5.4290E 01
34	8.6106E 01	5.6386E 01
35	8.8392E 01	5.8482E 01
36	9.0678E 01	6.0578E 01
37	9.2964E 01	6.2674E 01
38	9.5250E 01	6.4770E 01
39	9.75[illegible]6E 01	6.7627E 01
40	9.9[illegible]22E 01	7.0484E 01
41	1.0211E 02	7.3341E 01
42	1.0439E 02	7.6199E 01
43	1.0668E 02	7.9056E 01
44	1.0700E 02	8.1913E 01
45	1.0731E 02	8.4770E 01
46	1.0763E 02	
47	1.1012E 02	
48	1.1261E 02	
49	1.1511E 02	
50	1.1760E 02	
51	1.2009E 02	
52	1.2258E 02	
53	1.2508E 02	
54	1.2757E 02	
55	1.3006E 02	
56	1.3255E 02	
57	1.3505E 02	
58	1.3754E 02	
59	1.4003E 02	
60	1.4252E 02	
61	1.4502E 02	
62	1.4751E 02	
63	1.5000E 02	
64	1.5249E 02	
65	1.5499E 02	
66	1.5748E 02	

RADIAL AND AXIAL BOUNDARIES FOR CONFIGURATION II.B

I/J	Z (CM)	SET 1 R (CM)
1	0	0
2	3.0160E 00	2.4232E 00
3	6.0320E 00	3.2004E 00
4	9.0480E 00	5.2173E 00
5	1.2064E 01	6.4013E 00
6	1.5080E 01	8.3269E 00
7	1.8096E 01	9.6019E 00
8	2.1112E 01	9.9353E 00
9	2.4128E 01	1.0380E 01
10	2.7144E 01	1.0824E 01
11	3.0160E 01	1.1269E 01
12	3.0320E 01	1.1554E 01
13	3.0480E 01	1.2972E 01
14	3.1120E 01	1.4117E 01
15	3.3025E 01	1.5533E 01
16	3.7627E 01	1.6680E 01
17	4.2230E 01	1.8065E 01
18	4.6832E 01	1.9243E 01
19	5.1435E 01	2.0597E 01
20	5.6037E 01	2.1806E 01
21	6.0640E 01	2.3105E 01
22	6.0800E 01	2.4369E 01
23	6.0960E 01	2.6023E 01
24	6.3246E 01	2.6932E 01
25	6.5532E 01	2.7292E 01
26	6.7818E 01	2.7545E 01
27	7.0104E 01	2.7798E 01
28	7.2350E 01	2.8050E 01
29	7.4676E 01	2.8420E 01
30	7.6962E 01	2.8790E 01
31	7.9248E 01	2.9160E 01
32	8.1534E 01	3.1315E 01
33	8.3820E 01	3.3470E 01
34	8.6106E 01	3.5625E 01
35	8.8392E 01	3.7780E 01
36	9.0678E 01	3.7940E 01
37	9.2964E 01	3.8100E 01
38	9.5250E 01	3.9624E 01
39	9.7536E 01	4.1148E 01
40	9.9872E 01	4.2672E 01
41	1.0211E 02	4.4196E 01
42	1.0439E 02	4.5720E 01
43	1.0668E 02	4.7244E 01
44	1.0700E 02	4.8768E 01
45	1.0731E 02	5.0292E 01
46	1.0763E 02	5.1816E 01
47	1.1026E 02	5.3340E 01
48	1.1289E 02	5.3657E 01
49	1.1552E 02	5.3973E 01
50	1.1814E 02	5.4290E 01
51	1.2077E 02	5.6386E 01
52	1.2340E 02	5.8482E 01
53	1.2603E 02	6.0578E 01
54	1.2866E 02	6.2674E 01
55	1.3129E 02	6.4770E 01
56	1.3392E 02	6.7627E 01
57	1.3654E 02	7.0484E 01
58	1.3917E 02	7.3341E 01
59	1.4180E 02	7.6199E 01
60	1.4443E 02	7.9056E 01
61	1.4706E 02	8.1913E 01
62	1.4969E 02	8.4770E 01
63	1.5232E 02	
64	1.5494E 02	
65	1.5685E 02	
66	1.5748E 02	

RADIAL AND AXIAL BOUNDARIES FOR CONFIGURATION II.D

I/J	Z (CM)	SET 1 R (CM)	SET 2 R (CM)
1	-6.4516E 01	0	0
2	-6.2230E 01	2.4232E 00	7.4532E-01
3	-5.9944E 01	3.2006E 00	1.4906E 00
4	-5.7658E 01	5.2173E 00	2.2360E 00
5	-5.5372E 01	6.4013E 00	2.9813E 00
6	-5.3086E 01	8.3269E 00	3.7266E 00
7	-5.0800E 01	9.6019E 00	4.4719E 00
8	-5.0483E 01	9.9353E 00	5.2173E 00
9	-5.0167E 01	1.0380E 01	6.1435E 00
10	-4.9850E 01	1.0824E 01	6.6634E 00
11	-4.7221E 01	1.1269E 01	7.0841E 00
12	-4.4593E 01	1.1554E 01	7.5048E 00
13	-4.1964E 01	1.2972E 01	7.9255E 00
14	-3.9336E 01	1.4117E 01	8.0834E 00
15	-3.6707E 01	1.5533E 01	8.8427E 00
16	-3.4078E 01	1.6680E 01	9.6019E 00
17	-3.1450E 01	1.8065E 01	9.9353E 00
18	-2.8821E 01	1.9243E 01	1.0602E 01
19	-2.6193E 01	2.0597E 01	1.1269E 01
20	-2.3564E 01	2.1806E 01	1.1554E 01
21	-2.0935E 01	2.3105E 01	1.2767E 01
22	-1.8307E 01	2.4369E 01	1.3980E 01
23	-1.5678E 01	2.6023E 01	1.4414E 01
24	-1.3049E 01	2.6932E 01	1.4874E 01
25	-1.0421E 01	2.7292E 01	1.5296E 01
26	-7.7922E 00	2.7545E 01	1.5683E 01
27	-5.1636E 00	2.7798E 01	1.5947E 01
28	-2.5350E 00	2.8050E 01	1.6680E 01
29	-6.3000E-01	2.8420E 01	1.7412E 01
30	0	2.8790E 01	1.8145E 01
31	2.9972E 00	2.9160E 01	1.8877E 01
32	5.9944E 00	3.1315E 01	1.9609E 01
33	8.6616E 00	3.3470E 01	2.0341E 01
34	1.1329E 01	3.5625E 01	2.1074E 01
35	1.3996E 01	3.7780E 01	2.1806E 01
36	1.6663E 01	3.7940E 01	2.2503E 01
37	1.9330E 01	3.8100E 01	2.2837E 01
38	2.1998E 01	3.9624E 01	2.3307E 01
39	2.4665E 01	4.1148E 01	2.3797E 01
40	2.7332E 01	4.2672E 01	2.4305E 01
41	2.9999E 01	4.4196E 01	2.4761E 01
42	3.2666E 01	4.5720E 01	2.5846E 01
43	3.5334E 01	4.7244E 01	2.6932E 01
44	3.8001E 01	4.8768E 01	2.7292E 01
45	4.0334E 01	5.0292E 01	2.7671E 01
46	4.2668E 01	5.1816E 01	2.8050E 01
47	4.5001E 01	5.3340E 01	2.8605E 01
48		5.3657E 01	2.9160E 01
49		5.3973E 01	3.3470E 01
50		5.4290E 01	3.8100E 01
51		5.6386E 01	4.2672E 01
52		5.8482E 01	4.7244E 01
53		6.0578E 01	5.1816E 01
54		6.2674E 01	5.6386E 01
55		6.4770E 01	6.0578E 01
56		6.7627E 01	6.4770E 01
57		7.0484E 01	6.7627E 01
58		7.3341E 01	7.0484E 01
59		7.6199E 01	7.3341E 01
60		7.9056E 01	7.6199E 01
61		8.1913E 01	7.9056E 01
62		8.4770E 01	8.4770E 01

RADIAL AND AXIAL BOUNDARIES FOR CONFIGURATION II.E

I/J	Z (CM)	SET 1 R (CM)	SET 2 R (CM)
1	-2.5400E 00	0	0
2	-6.3500E-01	8.0773E-01	7.6793E-01
3	0	1.6155E 00	1.5359E 00
4	2.9972E 00	2.4232E 00	2.3038E 00
5	5.9944E 00	2.8119E 00	3.0717E 00
6	8.6616E 00	3.2006E 00	3.8397E 00
7	1.1329E 01	3.8713E 00	4.6076E 00
8	1.3996E 01	4.5420E 00	5.3755E 00
9	1.6663E 01	5.2128E 00	6.1435E 00
10	1.9330E 01	5.8070E 00	6.6634E 00
11	2.1998E 01	6.4013E 00	7.0805E 00
12	2.4665E 01	7.0432E 00	7.5048E 00
13	2.7332E 01	7.6850E 00	7.9255E 00
14	2.9999E 01	8.3269E 00	8.0045E 00
15	3.2666E 01	8.9644E 00	8.0834E 00
16	3.5334E 01	9.6019E 00	9.6019E 00
17	3.8001E 01	9.9353E 00	9.9353E 00
18	4.0334E 01	1.0602E 01	1.0602E 01
19	4.2668E 01	1.1269E 01	1.1269E 01
20	4.5001E 01	1.1554E 01	1.1554E 01
21	4.7382E 01	1.2263E 01	1.2767E 01
22	5.0875E 01	1.2972E 01	1.3980E 01
23	5.4367E 01	1.3545E 01	1.4414E 01
24	5.7304E 01	1.4117E 01	1.4874E 01
25	6.0241E 01	1.4723E 01	1.5296E 01
26	6.4051E 01	1.5328E 01	1.5683E 01
27	6.7861E 01	1.5947E 01	1.5947E 01
28	7.1671E 01	1.6680E 01	1.6624E 01
29	7.5481E 01	1.7373E 01	1.7301E 01
30	7.9291E 01	1.8065E 01	1.7977E 01
31	8.3101E 01	1.8654E 01	1.8654E 01
32	8.6911E 01	1.9243E 01	1.9442E 01
33	9.0721E 01	1.9920E 01	2.0230E 01
34	9.4531E 01	2.0597E 01	2.1018E 01
35	9.8341E 01	2.1201E 01	2.1806E 01
36	1.0215E 02	2.1806E 01	2.2503E 01
37	1.0596E 02	2.2456E 01	2.2837E 01
38	1.0977E 02	2.3105E 01	2.3307E 01
39	1.1358E 02	2.3737E 01	2.3797E 01
40	1.1739E 02	2.4369E 01	2.4305E 01
41	1.2120E 02	2.5196E 01	2.4761E 01
42		2.6023E 01	2.5196E 01
43		2.6932E 01	2.6932E 01
44		2.7292E 01	2.7292E 01
45		2.7671E 01	2.7671E 01
46		2.8050E 01	2.8050E 01
47		2.8615E 01	2.8615E 01
48		2.9180E 01	2.9180E 01
49		3.0590E 01	3.0200E 01
50		3.2000E 01	3.2000E 01
51		3.4750E 01	3.4750E 01
52		3.7500E 01	3.7500E 01
53		4.0250E 01	4.0250E 01
54		4.3000E 01	4.3000E 01
55		4.5750E 01	4.6000E 01
56		4.8500E 01	4.9000E 01
57		5.0920E 01	5.2000E 01
58		5.3340E 01	5.5000E 01
59		5.3815E 01	5.8000E 01
60		5.4290E 01	6.1000E 01
61		5.8000E 01	6.4000E 01
62		6.2500E 01	6.7000E 01
63		6.7000E 01	7.0000E 01
64		7.1500E 01	7.3000E 01
65		7.6000E 01	7.6000E 01
66		7.9000E 01	7.9000E 01
67		8.2000E 01	8.2000E 01
68		8.5000E 01	8.5000E 01

RADIAL AND AXIAL BOUNDARIES FOR CONFIGURATION III.F

I/J	Z (CM)	SET 1 R (CM)	SET 2 R (CM)	SET 3 R (CM)
1	-2.5400E 00	0	0	0
2	-6.3500E-01	8.0773E-01	7.6793E-01	7.0211E-01
3	0	1.6155E 00	1.5359E 00	1.4042E 00
4	2.5872E 00	2.4232E 00	2.3038E 00	2.1063E 00
5	5.9944E 00	2.8119E 00	3.0717E 00	2.8084E 00
6	8.6616E 00	3.2006E 00	3.8397E 00	3.5105E 00
7	1.1329E 01	3.8713E 00	4.6076E 00	4.1423E 00
8	1.3996E 01	4.5420E 00	5.3755E 00	4.7741E 00
9	1.6663E 01	5.2128E 00	6.1435E 00	5.4058E 00
10	1.9330E 01	5.8070E 00	6.6634E 00	6.0376E 00
11	2.1998E 01	6.4013E 00	7.0805E 00	6.5590E 00
12	2.4665E 01	7.0432E 00	7.5048E 00	7.0805E 00
13	2.7332E 01	7.6850E 00	7.9255E 00	7.6677E 00
14	2.9999E 01	8.3269E 00	8.0045E 00	8.2550E 00
15	3.2666E 01	8.9644E 00	8.0834E 00	8.8151E 00
16	3.5334E 01	9.6019E 00	9.6019E 00	9.3752E 00
17	3.8001E 01	9.9353E 00	9.9353E 00	9.9353E 00
18	4.0334E 01	1.0602E 01	1.0602E 01	1.0475E 01
19	4.2668E 01	1.1269E 01	1.1269E 01	1.1015E 01
20	4.5001E 01	1.1554E 01	1.1554E 01	1.1554E 01
21	4.8115E 01	1.2263E 01	1.2767E 01	1.2149E 01
22	5.1229E 01	1.2972E 01	1.3980E 01	1.2743E 01
23	5.3954E 01	1.3545E 01	1.4414E 01	1.3337E 01
24	5.6760E 01	1.4117E 01	1.4874E 01	1.3931E 01
25	5.9525E 01	1.4723E 01	1.5296E 01	1.4614E 01
26	6.2250E 01	1.5328E 01	1.5683E 01	1.5296E 01
27	6.5056E 01	1.5947E 01	1.5947E 01	1.5947E 01
28	6.7821E 01	1.6680E 01	1.6624E 01	1.6401E 01
29	7.0950E 01	1.7373E 01	1.7301E 01	1.7267E 01
30	7.4079E 01	1.8065E 01	1.7977E 01	1.8132E 01
31	7.7209E 01	1.8654E 01	1.8654E 01	1.8654E 01
32	8.0338E 01	1.9243E 01	1.9442E 01	1.9451E 01
33	8.3467E 01	1.9920E 01	2.0230E 01	2.0249E 01
34	8.6596E 01	2.0597E 01	2.1018E 01	2.1046E 01
35	8.9726E 01	2.1201E 01	2.1806E 01	2.1806E 01
36	9.2855E 01	2.1806E 01	2.2503E 01	2.2084E 01
37	9.5984E 01	2.2456E 01	2.2837E 01	2.2696E 01
38	9.9113E 01	2.3105E 01	2.3307E 01	2.3307E 01
39	1.0224E 02	2.3737E 01	2.3797E 01	2.3931E 01
40	1.0537E 02	2.4369E 01	2.4305E 01	2.4555E 01
41	1.0850E 02	2.5196E 01	2.4761E 01	2.5196E 01
42		2.6023E 01	2.5196E 01	2.5895E 01
43		2.6932E 01	2.6932E 01	2.6593E 01
44		2.7292E 01	2.7292E 01	2.7292E 01
45		2.7671E 01	2.7671E 01	2.7671E 01
46		2.8050E 01	2.8050E 01	2.8050E 01
47		2.8615E 01	2.8615E 01	2.8615E 01
48		2.9180E 01	2.9180E 01	2.9180E 01
49		3.0590E 01	3.0200E 01	3.0200E 01
50		3.2000E 01	3.2000E 01	3.2000E 01
51		3.4750E 01	3.4750E 01	3.4750E 01
52		3.7500E 01	3.7500E 01	3.7500E 01
53		4.0250E 01	4.0250E 01	4.0250E 01
54		4.3000E 01	4.3000E 01	4.3000E 01
55		4.5750E 01	4.6000E 01	4.6000E 01
56		4.8500E 01	4.8500E 01	4.8500E 01
57		5.0920E 01	5.1395E 01	5.1395E 01
58		5.3340E 01	5.4290E 01	5.4290E 01
59		5.3815E 01	5.8000E 01	5.8000E 01
60		5.4290E 01	6.1000E 01	6.1000E 01
61		5.8000E 01	6.4000E 01	6.4000E 01
62		6.2500E 01	6.7000E 01	6.7000E 01
63		6.7000E 01	7.0000E 01	7.0000E 01
64		7.1500E 01	7.3000E 01	7.3000E 01
65		7.6000E 01	7.6000E 01	7.6000E 01
66		7.9000E 01	7.9000E 01	7.9000E 01
67		8.2000E 01	8.2000E 01	8.2000E 01
68		8.5000E 01	8.5000E 01	8.5000E 01

RADIAL AND AXIAL BOUNDARIES FOR CONFIGURATION III.A

I/J	Z (CM)	SET 1 R (CM)
1	0	0
2	3.0160E 00	2.4232E 00
3	6.0320E 00	3.2006E 00
4	9.0480E 00	5.2173E 00
5	1.2064E 01	6.4013E 00
6	1.5080E 01	8.3269E 00
7	1.8096E 01	9.6019E 00
8	2.1112E 01	9.9353E 00
9	2.4128E 01	1.0158E 01
10	2.7144E 01	1.0380E 01
11	3.0160E 01	1.0602E 01
12	3.0320E 01	1.0905E 01
13	3.0480E 01	1.2367E 01
14	3.1120E 01	1.3491E 01
15	3.3025E 01	1.4968E 01
16	3.7627E 01	1.6077E 01
17	4.2230E 01	1.7527E 01
18	4.6832E 01	1.8664E 01
19	5.1435E 01	2.0076E 01
20	5.6037E 01	2.1250E 01
21	6.0640E 01	2.2592E 01
22	6.0800E 01	2.3836E 01
23	6.0960E 01	2.5489E 01
24	6.3246E 01	2.6422E 01
25	6.5532E 01	2.6790E 01
26	6.7818E 01	2.7210E 01
27	7.0104E 01	2.7630E 01
28	7.2350E 01	2.8050E 01
29	7.4676E 01	2.8427E 01
30	7.6962E 01	2.8803E 01
31	7.9248E 01	2.9180E 01
32	8.1534E 01	3.1330E 01
33	8.3820E 01	3.3480E 01
34	8.6106E 01	3.5630E 01
35	8.8392E 01	3.7780E 01
36	9.0678E 01	3.7940E 01
37	9.2964E 01	3.8100E 01
38	9.5250E 01	3.5624E 01
39	9.7536E 01	4.1148E 01
40	9.9822E 01	4.2672E 01
41	1.0211E 02	4.4196E 01
42	1.0439E 02	4.5720E 01
43	1.0668E 02	4.7244E 01
44	1.0700E 02	4.8768E 01
45	1.0731E 02	5.0292E 01
46	1.0763E 02	5.1816E 01
47	1.1026E 02	5.3340E 01
48	1.1289E 02	5.3657E 01
49	1.1552E 02	5.3973E 01
50	1.1814E 02	5.4290E 01
51	1.2077E 02	5.6386E 01
52	1.2340E 02	5.8482E 01
53	1.2603E 02	6.0578E 01
54	1.2866E 02	6.2674E 01
55	1.3129E 02	6.4770E 01
56	1.3392E 02	6.7627E 01
57	1.3654E 02	7.0484E 01
58	1.3917E 02	7.3341E 01
59	1.4180E 02	7.6199E 01
60	1.4443E 02	7.9056E 01
61	1.4706E 02	8.1913E 01
62	1.4969E 02	8.4770E 01
63	1.5232E 02	
64	1.5494E 02	
65	1.5685E 02	
66	1.5748E 02	

RADIAL AND AXIAL BOUNDARIES FOR CONFIGURATION IV.A

I/J	Z (CM)	SET 1 R (CM)
1	0	0
2	3.0160E 00	2.1079E 00
3	6.0320E 00	3.2006E 00
4	9.0480E 00	4.9152E 00
5	1.2064E 01	6.4013E 00
6	1.5080E 01	7.7014E 00
7	1.8096E 01	9.6019E 00
8	2.1112E 01	9.9353E 00
9	2.4128E 01	1.0380E 01
10	2.7144E 01	1.0824E 01
11	3.0160E 01	1.1269E 01
12	3.0320E 01	1.1554E 01
13	3.0480E 01	1.2471E 01
14	3.1120E 01	1.4117E 01
15	3.3025E 01	1.5170E 01
16	3.7627E 01	1.6680E 01
17	4.2230E 01	1.7799E 01
18	4.6832E 01	1.9243E 01
19	5.1435E 01	2.0280E 01
20	5.6037E 01	2.1806E 01
21	6.0640E 01	2.2812E 01
22	6.0800E 01	2.4369E 01
23	6.0960E 01	2.5490E 01
24	6.3246E 01	2.6932E 01
25	6.5532E 01	2.7292E 01
26	6.7818E 01	2.7545E 01
27	7.0104E 01	2.7798E 01
28	7.2350E 01	2.8050E 01
29	7.4676E 01	2.8427E 01
30	7.6962E 01	2.8803E 01
31	7.9248E 01	2.9180E 01
32	8.1534E 01	3.1330E 01
33	8.3820E 01	3.3480E 01
34	8.6106E 01	3.5630E 01
35	8.8392E 01	3.7780E 01
36	9.0678E 01	3.7940E 01
37	9.2964E 01	3.8100E 01
38	9.5250E 01	3.9624E 01
39	9.7536E 01	4.1148E 01
40	9.9822E 01	4.2672E 01
41	1.0211E 02	4.4196E 01
42	1.0439E 02	4.5720E 01
43	1.0668E 02	4.7244E 01
44	1.0700E 02	4.8768E 01
45	1.0731E 02	5.0292E 01
46	1.0763E 02	5.1816E 01
47	1.1026E 02	5.3340E 01
48	1.1289E 02	5.3657E 01
49	1.1552E 02	5.3973E 01
50	1.1814E 02	5.4290E 01
51	1.2077E 02	5.6386E 01
52	1.2340E 02	5.8482E 01
53	1.2603E 02	6.0578E 01
54	1.2866E 02	6.2674E 01
55	1.3129E 02	6.4770E 01
56	1.3392E 02	6.7627E 01
57	1.3654E 02	7.0484E 01
58	1.3917E 02	7.3341E 01
59	1.4180E 02	7.6199E 01
60	1.4443E 02	7.9056E 01
61	1.4706E 02	8.1913E 01
62	1.4969E 02	8.4770E 01
63	1.5232E 02	
64	1.5494E 02	
65	1.5685E 02	
66	1.5748E 02	

RADIAL AND AXIAL BOUNDARIES FOR CONFIGURATION IV.B

I/J	Z (CM)	SET 1 R (CM)	SET 2 R (CM)
1	-6.4516E 01	0	0
2	-6.2230E 01	2.1079E 00	7.0217E 01
3	-5.9944E 01	3.2006E 00	1.4043E 03
4	-5.7658E 01	4.9152E 00	2.1065E 00
5	-5.5372E 01	6.4013E 00	2.8087E 00
6	-5.3086E 01	7.7014E 00	3.5109E 00
7	-5.0800E 01	9.6019E 00	4.2130E 00
8	-5.0483E 01	9.9353E 00	4.9152E 00
9	-5.0167E 01	1.0380E 01	6.1435E 00
10	-4.9850E 01	1.0824E 01	6.6634E 00
11	-4.7221E 01	1.1269E 01	7.0805E 00
12	-4.4593E 01	1.1554E 01	7.5048E 00
13	-4.1964E 01	1.2471E 01	7.9255E 00
14	-3.9336E 01	1.4117E 01	8.0834E 00
15	-3.6707E 01	1.5170E 01	8.8427E 00
16	-3.4078E 01	1.6680E 01	9.6019E 00
17	-3.1450E 01	1.7799E 01	9.9353E 00
18	-2.8821E 01	1.9243E 01	1.0602E 01
19	-2.6153E 01	2.0280E 01	1.1269E 01
20	-2.3564E 01	2.1806E 01	1.1554E 01
21	-2.0935E 01	2.2812E 01	1.2767E 01
22	-1.8307E 01	2.4369E 01	1.3980E 01
23	-1.5678E 01	2.5490E 01	1.4414E 01
24	-1.3049E 01	2.6932E 01	1.4874E 01
25	-1.0421E 01	2.7292E 01	1.5296E 01
26	-7.7922E 00	2.7545E 01	1.5683E 01
27	-5.1638E 00	2.7798E 01	1.5947E 01
28	-2.5350E 00	2.8050E 01	1.6680E 01
29	-6.3000E-01	2.8427E 01	1.7412E 01
30	0	2.8803E 01	1.8145E 01
31	2.9972E 00	2.9180E 01	1.8877E 01
32	5.9944E 00	3.1330E 01	1.9609E 01
33	8.6616E 00	3.3480E 01	2.0341E 01
34	1.1329E 01	3.5630E 01	2.1074E 01
35	1.3996E 01	3.7780E 01	2.1806E 01
36	1.6663E 01	3.7940E 01	2.2503E 01
37	1.9330E 01	3.8100E 01	2.2837E 01
38	2.1998E 01	3.9624E 01	2.3307E 01
39	2.4665E 01	4.1148E 01	2.3797E 01
40	2.7332E 01	4.2672E 01	2.4305E 01
41	2.9999E 01	4.4196E 01	2.4761E 01
42	3.2666E 01	4.5720E 01	2.5846E 01
43	3.5334E 01	4.7244E 01	2.6932E 01
44	3.8001E 01	4.8768E 01	2.7292E 01
45	4.0334E 01	5.0292E 01	2.7671E 01
46	4.2668E 01	5.1816E 01	2.8050E 01
47	4.5001E 01	5.3340E 01	2.8605E 01
48		5.3657E 01	2.9160E 01
49		5.3973E 01	3.3470E 01
50		5.4290E 01	3.8100E 01
51		5.6386E 01	4.2672E 01
52		5.8482E 01	4.7244E 01
53		6.0578E 01	5.1816E 01
54		6.2674E 01	5.6386E 01
55		6.4770E 01	6.0578E 01
56		6.7627E 01	6.4770E 01
57		7.0484E 01	6.7627E 01
58		7.3341E 01	7.0484E 01
59		7.6199E 01	7.3341E 01
60		7.9056E 01	7.6199E 01
61		8.1913E 01	7.9056E 01
62		8.4770E 01	8.4770E 01

RADIAL AND AXIAL BOUNDARIES FOR CONFIGURATION VI.A

I/J	Z (CM)	SET I R (CM)
1	0	0
2	3.0160E 00	2.4232E 00
3	6.0320E 00	3.2006E 00
4	9.0480E 00	5.2173E 00
5	1.2064E 01	6.4013E 00
6	1.5080E 01	8.3269E 00
7	1.8096E 01	9.6019E 00
8	2.1112E 01	9.9353E 00
9	2.4128E 01	1.0046E 01
10	2.7144E 01	1.0158E 01
11	3.0160E 01	1.0269E 01
12	3.0320E 01	1.0581E 01
13	3.0480E 01	1.2097E 01
14	3.1120E 01	1.3179E 01
15	3.3025E 01	1.4693E 01
16	3.7627E 01	1.5776E 01
17	4.2230E 01	1.7259E 01
18	4.6832E 01	1.8374E 01
19	5.1435E 01	1.9816E 01
20	5.6037E 01	2.0972E 01
21	6.0640E 01	2.2338E 01
22	6.0800E 01	2.3570E 01
23	6.0960E 01	2.5219E 01
24	6.3246E 01	2.6167E 01
25	6.5532E 01	2.6583E 01
26	6.7818E 01	2.7072E 01
27	7.0104E 01	2.7561E 01
28	7.2350E 01	2.8050E 01
29	7.4676E 01	2.8427E 01
30	7.6962E 01	2.8803E 01
31	7.9248E 01	2.9180E 01
32	8.1534E 01	3.1330E 01
33	8.3820E 01	3.3480E 01
34	8.6106E 01	3.5630E 01
35	8.8392E 01	3.7780E 01
36	9.0678E 01	3.7940E 01
37	9.2964E 01	3.8100E 01
38	9.5250E 01	3.9674E 01
39	9.7536E 01	4.1148E 01
40	9.9822E 01	4.2672E 01
41	1.0211E 02	4.4196E 01
42	1.0439E 02	4.5720E 01
43	1.0668E 02	4.7244E 01
44	1.0700E 02	4.8768E 01
45	1.0731E 02	5.0292E 01
46	1.0763E 02	5.1816E 01
47	1.1026E 02	5.3340E 01
48	1.1289E 02	5.3657E 01
49	1.1552E 02	5.3973E 01
50	1.1814E 02	5.4290E 01
51	1.2077E 02	5.6386E 01
52	1.2340E 02	5.8482E 01
53	1.2603E 02	6.0578E 01
54	1.2866E 02	6.2674E 01
55	1.3129E 02	6.4770E 01
56	1.3392E 02	6.7627E 01
57	1.3654E 02	7.0484E 01
58	1.3917E 02	7.3341E 01
59	1.4180E 02	7.6199E 01
60	1.4443E 02	7.9056E 01
61	1.4706E 02	8.1913E 01
62	1.4969E 02	8.4770E 01
63	1.5232E 02	
64	1.5494E 02	
65	1.5685E 02	
66	1.5748E 02	

RADIAL AND AXIAL BOUNDARIES FOR CONFIGURATION II.F S-10 CALCULATION

I/J	Z (CM)	SET 1 R (CM)	SET 2 R (CM)	SET 3 R (CM)
1	-6.4516E 01	0	0	0
2	-6.2230E 01	9.6070E-01	7.6793E-01	7.0211E-01
3	-5.9944E 01	1.3717E 00	1.5359E 00	1.4342E 00
4	-5.7658E 01	2.1999E 00	2.3038E 00	2.1063E 00
5	-5.5372E 01	2.7434E 00	3.0717E 00	2.8084E 00
6	-5.3086E 01	3.5651E 00	3.8397E 00	3.5105E 00
7	-5.0800E 01	4.1151E 00	4.6076E 00	4.1473E 00
8	-5.0483E 01	4.9169E 00	5.3755E 00	4.7741E 00
9	-5.0167E 01	5.4869E 00	6.1435E 00	5.4058E 00
10	-4.9850E 01	6.2583E 00	6.6634E 00	6.0376E 00
11	-4.7222E 01	6.8585E 00	7.0805E 00	6.5590E 00
12	-4.4593E 01	7.6514E 00	7.5048E 00	7.0835E 00
13	-4.1965E 01	8.2302E 00	7.9255E 00	7.6577E 00
14	-3.9337E 01	9.0594E 00	8.0045E 00	8.2550E 00
15	-3.6708E 01	9.6019E 00	8.0834E 00	8.8151E 00
16	-3.4080E 01	9.9353E 00	9.6019E 00	9.3752E 00
17	-3.1452E 01	1.0602E 01	9.9353E 00	9.9353E 00
18	-2.8823E 01	1.1269E 01	1.0602E 01	1.0475E 01
19	-2.6195E 01	1.1554E 01	1.1269E 01	1.1015E 01
20	-2.3567E 01	1.2282E 01	1.1554E 01	1.1554E 01
21	-2.0938E 01	1.2836E 01	1.2767E 01	1.2148E 01
22	-1.8310E 01	1.3497E 01	1.3980E 01	1.2743E 01
23	-1.5682E 01	1.4117E 01	1.4414E 01	1.3337E 01
24	-1.3053E 01	1.4790E 01	1.4874E 01	1.3931E 01
25	-1.0425E 01	1.5399E 01	1.5296E 01	1.4614E 01
26	-7.7967E 00	1.6104E 01	1.5683E 01	1.5296E 01
27	-5.1684E 00	1.6680E 01	1.5947E 01	1.5947E 01
28	-2.5400E 00	1.7367E 01	1.6624E 01	1.6401E 01
29	-6.3500E-01	1.7961E 01	1.7301E 01	1.7267E 01
30	0	1.8637E 01	1.7977E 01	1.8132E 01
31	2.9972E 00	1.9243E 01	1.8654E 01	1.8654E 01
32	5.9944E 00	1.9905E 01	1.9442E 01	1.9451E 01
33	8.6614E 00	2.0524E 01	2.0230E 01	2.0249E 01
34	1.1329E 01	2.1196E 01	2.1018E 01	2.1046E 01
35	1.3996E 01	2.1806E 01	2.1806E 01	2.1804E 01
36	1.6663E 01	2.2495E 01	2.2503E 01	2.2084E 01
37	1.9330E 01	2.3087E 01	2.2837E 01	2.2694E 01
38	2.1998E 01	2.3683E 01	2.3307E 01	2.3307E 01
39	2.4665E 01	2.4369E 01	2.3797E 01	2.3931E 01
40	2.7332E 01	2.4876E 01	2.4305E 01	2.4555E 01
41	2.9999E 01	2.5650E 01	2.4761E 01	2.5196E 01
42	3.2666E 01	2.6764E 01	2.5196E 01	2.5895E 01
43	3.5334E 01	2.6932E 01	2.6932E 01	2.6593E 01
44	3.8001E 01	2.7297E 01	2.7292E 01	2.7292E 01
45	4.0334E 01	2.7671E 01	2.7671E 01	2.7671E 01
46	4.2668E 01	2.8050E 01	2.8050E 01	2.8050E 01
47	4.5001E 01	2.8615E 01	2.8615E 01	2.8615E 01
48	4.8115E 01	2.9180E 01	2.9180E 01	2.9180E 01
49	5.1229E 01	3.0590E 01	3.0200E 01	3.0200E 01
50	5.3994E 01	3.2000E 01	3.2000E 01	3.2000E 01
51	5.6760E 01	3.4750E 01	3.4750E 01	3.4750E 01
52	5.9525E 01	3.7500E 01	3.7500E 01	3.7500E 01
53	6.2290E 01	4.0250E 01	4.0250E 01	4.0250E 01
54	6.5056E 01	4.3000E 01	4.3000E 01	4.3000E 01
55	6.7821E 01	4.5750E 01	4.6000E 01	4.6000E 01
56	7.0950E 01	4.8500E 01	4.8500E 01	4.8500E 01
57	7.4079E 01	5.0920E 01	5.1395E 01	5.1395E 01
58	7.7209E 01	5.3340E 01	5.4290E 01	5.4290E 01
59	8.0338E 01	5.3815E 01	5.8000E 01	5.8000E 01
60	8.3467E 01	5.4290E 01	6.1000E 01	6.1000E 01
61	8.6594E 01	5.8000E 01	6.4000E 01	6.4000E 01
62	8.9726E 01	6.2500E 01	6.7000E 01	6.7000E 01
63	9.2855E 01	6.7000E 01	7.0000E 01	7.0000E 01
64	9.5984E 01	7.1500E 01	7.3000E 01	7.3000E 01
65	9.9113E 01	7.6000E 01	7.6000E 01	7.6000E 01
66	1.0224E 02	7.9000E 01	7.9000E 01	7.9000E 01
67	1.0537E 02	8.2000E 01	8.2000E 01	8.2000E 01
68	1.0850E 02	8.5000E 01	8.5000E 01	8.5000E 01

SPATIAL COARSE MESH

COARSE MESH BOUNDARIES FOR CONFIGURATION II.A

I/J	Z (CM)	SET 1 R (CM)
1	6.0320E 00	6.3889E 00
2	1.2064E 01	1.2578E 01
3	1.8096E 01	1.8767E 01
4	2.4128E 01	2.4955E 01
5	3.0160E 01	2.9160E 01
6	3.4250E 01	3.5625E 01
7	4.1790E 01	4.1148E 01
8	4.9330E 01	4.5720E 01
9	5.6870E 01	5.1816E 01
10	6.0960E 01	5.6386E 01
11	6.5532E 01	6.2674E 01
12	7.0104E 01	6.7627E 01
13	7.4676E 01	7.[illegible]61E 01
14	7.9248E 01	7.9056E 01
15	8.3820E 01	8.4770E 01
16	8.8392E 01	
17	9.2964E 01	
18	9.7536E 01	
19	1.0211E 02	
20	1.0763E 02	
21	1.1261E 02	
22	1.1760E 02	
23	1.2258E 02	
24	1.2757E 02	
25	1.3255E 02	
26	1.3754E 02	
27	1.4252E 02	
28	1.4751E 02	
29	1.5249E 02	
30	1.5748E 02	

COARSE MESH BOUNDARIES FOR CONFIGURATION II.B

I/J	Z (CM)	SET 1 R (CM)
1	3.0160E 00	3.7006E 00
2	6.0320E 00	6.4013E 00
3	9.0480E 00	9.6019E 00
4	1.2064E 01	1.1554E 01
5	1.5080E 01	1.5524E 01
6	1.8096E 01	1.9243E 01
	2.1112E 01	2.3105E 01
8	2.4128E 01	2.6932E 01
9	2.7144E 01	2.9160E 01
10	3.1120E 01	3.3470E 01
11	3.3029E 01	3.7780E 01
12	3.7627E 01	4.1148E 01
13	4.2230E 01	4.4276E 01
14	4.6832E 01	4.7344E 01
15	5.1435E 01	5.0452E 01
16	5.6037E 01	5.3540E 01
17	6.0960E 01	5.6386E 01
18	6.5532E 01	6.0578E 01
19	7.0104E 01	6.4770E 01
20	7.4676E 01	7.0484E 01
21	7.9248E 01	7.6199E 01
22	8.3820E 01	8.1913E 01
23	8.8392E 01	8.4770E 01
24	9.2964E 01	
25	9.7536E 01	
26	1.0211E 02	
27	1.0668E 02	
28	1.0763E 02	
29	1.1289E 02	
30	1.1814E 02	
31	1.2340E 02	
32	1.2866E 02	
33	1.3392E 02	
34	1.3917E 02	
35	1.4443E 02	
36	1.4969E 02	
37	1.5494E 02	
38	1.5748E 02	

COARSE MESH BOUNDARIES FOR CONFIGURATION II.D

I/J	Z (CM)	SET 1 R (CM)
1	-5.9944E 01	5.2173E 00
2	-5.5372E 01	9.6019E 00
3	-5.0800E 01	1.1554E 01
4	-4.4593E 01	1.6680E 01
5	-3.9336E 01	2.1806E 01
6	-3.4078E 01	2.6932E 01
7	-2.8821E 01	2.9160E 01
8	-2.3564E 01	3.3470E 01
9	-1.8307E 01	3.8100E 01
10	-1.3049E 01	4.2672E 01
11	-7.7923E 00	4.7244E 01
12	-2.5350E 00	5.1816E 01
13	0	5.6386E 01
14	5.9944E 00	6.0578E 01
15	1.1329E 01	6.4770E 01
16	1.6663E 01	6.7627E 01
17	2.1998E 01	7.0484E 01
18	2.7332E 01	7.3341E 01
19	3.2666E 01	7.6199E 01
20	3.8001E 01	7.9056E 01
21	4.1501E 01	8.4770E 01
22	4.5501E 01	

COARSE MESH BOUNDARIES FOR CONFIGURATION II.E

I/J	Z (CM)	SET 1 R (CM)
1	0	9.6019E 00
2	5.9944E 00	1.1554E 01
3	1.1329E 01	1.5947E 01
4	1.6663E 01	1.8654E 01
5	2.1998E 01	2.1806E 01
6	2.7332E 01	2.5196E 01
7	3.2666E 01	2.9180E 01
8	3.8001E 01	3.2000E 01
9	4.2668E 01	3.7500E 01
10	4.7380E 01	4.3000E 01
11	5.0875E 01	4.8500E 01
12	5.4370E 01	5.4290E 01
13	6.0240E 01	5.8000E 01
14	6.7860E 01	6.7000E 01
15	7.5480E 01	7.6000E 01
16	8.3100E 01	7.9000E 01
17	9.0720E 01	8.5000E 01
18	9.8340E 01	
19	1.0596E 02	
20	1.1358E 02	
21	1.2120E 02	

COARSE MESH BOUNDARIES FOR CONFIGURATION II.F

I/J	Z (CM)	SET 1 R (CM)
1	0	9.6019E 00
2	5.9944E 00	1.1554E 01
3	1.1329E 01	1.5947E 01
4	1.6663E 01	1.8654E 01
5	2.1998E 01	2.1806E 01
6	2.7332E 01	2.5196E 01
7	3.2666E 01	2.9180E 01
8	3.8001E 01	3.2000E 01
9	4.2668E 01	3.7500E 01
10	4.5001E 01	4.3000E 01
11	4.8115E 01	4.8500E 01
12	5.1229E 01	5.4290E 01
13	5.6760E 01	5.8000E 01
14	6.2290E 01	6.7000E 01
15	6.7821E 01	7.6000E 01
16	7.0950E 01	7.9000E 01
17	7.7209E 01	8.5000E 01
18	8.3467E 01	
19	8.9726E 01	
20	9.5984E 01	
21	1.0224E 02	
22	1.0850E 02	

COARSE MESH BOUNDARIES FOR CONFIGURATION III.A

I/J	Z (CM)	SET 1 R (CM)
1	3.0160E 00	3.2006E 00
2	6.0320E 00	6.4012E 00
3	9.0480E 00	9.6019E 00
4	1.2064E 01	1.2387E 01
5	1.5080E 01	1.6077E 01
6	1.8096E 01	2.9180E 01
7	2.1112E 01	3.3400E 01
8	2.4128E 01	3.7780E 01
9	2.7144E 01	4.1140E 01
10	3.1120E 01	4.4196E 01
11	3.3025E 01	4.7244E 01
12	3.7627E 01	5.0292E 01
13	4.2230E 01	5.3340E 01
14	4.6832E 01	5.3366E 01
15	5.1435E 01	5.9068E 01
16	5.6037E 01	6.4770E 01
17	6.0960E 01	7.0484E 01
18	6.5532E 01	7.6199E 01
19	7.0104E 01	8.1913E 01
20	7.4676E 01	8.4770E 01
21	7.9248E 01	
22	8.3820E 01	
23	8.8392E 01	
24	9.2964E 01	
25	9.7536E 01	
26	1.0211E 02	
27	1.0668E 02	
28	1.0763E 02	
29	1.1289E 02	
30	1.1814E 02	
31	1.2340E 02	
32	1.2866E 02	
33	1.3392E 02	
34	1.3917E 02	
35	1.4443E 02	
36	1.4969E 02	
37	1.5494E 02	
38	1.5748E 02	

COARSE MESH BOUNDARIES FOR CONFIGURATION IV.A

I/J	Z (CM)	SET 1 R (CM)
1	3.0160E 00	4.9152E 00
2	6.0320E 00	9.6019E 00
3	9.0480E 00	1.2471E 01
4	1.2064E 01	1.6680E 01
5	1.5080E 01	2.0280E 01
6	1.8096E 01	2.4359E 01
7	2.1112E 01	2.6932E 01
8	2.4128E 01	2.9180E 01
9	2.7144E 01	3.3400E 01
10	3.1120E 01	3.7780E 01
11	3.3025E 01	4.1140E 01
12	3.7627E 01	4.4196E 01
13	4.2230E 01	4.7244E 01
14	4.6832E 01	5.0292E 01
15	5.1435E 01	5.3340E 01
16	5.6037E 01	5.3366E 01
17	6.0960E 01	5.9068E 01
18	6.5532E 01	6.4770E 01
19	7.0104E 01	7.0484E 01
20	7.4676E 01	7.6199E 01
21	7.9248E 01	8.1913E 01
22	8.3820E 01	8.4770E 01
23	8.8392E 01	
24	9.2964E 01	
25	9.7536E 01	
26	1.0211E 02	
27	1.0668E 02	
28	1.0763E 02	
29	1.1289E 02	
30	1.1814E 02	
31	1.2340E 02	
32	1.2866E 02	
33	1.3392E 02	
34	1.3917E 02	
35	1.4443E 02	
36	1.4969E 02	
37	1.5494E 02	
38	1.5748E 02	

COARSE MESH BOUNDARIES FOR CONFIGURATION IV.B

I/J	Z (CM)	SET 1 R (CM)
1	-5.9944E 01	4.9152E 00
2	-5.5372E 01	9.6019E 00
3	-5.0800E 01	1.1554E 01
4	-4.4593E 01	1.6680E 01
5	-3.9336E 01	2.1806E 01
6	-3.4078E 01	2.6932E 01
7	-2.8821E 01	2.9160E 01
8	-2.3564E 01	3.3470E 01
9	-1.8307E 01	3.8100E 01
10	-1.3049E 01	4.2672E 01
11	-7.7923E 00	4.7244E 01
12	-2.5350E 00	5.1816E 01
13	0	5.6386E 01
14	5.9944E 00	6.0578E 01
15	1.1329E 01	6.4770E 01
16	1.6663E 01	6.7627E 01
17	2.1998E 01	7.0484E 01
18	2.7332E 01	7.3341E 01
19	3.2666E 01	7.6199E 01
20	3.8001E 01	7.9056E 01
21	4.1501E 01	8.4770E 01
22	4.5001E 01	

COARSE MESH BOUNDARIES FOR CONFIGURATION VI.A

I/J	Z (CM)	SET 1 R (CM)
1	3.0160E 00	3.2006E 00
2	6.0320E 00	6.4012E 00
3	9.0480E 00	9.6019E 00
4	1.2064E 01	1.2097E 01
5	1.5080E 01	1.5776E 01
6	1.8096E 01	1.9816E 01
7	2.1112E 01	2.3570E 01
8	2.4128E 01	2.6167E 01
9	2.7144E 01	2.9180E 01
10	3.1120E 01	3.3480E 01
11	3.3025E 01	3.7780E 01
12	3.7627E 01	4.1140E 01
13	4.2230E 01	4.4196E 01
14	4.6832E 01	4.7244E 01
15	5.1435E 01	5.0292E 01
16	5.6037E 01	5.3340E 01
17	6.0960E 01	5.3366E 01
18	6.5532E 01	5.9068E 01
19	7.0104E 01	6.4770E 01
20	7.4676E 01	7.0484E 01
21	7.9248E 01	7.6199E 01
22	8.3820E 01	8.1913E 01
23	8.8392E 01	8.4770E 01
24	9.2964E 01	
25	9.7536E 01	
26	1.0211E 02	
27	1.0668E 02	
28	1.0763E 02	
29	1.1289E 02	
30	1.1814E 02	
31	1.2340E 02	
32	1.2866E 02	
33	1.3392E 02	
34	1.3917E 02	
35	1.4443E 02	
36	1.4969E 02	
37	1.5494E 02	
38	1.5748E 02	

COARSE MESH BOUNDARIES FOR CONFIGURATION II.F S-10 CALCULATION

I/J	Z (CM)	SET 1 R (CM)
1	-5.9944E 01	9.6019E 00
2	-5.5372E 01	1.1554E 01
3	-5.0800E 01	1.5947E 01
4	-4.4593E 01	1.8654E 01
5	-3.9336E 01	2.1806E 01
6	-3.4080E 01	2.5196E 01
7	-2.8823E 01	2.9180E 01
8	-2.3566E 01	3.2000E 01
9	-1.8310E 01	3.7500E 01
10	-1.3053E 01	4.3000E 01
11	-7.7966E 00	4.8500E 01
12	-2.5400E 00	5.4290E 01
13	0	5.8000E 01
14	5.9944E 00	6.7000E 01
15	1.1329E 01	7.6000E 01
16	1.6663E 01	7.9000E 01
17	2.1998E 01	8.5000E 01
18	2.7332E 01	
19	3.2666E 01	
20	3.8001E 01	
21	4.2668E 01	
22	4.5001E 01	
23	4.8115E 01	
24	5.1229E 01	
25	5.6760E 01	
26	6.2290E 01	
27	6.7821E 01	
28	7.0950E 01	
29	7.7209E 01	
30	8.3467E 01	
31	8.9726E 01	
32	9.5984E 01	
33	1.0224E 02	
34	1.0850E 02	

2-D R-Z GEOMETRY PLOTS

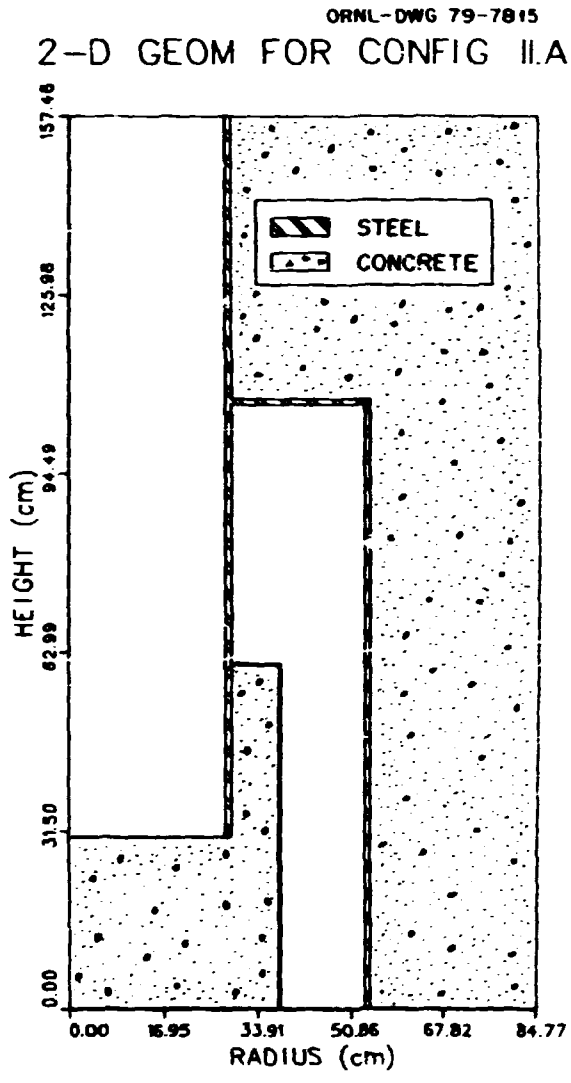

Fig. E.1. Plot of 2-D Geometry Model for GCFR Grid-Plate Shield Experiment Configuration II.A.

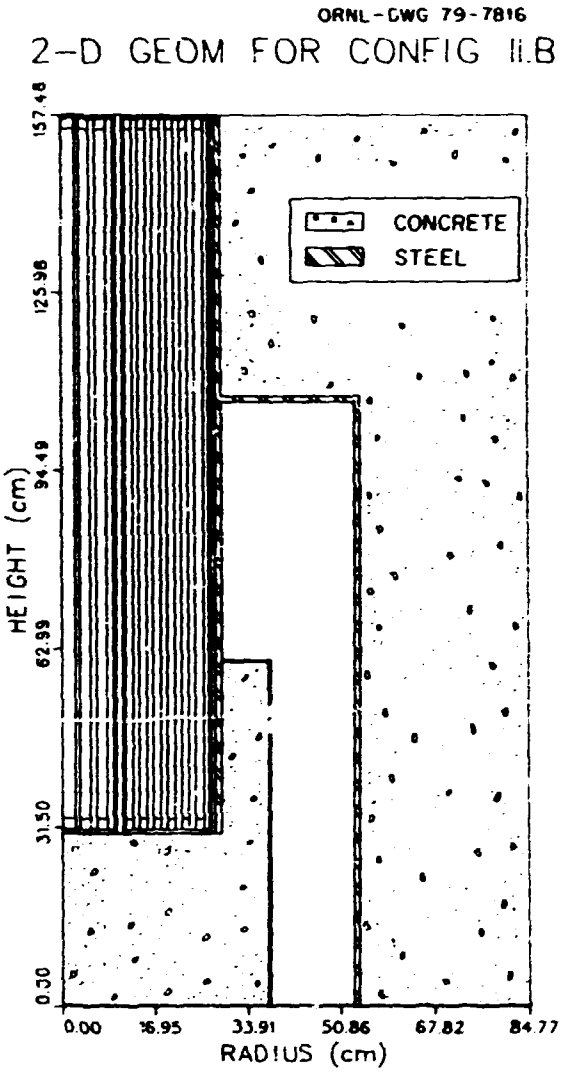

Fig. E.2. Plot of 2-D Geometry Model of GCFR Grid-Plate Shield Experiment Configuration II.B.

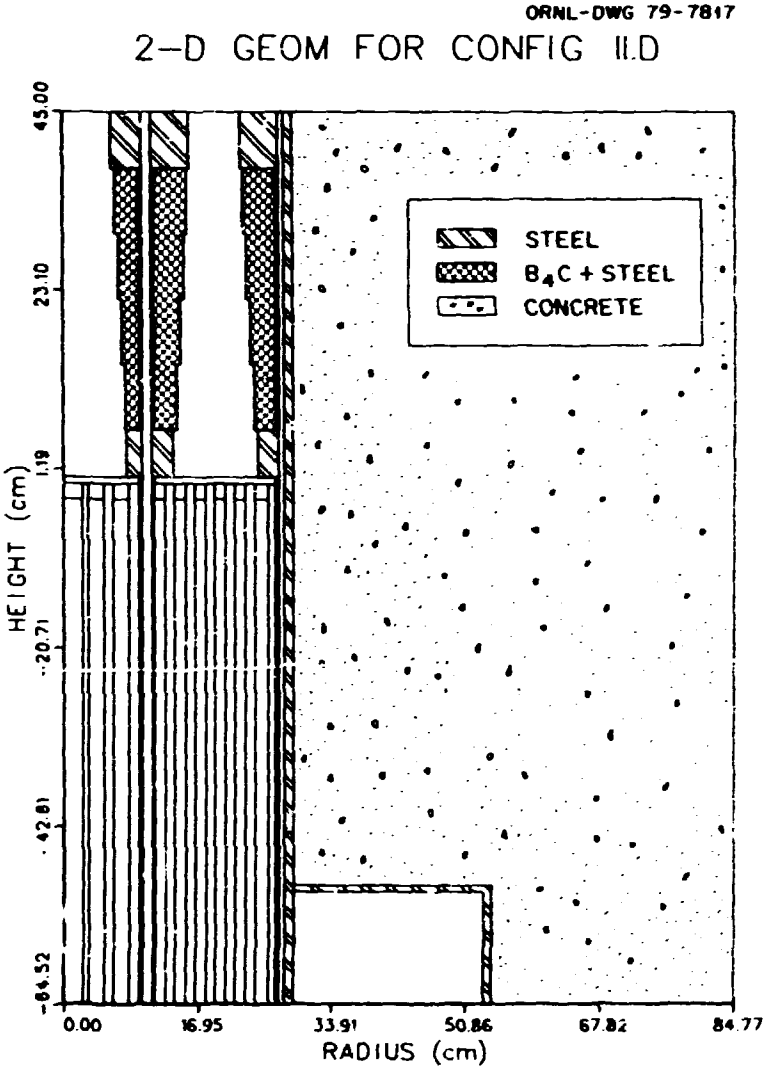

Fig. E.3. Plot of the 2-D Geometry Model for GCFR Grid-Plate Shield Experiment Configuration II.D.

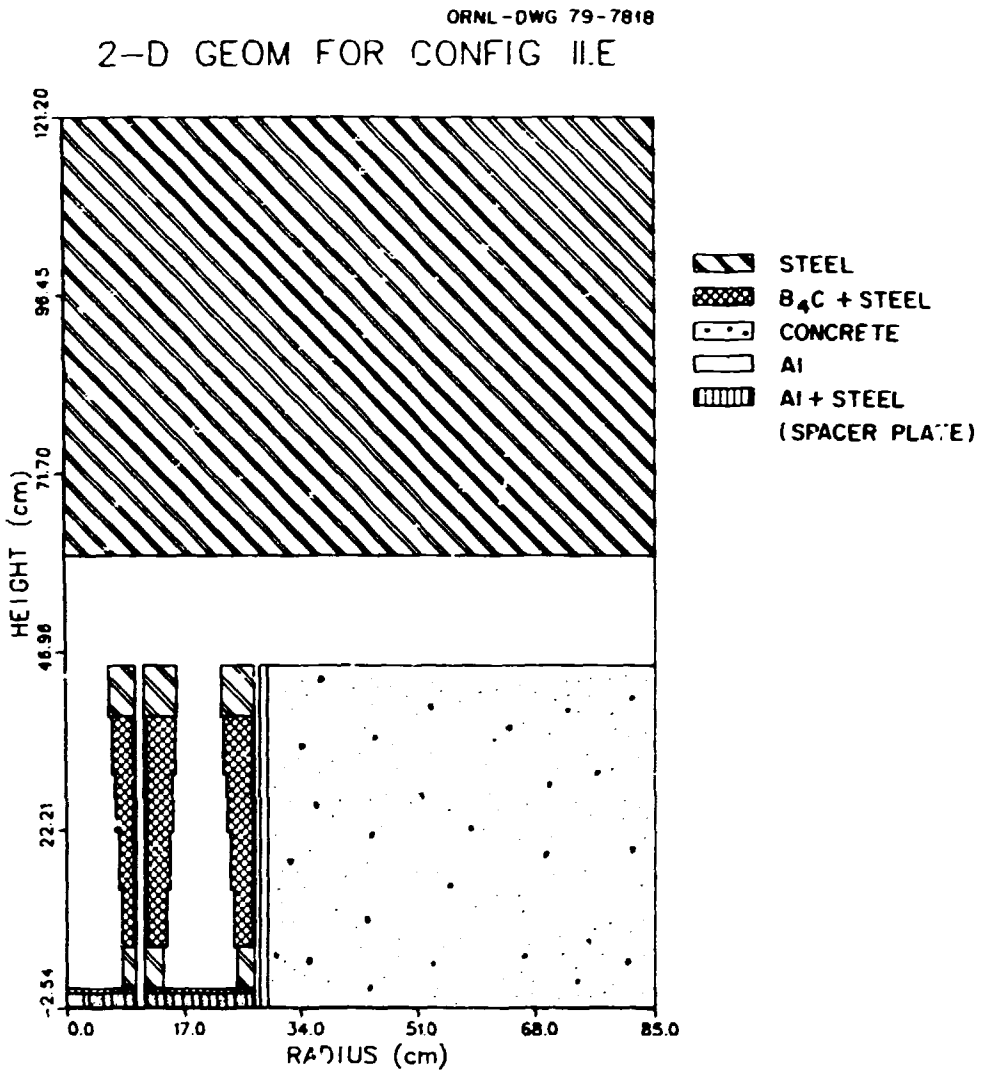

Fig. E.4. Plot of the 2-D Geometry Model of GCFR Grid-Plate Shield Experiment Configuration II.E.

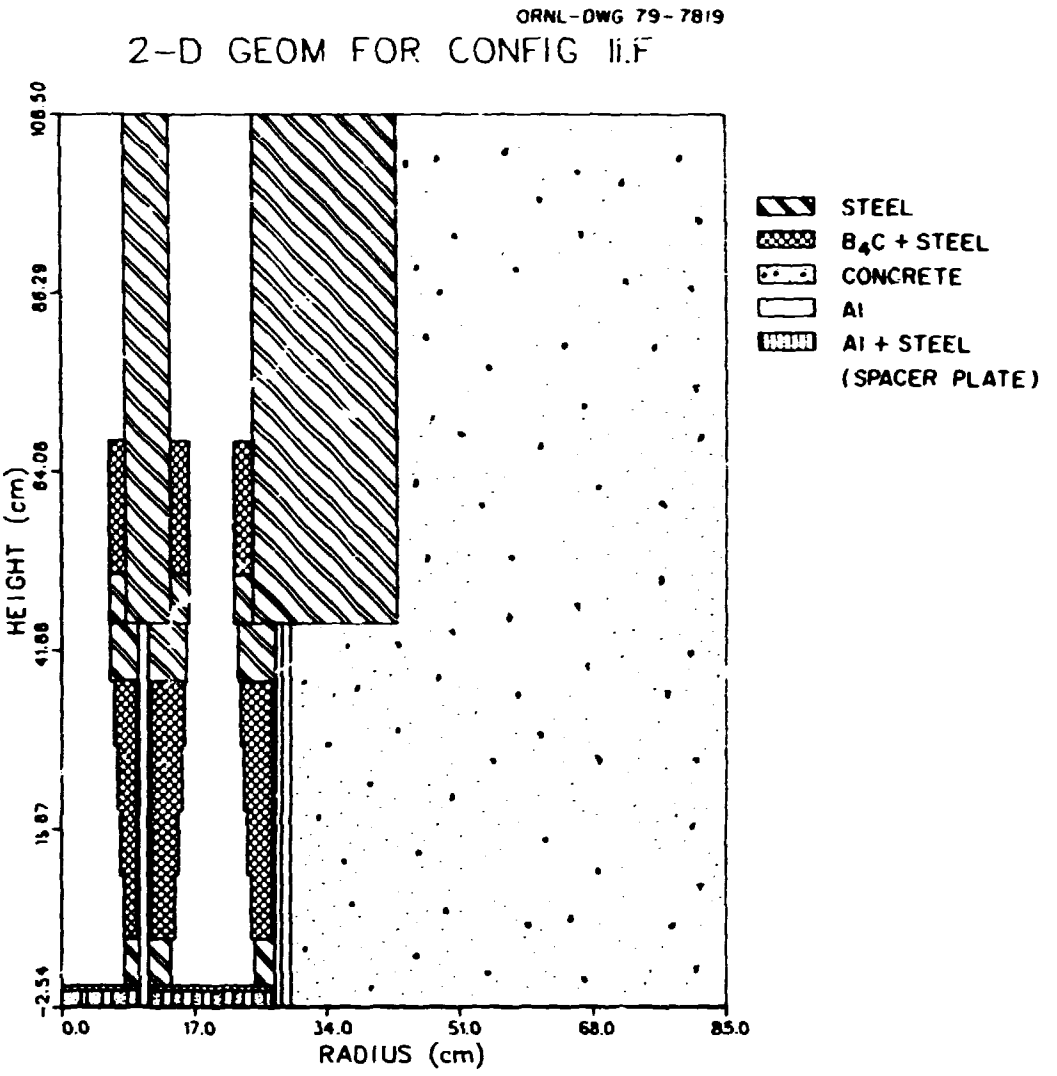

Fig. E.5. Plot of the 2-D Geometry Model of GCFR Grid-Plate Shield Experiment Configuration II.F.

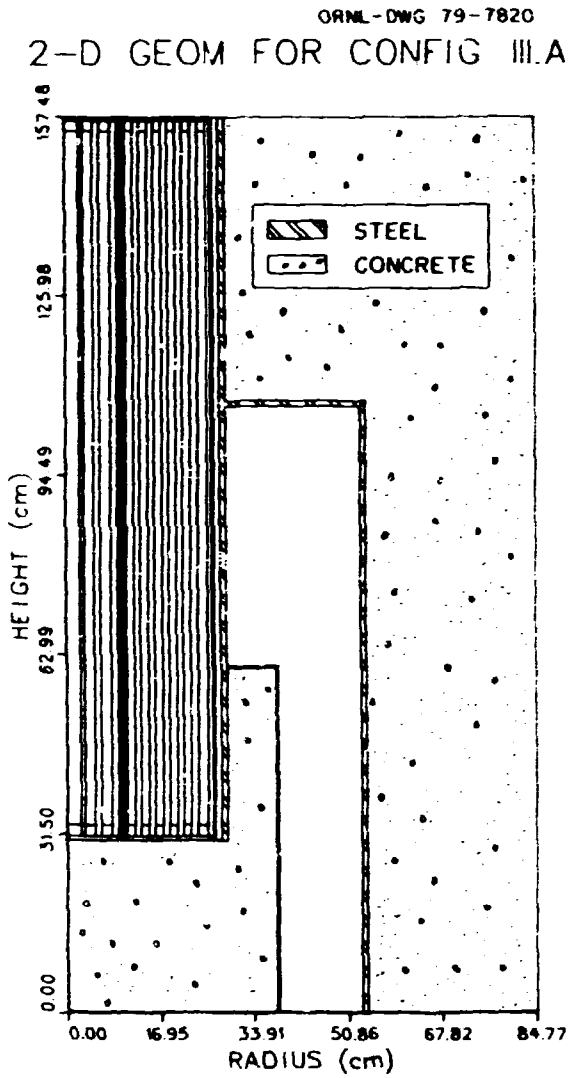

Fig. E.6. Plot of 2-D Geometry Model of GCFR Grid-Plate Shield Experiment Configuration III.A.

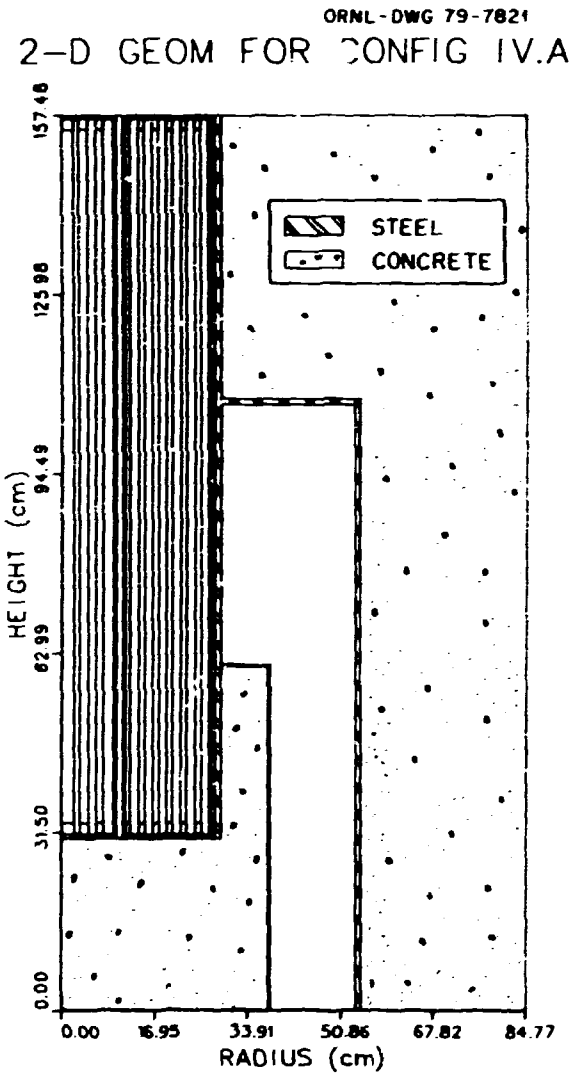

Fig. E.7. Plot of 2-D Geometry Model of GCFR Grid-Plate Shield Experiment Configuration IV.A.

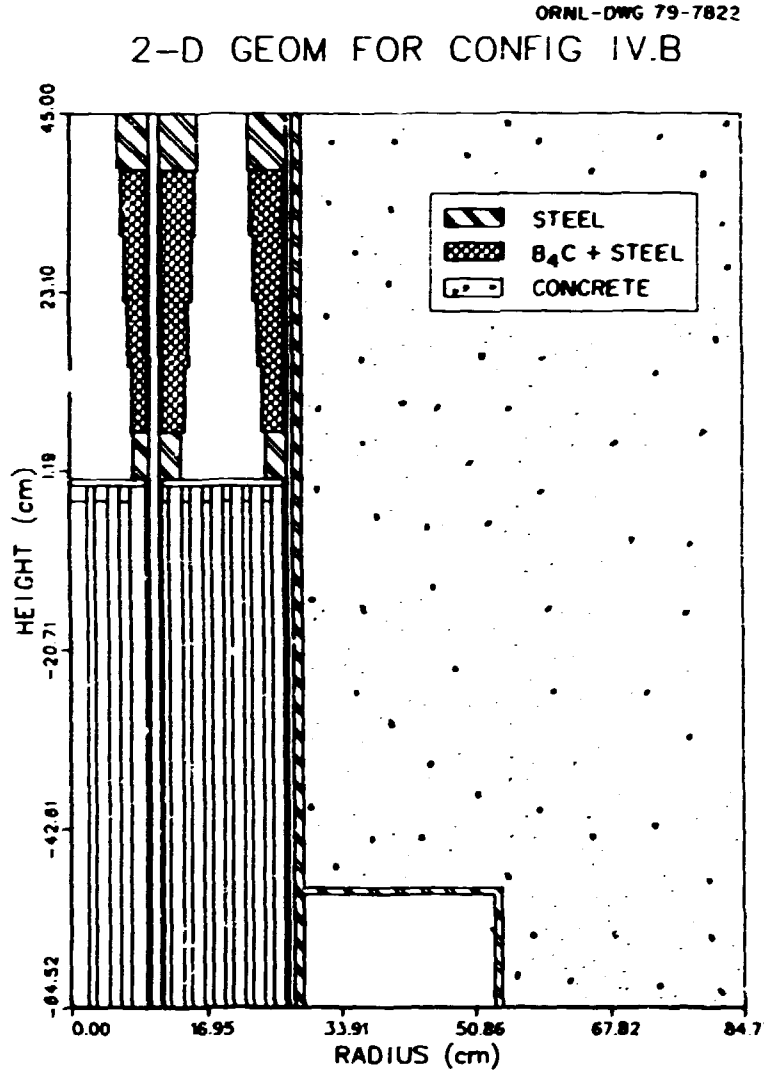

Fig. E.8. Plot of 2-D Geometry Model of GCFR Grid-Plate Shield Experiment Configuration IV.B.

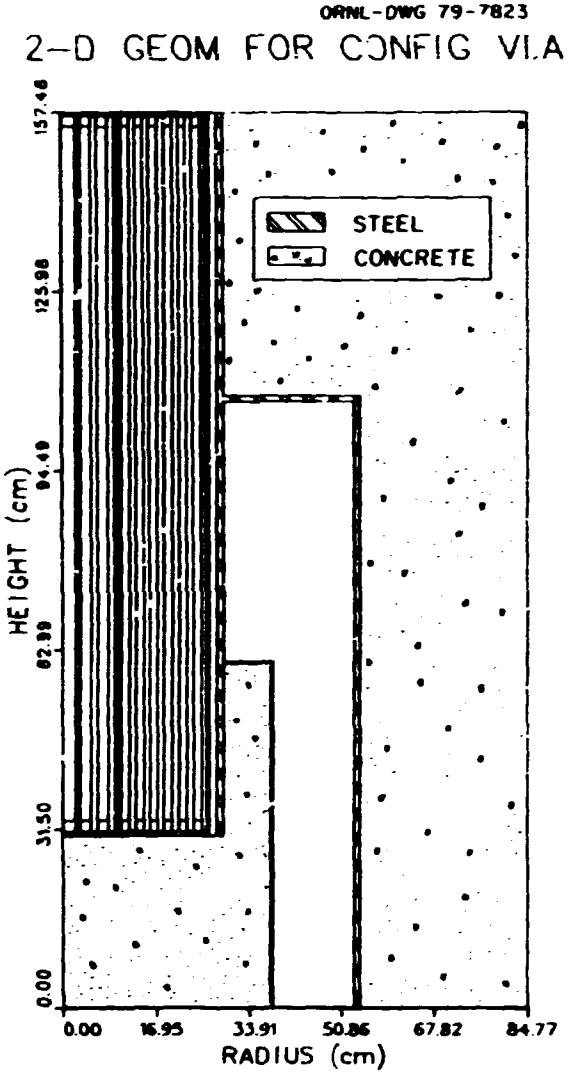

Fig. E.9. Plot of 2-D Geometry Model of GCFR Grid-Plate Shield Experiment Configuration VI.A.

ORNL-DWG 79-10956

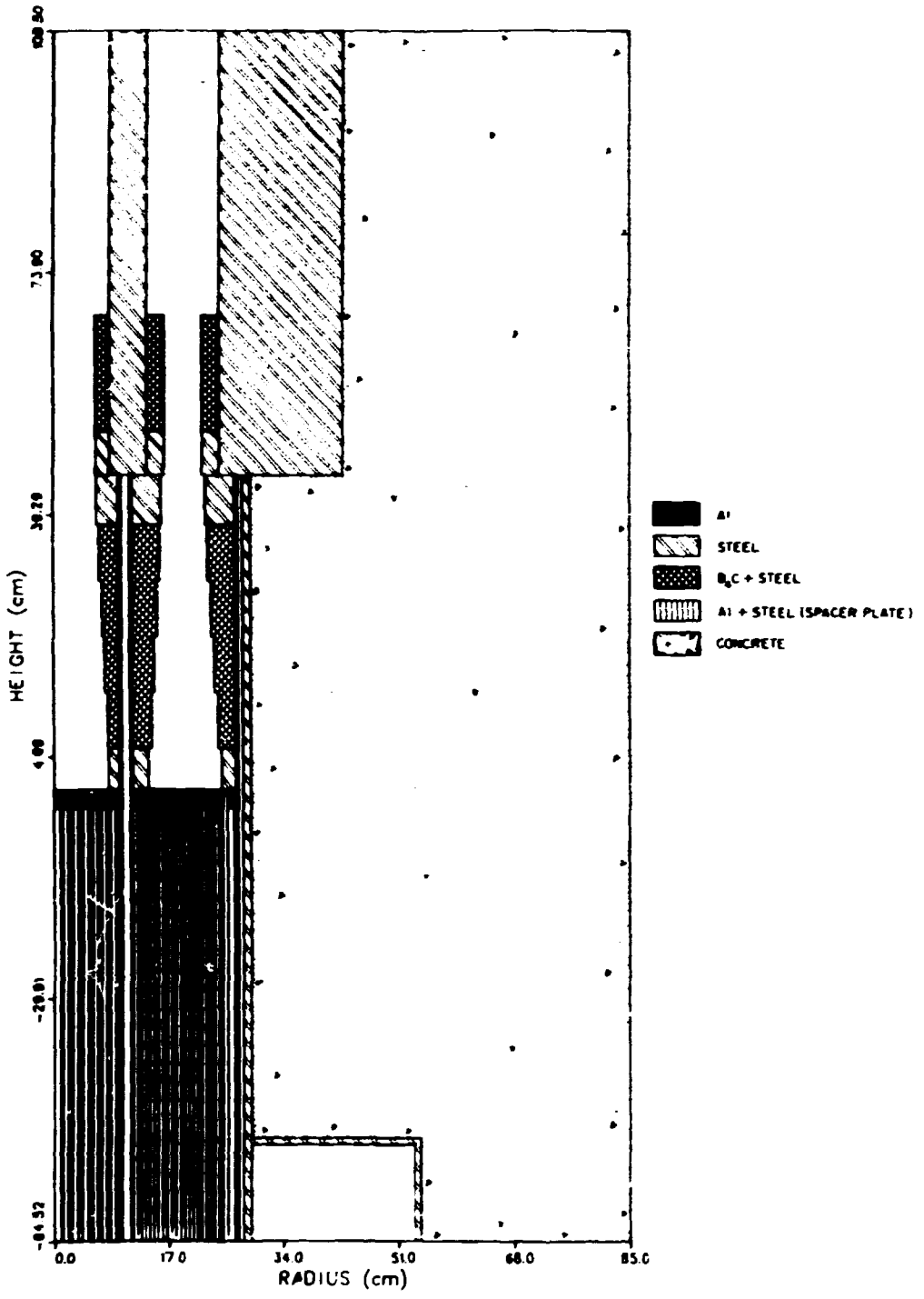

Fig. E.10. Plot of 2-D Geometry Model Used in the Calculation of GCFR Grid-Plate Shield Experiment Configuration II.F with the S_{10} Symmetric Quadrature.

ORNL-5551
Distribution Category UC-77
Gas Cooled Reactor Technology

INTERNAL DISTRIBUTION

1. L. S. Abbott
2. R. G. Alsmiller, Jr.
3. S. J. Ball
4. D. E. Bartine
5. M. Bender
6. T. J. Burns
7. J. P. Callaghan
8. R. L. Childs
9. J. C. Cleveland
10-11. S. N. Cramer
12. M. B. Emmett
13. W. W. Engle, Jr.
14. G. F. Flanagan
15. M. H. Fontana
16. Uri Gat
17. E. H. Gift
18. H. Goldstein (Consultant)
19. A. G. Grindell
20. F. J. Homan
21-22. D. T. Ingersoll
23-30. P. R. Kasten
31. A. L. Lotts
32. R. E. Maerker
33. RSIC
34. F. C. Maienschein
35. F. J. Muckenthaler
36. E. M. Oblow
37. R. W. Peelle
38. J. P. Renier
39-53. C. O. Slater
54. I. Spiewak
55. H. E. Trammell
56. D. B. Trauger
57. D. R. Vondy
58. J. R. Weir
59. C. R. Weisbin
60. G. E. Whitesides
61. L. R. Williams
62. M. L. Williams
63. B. A. Worley
64. A. Zucker
65. P. Greebler (Consultant)
66. W. B. Loewenstein (Consultant)
67. R. Wilson (Consultant)
68-69. Central Research Library
70. Y-12 Document Reference Section
71-72. Laboratory Records Department
73. Laboratory Records ORNL-RC
74. ORNL Patent Office

EXTERNAL DISTRIBUTION

75. Director, Nuclear Power Development Division, Department of Energy, Washington, D.C. 20545.

76. G. A. Newby, GCFR Branch, Nuclear Power Development Division, Department of Energy, Washington, D.C. 20545.

77. Director, Department of Energy, Office of Program Management, P. O. Box 81325, San Diego, California 92138.

78-79. Office of the Assistant Manager for Energy Research and Development, DOE-ORO, Oak Ridge, Tennessee 37830.

80-81. Director, Nuclear Research and Development Division, DOE-ORO, Oak Ridge, Tennessee 37830.

82-257. Given distribution as shown in TID-4500, Distribution Category UC-77 - Gas Cooled Reactor Technology.

☆U.S. GOVERNMENT PRINTING OFFICE: 1979-640-079-159